TU Delft

Delft University of Technology

Document Version
Final published version

Citation (APA)
Kiouranakis, K. I. (2026). *Experimental thermodynamic analysis of premixed methanol marine engines*. [Dissertation (TU Delft), Delft University of Technology]. https://doi.org/10.4233/uuid:c8397dc4-301d-4d15-8cb0-398127337786

Important note
To cite this publication, please use the final published version (if applicable).
Please check the document version above.

Copyright
In case the licence states “Dutch Copyright Act (Article 25fa)”, this publication was made available Green Open Access via the TU Delft Institutional Repository pursuant to Dutch Copyright Act (Article 25fa, the Taverne amendment). This provision does not affect copyright ownership.
Unless copyright is transferred by contract or statute, it remains with the copyright holder.

Sharing and reuse
Other than for strictly personal use, it is not permitted to download, forward or distribute the text or part of it, without the consent of the author(s) and/or copyright holder(s), unless the work is under an open content license such as Creative Commons.

Takedown policy
Please contact us and provide details if you believe this document breaches copyrights.
We will remove access to the work immediately and investigate your claim.

This work is downloaded from Delft University of Technology.

Experimental Thermodynamic Analysis of Premixed Methanol Marine Engines

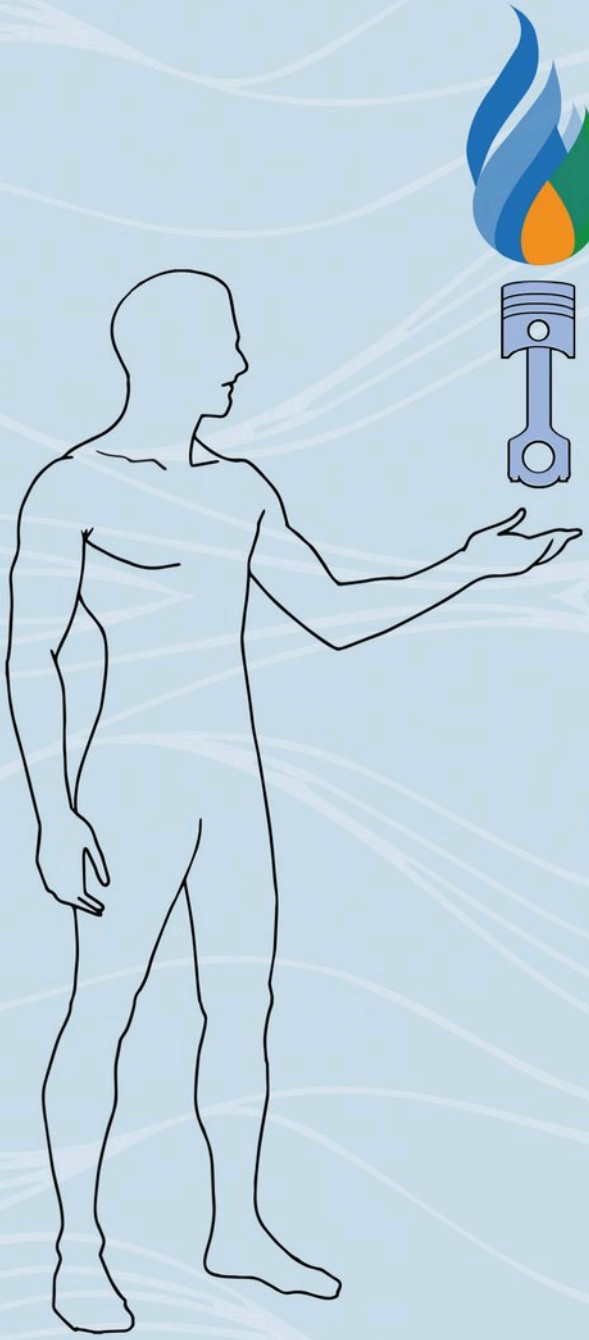

TU Delft Delft University of Technology

Konstantinos Ioannis Kiouranakis

EXPERIMENTAL THERMODYNAMIC ANALYSIS
- OF -
PREMIXED METHANOL MARINE ENGINES

KONSTANTINOS IOANNIS KIOURANAKIS

Konstantinos Ioannis Kiouranakis: *Experimental Thermodynamic Analysis of Premixed Methanol Marine Engines*, © April 2026

EXPERIMENTAL THERMODYNAMIC ANALYSIS OF PREMIXED METHANOL MARINE ENGINES

Dissertation

for the purpose of obtaining the degree of doctor
at Delft University of Technology
by the authority of the Rector Magnificus
Prof.dr.ir. H. Bijl
chair of the Board of Doctorates
to be defended publicly on
Friday, 5 June 2026, 10:00

BY

Konstantinos Ioannis KIOURANAKIS

This dissertation has been approved by the promotor, the copromotor and the external advisor.

Composition of the doctoral committee:

Rector Magnificus	chairperson
Dr.ir. P. de Vos	Delft University of Technology, promotor
Dr.ir. R.D. Geertsma	Delft University of Technology / Netherlands Defence Academy, copromotor
Dr.ir. R.C. Willems	Netherlands Organisation for Applied Scientific Research (TNO), external adviser

Independent members:

Prof.dr. A. Gangoli Rao	Delft University of Technology
Prof.dr.ir. B.J. Boersma	Delft University of Technology
Prof.dr.ir. S. Verhelst	Ghent University, Belgium / Lund University, Sweden
Prof.dr.-ing. B. Buchholz	Rostock University, Germany
Dr.ing. A. Coraddu	Delft University of Technology, reserve member

This research is part of the MENENS project (Methanol als Energiestap Naar Emissieloze Nederlandse Scheepvaart). The project is funded by the Netherlands Enterprise Agency (RVO: Rijksdienst voor Ondernemend Nederland) under the grant number MOB21012.

MENENS partners: Bakker Sliedrecht, Boskalis, C-Job, DAMEN, DC Systems B.V., Discom, EST-Floattech, Feadship, Fugro, LPS Twin Turbine, MARIN, Marine Service Noord, Nederlandse Defensie Academie, NIM, RH Marine, Royal IHC, Royal T Shipyards, Royal Wagenborg, TNO, Van Oord, Van Oossanen, VT, Wärtsilä.

Keywords:	Internal combustion engine, spark ignition, compression ignition, diesel, natural gas, methanol, maritime, defossilization, experimental study, combustion, efficiency, emissions.
Front cover:	Prometheus' figure holding an engine piston cup with combustion fire by methanol.
Back cover:	Waves and methanol's chemical structure filled with keywords of this dissertation.
Printed by:	Ridderprint
Cover design:	Georgia Perra
Typesetting:	LaTeX
AI use:	The author acknowledges the use of AI tools (OpenAI; Perplexity AI) as aids for language refinement and brainstorming, and takes responsibility for the dissertation's content.

Copyright © 2026 by Konstantinos Ioannis Kiouranakis

ISBN: 978-94-6537-557-1

An electronic version of this dissertation is available at:
http://repository.tudelft.nl/.

Τῶν ὄντων τὰ μέν ἐστιν ἐφ᾽ ἡμῖν
τὰ δὲ οὐκ ἐφ᾽ ἡμῖν.

From things, some are up to us
and some are not up to us.

Epictetus

SUMMARY

The defossilization of marine power systems remains a central challenge in the ongoing energy transition of transportation. Despite the progress of alternative technologies, the reciprocating internal combustion engine (ICE) will continue to dominate marine applications in the foreseeable future due to its unparalleled robustness, reliability, and efficiency. Shipping's transition toward carbon neutrality therefore relies on adapting this well-established technology to operate with sustainable fuels.

This dissertation addresses the growing need for sustainable marine fuels by exploring premixed combustion strategies to adopt methanol in marine engines. Because low reactivity of methanol limits its suitability for conventional compression ignition (CI) diesel engines, alternative premixed combustion concepts emerge. Lean-burn spark-ignition (LBSI) and premixed dual-fuel (PRDF) strategies share a premixed combustion concept and robust ignition control. In addition to new engine design architectures, the ability to convert existing diesel platforms to premixed methanol combustion with only relatively minor modifications makes these concepts highly attractive. Given the long operational lifespan of marine engines, such retrofit capability can smoothen and accelerate maritime defossilization. To inform the development of retrofit and next-generation methanol marine engines, this research offers an in-depth examination of these engine technologies, elucidating their potential and limitations.

The primary objective of this dissertation is to *develop an experimentally based thermodynamic analysis framework for premixed methanol engine technologies*, linking in-cylinder pressure-based and combustion-informed heat release analysis with engine performance indicators. This framework is tailored to the two premixed concepts of LBSI and PRDF. Building on these frameworks, the overarching goal of the thesis is *to enhance the understanding of the performance of methanol-fueled premixed concepts*, including their distinct combustion behavior, stability limits, efficiency, and emission characteristics. To this end, the frameworks are applied to two marine engine testbeds through targeted experimental campaigns: 1) a 34.7 liter multi-cylinder LBSI engine, and 2) a 4.1 liter single-cylinder PRDF engine.

To realize this research goal, this dissertation first reviews the research landscape of methanol engines and establishes the conceptual basis for the subsequent analysis frameworks. Beyond conducting a comprehensive literature review and identifying research gaps in SI and PRDF methanol operation, the review clarifies the inconsistent terminology used for injection, ignition, and combustion strategies for methanol use. To further address this, a unified classification framework is proposed that links injection and ignition strategies to combustion modes.

Building on this foundation, this thesis introduces a combustion chamber geometry- and concept-driven combustion characterization framework for *LBSI multi-cylinder engines* and applies it in experimental campaigns using natural gas as a fuel, as the LBSI engine cannot yet run on methanol. By resolving the distinct combustion phasing and linking it to engine performance indicators, this research shows that advancing the transition point at which the flame enters the squish region improves combustion stability as well as brake thermal and combustion efficiency, albeit with increased heat losses and NO_x formation. The experimental framework integrates a multi-stage Wiebe formulation as an additional quantitative diagnostic tool for characterizing dual-stage combustion behavior. Because the combustion-phasing framework is rooted in the premixed flame-propagation dynamics associated with the chamber geometry, rather than in fuel-specific properties only, its qualitative conclusions are expected to remain valid for methanol LBSI operation. To this end, the diagnostic approach is deemed conceptually suited for direct application in future methanol-LBSI engine experiments.

Subsequently, this dissertation proposes a methodological analysis framework tailored to *methanol PRDF operation*. This framework enables both qualitative and quantitative analysis of heat release profiles and is applied in an experimental campaign on the single-cylinder test engine operating at high methanol energy fractions (MEFs). The qualitative analysis reveals three distinct combustion modes—characterized by m-, h-, and n-shaped profiles—unique to methanol PRDF operation, and associates them with specific underlying mechanisms. A systematic quantitative method based on two heat release morphology indicators—the Combustion Mechanism Index (CMI) and Phase Magnitude Ratio (PMR)—is proposed to map and classify these combustion modes. Methanol PRDF operation achieves lower NO_x emissions than diesel-only (DO) baseline operation, but at the expense of higher NO_2/NO ratios and substantial rise in CO and UHC emissions. While transitioning from DO to methanol PRDF offers potential efficiency gains for marine engines, especially under high-load operation, combustion losses remain the primary barrier.

Building on the investigation of MEF effects and leveraging the developed framework, this thesis explores certain boundary conditions to assess their potential in mitigating methanol PRDF challenges. The parametric analysis of intake temperature and intake/exhaust pressures highlights the critical role of boundary conditions in enabling high-MEF, high-load PRDF operation, especially for diesel engines with mechanically controlled injection. Increasing intake temperature enhances combustion, allowing MEF to reach 93% without significant penalties in heat losses or NO_x emissions. Similarly, reducing intake pressure enriches the mixture and improves combustion efficiency without compromising the high temperature related aspects. The morphological analysis during this reduction reveals a transition from h-shaped to bell-shaped heat release profiles, indicating a shift in the dominant combustion mechanism from flame propagation toward premixed autoignition.

On a final note, this dissertation aims not only to advance understanding of premixed methanol combustion in large-bore engines but also to provide practical diagnostic methodologies that support research and development of marine power systems powered by sustainable fuels. Therefore, the developed frameworks are intended to be refined and expanded to other engines and fuels, and as such this thesis contributes to more sustainable shipping.

SAMENVATTING

Binnen de lopende energietransitie in de transportsector vormt het defossiliseren van energie aan boord van schepen een grote uitdaging. Niettegenstaande de recente ontwikkelingen van alternatieve technologieën, zal de zuigermotor met inwendige verbranding (Internal Combustion Engine, ICE) naar alle waarschijnlijkheid in de toekomst dominant blijven in maritieme toepassingen, als gevolg van haar ongeëvenaarde robuustheid, betrouwbaarheid en relatief hoge efficiëntie. De transitie van de scheepvaart naar koolstofneutraliteit is daarom sterk afhankelijk van het aanpassen van deze beproefde technologie naar werking op alternatieve, duurzame brandstoffen.

Dit proefschrift adresseert de groeiende behoefte naar duurzame maritieme brandstoffen door de toepassing van methanol in scheepsmotoren middels zogenoemde voorvermengde verbrandingsconcepten te onderzoeken. De lage reactiviteit van methanol beperkt de geschiktheid ervan voor conventionele Compression Ignition (CI) dieselmotoren, waardoor alternatieve voorvermengde verbrandingsconcepten aantrekkelijk zijn. De Lean-Burn Spark Ignition (LBSI) en Premixed Dual-Fuel (PRDF) verbrandingsconcepten verbrandingsstrategieën ze delen een concept voor voorgemengde verbranding en een robuuste ontstekingsregeling. Naast nieuwe motorontwerparchitecturen, de mogelijkheid om bestaande dieselmotoren met slechts beperkte aanpassingen geschikt te maken voor voorvermengde methanolverbranding maakt deze concepten bijzonder aantrekkelijk. Gezien de lange operationele levensduur van maritieme motoren, kan de mogelijkheid tot het retrofitten van bestaande motoren de defossilisatie van de scheepvaart versnellen en vergemakkelijken. Dit onderzoek biedt daarom een diepgaande analyse van deze motortechnologieën en belicht hun potentieel en beperkingen ter ondersteuning van de ontwikkeling van zowel retrofit- als next-generation methanolmotoren voor maritieme toepassingen.

Het primaire doel van dit proefschrift is het *ontwikkelen van thermodynamische analysekaders gebaseerd op experimenten voor voorvermengde methanolmotortechnologieën*, waarin gemeten cilinderdruk gebaseerde analyse en verbrandingsgeïnformeerde warmteafgifte-analyse worden gekoppeld aan prestatie-indicatoren van de motor. Dit analysekader is specifiek toegespitst op de voorvermengde concepten LBSI en PRDF voor motoren met een typische diesel verbrandingskamergeometrie. Gebruikmakend van de ontwikkelde analysekaders is het overkoepelende onderzoeksdoel van het proefschrift het *vergroten van het inzicht in de prestaties van methanol-lucht voorvermengde motorconcepten*, waaronder hun unieke verbrandingsgedrag, operationele limieten, efficiëntie en emissiekenmerken. De ontwikkelde analysekaders worden toegepast op twee maritieme motorproefopstellingen via gerichte experimentele campagnes: (1) een 34,7-liter multi-cilinder LBSI-motor en (2) een 4,1-liter één-cilinder PRDF-motor.

Ter realisatie van het onderzoeksdoel begint het proefschrift met een uitgebreide literatuurstudie die het onderzoekslandschap van methanolmotoren in kaart brengt en de conceptuele basis legt voor de daaropvolgende analysekaders. Naast het identificeren van onderzoekshiaten in Spark Ignition (SI) en PRDF methanolbedrijf, adresseert dit proefschrift ook de inconsistente terminologie die wordt gebruikt voor injectie-, ontstekings- en verbrandingsstrategieën bij methanoltoepassing. Er wordt een eenduidig classificatiekader voorgesteld dat injectie- en ontstekingsstrategieën systematisch koppelt aan specifieke verbrandingsmodi.

Op basis van dit classificatiekader introduceert het proefschrift een op verbrandingskamergeometrie en motorconcept gebaseerd karakteriseringskader voor *multi-cilinder LBSI-motoren*, welke vervolgens wordt toegepast in experimentele campagnes waarbij aardgas als brandstof is gebruikt, aangezien de betreffende LBSI-motor nog niet op methanol kan draaien. Door de verschillende unieke fases van de verbranding te onderscheiden en deze te relateren aan motorprestatie-indicatoren wordt aangetoond dat het vervroegen van het overgangspunt waarop het vlamfront het squish-gebied bereikt, leidt tot verbeterde verbrandingsstabiliteit en hoger motor- en verbrandingsrendement, zij het dat dit ook gepaard gaat met verhoogde warmteverliezen en een toename van NO_x-emissies. Het ontwikkelde experimentele analysekader integreert een meerfasige Wiebe-formulering als aanvullend kwantitatief diagnostisch hulpmiddel voor het karakteriseren van tweestapsverbrandingsgedrag. Aangezien dit verbrandingsfasemodel gebaseerd is op de vlamvoortplantingsdynamica van voorvermengde brandstof-lucht mengsels in de specifieke verbrandingskamergeometrie, en niet alleen in brandstofspecifieke eigenschappen, worden de kwalitatieve conclusies als geldig beschouwd voor toepassing op toekomstige methanol-LBSI motorexperimenten.

Vervolgens presenteert het onderzoek een methodologisch analysekader dat specifiek is afgestemd op *methanol PRDF-bedrijf*. Dit kader maakt zowel kwalitatieve als kwantitatieve analyse van warmteafgifteprofielen mogelijk en wordt toegepast in een experimentele campagne op een één-cilinder motorplatform bij hoge methanol energy fractions (MEFs). De kwalitatieve analyse identificeert drie duidelijk te onderscheiden verbrandingsmodi, gekarakteriseerd door m-, h- en n-vormige warmteafgifteprofielen, die specifiek zijn voor methanol PRDF-bedrijf en worden gekoppeld aan onderliggende fysische verbrandingsmechanismen. Daarnaast wordt een systematische kwantitatieve methode voorgesteld op basis van twee morfologische indicatoren voor vrijkomende warmte, de Combustion Mechanism Index (CMI) en de Phase Magnitude Ratio (PMR), waarmee deze verbrandingsmodi kunnen worden geclassificeerd en gekwantificeerd. Methanol PRDF-bedrijf resulteert in lagere NO_x-emissies dan diesel-only operationeel bedrijf, maar leidt tot hogere NO_2/NO-verhoudingen en significante toenames in CO- en UHC-emissies. Hoewel de overgang van diesel-only naar methanol PRDF-bedrijf mogelijk verbetering van rendement biedt voor maritieme motoren, met name bij hoge belasting, vormen verbrandingsverliezen blijven de belangrijkste belemmering.

Voortbouwend op de analyse van MEF-invloeden en gebruikmakend van het ontwikkelde analysekader, onderzoekt dit proefschrift tevens specifieke randvoorwaarden m.b.t. luchtcondities om hun potentieel te beoordelen in het mitigeren van de uitdagingen kenmerkend voor methanol PRDF-bedrijf. De parametrische analyse van inlaattemperatuur en inlaat- en uitlaatdrukken benadrukt het cruciale

belang van de juiste luchtcondities voor en na de cilinders voor het mogelijk maken van stabiel PRDF-bedrijf bij hoge MEF en hoge motorbelasting, met name voor dieselmotoren met mechanisch aangestuurde dieselinjectie. Het verhogen van de inlaattemperatuur verbetert de verbranding en maakt MEFs tot 93% mogelijk zonder significante nadelen in warmteverliezen of NO_x-emissies. Even zo leidt verlaging van de inlaatdruk tot mengselverrijking en verbetering van het verbrandingsrendement zonder nadelige gevolgen voor hoge-temperatuurgerelateerde processen. De morfologische analyse van de warmteafgifteprofielen tijdens deze drukverlaging toont een overgang van h-vormige naar belvormige warmteafgifteprofielen, wat wijst op een verschuiving van het dominante verbrandingsmechanisme van vlamfrontvoortplanting naar voorvermengde spontane ontsteking.

Tot slot beoogt dit proefschrift niet alleen het fundamentele inzicht in voorvermengde methanolverbranding in motoren met grote cilinderdiameters te vergroten, maar ook praktische diagnostische analysemethodes aan te reiken ter ondersteuning van onderzoek en ontwikkeling van maritieme aandrijvingen op basis van duurzame brandstoffen. De ontwikkelde analysekaders zijn daarom bedoeld om verder te worden verfijnd en toegepast op andere motorconfiguraties en brandstoffen. Zodoende draagt dit proefschift bij aan een duurzamere scheepvaart.

CONTENTS

LIST OF FIGURES

LIST OF TABLES

NOMENCLATURE (SYMBOLS AND PARAMETERS)

Symbol	Definition	Unit
aHRR / gHRR	apparent/gross Heat release rate	J/°CA
BTE	Brake thermal efficiency	%
CA	Crank angle	°CA
CAx	Crank angle for x% of MFB	°CA
CD	Combustion duration	°CA
COV	Coefficient of variance	%
CMI	Combustion mechanism index	%
ID	Ignition delay	°CA
(g)IMEP	(gross) Indicated mean effective pressure	bar
LHV	Lower heating value	MJ/kg
MFB	Mass fraction burnt	–
MEF	Methanol energy fraction	%
PMR	Phase magnitude ratio	%
PRR	Pressure rise rate	bar/°CA
IVC / EVO	Inlet/Exhaust valve	°CA
EVC / IVO	closing/opening	
SOC / EOC	Start/End of combustion	°CA
SOI	Start of injection	°CA
ST	Spark timing	°CA
c_p, c_v	Specific heat at constant pressure/volume	J/(kgK)
p	Pressure	bar
$\dot{p}$	Pressure derivative	bar/s
m	Mass	kg
n	Engine speed	rpm
$\dot{m}$	Mass-flow rate	kg/s
V	Volume	m^3
P	Power output (mechanical)	kW
$\dot{P}$	Heat-transfer rate	W
R	Specific gas constant	J/(kgK)
T	Temperature	K

GREEK SYMBOLS

α	Wiebe efficiency parameter	–
β	Wiebe weight factor	–
γ	Specific heat ratio (c_p/c_v)	–
$\Delta\theta$	Wiebe combustion duration parameter	–
ϵ	Compression ratio	–
η	Efficiency	–
θ	Crank angle	°CA
λ	Air excess ratio	–
ϕ	Equivalence ratio	–
ρ	Gas density	kg/m^3
τ	Characteristic time	s

ACRONYMS AND ABBREVIATIONS

Combustion concepts and engine modes

CDC	Conventional diesel combustion
CI	Compression ignition
CN	Cetane number
DDFS	Direct dual-fuel stratification
DF	Dual-fuel
DFDC	Dual-fuel diffusion combustion
DMDF	Diesel–methanol dual-fuel
DO	Diesel-only operation
HCCI	Homogeneous charge CI
HP / LP	High / Low pressure
HRF / LRF	High-/low-reactivity fuel
JCCI	Jet-controlled CI
LB / LBSI	Lean-burn / Lean-burn SI
MCCI	Mixing-controlled CI
MF	Mono-fuel
MPDF	Micro-pilot dual-fuel
ON	Octane number
PCCI	Premixed charge CI
PPC / PPCI	Partially premixed CI
PRDF	Premixed dual-fuel
PREMIER	Premixed mixture ignition in the end-gas region
RCCI	Reactivity-controlled CI
SACI	Spark-assisted CI
SI	Spark ignition
TJI	Turbulent jet ignition

Performance and engine parameters

aTDC / bTDC	After / before top dead center
CCV	Cycle-to-cycle variation

CL	Combustion losses
CR	Compression ratio
DOE	Design of experiments
EC	Experimental campaign
EGR	Exhaust gas recirculation
EL	Exhaust losses
EOC	End of combustion
EVO	Exhaust valve open
DAS	Data acquisition system
HL	Heat losses
ICE	Internal combustion engine
MSP	Methanol substitution percentage
RG	Residual gases
RSS	Residual sum of squares
TKE	Turbulent kinetic energy

FUEL AND EMISSIONS

CO	Carbon monoxide
CO_2	Carbon dioxide
HO_2	Hydroperoxyl
MeOH	Methanol
NG	Natural gas
NO_x	Nitrogen oxide
NO	Nitrogen monoxide
NO_2	Nitrogen dioxide
PM	Particulate matter
SO_x	Sulfur oxide
SOF	Soluble organic fraction
UHC	Unburned hydrocarbons

1

INTRODUCTION

The world has enough for everyone's need,
but not enough for everyone's greed.

— Mahatma Gandhi

It was nearly two centuries ago that the first connection between atmospheric carbon dioxide (CO_2) and global warming was established [1]. In 1856, Eunice Foote [2] became the first scientist to suggest that rising CO_2 concentrations in the atmosphere could increase the Earth's temperature. Since then, scientific understanding has advanced significantly, yet the threat of climate change caused by excessive and ever-increasing CO_2 emissions has become an even greater global concern [3, 4]. Fossil fuels, our primary energy sources since the industrial revolution, are the main contributors to the increase in atmospheric CO_2 [5]. Addressing this challenge requires a fundamental shift in how we extract and use energy, calling for the adoption of alternative energy carriers to support the continued development of modern society.

The maritime industry, as a critical enabler of global trade, bears significant responsibility for its contribution to CO_2 and other greenhouse gas (GHG) emissions. Acknowledging this responsibility, maritime stakeholders have committed to ambitious defossilization targets by continuously formulating and adopting new sustainability frameworks [6]. In this context, a wave of technological innovation is needed to enable what has been termed the *fourth propulsion revolution* [7]. While continued efforts to further improve the efficiency of marine power systems remain crucial, the gains achievable through efficiency improvements are insufficient to achieve carbon neutrality. Consequently, the transition toward low- and zero-carbon fuels is essential, with synthetic fuels emerging as key candidates for the defossilization of shipping. Despite emerging alternative propulsion and power technologies, the reciprocating internal combustion engine (ICE) continues to dominate maritime transport thanks to its unmatched robustness, efficiency, and power density [8, 9]. Therefore, facilitating the safe and optimized use of renewable fuels in ICE-based

power systems represents one of the most pragmatic and effective pathways to defossilize the maritime industry [10].

1.1 METHANOL AS A MARINE ENGINE FUEL

Methanol has emerged as a promising alternative fuel due to its favorable combustion properties [11], scalable renewable production [12], and liquid state at ambient conditions—making it particularly suitable for long-haul and ocean-going applications. These attributes position methanol as a practical and cost-effective option, especially in heavy-duty (HD) sectors where full electrification faces considerable limitations [13, 14].

Methanol's unique molecular structure presents both opportunities and challenges for its use as a combustion engine fuel. The presence of a hydroxyl (OH) group renders methanol a polar compound with strong hydrogen bonding between molecules, which is advantageous for marine applications—such as enabling storage in double-bottom tanks due to water miscibility [15]. The strong intermolecular forces of methanol also result in its high latent heat of vaporization, which lowers in-cylinder temperatures during combustion and contributes to reduced NO_x emissions. However, methanol's relatively low energy density, owing to its oxygen content, and high latent heat of vaporization pose challenges for fuel evaporation and combustion stability.

The second core challenge of methanol in HD applications lies in its chemical reactivity profile. Like other promising sustainable fuels such as hydrogen and ammonia, methanol is highly suitable for spark-ignition (SI) engines owing to its high octane number, which enhances knock resistance and allows for higher compression ratios [16–18]. However, its low reactivity creates significant hurdles in diesel compression ignition (CI) engines, which remain the dominant choice in the maritime industry due to superior fuel efficiency and power density [9, 19]. Although high octane fuels can enhance the performance of SI engines, their advantages have not yet been sufficient to displace diesel engines in HD applications. To address these challenges, research has predominantly focused on two main approaches for methanol use in CI engines: low-temperature combustion (LTC) strategies, such as homogeneous charge compression ignition (HCCI), and dual-fuel concepts [20, 21].

In summary, despite the inherent challenges with the application of methanol in marine engines, the long experience with it in engine applications has demonstrated its technical viability. Combined with the potential for large-scale renewable methanol production, methanol remains one of the most promising fuels to defossilize shipping. This promise has resulted in growing interest in advancing research and development of methanol-fueled marine engine technologies.

1.2 DEVELOPMENT IN METHANOL MARINE ENGINES

The momentum for methanol as a marine fuel has led to numerous research initiatives, evolving from initial feasibility studies to full-scale demonstrations. Fig. 1.1 presents the timeline of a range of consortium projects that have explored methanol use as a marine engine fuel.

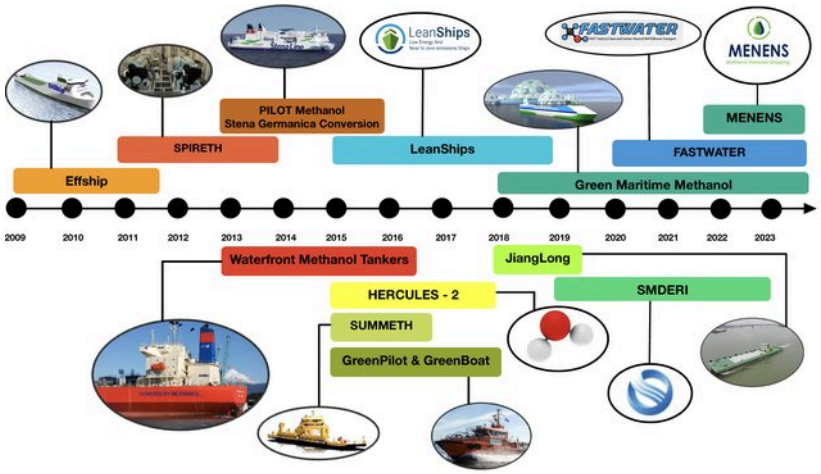

Figure 1.1: Timeline of methanol marine engine projects [22]

Early efforts, such as the Effship project [23], evaluated methanol's potential, leading to the SPIRETH project [15], which conducted the first experimental conversions of diesel engines to methanol direct injection (DI) with mixing-controlled (diffusion) combustion. This paved the way for on-board applications, including the conversion of four Wärtsilä four-stroke engines on the Stena Germanica ferry using dual-channel high-pressure injectors. Subsequent projects expanded to two-stroke engines: HERCULES-2, involving the WinGD manufacturer, explored multi-fuel capabilities [24], while MAN's Waterfront initiative developed methanol-powered tankers employing high-pressure DI for diffusion combustion. Later, SUMMETH investigated alternative concepts like SI engines for smaller vessels, influencing ScandiNAOS's MD97 engine with ignition improvers for mixing-controlled combustion mode [25, 26]. Parallel demonstrations in GreenPilot and GreenBoat projects validated SI conversions for small crafts and recreational boats, respectively [27]. The Shanghai Marine Diesel Engine Research Institute (SMDERI) also advanced diesel-methanol diffusion combustion conversions [28]. These initiatives underscore a predominant focus on diffusion-based combustion strategies, which employ direct injection of methanol and its subsequent mixing-controlled combustion.

However, for a wide range of engine sizes, such as high-speed four-stroke marine and locomotive engines, this mixing-controlled concept presents significant challenges [29]. These engines often face spatial constraints in the cylinder head that complicate the integration of additional injection systems necessary for such a dual-fuel operation. Additionally, the high-pressure fuel system required for injecting methanol further limits its feasibility for retrofitting existing diesel engines.

Premixed strategies offer a more practical alternative for diverse engine sizes. Recognizing these gaps, projects like LeanShips and its subsequent project FASTWATER explored and enhanced the understanding of methanol as a fuel in premixed dual-fuel strategies [30, 31]. Similar diesel engine conversions to premixed methanol dual-fuel operation were pursued by Jianglong and other knowledge institutes [32], while the Green Maritime Methanol project focused on SI premixed approaches [33].

Despite these efforts, data on premixed methanol concepts remain scarce, limiting our understanding of these strategies, while challenges with knocking and combustion instabilities still restrict significant diesel displacement by methanol in dual-fuel modes. Thus, premixed strategies represent a critical underexplored area for expanding methanol's role in sustainable marine powertrains.

1.3 MENENS PROJECT

Building on these foundations, the MENENS[1] project (Methanol as an Energy Step Toward Zero-Emission Dutch Shipping), represents a crucial advancement in methanol's integration into marine propulsion. Launched as a collaborative effort involving academic institutions and industry partners (e.g., engine manufacturers and shipping operators), MENENS aims to accelerate the defossilization of the maritime sector by exploring several marine engine strategies for methanol. In particular, the engine research of MENENS prioritizes premixed approaches in medium- and high-speed ICEs, with a core emphasis on enhancing efficiency and minimizing emissions. Embedded within MENENS, this PhD research concentrates on experimental exploration and thermodynamic analysis to elucidate methanol's combustion behavior in marine engines and its impact on their overall performance.

1.4 RESEARCH GAPS AND QUESTIONS

Despite methanol's promise as a sustainable marine fuel, knowledge gaps persist regarding its application in premixed combustion strategies for large-bore engines. These gaps limit the current understanding of methanol combustion behavior, its governing mechanisms, and the influence of boundary and control parameters on the performance of HD engines, especially for marine applications. In light of these challenges the main objective of this dissertation is:

The development of experimentally based thermodynamic analysis framework to enhance the understanding of the behavior of premixed methanol marine engines.

To achieve this objective, the overarching research problem is divided into four targeted knowledge gaps, each addressed by a specific research question (RQ). Together, these RQs structure the experimental and analytical scope of the dissertation, are each linked to a specific knowledge gap, and are summarized below following the chronological progression of this work. The experimental part of this thesis comprises four distinct experimental campaigns (EC I-IV), each directly related to its corresponding research scope. Accordingly, this dissertation explores and aims to resolve the following research gaps:

- **Gap 1: Inconsistent terminology in injection, ignition, and combustion strategies for methanol**
  Distinctions among various injection and ignition strategies for ICEs fueled by alternative fuels like methanol, along with their resulting combustion mechanisms, suffer from inconsistent naming and definitions. This ambiguity

1 Actual abbreviation in Dutch: Methanol als Energiestap Naar Emissieloze Nederlandse Scheepvaart

hinders effective knowledge transfer within the research community and complicates comparative analyses between studies. The objective is to delineate engine technologies and resolve inconsistencies, thereby aiming to address:
***RQ1**: How to develop a classification framework resolving methanol combustion terminology inconsistencies?*

- **Gap 2: Limited insights into dedicated mono-fuel lean-burn spark ignition concepts for alternative fuels**
  While dual-fuel concepts prevail in methanol marine engine research, dedicated mono-fuel strategies—such as lean-burn SI—provide a pathway for 100% substitution of diesel, removing dependency on fossil pilot fuels. However, limited research exists on the combustion behavior and overall performance of such systems in marine engines. Fundamental aspects such as the interaction between boundary conditions with distinct combustion behavior and engine performance of marine LBSI engines remain underexplored. The objective is to utilize a multi-cylinder LBSI marine engine to generate transferable insights for methanol operation and prepare for future methanol experiments on the same testbed, thereby aiming to address:
  ***RQ2**: How can natural gas lean-burn spark ignition experiments inform the development of a combustion-informed diagnostic framework for future methanol experiments?*

- **Gap 3: Underexplored combustion mechanisms and transitions in premixed methanol dual-fuel engines**
  Existing experimental studies on methanol-fueled premixed dual-fuel (PRDF) engines frequently lack a systematic investigation of the fundamental combustion mechanisms and transitions that occur across varying methanol energy fractions (MEFs). This gap is critical because methanol's distinct thermophysical and chemical properties are expected to influence these mechanisms in PRDF concepts differently from other low reactivity fuels (LRFs) such as methane. As a result, our understanding of methanol combustion behavior in PRDF concepts, particularly in marine-scale engines and at high methanol energy fractions (MEFs), remains limited. The objective is to conduct a detailed experimental investigation to elucidate methanol combustion characteristics and overall performance in PRDF marine engines, thereby aiming to address:
  ***RQ3**: How can qualitative and quantitative analysis be developed to reveal distinct methanol premixed dual-fuel combustion behavior?*

- **Gap 4: Limited mechanistic understanding of the influence of key boundary conditions on methanol premixed dual fuel marine engine performance**
  The sensitivity of methanol PRDF operation to boundary conditions remains insufficiently explored for marine-scale engines and high-MEF operation. This limits understanding of how various control parameters, especially retrofit-friendly[2], can be adjusted to improve combustion and overall performance in these engines. Consequently, a systematic exploration is needed to assess

2 Retrofit-friendly control parameters refer to operating variables that modify key boundary conditions and can be implemented on existing engines with minimal hardware modifications. These include intake or exhaust throttling and intake air heating, which do not require major redesign of core components like the fuel injection system or combustion chamber geometry.

how boundary conditions influence combustion characteristics, efficiency, and emissions. Practical and suitable control levers can be identified to assist methanol PRDF retrofit implementation and optimize engine performance. The objective is to utilize the developed diagnostic framework and dedicated parametric sweeps of retrofit-friendly control parameters to better understand their impact on combustion and overall performance of high-MEF, high-load PRDF operation, thereby aiming to address:
***RQ4**: What is the effect of boundary conditions on combustion and overall performance of methanol PRDF engines?*

1.5 STRUCTURE OF THE THESIS

The remainder of this dissertation is organized into four main chapters, each addressing one of the identified knowledge gaps in methanol use for marine reciprocating ICEs. Chapter 2 establishes the foundational background on methanol as an engine fuel by reviewing the current research landscape, highlighting key knowledge gaps, and resolving inconsistencies in terminologies for engine strategies, addressing *RQ1*. To bridge the gap in methanol application for HD SI engines (*RQ2*), Chapter 3 employs a natural-gas LBSI testbed and two experimental campaigns (EC I & II) to develop a chamber geometry- and concept-driven combustion characterization methodology. Focusing on *RQ3*, Chapter 4 develops an in-depth and systematic analysis framework for methanol PRDF operation and applies it in the experimental campaign of the single-cylinder research engine platform. Moreover, it touches upon *RQ4* by incorporating small intake air temperature adjustments to improve combustion performance at high MEFs and engine load. Building on this foundation, Chapter 5 further elaborates on *RQ4* by extending the analysis framework through comprehensive parametric studies of intake and exhaust pressure using an additional experimental campaign (EC IV). To summarize, Chapter 6 consolidates the findings from all chapters addressing the distinct RQs, presenting the main conclusions, recommendations, and reflections on methanol PRDF engines derived from this PhD research. An overview of the thesis structure is illustrated in Fig. 1.2.

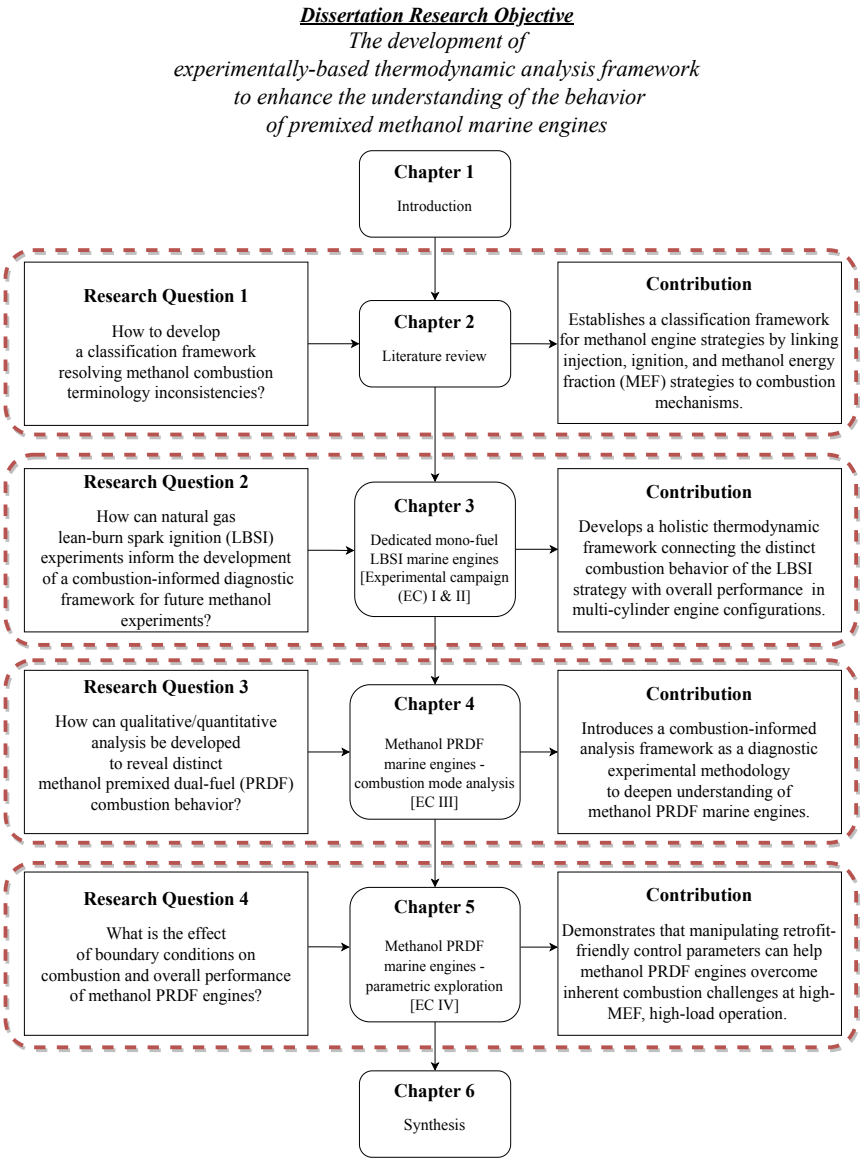

Figure 1.2: Structure of the dissertation

1.6 CONTRIBUTIONS

Beyond the chapter-wise structure, the contributions of this dissertation can be summarized as follows:

- Developed a combustion-informed thermodynamic analysis for premixed marine engines that unifies in-cylinder pressure-based heat release analysis with whole-engine performance indicators, and demonstrated it on multi-cylinder natural-gas fueled LBSI and methanol-fueled single-cylinder PRDF marine research engine platforms. [Chapter 3 & 4]
- Introduced a morphology-based classification framework for methanol PRDF engines using two shape indicators—combustion mechanism index (CMI) and phase magnitude ratio (PMR)—identifying three distinct combustion modes (m-, h-, and n-shaped) and their transitions across different MEFs and boundary conditions. [Chapter 4 & 5]
- Established a unified classification framework resolving inconsistencies in methanol engine research by systematically linking injection, ignition and MEF strategies to dominant combustion mechanisms across mono- and dual-fuel pathways. [Chapter 2]
- Identified key combustion-mechanism sensitivities governing premixed methanol performance: LBSI squish-entry phasing controls efficiency-stability-NO_x trade-offs, PRDF pilot ignition timing effects dominate over its ignition energy, combustion behavior is very sensitive to several boundary conditions in methanol PRDF operation. [Chapter 3, 4, & 5]
- While confirming the diminishing effect of advanced ignition timing on combustion efficiency in LBSI engines due to the squish phase, both mixture enrichment and spark timing advancement consistently improved overall performance. [Chapter 3]
- Revealed that diesel-only to methanol PRDF transition fundamentally alters the energy balance: although thermodynamic efficiency is slightly compromised, methanol operation enhances conversion of released fuel energy into work output by significantly decreasing heat losses; however, high combustion losses remain the main barrier to match diesel engine efficiency. [Chapter 4]
- Demonstrated through parametric studies that manipulation of intake temperature, intake and exhaust pressure, can substantially improve high-MEF PRDF combustion efficiency with minimal heat loss penalties, underscoring practical control levers for diesel-to-methanol conversion. [Chapter 4 & 5]

2

LITERATURE REVIEW [1]

We are like dwarfs,
on the shoulders of giants,
so that we can see more than they.

— Bernard of Chartres

This chapter delivers an in-depth background and literature review of methanol utilization in heavy-duty (HD) internal combustion engines (ICEs), with a focus on both recent scientific advancements and practical challenges in the field. Its aim is twofold: to consolidate the foundational understanding required for the subsequent thesis chapters—particularly the combustion mode framework for Chapter 4 and Chapter 5—and to highlight emerging research needs that frame the overarching research questions.

Section 2.1 presents the principal combustion pathways for methanol in ICEs. In addition to reviewing current knowledge, this section introduces a systematic classification framework for injection and ignition strategies that form the pathways for the various combustion concepts in ICEs, and applies it to methanol fuel. This framework aims to address the current ambiguity in terminology found across the literature, advocating for greater consistency. In connection with the first sub-research question of this dissertation, it proposes that established shared frameworks and a more universal vocabulary for engine combustion concepts are essential to streamline scientific discussion, foster efficient knowledge transfer within the research community, and make it easier for new researchers to engage in the ICE field. Section 2.2 reviews the key findings from experimental studies conducted on low- and medium-speed HD engines operating on methanol. The discussion centers on combustion processes, engine performance metrics, and emissions characteristics, distinguishing patterns and identifying knowledge gaps for future studies. Section 2.3 focuses specifically on the methanol premixed dual-fuel strategy, considered among the most promising pathways for accelerating methanol's adoption in HD and marine applications. Here, prior experimental work is synthesized to evaluate the influence of various design and operational parameters on the performance of

1 This chapter is partly reproduced from Kiouranakis et al. [34, 35], and co-authored with Konstantinos Zoumpourlos and Andrea Coraddu, in addition to the author's supervisors

PRDF engines and their diesel displacement capabilities, providing practical insights for both researchers and engine developers. Ultimately, Section 2.4 provides a synthesis of the key findings throughout Chapter 2, highlighting both the contribution of the current chapter and the major research gaps that have guided the direction of this thesis.

2.1 COMBUSTION PATHWAYS FOR METHANOL IN ICES

Combustion in an ICE can fundamentally occur in three ways: premixed flame propagation (Gasoline SI engine), premixed autoignition (HCCI engine), and non-premixed mixing-controlled diffusion combustion (Diesel CI engine). Fig. 2.1 illustrates how combustion occurs in each distinct mode.

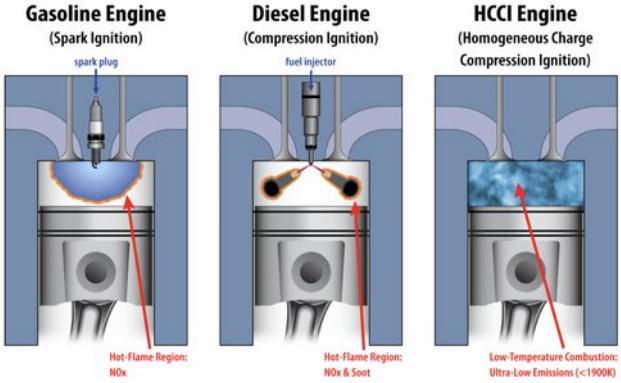

Figure 2.1: Combustion concepts in ICEs [36]

2.1.1 *SI engines*

High octane number (ON) alcohol fuels, such as methanol and ethanol, are suitable for use in gasoline engines [37, 38]. In SI engines, the fuel is typically injected at low-pressure (LP) in the intake air, resulting in a nearly homogeneous air-fuel mixture in the cylinder. Air-path injection (API) can be implemented through a single-point injection (SPI) by carburating or spraying along the intake path, or through multipoint injection (MPI) using port-fuel injection (PFI) [39, 40]. The former is often used for gaseous fuels such as NG [41], while for liquid fuels like methanol, the PFI strategy is typically employed [42]. Fig. 2.2 depicts the injection strategies found in SI engines.

In SI engines, injection strategies are generally designed to create a premixed air-fuel charge so that combustion proceeds via flame propagation initiated by a spark, with the resulting combustion duration being highly sensitive to flame-turbulence interaction [20]. Enhancing turbulence intensity increases the flame velocity [43]. This is the foundation of the turbulent jet ignition (TJI) concept, which uses a pre-chamber to ignite a lean air-fuel mixture [44, 45]. Apart from homogeneous premixed strategies, direct injection (DI) into the cylinder or combining API with

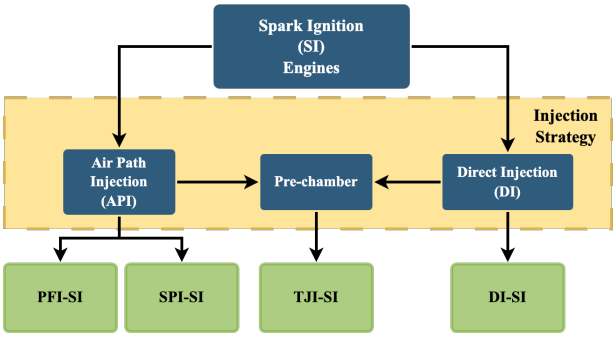

Figure 2.2: Engine strategies in SI engines

a pre-chamber can enhance the efficiency of SI engines by stratifying the charge and allowing leaner mixtures [46, 47]. These lean mixtures can simultaneously improve engine efficiency and lower emissions [48]. The TJI concept appears to be the most common strategy when applying the SI engine technology for HD applications like marine [49, 50]. Despite the various injection strategies in SI engines, combustion is intended to occur via premixed flame propagation [51], while any premixed autoignition must be avoided. For instance, while gasoline direct injection is typically employed to create stratified charge within the cylinder to enhance performance, the fundamental and intended combustion mechanism remains flame propagation [52].

2.1.2 *CI engines*

In contrast to SI engines, CI engines can employ two distinct combustion concepts—LTC and conventional diesel combustion (CDC)—which complicates the definition of combustion strategies. Furthermore, the introduction of DF concepts has further expanded research on various combined approaches aimed at improving engine performance and incorporating alternative fuels. However, this growing body of research has also led to confusion, as inconsistent and overlapping terminologies are frequently used to describe different combustion strategies. The confusion is particularly evident when discussing alternative fuels, which also applies to methanol. For example, direct dual fuel stratification (DDFS), originally proposed as a new combustion concept based on a distinct injection strategy [53], has been used differently in some studies exploring methanol [54, 55]. Such inconsistencies in terminology are not unique to methanol, as similar issues have been observed in the literature on other low reactivity fuels, such as NG [21].

Thus, the primary objective of this subsection is to establish common ground and propose a practical classification framework to help researchers better categorize and identify different strategies. To this end, this thesis aims at clarifying methanol CI engine strategies by focusing on four degrees of freedom (DoF): fuel strategy (mono-fuel (MF) or DF), injection location of methanol, ignition strategy, and methanol to HRF ratio in premixed DF engines. These parameters influence the leading combustion mechanism. Fig. 2.3 illustrates the strategies for methanol utilization

in CI engines, showing that regardless of the chosen strategy, combustion typically follows one of the three combustion mechanisms. While specific engine calibration strategies may intend to involve a combination of combustion modes, this figure focuses on capturing the intended and dominant mechanism in each case [56]. The ignition strategy depends on the fuels' injection timing, further illustrated in Fig. 2.4, complementing the information in Fig. 2.3.

2.1.2.1 *Mono-fuel strategies*

Using neat methanol in CDC necessitates much higher compression ratios (CRs) compared to diesel fuel [57], along with higher intake air temperatures [58] or hot recirculated exhaust gases [59], potentially increasing nitrogen oxide (NO_x) emissions and risking engine durability. To facilitate combustion under such conditions, ignition aids like glow plugs are also employed [60], particularly during low-load and cold-start conditions [61]. For LRFs, a strategy that resembles CDC, wherein diffusion combustion is the intended mode, is often referred to as mixing-controlled compression ignition (MCCI) [62]. MCCI is commonly facilitated by two-stage HP-DI of the LRF, such as methanol, near TDC [63].

The challenging requirements, such as high CRs, needed to operate MCCI with neat methanol, have led most research studies to focus on the methanol use with ignition improvers for HD applications, including marine-size engines. The effects of various ignition and lubricity improvers, along with their different ratios, on methanol diffusion combustion have been explored [64, 65], reporting that stable combustion was not feasible with ignition improver ratios below 5%. However, a subsequent study demonstrated stable combustion with a reduced ignition improver ratio of 3% [66]. This strategy, termed MD97 [66], is classified as an MF strategy [67].

An alternative approach to address the low reactivity of methanol in CI engines, without the need of ignition improver or an additional HRF, involves utilizing pre-chamber technology, commonly employed in SI engines [45]. This pre-chamber-based concept, often referred to as the TJI-HPDI mode [68], operates as an MCCI-type combustion mechanism and aims to mitigate the risk of knocking, which is a primary limitation of premixed injection strategies in HD engines to reach diesel engine-level efficiencies. In this concept, a small quantity of methanol is injected into the pre-chamber and ignited by a spark plug. The resulting hot jets are expelled through small orifices into the main combustion chamber, where the remaining methanol fuel is sprayed using HP-DI directly into these induced jets. Due to the complexity of this technology and its relatively recent introduction in engine research, most studies to date have been limited to numerical simulations [69].

Alternative MF approaches, such as the LTC concepts, are notable for their potential to reduce NO_x and PM emissions while maintaining or even increasing efficiency [20]. LTC strategies aim to decouple injection and combustion phases in CI engines, thereby avoiding the diffusion combustion phase [70]. HCCI is often regarded as the foundational LTC concept, employing a combustion mechanism distinct from traditional gasoline SI and diesel CI processes. Historically, this concept appeared under different names, such as active thermo-atmosphere combustion (ATAC) in 1979 [71], toyota-soken (TS) combustion [72], and compression-ignited homogeneous charge (CIHC) in 1983 [73]. In all cases, combustion is initiated and

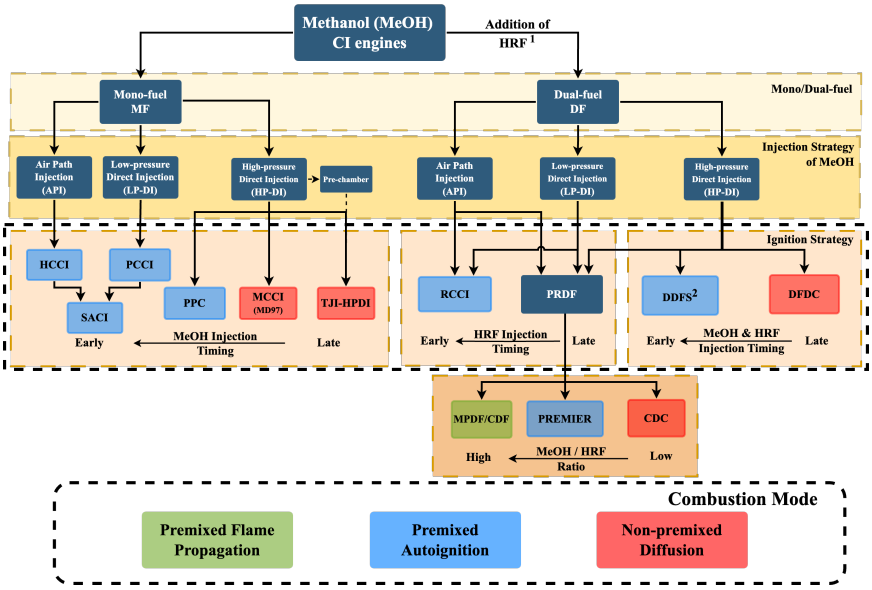

[1] High Reactivity Fuel (HRF) (e.g., Biodiesel)
[2] RCCI-type of combustion strategy

Figure 2.3: Classification framework for methanol CI engine strategies

governed by spontaneous autoignition driven by chemical kinetics. This thesis adopts the widely accepted term HCCI, which introduces fuel into the cylinder via an API strategy to ensure a well-mixed charge [74]. The HCCI strategy has been studied for fuels that are typically used in diesel engines [75], i.e., high-cetane-number fuels, as well as for fuels used in gasoline engines, i.e., high-octane-number fuels,such as methanol [76].

Similar to HCCI, the premixed charge compression ignition (PCCI) concept aims for fully lean premixed combustion initiated by autoignition [77]. PCCI can be considered a DI version of HCCI [78]. To address the challenges of controlling combustion phasing in fully premixed strategies, a subsequent concept emerged involving a two-stage injection: an early main injection to form the premixed mixture, followed by a second injection at the desired start of combustion. This strategy was characterized as an HCCI concept, as it still relies on bulk autoignition, and has been termed as uniform bulky combustion system (UNIBUS) [79] and two-stage PCCI [80]. Multi-pulse ultra-HP injection strategy has also been explored in such PCCI combustion strategies [81, 82].

The two- or multi-stage version of this injection strategy is typically referred to as partially premixed combustion (PPC) [83, 84], which also aims to separate the first injection stage from the start of combustion [85]. Similar approaches in diesel engines are also referred to by terms like split-premixed compression ignition (split-PCI) [86] and partially premixed compression ignition (PPCI) [87]. Furthermore, this thesis differentiates PPC from MCCI strategy to avoid confusion, as these terms have often been used in research to characterize the same strategy, where a first

injection takes places before TDC to partially premix the mixture followed by a second that aims to control the combustion phasing with a diffusion-like combustion of the second injection spray [83]. In this thesis, PPC will refer to when most of the fuel is injected away from the TDC [88], compared to MCCI in which the first injection phase is very close to TDC [89]. While this thesis aims to distinguish PPC from PCCI, it should be noted that these terms may have sometimes been used interchangeably in other sources. Furthermore, due to variations in conventions, this may hold true for other combustion strategies discussed in this chapter as well. Finally, spark assisted compression ignition (SACI) is another prominent strategy that relies on premixed autoignition as the dominant combustion mechanism [90]. In SACI, a spark discharge initiates reaction kinetics near the spark plug, which cascades into premixed autoignition throughout the charge [91].

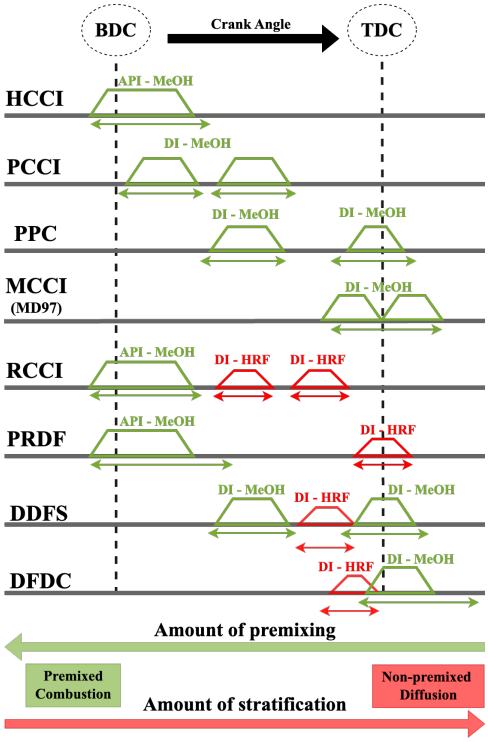

Figure 2.4: Fuel injection timing in different ICE strategies

2.1.2.2 *Dual-fuel strategies*

Although the term *DF strategy* is commonly linked with natural gas DF engines, it can accommodate any LRF, including liquid fuels such as alcohols [21]. It should be noted that Fig. 2.3 does not include the diesel-methanol blending strategies, such as splash blends [92], emulsions [93], and the combination of more than two co-solvent fuels [94], because of methanol's miscibility issues, thereby restricting

methanol ratios up to 20% and subsequently limiting its applicability in these engine strategies [95]. DF engines rely on HRFs like diesel to ignite low cetane number (CN) fuels like methanol. CN is a measure of suitability of a fuel for diesel engines, quantifying its delay to autoignite when injected in the engine [96]. In addition to conventional diesel pilots, concepts have been proposed in which dimethyl ether (DME) is produced on board from methanol and supplied as the HRF, enabling single-fuel systems in which the combustion strategy still relies on two fuels in the cylinder [97, 98]. From a combustion-mode perspective, such DME-methanol concepts still map onto the same framework as systems using other HRFs and can realize the same DF strategies, such as RCCI, PRDF, DDFS, and DFDC depending on the ignition strategy [99]. In DF engines, only methanol's injection location varies, with the three typical injection strategies: API, LP-DI, and HP-DI. Currently, the most commonly applied technology is the HP-DI injection strategy for the HRF. Similar to mono-fuel SI engines, the LP-API strategy is the most straightforward method for injecting methanol in DF engines, either using SPI or multi-point PFI strategy.

This injection technique has been termed "fumigation" in the context of alcohol DF engines [100]. Alperstein et al. [101] introduced the term "fumigation" in 1958 to describe LP-PFI of diesel in the intake to address, among others, mixing hurdles and smoke formation in diesel engines. Fumigation was defined as introducing a liquid fuel, such as diesel, as a fine mist or "fumes" in the intake manifold. However, fumigation has evolved to describe the introduction of alternative fuels in the air upstream of the manifold by a carburetor or LP injector [102, 103]. Today, "fumigation" typically refers to methanol injection along the air path [104]. This thesis suggests that "fumigation" may not be an adequate descriptor for this injection strategy, as it deviates too much from the initial meaning and led to questions about injection location and evaporation. This work suggests to abandon the term "fumigation" and use the more fitting term *air-path injection (API)*, as a synonym and general term for any air-path injection technique.

An alternative LP injection strategy is to inject methanol directly in the cylinder, a technique that is typically applied in large two-stroke marine NG DF engines [29, 34]. In these premixed strategies, combustion is primarily influenced by the DI of a HRF, such as diesel. Two combustion strategies can arise from this manner: the reactivity controlled compression ignition (RCCI) [105] and the premixed dual-fuel (PRDF). RCCI evolved from efforts to better control premixed autoignition strategies such as HCCI and PCCI, introducing the LRF via API to create a homogeneous charge. The HRF is then directly injected well before TDC to modulate reactivity, differing from PRDF in which diesel injection timing remains similar to CDC, i.e., a late pilot injection near TDC, to ignite the premixed methanol-air mixture. PRDF is commonly referred to as the conventional dual-fuel (CDF) strategy [21, 106, 107]. In methanol DF engines, this premixed strategy is often called diesel methanol dual-fuel (DMDF) [108–110], or diesel methanol compound combustion (DMCC) [111–113]. However, since these terms do not clearly describe the injection or combustion mechanisms, this thesis proposes the term methanol PRDF to better convey the combustion strategy employed.

In strategies that use HP-DI of both fuels, methanol injection timing can be adjusted to offer a range of combustion regimes [54]. The methanol non-premixed

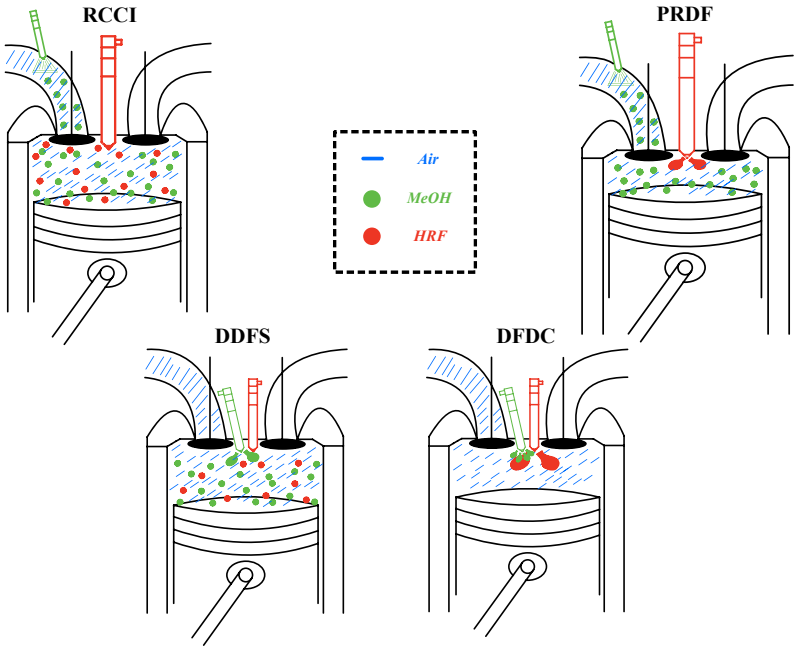

Figure 2.5: Dual-fuel main ignition combustion strategies

combustion strategy, which dominates current large marine DF engine developments [34], involves HP-DI of both fuels close to TDC, resembling CDC combustion but applied to both fuels [114]. This strategy typically follows the conventional late diesel injection near TDC, followed by the LRF's injection [49], as explored in several studies on methanol [115, 116]. When methanol is injected prior to diesel [117, 118], the increased ignition delay due to methanol's cooling effect often results in a more premixed burn, akin to the PRDF combustion strategy [119]. To assist experimental studies and explore the optimization parameters of the DFDC concept, numerical simulations have been conducted. Li et al. [120] investigated injection strategies involving the splitting of methanol injection before and after the diesel injection, referred to as methanol/diesel/methanol (M/D/M). Yang et al. [121] examined how the structure of the pilot fuel injection could enhance the combustion performance of methanol. This thesis proposes the term methanol dual-fuel diffusion combustion (DFDC) for these concepts, as it appropriately describes the intended combustion mechanism—primarily diffusion-driven combustion for both fuels.

Additionally, premixed autoignition-driven combustion mechanisms, such as in RCCI, can be achieved with HP-DI injection of both fuels early in the compression stroke. DDFS combines elements of RCCI and PPC [53, 122], allowing for flexible injection pulses between the fuels [55]. This flexibility enables better control over concentration and reactivity gradients compared to traditional RCCI. In similar studies that explore flexible stratification combustion concepts, this approach is referred to as intelligent charge compression ignition (ICCI) combustion mode [123]

and premixed micro pilot combustion (PMPC) [124]. To unify terminologies and avoid confusion, this thesis proposes to use DDFS to describe strategies aiming to achieve LTC via stratification controlled by the direct injection of both fuels. Fig. 2.5 illustrates the cylinder layout for the four typical DF ignition strategies.

An interesting and distinct strategy is the jet controlled compression ignition (JCCI) concept [125], also developed to address the combustion control challenges faced by HCCI and PCCI. In JCCI, a small ignition chamber, similar to the (TJI) concept, is mounted on the cylinder and contains an HRF injector and a spark plug [126]. Combustion-rich gases, controlled by spark discharge, are then expelled through small orifices into the main combustion chamber to trigger the premixed autoignition of the charge. Therefore, it differs from the conventional TJI concept, which relies on flame propagation, as the intended combustion mechanism in JCCI is premixed autoignition, similar to HCCI, SACI, PCCI, PPC, RCCI, and DDFS. This strategy has also been explored with ammonia-methanol mixtures in the main chamber, where hydrogen-fuelled jets, ignited in the pre-chamber, initiate combustion in the main charge [127]. While this concept introduces additional combustion pathways for both mono-fuel [45] and dual-fuel [127] in CI engines, incorporating it into the framework of Fig. 2.3 would add complexity, which contradicts the framework's goal of simplification.

PREMIXED DUAL-FUEL STRATEGY (PRDF)

In PRDF engines, the goal is to minimize diesel pilot fuel required to initiate combustion [128]. Nevertheless, challenges like misfiring and knocking necessitate reducing the methanol quantity to protect the engine [129]. Numerous studies have shown that combustion mechanisms in methanol PRDF engines is highly sensitive to varying methanol-to-HRF ratios [56, 129–132].

Combustion in PRDF engines is a hybrid between the combustion principles in diesel CI and gasoline SI engines: the premixed autoignition and mixing-controlled combustion of CI, and the premixed flame propagation and autoignition typical of SI engines. To assist the conceptualization of combustion mechanisms in PRDF engines, this study incorporates the theoretical DF model by Karim [21], defined in three overlapping combustion stages, as illustrated in Fig. 2.6:

- **Stage I** encapsulates the premixed autoignition of pilot diesel, including any entrained LRF.
- **Stage II** defines the combustion deriving from the premixed autoignition of the LRF-air mixture.
- **Stage III** reflects the bulk turbulent flame propagation, along with any remaining diffusion combustion of diesel.

It should be noted that the main deviation from Karim's definition of the three stages lies in the third stage, in which Karim also included premixed autoignition. However, this work redefined the third stage to conceptually separate autoignition-driven [133] from flame propagation-driven in the unburned mixture [134]. This adjustment follows the approach of Ahmad et al. [132], which characterized distinct

combustion phases in a methane PRDF single-cylinder engine by combining HRR analysis with optical diagnostics.

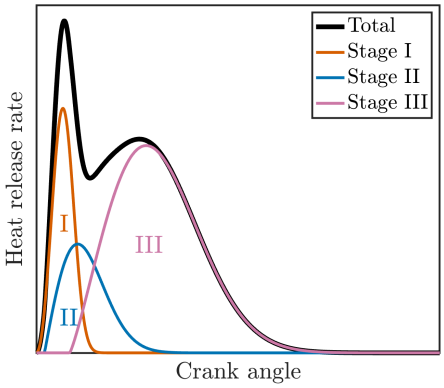

Figure 2.6: Dual-fuel conceptual model distinguishing three main combustion stages

The interaction between the pilot diesel's premixed combustion and the subsequent LRF combustion stages is a defining aspect of the multi-stage process in PRDF engines. The Stage I autoignition event governs the amount of LRF that undergoes premixed autoignition near the jets (Stage II), as well as the number and spatial distribution of flame kernels that propagate through the mixture (Stage III) [135, 136]. This intricate interplay has a profound influence on overall combustion dynamics and engine performance. Micro-pilot dual-fuel (MPDF) strategies, which minimize the pilot diesel quantity, substantially reduce the influence of Stage I [137]. The resulting ignition energy is often insufficient to robustly initiate Stage II, causing the majority of LRF combustion to shift to Stage III. However, fewer and likely weaker generated flame kernels might have insufficient ignition energy to result in an efficient Stage III, which becomes very sensitive to end-gas mixture reactivity properties, such as temperature and equivalence ratio. Low reactivity in the end-gas mixture can lead to slower overall burn rates and increased cycle-to-cycle variability (CCV). This deterioration in combustion quality has been experimentally observed by Choi et al. [138] in a methane-fueled MPDF engine, with the slowest combustion rates and highest cyclic variations recorded at the maximum methane energy fraction of 97.86%. Similar trends have been reported by Li et al. [139]. These combustion challenges highlight a fundamental limitation of PRDF strategies at lower load conditions: lower in-cylinder temperatures and leaner mixtures—typical of unthrottled operation—with decreasing loads require the maximum attainable MEF to be drastically reduced to maintain stable combustion [140].

Consequently, although maximizing diesel replacement with LRF is a desirable goal for reducing carbon intensity in DF engines, stable flame propagation in the methanol-air charge, beyond critical mixture factors such as temperature and equivalence ratio, relies on the ignition dynamics of the pilot fuel, i.e., the size and intensity of the initial autoignition region as well as the number and strength of flame kernels. As the pilot quantity is likely increased to enhance combustion stability, the

number and strength of ignition kernels grow, and the system gradually transitions toward a more complex interplay of combustion mechanisms. Consequently, the primary challenge shifts from avoiding slow burn and misfire to controlling the onset of knock-related phenomena associated with intensified pilot premixed combustion and end-gas autoignition—namely:

- **Diesel knock**, associated with intensified Stage I combustion.
- **End-gas knock**, related to the induced autoignition in the end-gas region.

PRDF engines often encounter pronounced premixed diesel combustion (Stage I) due to extended IDs caused by air displacement by the LRF. When this coincides with the autoignition of the unburned LRF-air mixture (Stage II), triggered by pressure waves from multiple flame fronts, the combination produces high PRRs that can be detrimental to both engine efficiency and mechanical integrity [141]. It should be noted that PRDF knock more closely resembles the knock observed in reactivity-controlled combustion systems—such as HCCI and RCCI—where ringing intensity caused by strong premixed autoignition defines the practical limit, rather than the limiting knock in SI engines [142–145]. To mitigate these challenges, the premixed mixture ignition in the end gas (PREMIER) strategy has been proposed, aiming to harness end-gas autoignition and improve PRDF operation [146]. This PREMIER approach is analogous to the SACI concept, in which a spark discharge is used to initiate ignition and enable phasing control over the otherwise compression-ignited mixture, thereby offering a lever for combustion phasing in HCCI-type engines [39]. Unlike knocking combustion, the PREMIER strategy enables a controlled and more gradual premixed autoignition that avoids damaging pressure oscillations [147]. Instead, utilizing a very lean mixture it aims to initiate ignition around the pilot jets and promote multiple flame propagation in the LRF-air charge, which can improve combustion quality and thermal efficiency [148]. Conversely, if the diesel fraction is further increased to suppress knock and further improve combustion control, the influence of the LRF diminishes, resulting in its passive co-combustion role as the combustion process transitions toward two-stage conventional diesel combustion (CDC) [149].

2.2 EXPERIMENTAL STUDIES ON METHANOL HD ICES

Although methanol has been subject to substantial experimental research in recent decades, most investigations have explored its use in high-speed LD engines. Nonetheless, low-medium speed HD engines' operating regimes and thermal conditions are significantly different [29, 150, 151]. The classification of engines as low-, medium-, or high-speed follows the speed ranges provided in Table 2.1 [152], according to the absolute rated operating speed of the marine engine. This section reviews the results of previous experimental studies on low-medium speed HD engines using methanol. It evaluates the impact of methanol on combustion characteristics, engine performance, and emissions of these engines. The analysis targets previous experimental studies on engines designed for HD applications under steady-state conditions. These engines typically operate at lower speeds and have larger bore and stroke sizes.

2.2.1 *Dual-fuel engines*

Introducing methanol in DF engines aims to maximize the substitution of diesel fuel. The extent of this substitution is vital for the decarbonization of HD engines and depends on various factors such as combustion strategy and load. For a consistent analysis of DF engines, a standardized variable indicating diesel replacement by a LRF like methanol is vital. However, terminology in the literature varies and lacks consistency.

2.2.1.1 *Methanol energy fraction*

The oxygen content of alcohol fuels results in lower LHVs compared to conventional hydrocarbons, with methanol's LHV being approximately half that of diesel fuel. This results in a nonlinear relationship between methanol mass fraction (MMF) and methanol energy fraction (MEF) in methanol DF engine, as illustrated in Fig. 2.7. The MEF, MMF, and their functional relationship are defined respectively as:

$$\mathrm{MEF} = \frac{\dot{m}_\mathrm{m} \cdot \mathrm{LHV}_\mathrm{m}}{\dot{m}_\mathrm{m} \cdot \mathrm{LHV}_\mathrm{m} + \dot{m}_\mathrm{d} \cdot \mathrm{LHV}_\mathrm{d}} \cdot 100\% \tag{2.1}$$

$$\mathrm{MMF} = \frac{\dot{m}_\mathrm{m}}{\dot{m}_\mathrm{m} + \dot{m}_\mathrm{d}} \cdot 100\% \tag{2.2}$$

$$\mathrm{MEF} = f(\mathrm{MMF}) = \frac{\mathrm{LHV}_\mathrm{m}}{\mathrm{LHV}_\mathrm{m} + \frac{1-\mathrm{MMF}}{\mathrm{MMF}} \cdot \mathrm{LHV}_\mathrm{d}} \tag{2.3}$$

where $\dot{m}$ is the mass flow rate of each fuel, and subscripts m and d correspond to methanol and diesel fuel, respectively.

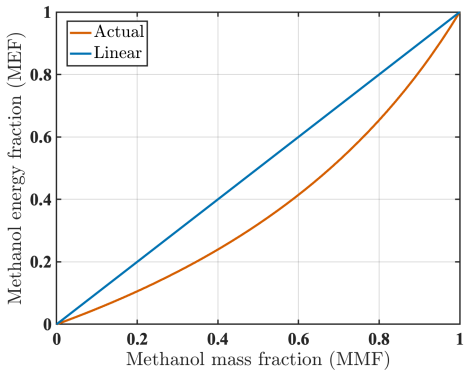

Figure 2.7: Methanol energy-based fraction against mass-based

Given methanol's low-energy content, using an energy-based ratio seems reasonable. Yet, there's inconsistency in the literature regarding naming conventions. For instance, on the energy ratio basis, several terms have been used, such as energy ratio of methanol (Rme) [153], methanol diesel energy share (MDES) [154], and methanol co-combustion ratio (CCR) [54]. This ambiguity also exists for mass ratio terms [110, 123, 155, 156]. In the subsequent analysis, this thesis adopts MEF

and MMF for the respective ratio definitions to minimize confusion and ensure consistency.

2.2.1.2 *Methanol substitution limitations in DF engines*

Blending methanol with diesel offers a straightforward way to introduce methanol into diesel engines. Yet, miscibility issues with methanol often limit its fractions in the blend [95]. Tol [157] evaluated the effect of blending diesel with methanol on the performance of a MAN 4L20/27 four-stroke CI engine, using two different methanol/diesel blends (MEF of 10 and 20%) and compared them to conventional diesel-only mode. His study revealed that the engine could not maintain stable operation across its entire operating range when 20% of MEF was used. Previous studies have highlighted the importance of injecting methanol and diesel separately into the cylinder to achieve higher MEF [95].

Table 2.1: Engine classification by speed [152]

	Engine Speed (rpm)
Low-speed	50-275
Medium-speed	275-1000
High-speed	1000-3600

As a result, the majority of research has focused on the more simplistic API [158], LP-DI [159], or HP-DI methods, employing either an additional [116] or single dual-channel [160] injector. Given the prevalent use of diesel engines in HD transport systems, the API strategy presents a promising pathway for transforming existing engines toward sustainable operation. Dierickx et al. [161] adapted a high-speed marine diesel engine for methanol operation through different API strategies, an SPI and a PFI strategy. Their objective was to evaluate the influence of methanol on the engine performance across multiple operating points and to determine the maximum MEF for each point. Misfiring at low loads and knocking at high loads limited MEF. The highest MEF reached was 84% using SPI at medium load and high speed, compared to a maximum MEF of 80% with PFI found at low load and speed. However, PFI proved more robust, achieving greater MEF across more operating points, with an average maximum MEF above 60%.

Wang et al. [113] further explored methanol's impact on a marine diesel engine using an API with SPI. Roar combustion restricted MSP to 60.6% at 75% load and 39.4% at 100% load. On the other hand, using PFI strategy, Guan et al. [158] investigated the influence of methanol on a single cylinder HD diesel engine. Increasing MEF, both the pressure rise rate (PRR) and peak pressure increased, reaching engine design limits of 30bar/CAD and 180bar, respectively. This restricted MEF to 28%. Due to methanol's cooling effect, prolonged ignition delay and increased diesel premixed combustion occur in PRDF engines, which often result in elevated PRR and peak pressure.

The DFDC strategy shows great potential to overcome MEF restrictions deriving from combustion instability found in premixed modes such as PRDF and RCCI [24].

DFDC can mitigate issues like misfiring at low loads and diesel knock combustion at high loads. Notably, MAN has reported attainable MEF of up to 95% in one of its commercially available methanol two-stroke marine engines by incorporating an additional injector [162]. These attainable MEF in DFDC mode align with the experimental studies of Saccullo et al. [116] and Dong et al. [114], who reported MEF of up to 96.6% and 95.3% using two separate methanol and diesel injectors, respectively. Similarly, Wärtsilä, using a single co-axial dual-channel injector [160], has achieved MEF up to 92% in its commercial medium-speed four-stroke engines [163].

2.2.1.3 *Impact of methanol on combustion characteristics*

In ICEs, several parameters are needed to characterize the combustion process [20, 164]. For example, the ignition delay (ID) represents one of the crucial factors that influence the engine performance, defining the time duration between the start of injection and that of combustion. Combustion phasing (CA50) and duration (CD) are also critical metrics necessary in the combustion evaluation. Typically, HRR analysis is used to study these parameters. Maximum pressure (Pmax) and PRR are also important parameters affecting the engine design.

IGNITION DELAY, MAXIMUM PRESSURE, AND PRESSURE RISE RATE

Wang et al. [113] explored the effect of methanol on the combustion characteristics of a PRDF engine at different engine loads. They found that ID significantly increases with increasing MEF in the whole load range. This correlation aligns with the experimental studies in similar engines [155, 161, 165]. Adding methanol reduces the frequency at which pilot diesel will collide with oxygen molecules resulting in an ID rise [166]. However, two main factors are expected to contribute the most to the increase in ID in engines using the PRDF strategy. First, methanol's cooling effect draws heat from the charge, reducing both temperature and pressure in the cylinder. Second, methanol's presence within the cylinder influences the low temperature chemical oxidation of the injected diesel. Xu et al. [167] employed a skeletal model to investigate the effect of methanol in the oxidation mechanism of n-heptane in a diesel engine. Their simulation revealed that the addition of methanol to n-heptane leads to the conversion of active radicals $OH^{\cdot}$ to inactive H_2O_2 species at temperatures below 1000 K, decreasing the overall reactivity and increasing the ID. However, once the temperature surpassed 1000 K, the H_2O_2 species started decomposing back into $OH^{\cdot}$ radicals before completely disappearing at around 1200 K.

To better understand this chemically driven ID effect, it is useful to briefly recall the fundamental sequence of low- and high-temperature autoignition events in conventional diesel spray combustion [20, 168–173]. In CDC, autoignition is initiated in the leaner, near-stoichiometric regions at the periphery of the spray tip, where low-temperature reactivity produces radicals and raises the local temperatures. This influences the following stronger high-temperature fuel-rich autoignition event in the core of the diesel jet, which gives the characteristic premixed HRR peak. In PRDF concepts, LRF such as methane and methanol alter this sequence by chemically inhibiting the low-temperature diesel oxidation in the lean pilot regions, retarding

the cool-flame stage and ultimately delaying the high-temperature autoignition of the diesel jet core and the overall ID [136, 174–176].

Prolonged ID due to methanol addition results in a larger fraction of diesel participating in premixed combustion with methanol, generally leading to increased PRR and Pmax [100]. High PRR induces roar combustion, limiting the maximum MEF achievable in PRDF engines, as discussed in Section 2.2.1.2. Wang et al. [113] found that maximum PRR was higher in the PRDF mode using methanol compared to CDC at all loads except for the low load points. In a similar study on a modified single-cylinder engine, Guan et al. confirmed similar patterns. However, this study optimized diesel injection timing as the MEF was increased. It becomes more challenging to distinguish the specific impact of MEF on combustion characteristics when other variables are altered simultaneously. On the contrary, using the DDFS strategy, Jia et al. [177] reported that while increasing MEF from 53% to 63% lengthened ID but reduced PRR and Pmax. This behavior was attributed to the cooling effect of methanol, which lowered in-cylinder temperatures, reduced overall reactivity, and thus retarded combustion phasing. The resulting poorer combustion stability was the factor that ultimately limited MEF to 63% in this sweep.

In DFDC strategy, an additional HP-DI system injects methanol at high pressure near TDC, typically after the diesel injection. Saccullo et al. [116] investigated methanol DFDC on a large-bore marine engine comparing two injector configurations: 1) a diesel-only case with a centrally mounted Delphi 6-hole diesel injector and an additional side-mounted Bosch pilot 3-hole injector, and 2) a methanol case where main central diesel injector was replaced by an methanol Delphi 8-hole injector while retaining the side diesel pilot. To compensate for methanol's lower LHV, the methanol injector had approximately twice the flow capacity of the diesel injector and was operated at 1000 bar (versus 800 bar for diesel) with a slightly later SOI at 5.5 °CA bTDC(versus 6 °CA bTDC for diesel), so that both cases produced predominantly mixing-controlled combustion following the prior diesel pilot. Despite the slightly advanced diesel injection timing, ID decreased from 0.37 to 0.15 ms shifting from diesel to methanol operation. Siebers and Edwards [182] reported that methanol requires temperatures above 950K to reach a similar ID to diesel fuel. When the temperature is higher than 1100K, ID of methanol is slightly shorter than isooctane and normal hexadecane. Therefore, the combination of higher reactivity of methanol at these temperatures and its oxygen content might explain this ID trend in the DFDC mode. Regarding PRR and Pmax, experimental studies have identified similar trends using the methanol DFDC [116, 180, 183], as seen in PRDF. A summary of the previous studies exploring the impact of methanol on the combustion characteristics of HD DF engines is shown in Table 2.2. The trends presented in Table 2.2 regarding the impact of methanol are compared to the diesel-only mode of the same engine, which serves as the baseline.

HEAT RELEASE AND COMBUSTION PHASING

Ma et al. [129] explored the possible combustion profiles in a methanol PRDF engine using experiments in a constant volume combustion chamber coupled with a computational model. Analyzing the HRR profiles, the study identified four combustion modes, termed DMDF modes:

Table 2.2: Methanol impact on combustion characteristics of HD DF engines from experimental studies

Ref.	Engine Type	CR [-]	Bore x Stroke [mm]	Rated Power [kW/c]	Injection (Ignition) Strategy	MEF test [%]	Speed [rpm]	Load	Combustion Characteristics					
									ID	CD	CA50	PRR	Pmax	HRR max
[113]	Marine 4x 6c	16.8	-	43	API (PRDF)	51	1134	Low	↑	∼	∼	↓	↓	↓
						39.4	1800	High	↑	∼	A	↑	↓	↑
[161, 178]	Marine 4x 6c	19	108 x 130	32.5	API (PRDF)	44	1500	Low	↑	↓	D	-	-	-
						78		High	↑	↓	A	↑	↑	↑
[158]	Marine 4x 1c	16.8	129 x 155	49	API (PRDF)	28	1200	High	-	↓	D	↑	↓	↑
[155]	Truck/ Bus 4x 6c	17	126 x 130	42	API (PRDF)	40	1500	High	↑	↓	A	-	-	↑
[179]	Truck/ Bus 4x 6c	18.1	108 x 130	32	API (PRDF)	30	1400	Low	-	↓	A	-	-	↑
[165]	Truck/ Bus 4x 6c	17	126 x 130	42	API (PRDF)	60	1900	High	↑	∼	A	∼	∼	↑
[116]	Truck/ Bus 4x 1c	16.7	131 x 158	73.5	HP-DI (DFDC)	96.6	1262	High	↓	↓	A	↑	↑	↑
[177]	Truck/ Bus 4x 1c	16.6	131 x 158	73.5	HP-DI (DDFS)	53 to 63	1500	High	↑	↑	D	↓	↓	↓
[24]	Marine 2x 4c	-	500 x 2,250	1,624	HP-DI (DFDC)	High*	105	Low-High	-	↓	A	-	-	↑
[180]	Marine 2x 6c	-	500 x 2,500	1,264	HP-DI (DFDC)	High	88.5	High	-	↓	A	-	↑	↓
[181]	Marine 4x 8c	-	320 x 400	500	HP-DI (DFDC)	High	720	High	-	↓	A	-	-	↓
[28]	Marine 4x 6c	-	210 x 320	220	HP-DI (DFDC)	95	1000	Low-High	-	↓	∼	∼	↑	↑

[1] The baseline is the corresponding engine operating in diesel-only mode
[2] A: Advanced, D: Delayed, ↑: Increase, ↓: Decrease, ∼ : Constant , - : Data not available
[3] c: cylinder, 2x: two-stroke, 4x: four-stroke
* Ethanol used in engine experiments

- In DMDF mode 1, combustion is dominated by the premixed combustion of both fuels.
- The DMDF mode 2 displays a two-phase combustion profile: starting with a premixed combustion of diesel and surrounded methanol, followed by the diffusion combustion of diesel and the flame propagation through the remaining methanol-air mixture.
- In DMDF mode 3, autoignition of methanol occurs before diesel injection, leading to knocking and misaligned combustion phasing between the two fuels.
- In DMDF mode 4, misfire occurs, with the majority of methanol charge failing to combust following pilot diesel ignition.

These modes, illustrated in Fig. 2.8, are mostly sensitive to the MEF ratio. DMDF mode 1, typically found at relatively high MEF, is dominated by an HCCI-like

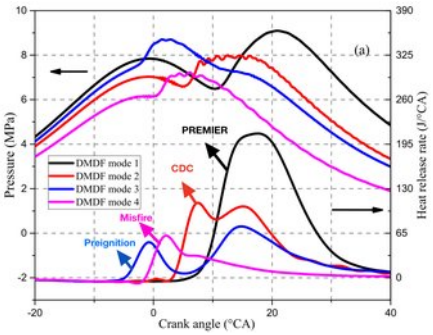

Figure 2.8: Methanol PRDF combustion modes (adapted from [129])

premixed combustion of methanol-air mixture in the vicinity of diesel flame. Conversely, DMDF mode 2, observed at lower MEF, mirrors the CDC mode. These trends align with the analysis in Section 2.1.2.2 and the sensitivity of the combustion profile to LRF ratio in the PRDF combustion strategy. DMDF mode 1, similar to the PREMIER mode [56], might require exhaust gas recirculation (EGR) and delayed diesel injection timing to control the spontaneous autoignition of methanol-air mixture [129]. Both PREMIER and CDC combustion modes were observed during the experimental studies of Dierickx et al. [161], as shown in Fig. 2.9. Additionally, the spontaneous autoignition of methanol before diesel injection, as seen in DMDF mode 3, was identified in this study. Referring to DMDF modes 3 and 4 as 'combustion abnormalities' rather than combustion modes might be more appropriate. This type of autoignition found in these modes can also be characterized as preignition knock [20]. Introducing methanol through the PRDF strategy in a diesel engine has shown that combustion can become faster, with overall more advanced phasing than in diesel-only operation due to a greater fraction of isochoric combustion. However, this is not always the case, as shown earlier in the RCCI experimental study of Jia et al. [177], and careful control of boundary conditions remains essential.

In premixed strategies, methanol is typically evaporated before combustion. On the other hand, in non-premixed DFDC mode, evaporation and combustion phases occur consecutively and simultaneously. In the study of Sacculo's et al. [116], both the diesel and methanol cases exhibited HRR traces dominated by a single mixing-controlled combustion, with the typical premixed combustion of CDC being absent due to the pilot strategy. This closer to unimodal HRR shape align with similar experimental studies using the DFDC strategy for methanol [28, 180]. Methanol DFDC showed a higher initial HRR peak and more advanced combustion phasing than the diesel case, indicating a faster early diffusion burn and shorter CD (≈ 10°CA shorter), while leaving less fuel for the late combustion phase. These observations highlight that in DFDC concept the heat release is strongly governed by mixing-controlled combustion of the main injection, thereby making factors like injection pressure, nozzle geometry and angle important for the combustion and overall performance.

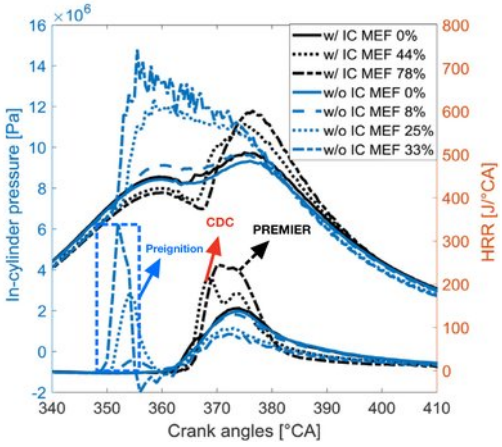

Figure 2.9: Combustion mechanisms found in a methanol PRDF marine engine (adapted from [161])

2.2.1.4 *Impact of methanol on engine performance*

Methanol can potentially improve brake thermal efficiency (BTE) in ICEs by reducing in-cylinder heat losses, likely adding room for combustion phasing optimization. PRDF operation can promote a higher degree of isochoric combustion, with methanol under DFDC concept also being promising concerning the combustion phasing. While methanol can increase engine efficiency and reduce emissions, its evaporation challenges may increase combustion variability in premixed strategies [158], particularly at low loads, potentially offsetting these benefits. Most studies report a positive impact of methanol on BTE using either the PRDF or DFDC strategy, as seen in Table 2.3. Despite methanol's lower calorific value and the API in the PRDF strategy, its use can improve both the volumetric efficiency and specific fuel consumption. Only Wei et al. [165] reported a decrease in these two efficiencies. Their study, which assessed the effect of methanol in a six-cylinder truck engine using the PRDF strategy, showed a 2% reduction in BTE compared to diesel-only mode, likely due to delayed combustion phasing away from TDC.

Although the PRDF may not achieve as high MEF as the DFDC strategy, most studies demonstrate that both can achieve higher BTE with methanol addition. In the PRDF strategy, the efficiency boost primarily derives from methanol's cooling effect as well as advanced and/or shorter combustion. This is supported by the study of Guan et al. [158], which reported faster combustion rates and a maximum increase in efficiency of approximately 2% in methanol operation compared to diesel-only, despite an increase in coefficient of variance (COV) of IMEP and decrease in combustion efficiency. Dierickx et al. [178] observed a relative increase up to 12% in BTE compared to DO operation in a high-speed marine diesel engine converted to methanol PRDF, exhibiting the greatest gains at higher load points at the expense of a slight decrease at low loads. Wang et al. [113] similarly reported BTE relative gains of up to 10% in methanol mode compared to diesel, while an efficiency gain was also found at low loads.

The increasing trend in BTE with methanol is also confirmed in DFDC strategies for large marine engines. Repo et al. [163] reported a 2% efficiency gain during methanol operation compared to diesel, with the highest gains at maximum load points. Aabo et al. [180] showed that large two-stroke MAN marine diesel engines exhibited an increase in indicated efficiency at all load points, with gains up to 4% in methanol mode. Although the comparison is made between tuned diesel-only and methanol–diesel operation, and despite differences in certain boundary conditions and injector geometry, the observed improvements are primarily attributed to slightly faster combustion under methanol operation and to methanol's cooling effect, which reduces heat losses. Similar BTE improvements have been observed in developing other large marine engines using the DFDC strategy [181, 183].

2.2.1.5 *Impact of methanol on emissions*

Utilizing renewable methanol in next-generation HD engines offers significant potential to reduce greenhouse gas and other harmful emissions in transportation, especially for hard-to-abate transport sectors like maritime [12]. Methanol contains no sulfur and no carbon-to-carbon bonds in its molecule, so the fuel itself eliminates sulfur oxide (SO_x) and does not form any soot [11].

NITROGEN OXIDE EMISSIONS

NO_x emissions remain a great challenge in diesel engines. Very high temperatures near the diffusion flame and high oxygen concentration due to lean combustion contribute to high levels of NO_x in diesel engines. The key factors influencing NO_x formation include maximum in-cylinder temperatures, air residence at high temperatures, and oxygen concentration within the cylinder [20]. In diesel engines, high NO_x levels are driven by local conditions in the diffusion flame, where intense heat release in near-stoichiometric reaction zones leads to very high local temperatures and finite residence times that strongly promote thermal NO formation.

Across various combustion strategies and engine sizes, studies consistently report a decrease in in-cylinder temperatures when methanol is used in diesel engines [180, 184]. While methanol's oxygen content might proportionally promote NO_x formation as methanol is added, its cooling effect and resulting temperature drop has significantly stronger impact, thereby leading to the net NO_x decrease compared to diesel-only mode. In methanol PRDF engines, higher MEFs are expected to result in lower NO_x emissions for three main reasons. First, the cooling effect of methanol increases as MEF rises. In addition, higher MEF promotes a more dominant premixed lean combustion mode through flame propagation, reducing the amount of diesel undergoing diffusion combustion. This effect is also supported by experimental studies on PRDF strategies with NG, where increasing NG-to-diesel ratio decreased NO_x due to smaller hot-flame diffusion regions [138]. These trends are corroborated by the studies of Wang et al. [113] and Dierickx et al. [178] that reported reduced NO_x emissions at all tested load conditions. Wang et al. [113] reported a reduction range of 15% to 40%, with the maximum reduction at 75% load where the highest MEF was achieved, while Dierickx et al. [178] reported a reduction between 40% up to 75%.

While all reviewed combustion strategies with methanol demonstrate NO_x reduction, directly comparing different combustion strategies is challenging due to parameter variations like engine size and load points. For instance, in methanol PRDF concepts, some studies report lower NO_x reduction [113, 155, 158], while others demonstrate stronger NO_x reduction capabilities [161, 178]. Similar trends are observed for methanol DFDC engines compared to their diesel baseline. The study of Wang et al. [115] on a high-speed LD engine showed a 60% NO_x reduction with approximately 80% MEF across all load points compared to CDC, while Saccullo [116] reported a 20% reduction in a HD single-cylinder setup with a higher MEF of 96%.

Despite methanol's NO_x reduction potential, it remains unclear whether this reduction is sufficient to comply with stringent regulations such as International Maritime Organization (IMO) Tier III for shipping. Several studies suggest that exhaust gas after-treatment may still be required for marine engines to meet Tier III levels [161, 183]. Fridell et al. [185] investigated the exhaust emissions from a large marine four-stroke medium-speed diesel engine converted to methanol DFDC. Although NO_x levels ranged from 6.5 to 12.3 g/kWh in methanol mode, which are lower than the typical values in diesel-only mode, after-treatment is still required to meet Tier III levels. MD97 remains the only methanol-based combustion strategy to meet the Tier III standards without exhaust after-treatment [26, 66, 186].

Introducing water into the cylinder is a viable direct strategy to further reduce NO_x emissions in methanol engines [187]. Dierickx et al.[188] tested various methanol-water (MeOH-W) blends to investigate the potential of water addition in a marine diesel engine. They concluded that a higher water ratio (MeOH-50 and MeOH-64 blends) could help the engine reach Tier III NO_x legislation but at the cost of reducing the maximum MEF that could be used. Although water addition generally leads to a small decrease in engine efficiency [189], this experimental study demonstrated an increase in BTE compared to pure methanol. The MeOH-50 blend resulted in a 3.3% and 4.9% increase in BTE compared to pure methanol and diesel-only modes, respectively. According to the study, this improvement can be attributed to the advancement of combustion phasing caused by the enhanced cooling effect and longer ID with water addition. The extended ID led to a greater portion of isochoric combustion closer to TDC, thereby increasing thermodynamic efficiency. Additionally, water addition mitigates the inhibition effect of methanol on $OH^{\cdot}$ radical production, which improves mixture reactivity [190], further enhancing combustion efficiency.

While methanol generally reduces NO_x emissions, special attention should be paid to NO_2 emissions when methanol is employed in ICEs. Several experimental studies have confirmed an increase in NO_2 emissions despite the overall decrease in NO_x emissions [112, 155, 184, 191]. This rise occurs when NO rapidly converts to NO_2 in certain areas of the charge, due to leaner mixtures and cooler temperatures [192]. The direct NO_2 tailpipe emissions rising trend raises health concerns as they increase the direct exposure to humans and are linked with respiratory issues [193], to which engine research has given little attention.

Table 2.3: Methanol impact on engine performance and emission characteristics of HD DF engines

Ref.	Engine Type	CR [-]	Bore x Stroke [mm]	Rated Power [kW/c]	Injection (Ignition) Strategy	MEF test [%]	Speed [rpm]	Performance		Emissions				
								VE	BTE	NO_x	PM	UHC	CO	CH_2O
[113]	Marine 4x 6c	16.8	-	43	API (PRDF)	51	1800	↑	↑	↓	↓	↓**	↓**	↓**
[161, 178]	Marine 4x 6c	19	108 x 130	32.5	API (PRDF)	60	1500	∼	∼	↓	↓	-	-	-
[158]	Marine 4x 1c	16.8	129 x 155	49	API (PRDF)	28	1200	↑	↑	↓	-	↑	↑	-
[155]	Truck/ Bus 4x 6c	17	126 x 130	42	API (PRDF)	40	1500	-	↑	↓	↓	↑	↑	↑
[179]	Truck/ Bus 4x 6c	18.1	108 x 130	32	API (PRDF)	30	1400	-	-	-	↑	-	-	-
[165]	Truck/ Bus 4x 6c	17	126 x 130	42	API (PRDF)	60	1900	↓	↓	↓	↓	↑	↑	-
[116]	Truck/ Bus 4x 1c	16.7	131 x 158	73.5	HP-DI (DFDC)	96.6	1262	-	↑	↓	↓	-	-	-
[24]	Marine 2x 4c	-	500 x 2,250	1,624	HP-DI (DFDC)	High	105	-	∼	↓	↓	↑	∼	-
[163, 185]	Marine 4x 8c	-	400 x 560	660	HP-DI (DFDC)	High	530	-	-	↓	↓	↑	-	-
[163]	Marine 4x 16c	-	320 x 400	580	HP-DI (DFDC)	High	750	-	↑	↓	-	-	-	-
[180]	Marine 2x 6c	-	500 x 2,500	1,264	HP-DI (DFDC)	High	88.5	-	↑	↓	-	-	-	-
[181]	Marine 4x 8c	-	320 x 400	500	HP-DI (DFDC)	High	720	-	↑	↓	↓	-	-	-
[28, 183]	Marine 4x 6c	-	210 x 320	220	HP-DI (DFDC)	93	1000	-	↑	↓	↓	-	-	-

[1] The baseline is the corresponding engine operating in diesel-only mode
[2] A: Advanced, D: Delayed, ↑: Increase, ↓: Decrease, ∼ : Constant , - : Data not available
[3] c: cylinder, 2x: two-stroke, 4x: four-stroke
[*] Ethanol used in engine experiments
[**] After diesel oxidation catalyst (DOC)

PM AND SOOT EMISSIONS

PM emissions pose another challenge in diesel engines [194], with a typical trade-off existing between NO_x and soot emissions. Soot, which appears as black smoke, is the primary constituent of PM emissions in diesel engines, with methanol having the potential to mitigate soot formation due to its oxygen content and lack of carbon-to-carbon bonds. Geng et al. [179] conducted an experimental study on a 6-cylinder HD diesel engine using the methanol PRDF strategy to assess methanol's impact on PM emissions. Methanol operation resulted in a reduction of dry-soot emissions by up to 92% compared to CDC at low to medium loads, with PM distribution shifting toward smaller particles. This trend aligns with findings from similar studies on smaller engines [194, 195]. However, at higher load points, an increase in soot particles was observed in methanol mode, which can be explained by the

methanol combustion before diesel injection, which reduced oxygen availability during diesel combustion. Under normal operating conditions, methanol typically reduces soot emissions at all load points, as shown by Dierickx et al. [161, 178], with the reduction reaching up to 86% at the highest MEF.

Methanol's great potential in diesel engines lies in its potential to eliminate their typical soot-NO_x trade-off [104]. Although previous studies have reported this elimination in methanol PRDF engines [155, 165], Dierickx et al. [178] found that this trade-off elimination was not evident at all operating points. Specifically, at higher loads, there was a threshold beyond which the trade-off was reintroduced, as NO_x began to rise again. According to the study, this probably originated from the elevated temperature of more premixed combustion taking place at higher MEF. Using methanol with DFDC strategy, all reviewed studies report a reduction of both PM and NO_x emissions, as summarized in Table 2.3. Fridell et al. [185] observed PM levels as low as 0.1 g/kWh, significantly below those in diesel-only mode, along with NO_x reduction. Similarly, Sacculio [116] reported decreasing soot emissions from 3.2 to 0.05 mg/kWh in methanol DFDC mode.

Despite the general reduction in PM emissions with methanol, an increase in the soluble organic fraction (SOF) of PM can be expected [179, 196]. Zhang et al. [112] confirmed that methanol operation results in higher SOF proportions in PM. While SOF poses additional health concerns, there is limited research on such unregulated emissions in methanol-fueled HD engines, highlighting the need for further investigation.

UNREGULATED EMISSIONS

Introducing methanol in CI engines, particularly through premixed strategies, often leads to higher levels of unburned hydrocarbons (UHCs), including methanol (CH_3OH) and formaldehyde (CH_2O), as well as increased carbon monoxide (CO) emissions [197]. The increase in these emissions in PRDF engines with methanol can be attributed to three main factors: 1) incomplete combustion due to lower in-cylinder temperature and leaner mixtures, 2) 'wall wetting effect', causing a portion of methanol to stick to the walls and crevices, and 3) absorption of methanol into oil layers [104, 117]. CO is particularly sensitive to the first, whereas UHC is more sensitive to the last two. The mechanism of the UHC is similar to that in SI engines [198]. Ning et al. [117] compared the emissions of methanol, ethanol, and n-pentanol in a non-road PRDF engine and reported that all alcohols resulted in lower CO and soot but higher UHC levels compared to the diesel baseline. Among the three alcohols, methanol showed the best CO and soot reduction performance but had the highest UHC emissions, likely due to increased wall wetting and absorption into oil layers [199]. At 40% MEF, UHC increased from around 0.14 to 0.57 g/kWh, while CO decreased from around 3.15 to 1.55 g/kWh.

Unoxidized methanol, after combustion, escapes in the exhaust, with some partial oxidation to formaldehyde taking place in the exhaust stream. While both molecules are intermediate products from the combustion of diesel fuel, they are relatively low in CDC [112]. Diesel combustion involves a range of species during its oxidation reactions, whereas the only methanol oxidation path is through formaldehyde [100]. Aniolek and Wilk [200] investigated the low-temperature oxidation of methanol

in a constant volume stirred reactor, which could mimic the lower-temperature oxidation process occurring during the exhaust stroke. They observed that methanol is quickly oxidized at low temperatures, while formaldehyde, its principal intermediate product, accumulates rapidly before being oxidized to CO. They also concluded that formaldehyde oxidation results in a high increase in CO but few CO_2 at low temperatures, consistent with the expected slower reaction rates of CO to CO_2 [201, 202].

While numerous studies have examined methanol's impact on UHC in diesel engines using the PRDF strategy, detailed data on methanol and formaldehyde emissions are still scarce, particularly for HD DF engines. Investigating the impact of methanol on the performance of six-cylinder HD methanol PRDF engine, Wang et al. [113] reported almost no methanol emission in all tested load conditions and only slightly higher formaldehyde levels after the diesel oxidation catalyst (DOC) compared to baseline CDC mode. These findings are consistent with the results of Zhang et al. [113] in a LD four-cylinder methanol PRDF engine, which also reported low methanol levels post-DOC (around 0.028 g/kWh) but found the DOC having less impact on formaldehyde emissions. However, without the DOC, this study demonstrated that unburned methanol emissions are expected to increase significantly in methanol PRDF engines. At 30% MEF, methanol PRDF engines emitted 0.86 g/kWh of methanol and approximately 0.92 g/kWh of formaldehyde, while in the CDC mode, both emissions were low at 0.03 g/kWh.

In methanol DFDC engines, information about unregulated emissions is even more limited. However, an increase might not be as significant as in PRDF strategy due to the nature of diffusion combustion. The absence of a premixed fuel-air mixture eliminates the risk of unburned methanol due to the aforementioned reasons. This might explain this lack of data on such emissions in methanol DFDC engines. In the study of Fridell et al. [185], engine-out UHC emissions were 1.6 g/kWh at 80% engine load, which are higher than the typical UHC emissions seen in these engines of around 0.2 g/kWh [203]. Aldehyde emissions were minimal, with CO emissions ranging from 3.7 g/kWh at high loads to 6.6 g/kWh at low loads. Schmid et al. [24] reported an increase in UHC with ethanol use, but the rise was much smaller compared to the increase observed in methanol PRDF engines. This trend is also mirrored in CO emissions.

To mitigate the expected rise in engine-out UHC, the DOC technology can be employed, which can effectively reduce not only CO and UHC but also PM emissions, including SOF [204, 205]. The DOC performance is also highly sensitive to exhaust temperature [206], supported by the study of Geng et al. [179] where the reduction of PM concentration increased at higher loads. This study also demonstrated that DOC could significantly lower SOF and UHC in the exhaust from a PRDF engine with methanol, with a total particulate number concentration reduction of up to 60%. Wang et al. [113] reported similar findings, showing DOC's capability to eliminate methanol from the exhaust and substantially decrease CO and UHC. Methanol operation with DOC exhibited unburned methanol emissions that were even lower than the diesel baseline. However, formaldehyde emissions were found higher than the diesel baseline, even with DOC use. It should be noted that, depending on catalyst and exhaust gas temperature, formaldehyde emissions can even increase downstream of the DOC, underscoring the need to carefully assess DOC

characteristics and exhaust temperature profiles for methanol engines [207]. The maximum increase occured at 75% load, where emissions rose from approximately 0.015 g/kWh in diesel-only mode to 0.045 g/kWh, which load points corresponds to the highest MEF used of 60.6%.

2.2.2 *Dedicated mono-fuel methanol engines*

Because diesel engines dominate HD transport, research has mainly focused on methanol use in DF schemes. However, exploring other strategies like mono-fuel SI and low-temperature combustion could offer improved trade-offs between emissions and efficiency and enable operation fully on renewable fuels like methanol, thus reducing the reliance on diesel. Despite limited research on these alternative concepts, this subsection seeks to gather and review experimental research on HD engines that have utilized MF approaches with methanol.

2.2.2.1 *HD SI engines*

The gasoline engine's affordability and low emissions have made it prevalent in the LD automotive sector. In contrast, the diesel engine is favored in HD applications due to its superiority in power density, robustness, and efficiency [9]. As engine bore size increases for heavier applications, so does the flame distance within the combustion chamber. This, along with higher pressure and lower flame velocities associated with typically slower speed regimes, exacerbates knocking in SI engines, thus limiting their capability to meet higher load torque demands and consequently their efficiency due to restricted CR [19].

Despite DF concepts currently leading in HD applications, growing experience with methanol can pave the way for dedicated methanol HD SI engines [30, 208]. Methanol allows for higher CR in SI engines than traditional gasoline-type fuels due to its higher ON. Wouters et al. [209] explored the CR limits in a methanol DI SI engine, testing CR from 10.8 to 20.6. The authors reported that the engine could operate at high loads, including the highest of 18 bar indicated mean effective pressure (IMEP), resulting in higher efficiencies. The greatest gain in efficiency was observed at the highest CR, with an IMEP of 16 bar and lean mixture. The study of Güdden et al. on a large-bore 5-liter PFI SI engine showed that despite knock limitations, an efficiency of 44 % at 17 bar IMEP can be achieved while meeting the IMO Tier III regulations without the need for additional exhaust after-treatment technologies [210]. Nevertheless, a rise in formaldehyde might necessitate the use of an oxidation catalyst in the exhaust system.

Bosklopper et al. [211, 212] studied an eight-cylinder NG engine converted to methanol, achieving stable operation across all test loads (25%, 50% and 75%) with improved efficiency over NG. Zhu et al. [213] also converted an NG HD SI engine to methanol, observing a BTE over 40% across 12.7 to 21.7 bar BMEP and 1000 to 1700 rpm, together with a reduction in NO_x and CO emissions compared to NG. However, an increase in UHC was observed. Björnestrand [214] investigated an HD DI SI engine with methanol, noting knock limiting high load operation. Retarding spark discharge and employing EGR mitigated knock and resulted in gross indicated efficiency of 54%. Similarly, Mahendar et al. [215] explored methanol's diluted

combustion characteristics in an HD SI engine, comparing it with gasoline and ethanol. Methanol could operate at the highest load, over 25 bar IMEP and even at stoichiometric conditions, increasing indicated efficiency at 48%.

2.2.2.2 *Partially premixed combustion*

The PPC concept, an emerging low-temperature combustion (LTC) strategy, involves adjusting injection timing during the compression stroke to create a partially premixed charge and separate the injection and combustion events [85, 216]. To explore methanol's potential in PPC, a series of experimental studies were conducted in a converted marine six-cylinder Scania D13 engine into a single-cylinder configuration [66, 217–221]. Shamun et al. [217] explored the PM characteristics in the exhaust gas from the PPC engine fueled with naphtha gasoline, ethanol, and methanol and compared them with CDC. Intake concentration of O_2, intake temperature and injection pressure were varied during the experiments. The study demonstrated extremely low PM emissions and elimination of the NO_x-soot trade-off when both alcohol fuels were employed. Although neither methanol nor ethanol produced any particle with diameters greater than 30 nm, methanol resulted in more particles than ethanol. The authors speculated that the rise in number of particles could be linked to material-compatibility of methanol with the contacting metallic components.

Subsequently, the same authors attempted to quantify the cooling effect of methanol and compare it to that of iso-octane fuel [218]. Analyzing the in-cylinder pressure measurements, methanol's cooling effect resulted in lower compression work, leading to a slightly higher BTE. Lower achieved temperatures with methanol reduced both the heat losses and NO_x emissions. Zincir et al. [219] later conducted a study to investigate the potential of a methanol PPC engine in the context of slow-speed and low loads, a strategy increasingly adapted by ships to lower emissions [222]. Compared to marine gas oil, the methanol-fueled PPC engine resulted in higher BTE, increased from 31% to 43% in the low-load range. Methanol use reduced CO_2 and led to NO_x levels below the IMO Tier III while eliminating both SO_x and PM emissions. In a follow-up study, Zincir et al. [84] investigated the impact of intake air temperature on these low load operating conditions. The results showcased that decreasing the intake air temperature led to lower combustion stability and longer ID, similar to the PRDF engine concept.

Svensson et al. [221] investigated the timing and duration of dual methanol injections in low load operation with neat methanol. Their strategy included an early pilot injection coupled with a diffusion-controlled main injection in the context of PPC combustion (Fig. 2.4). The study's findings demonstrated that low levels of CO, UHC, and NO_x emissions can be obtained by optimizing the dwell time and injection duration. This highlights the potential reductions in hazardous emissions through injection optimization in methanol PPC engines.

2.2.2.3 *Additized methanol in CI engines*

In addition to SI and PPCI, using methanol with an ignition improver demonstrated promising conventional diffusion combustion performance. Aakko-Saksa et al. [67] explored the potential of renewable methanol blended with ignition improvers and lubricity additives in a Scania ethanol engine. Operating the engine on MD95 (95%

of methanol and 5% of ignition improvers), the engine exhibited lower emissions compared to the ethanol mode. This study concluded that this engine strategy could be suitable for HD applications such as smaller marine vessels with engines ranging from 800 to 1200 kW of power. In a subsequent study, a higher methanol ratio of 97% (MD97) was achieved, leading to the certification of a commercial engine capable of meeting IMO Tier III NO_x levels without additional treatment system [66].

2.3 IMPACT OF DESIGN AND OPERATING PARAMETERS ON DIESEL-METHANOL DUAL FUEL ENGINES

DF technology is often regarded as the most effective strategy to utilize methanol in HD engines due to its potential to lower emissions and enhance efficiency in the diesel engine [11, 163, 180] while offering the flexibility of switching between methanol and diesel operation. The flexibility provided by the DFDC strategy is crucial to meet the growing demand for global trade power [223]. While the DFDC strategy can reach high MEF and offer this adaptability for HD diesel engines, it is restricted to a certain range of engine sizes due to space constraints in the cylinder head when an additional injection system needs to be mounted. A highly complex injection system is required to realize DFDC strategy in smaller engine sizes [163]. Moreover, DFDC still faces challenges with the relatively high levels of NO_x deriving from the diffusive nature of combustion.

In contrast, the simpler-to-adopt PRDF strategy applies to a broader spectrum of engine sizes while having the potential of significantly reducing NO_x emissions. This approach can contribute to the sustainable conversion of existing engines. Yet, PRDF combustion faces challenges like misfires at low loads and knocking at high loads [129]. Optimizing design and operational parameters could extend MEF limits and enhance the performance of these methanol PRDF engines. This section reviews experimental studies on PRDF engines using methanol to evaluate the impact of several design and operating parameters on engine performance of these DF engines. Table 2.4 compiles these findings, offering insights into optimizing PRDF engine performance.

2.3.1 *Engine speed*

The lower speed operating regime is a distinct feature of HD engines compared to LD applications, highlighting the importance of better understanding how engine speed influences the behavior of methanol DF engines. Chen et al. [224] examined a methanol-fueled engine using the PRDF strategy across various speeds. At 25% MEF, increasing engine speed resulted in higher peak pressure, reduced cylinder-to-cylinder variation, and slightly delayed combustion phasing. The reduced variation and higher Pmax were likely due to improved mixing from increased turbulence [225], while delayed combustion phasing is expected as timing narrows with increasing speed. This effect in combustion phasing might be confirmed by Cheung et al. [226], who reported rising exhaust temperatures with increasing speed from 1280 to 2560 rpm, exhibiting a drop in BTE from 30.8% to 24.8%. These findings might also be confirmed by studies suggesting that lower engine speeds extend the

maximum achievable MEF [100, 178, 227], possibly due to more favorable combustion phasing and more time available for methanol to evaporate and properly mix. Dierickx et al. [178] found the maximum MEF to be 70% at 1000 rpm, decreasing to 37% at 2000 rpm. In a subsequent study by the authors, which compared SPI with PFI strategy, confirmed the higher maximum MEF at lower engine speeds for PFI, yet for SPI the trend was reversed [161]. Wang et al. [227] also reported higher brake specific fuel consumption at 2090 rpm compared to 1660 rpm at all tested MSP. Despite these findings, drawing definitive conclusions about the effect of engine speed on methanol PRDF engine performance remains challenging, as multiple factors that are not kept constant might influence engine behavior across different studies. However, a general hypothesis from the literature reviewed is that lower engine speeds typically lead to delayed combustion phasing, which can decrease thermodynamic efficiency. The overall impact may reflect a trade-off between higher thermodynamic efficiency at lower speeds and the corresponding increase in heat losses due to prolonged exposure to high temperatures within the cylinder. This is supported by Dierickx et al. [178] and Cheung et al. [226], who reported that lower speeds resulted in reduced soot but increased NO_x emissions. Extended combustion gas residence time at high temperatures at lower speeds could explain the increase in NO_x and an expected rise in heat losses.

These research findings underscore the impact of engine speed on the overall performance of these PRDF engines fueled by methanol. Methanol's better performance at lower speeds could benefit larger engines operating at lower speed regimes. However, the scarcity of experimental results calls for further investigation into how engine speed affects MEF limitations in engines using the PRDF strategy.

2.3.2 *Methanol injection location*

Injecting methanol at LP with the API strategy is the simplest and most cost-effective way to retrofit diesel engines compared to more complex and expensive HP-DI systems [161]. Depending on the intake geometry of each engine design, there are several API locations for methanol when SPI strategy is employed. Therefore, the PRDF ignition concept can be facilitated via the different SPI, PFI and LP-DI strategies, as discussed in Section 2.1.2.2. The injection location is expected to affect the overall performance of the engine. This subsection reviews experimental studies that compare different injection locations for the PRDF concept and their impact on engine performance.

Xu et al. [39] experimentally evaluated the effects of methanol API locations on a four-cylinder common rail diesel engine at varying loads, exploring three alternative locations: 1) pre-intercooler (I/C) SPI, post-I/C SPI, and PFI. Four injectors were employed for each case of the SPI strategies. The authors observed that the optimal API location was highly sensitive to the operating load. The pre-I/C SPI strategy was the most effective in promoting combustion at low loads, post-I/C SPI at medium loads, and PFI at high loads. The improved combustion was characterized by lower ignition delay and greater combustion efficiency resulting in lower UHC and CO but higher NO_x emissions. At all load points, regardless of the injection strategy, methanol operation resulted in higher efficiency compared to diesel-only mode. At

high load and 40% MSP, PFI strategy resulted in 42.5% BTE compared to 41% for diesel baseline, 41.5% for post-I/C SPI, and 42% for pre-I/C SPI.

As previously discussed in Section 2.2.1.2, the study of Dierickx et al. on the pre-I/C SPI strategy chose to bypass the I/C to prevent methanol condensation [161]. In this study, the PFI strategy was found to be the most effective API strategy for maximizing MEF. However, comparing SPI and PFI directly from this study is challenging due to variations in air conditions induced by the I/C. The authors highlight the importance of controlling the I/C's cooling effect in pre-I/C SPI setups for methanol. Investigating the impact of this cooling effect on the performance of these engines is interesting for further studies.

Chen et al. [40] explored different methanol injection locations and their effect on COV and emissions of a four-cylinder diesel engine, investigating three strategies: SPI at two points and PFI. PFI exhibited the greatest cooling effect on the intake charge, increasing volumetric efficiency and allowing more methanol to enter the engine in gaseous form At 50% MSP, the temperature of the intake manifold dropped around 40 K relative to diesel-only, while both SPI strategies led to a decrease of around 20K. The increased cooling effect was confirmed by the lower NO_x emissions across the entire operating range and tested MSPs. This can be attributed to a more effective cooling of the intake air compared to early SPI, where cooling losses occur in the intake pipes.

Ning et al. [159] compared PFI and LP-DI strategies of methanol injection in a single-cylinder diesel engine using the PRDF concept. A high-pressure common rail system was used for LP-DI, while a LP system was used for PFI. LP-DI resulted in higher BTE, lower UHC and CO emissions, despite exhibiting higher COV. The lower COV in PFI might be attributed to better mixing, which could also explain the reduced NO_x emissions. The earliest LP-DI tested showed better overall performance than PFI, but it is difficult to directly compare the injection location impact between the LP-DI and PFI due to the different injection systems used in the two strategies. Additionally, comparing trends across different studies poses challenges, as the specific fuel injection equipment employed for the pilot fuel may influence the results. For instance, one study used a common rail system [117], while another [161] used a pump-line-nozzle system.

2.3.3 *Intake conditions*

Despite methanol's cooling effect and its potential to enhance the engine efficiency, great attention should be given to the intake air conditions in methanol-fueled engines, especially when API schemes are considered. Methanol's high heat of evaporation makes its mixture formation highly sensitive to intake conditions, eventually affecting engine operation. Strategies like EGR can modify the intake air conditions, such as the reactivity gradients in the mixture, and subsequently affect overall engine performance. This subsection will examine the effect of variations in intake conditions, such as temperature, pressure, and EGR, on the methanol PRDF engine operation.

To explore the potential of higher intake air temperatures and overcome the part load challenges in a methanol PRDF engine, Wang et al. [229] conducted experiments on a diesel engine at low loads. At nominal conditions and MEF of 60%,

Table 2.4: Impact of operating/design parameters on the performance of methanol dual-fuel engines

Ref.	Parameter Varying	Combustion Characteristics					Performance (BTE)	Emissions				MEF maximum
		ID	CD	CA50	COV	Pmax		NO_x	PM	UHC	CO	
[224]	Speed ↑	↑	↑	D	-	↑	↓	-	-	-	-	-
[226]	Speed ↑	-	-	-	-	-	↓	↓	↓	↓	↑	-
[100]	Speed ↑	-	-	-	-	-	↓	↑	-	↑	↑	↓
[227]	Speed ↑	↑	↑	D	-	↓	↓	↑	↑	↑	↓	↓
[178]	Speed ↑	-	-	-	-	-	↑	↓	↑	-	-	↓
[39]	Injection Location (SPI to PFI)	↓	↓	A	↓	↑	↑	↑	-	↓	↓	-
[161]	Injection Location (SPI to PFI)	-	-	-	↓	-	↓	↓	-	-	-	↑
[40]	Injection Location (SPI to PFI)	-	-	-	↑	∼	-	↓	↑	↓	↓	-
[159, 228]	Injection Location (PFI to LP-DI)	↑	↑	-	↑	↑	↑	↑	↑	↓	↓	-
[229]	Intake air Temperature (low load) ↑	↓	↓	A	-	↑	↑	↑	↓	-	-	-
[191]	Intake air Temperature (low load) ↑	↓	↓	A	-	↑	↑	↑	↓	↓	↓	-
[155]	Intake air Temperature (high load) ↑	↓	↓	A	-	↑	↑	↑	↑	↓	↓	-
[194]	Intake air Temperature (high load) ↑	↓	↓	A	-	↑	↓	-	-	-	-	-
[158]	Intake air Temperature (high load) ↓	↑	↓	-	↑	↑	↑	↓	↑	↑	↑	-
[230]	Intake air Temperature (low load) ↑	↓	↓	A	-	↑	↑	↑	-	-	↓	↑
[230]	Intake air Pressure ↓	↑	↑	D	-	↓	↓	↑	↓	-	↑	↓
[230]	EGR ↑	-	-	-	-	-	↓	↓	-	-	↑	↑
[227]	EGR ↑	↑	∼	-	-	↓	-	↓	↑	-	-	∼
[231]	Injection Timing (A)	↓	↓	-	↑	↑	-	↑	↓	↓	↓	-
[229]	Injection Timing (A)	↑	↓	A	↑	↑	↑	↑	↓	↓	↓	-
[232]	Injection Pressure ↑	↓	↓	A	∼	↑	↑	↑	↓	↓	↓	-
[231]	Injection Pressure ↑	↓	↓	-	↓	↑	-	↑	↓	↓	↓	-

[1] The baseline is the corresponding engine operating in methanol-diesel mode prior to the corresponding adjustment of the operating/design parameter.
[2] A: Advanced, D: Delayed, ↑: Increase, ↓: Decrease, ∼ : Constant , - : Data not available

methanol PFI decreased the intake temperature by 27.45 K, showcasing its dominant cooling effect during the evaporation phase. This slowed flame propagation due to low-temperature and lean mixtures after diesel injection. Pre-heating of intake air could help overcome these combustion challenges at low loads, as corroborated by the findings showing that increasing the intake air temperature to 348.15 K and 388.15 K advanced the combustion phasing and improved BTE. Thus, MEF ratios at low loads can be increased by assisting heating strategies, as also reported by Kumar et al. [191]. Improved combustion efficiency is observed with higher temperatures, and can lead to stable operation at higher MEF, lower CO and UHC; yet attention should be given to the trade-off between combustion efficiency and NO_x emissions.

On the contrary, increasing intake air temperature at high loads has a reverse effect on the efficiency of methanol PRDF engines while leading to further rise in NO_x emissions [191]. Exploring the impact of various intake air temperatures at high loads in an HD methanol PRDF engine, Pan et al. [155] reported an increase in both NO_x and soot emissions with higher intake air temperatures. Specifically, increasing the intake air temperature initially led to rising BTE until its maximum value at 333.15 K of intake air temperature. However, further increasing intake air temperature deteriorated BTE. This trend aligns with the experimental results reported by Chen et al. [194], who concluded that higher intake temperatures at high loads can lead to auto-ignition of methanol, affecting combustion stability and emissions. At high loads, methanol PRDF engines encounter the opposite challenges with uncontrolled combustion compared to low loads when partial combustion occurs. To address high PRR and Pmax resulting from roar combustion at high loads, Guan et al. [158] reduced the intake air temperature using an air-to-water cooler in a single cylinder HD methanol PRDF engine. By decreasing the intake temperature from 323K to 305K, they lowered average in-cylinder temperatures during compression and allowed for more advanced diesel injection timing. This intake condition resulted in lower PRR, improved volumetric and thermal efficiency, and less NO_x emissions. However, COV and combustion efficiency slightly decreased, leading to higher soot, CO, and UHC emissions.

Besides the impact on performance, it is crucial to explore the effects of these variations in intake conditions on MEF limitations in methanol DF engines. To this end, Dierickx et al. [230] investigated the impact of intake air temperature, pressure, and EGR on the MEF limits, as well as the engine performance. At low loads, misfiring was the main limiting factor for higher MEF ratios. Increasing intake air temperature resulted in greater MEF until the maximum level of 74% at 333.15 K. Instead of misfiring, knocking and pre-ignition were the limiting factors for further increasing MEF beyond 333.15 K. Moreover, the impact of higher temperature aligns with the experimental studies discussed earlier, leading to better combustion phasing, BTE, and higher NO_x. By varying the waste-gate valve in the exhaust, the effects of intake air pressure were studied at a constant air temperature of 303.15 K. Lower intake air pressures resulted in decreased attainable MEF ratios while knocking transitioned to misfiring as the main limiting factor. Additionally, lower intake pressure deteriorated combustion phasing and BTE, while it also resulted in higher NO_x emissions. This NO_x trend at lower intake pressure might result from poorer volumetric efficiency that led to higher maximum temperature during combustion. Finally, employing EGR at medium load and two set intake

temperatures, the authors reported that EGR can improve diesel displacement ratios and lower NO emissions, albeit at the expense of combustion and thermal efficiency. EGR is promising at extending MEF limits, particularly at high loads, where knocking is the main constraint [230]. However, Wang et al.'s similar studies indicated that using EGR did not contribute to any extension of MEF limits [227]. The scarce information on the effect of EGR in methanol PRDF engines necessitates further exploration to understand the capabilities of this technology better.

2.3.4 *Injection parameters of pilot diesel*

Combustion control in PRDF engines depends on the injection characteristics of the HRF, like diesel. Injection timing dominates the combustion dynamics, similar to pilot diesel used in PRDF strategies. Knocking at high loads could be overcome by optimizing diesel injection parameters. This subsection reviews experimental studies to identify the effect of pilot fuel injection parameters on combustion characteristics, performance, and emissions of methanol PRDF engines.

Li et al. [231] studied the effects of pilot fuel injection pressure and timing in a methanol PRDF engine. Similar to CDC, they observed that advancing diesel injection resulted in earlier combustion phasing, with higher Pmax and HRR. Advancing injection timing from 4 to 12 °CA before TDC at 35.7% MEF increased IMEP from 7.4 to 8.3 bar and advanced Pmax by 5 °CA. This advancement in combustion reduced soot, CO, and UHC emissions due to higher in-cylinder temperatures, albeit with an increase in NO_x emissions. Wang et al.[229] reported similar trends, including improved BTE, with advanced diesel injection timing across all tested operating points [229]. The sweep in injection timing ranged from 4.6 °CA after TDC to 17.4 °CA before TDC. The BTE improvement came at the expense of higher NO_x emissions, with a 70% increase at 60% MSP and an intake temperature of 348.15 K, compared to the most retarded timing.

Liu et al. [232] explored the influence of diesel injection pressure on methanol PRDF engine performance in a 6-cylinder HD diesel engine. Similar to injection timing, diesel injection pressure effects in PRDF strategy resembles those in CDC mode. Increasing injection pressure from 700 to 1300 bar shortened CD from 66.9 to 23.5 °CA, advanced combustion phasing from 28.6 to 13.6 °CA, lowered specific fuel consumption from 202.3 to 187.3 g/kWh, and reduced UHC emissions from 1850 to 950 ppm. However, NO_x emissions rose from 450 to 800 ppm, while both soot and CO exhibited a decreasing trend. Li et al. [231] similarly observed that increasing injection pressure from 721 to 1082 bar led to faster combustion, higher Pmax, and IMEP, along with reduced CO and UHC emissions while increasing NO_x emissions. These trends are consistent with the general understanding from CDC, where higher injection pressures enhance atomization and mixing, leading to shorter ID and advanced combustion phasing [233]. In PRDF operation, the pilot fuel ignition dynamics play a pivotal role in setting the overall combustion phasing by governing the ignition timing and energy, which subsequently control the combustion of the unburned methanol-air mixture [135]. Compared with conventional SI engines, beyond the inherent multi-point pilot ignition effects, PRDF combustion is influenced by pilot injection wave dynamics, which affect ignition kernel formation, turbulent flame development, and flame propagation speed [136]. A key conclusion

from the studies of Srna et al. [135, 136] on methane-air PRDF combustion is that pilot injection parameters exert a relatively minor influence on pilot combustion dynamics—and thus on combustion performance—compared to more dominant factors such as in-cylinder temperature and, in particular, the LRF to pilot fuel ratio.

2.4 CONCLUSIONS

In summary, this chapter has established and proposed a unified classification framework designed to clarify the diverse injection and ignition strategies found in ICEs powered by alternative fuels like methanol. Addressing the first sub-research question, this framework positioned as a critical tool for advancing collective understanding and supporting the development of new methodologies in the field. The review also underscored significant research gaps regarding dedicated monofuel strategies, such as those related to SI engines, which formulates the second sub-research question of this thesis, which will be addressed in Chapter 3. Additionally, the synthesis recognizes PRDF concept as the current most accessible and potentially impactful pathway for the near-term adoption of methanol in heavy-duty and marine engines. This insight sets the stage for the third sub-research question which will be dealt with in Chapter 4, where the combustion behavior and practical challenges of this concept will be investigated in depth. Finally, the chapter highlights how various design and operation parameters influence the efficiency, emissions, and achievable methanol energy fractions in premixed dual-fuel engines. These parameters can further expand the performance and technical frontier of PRDF concept, and formulate the fourth sub-research questions of this thesis, addressing it in Chapter 5. Based on the identified importance of boundary conditions governing combustion and performance in PRDF engines, this thesis focuses on the effects of MEF, intake temperature, equivalence ratio, and residual gas fraction in the experimental analyses presented in Chapter 4 and Chapter 5. Overall, this chapter aimed at both framing and propelling research by delivering actionable insights and mapping the trajectory from foundational review to experimental exploration.

3

COMBUSTION CHARACTERIZATION ANALYSIS IN LBSI MARINE ENGINES[1]

ἔδωκα γὰρ αὐτοῖς πῦρ καὶ τούτου διδάσκαλος
τεχνῶν ἅπασαν ἕσχεν ἀνθρωπότης ὁδόν.

I gave them fire, and by that gift
mankind shall learn every art.

— Aeschylus

This chapter addresses the second research question (**RQ2**) of the thesis, focusing on the key combustion characteristics and overall engine performance, including efficiency and emissions, in lean-burn spark-ignition (LBSI) marine engines using high-octane fuels. Natural gas (NG) is used in a multi-cylinder heavy-duty (HD) LBSI engine testbed as a convenient high-octane fuel to study multi-stage combustion behavior in premixed LBSI engines and overall performance, with insights being relevant under methanol operation. However, despite the combustion characteristic similarities between methanol and NG, these fuels still differ fundamentally, e.g., in their physical state and the typical strategy that they are introduced in the engine. To this end, the transfer of insights from NG to methanol is discussed explicitly in a dedicated reflection subsection at the end of this chapter. This work tackles *Research Gap 2* by providing a holistic experimental thermodynamic analysis framework to diagnose the dedicated mono-fuel LBSI strategy, a technology that can eliminate diesel dependency. It further seeks to enhance understanding of cycle-to-cycle variations, multi-stage combustion (e.g., bowl-in and squish phases), and emissions like unburned hydrocarbons, in HD LBSI technology, which are crucial for maritime applications.

The structure begins with Section 3.1 offering a brief background on LBSI marine engines. Section 3.2 details the experimental setup, data acquisition system, and analysis methodology including the multi-stage combustion methodology developed for the LBSI strategy. In Section 3.3 combustion stability is explored, with an emphasis on cycle-to-cycle variability and determination of combustion stability regions in these engines. Section 3.4 delves into fundamental combustion characteristics, providing a thorough analysis of multi-stage combustion processes and

1 This chapter is partly reproduced from Kiouranakis et al. [234–236]

their interplay with overall engine performance. Section 3.5 presents the Wiebe function analysis as a subsequent modeling analysis that can couple the developed experimental analysis to study the combustion characteristics in LBSI engines. This chapter concludes with Section 3.6, synthesizing the main conclusions and recommendations for future research, as well as the insights and hypotheses that can be transferred to LBSI powered by methanol and tested in future studies.

3.1 INTRODUCTION

Diesel engines remain the dominant power source for HD and marine transportation due to their operational robustness and efficiency [9], with spark ignition (SI) engine technology traditionally used in light-duty (LD) automotive applications [19]. SI engines can be particularly well-suited for emerging alternative fuels, such as ammonia [237], methanol [11], and hydrogen [238], due to the autoignition challenges of these fuels with compression ignition (CI) engines. Nevertheless, the maritime sector has largely focused on dual-fuel (DF) strategies for using alternative fuels, particularly NG in recent years, retaining diesel combustion principles [29, 239]. Although this approach is effective, it still relies on a high reactive fuel like diesel for ignition, which reliance in many cases is still significant, limiting the upscale and full transition to alternative fuels [22].

A promising alternative involves converting existing diesel engines to SI operation with minimal modifications by replacing the fuel injector with a spark plug and incorporating a low-pressure fuel injection system into the intake path [240, 241]. This approach is relatively straightforward, requiring no major engine redesign, and could be particularly suitable for compact marine engines where limited cylinder head space poses challenges for pre-chamber integration [242]. Additionally, this strategy often includes modifying the piston crown to slightly lower the compression ratio (CR) and optimize the in-cylinder flow regime for flame propagation rather than spray combustion [240]. Unlike conventional SI engines, which aim to minimize heat losses by reducing combustion chamber surface areas, this conversion approach leverages an enhanced flow regime that supports faster combustion and enables leaner mixture operation. In contrast to pre-chamber-based SI technology, this concept relies on a relatively well-homogenized charge through the combustion chamber [243]. Notably, pre-chamber designs have not yet been applied to smaller marine engines, as evidenced by prior research [49, 50, 244].

Retaining a diesel-like combustion chamber and swirl-inducing inlet ports [245], as implemented in the patented nebula combustion system [242, 246], provides optimum conditions for ignition and fast burning by the 'swirl killing' phenomenon as the piston approaches top dead center (TDC) [242]. This phenomenon, combined with enhanced tumble flow in bowl-in pistons, leads to greater turbulence levels in the combustion chamber [247, 248]. The greater turbulence subsequently enhances flame stability and significantly increases the potential of these engines to run on lean mixtures, thereby extending their capacity to reduce certain emissions and improve fuel economy [249]. Additionally, alternative fuels like NG and methanol, which have wider flammability ranges, can further improve the lean-burn capabilities of these engines [208, 250]. This makes this technology very promising to meet environmental targets without the need for extra exhaust treatment systems such as three-way

catalysts in conventional stoichiometrically operated SI engines [215, 249] or selective catalytic reduction technology in marine DF engines [185, 251]. Improving lean-burn capabilities in SI engines reduces NO_x by lowering combustion temperatures, while it also decreases CO and unburned hydrocarbon (UHC) emissions thanks to the greater oxygen availability [252, 253]. Moreover, the extension of dilution limits, combined with the high octane rating of alternative marine fuels, allows these LBSI concepts to extend their knock limits [254]. This enables them to operate at higher CRs and efficiencies than their conventional SI counterparts [38, 255].

As outlined in Section 1.4, there are still limited insights into mono-fuel LBSI concepts that could enable 100% utilization for alternative fuels like methanol. Additionally, recent research on LBSI strategies for heavy-duty and marine engines has predominantly focused on advanced pre-chamber stratification concepts, both in fundamental studies [256–258] and in the development of commercial marine SI products [49, 50, 259, 260]. As a result, the optimization potential and practical advantages of homogeneous open-chamber LBSI concepts—especially suitable for retrofitting diesel engines—have received comparatively little attention. This gap is particularly significant for marine-scale, multi-cylinder engines, which engines could play a key role in the energy transition. While single-cylinder experimental setups and numerical studies have provided valuable insights into alternative fuels [208, 261, 262], combustion chamber designs and operating strategies [263–266], there remains a lack of experimental data on multi-cylinder engines that can capture overall performance, and the relationships between efficiency and emissions with the inter-cylinder combustion dynamics.

3.2 EXPERIMENTAL SETUP AND METHODOLOGY

The experimental setup, as illustrated in Fig. 3.1, uses an 8-cylinder, four-stroke, turbocharged, marine high-speed NG LBSI engine. The engine is rated at 500 kWe at 1500 rpm and features a minimal valve overlap, with the specifications of the test engine given in Table 3.1. The engine, originally designed as a diesel engine, was converted into gas-powered with minimal modifications to facilitate its transition to SI operation. As part of this conversion, the piston geometry was redesigned with a new bowl-in piston, reducing the compression ratio to 12:1. The design aimed to harness squish flow to enhance turbulence within the cylinder near TDC, promoting faster flame propagation and improving lean-burn combustion capabilities, while retaining the core architecture of the original diesel design. The hemispherical bowl-in piston crown is shown in Fig. 3.2, with the intended squish-to-tumble flow transition illustrated in Fig. 3.3.

3.2.1 *Apparatus*

The data acquisition system (DAS) in the engine setup typically comprises two main components: one for in-cylinder measurements using a Kistler Type 2893A Kibox and another for external cylinder data collection, including emissions measurements by a HORIBA PG-350 analyzer. All cylinders are equipped with uncooled Kistler 7061C piezoelectric pressure sensors, connected to a Kistler 5064C charge amplifier.

Figure 3.1: Marine LBSI engine testbed

Table 3.1: LBSI engine specifications

Engine type	8-cylinder, turbocharged, lean-burn, 4-stroke
Ignition mode	Spark Ignition
Combustion chamber	Flat head and bowl-in piston
Bore x Stroke [mm]	170 x 190
Displacement [L]	34.5
Rated power/speed [kWe/rpm]	500/1500
Compression Ratio [-]	12:1
Number of valves [-]	4
Intake valve opens/closes [°CA aTDC]	337/-122
Exhaust valve opens/closes [°CA aTDC]	140/377

Additionally, an optical crank angle encoder with 720 marks is used to measure the crankshaft angle, enabling pressure data collection with a resolution of 0.5 °CA. While this engine has been previously used in studies [212, 267], new pressure sensors were mounted in a minimal and controlled recessed fashion on the periphery of all cylinder heads, as shown in Fig. 3.4. After installing the new sensors, several offline evaluation techniques were used to verify the accuracy of the updated measurement setup [268, 269].

Fig. 3.4 demonstrates a detailed scheme with the experimental apparatus in the engine lab. For this experimental campaign, an additional flame ionization detector, a Thermo-FID PT84 analyzer, was used to capture methane and total UHC emissions. NG is injected upstream of the compressor, with its flow rate being monitored by a Bronkhorst F-106Cl gas flow meter. It should be noted that NG is characterized as a low calorific value gas due to the high amount of nitrogen it contains, with its composition and properties summarized in Table 3.2.

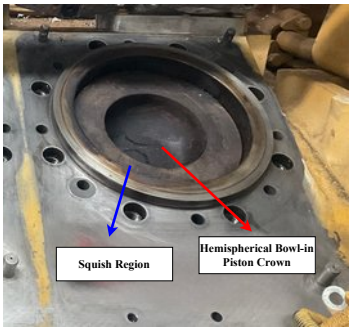

Figure 3.2: LBSI engine piston Crown

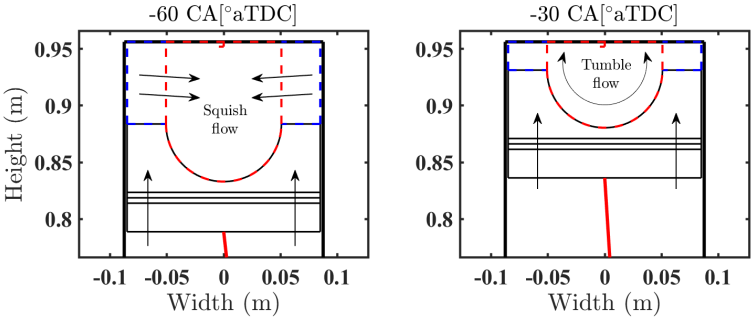

Figure 3.3: Squish to tumble flow transition during compression approaching TDC

3.2.2 *Operating test conditions*

The primary objective of this research is to examine the steady-state operation of the NG LBSI engine. To ensure stability during testing, the engine is operated for at least five minutes between the operating points' transitions, with a continuous monitoring of parameters such as exhaust temperature, fuel flow, and emissions to ensure steady-state conditions. Two main experimental campaigns are involved in this research. The first experimental campaign (EC I), related to the stability analysis discussed in Section 3.3, encompasses tests at 18 distinct operating points, and is defined in this thesis as the experimental campaign (EC) I. These operating conditions include load sweeps from 100 to 450 kWe, as well as air excess ratio and spark timing sweeps, as illustrated in Table 3.3. The in-cylinder pressure measurements for the top in-line cylinders 1, 3, 5, and 7 were captured for 600 consecutive cycles at each measuring point.

The second experimental campaign (EC II), concerning the more fundamental combustion characteristics in LBSI engines elaborated in Section 3.4, builds on the EC I. Key differences in the new dataset include: 1) an increased number of operating points tested, 2) the addition of intake air temperature sweeps, and 3) the use of the FID analyzer for a better quantification of combustion efficiency, methane

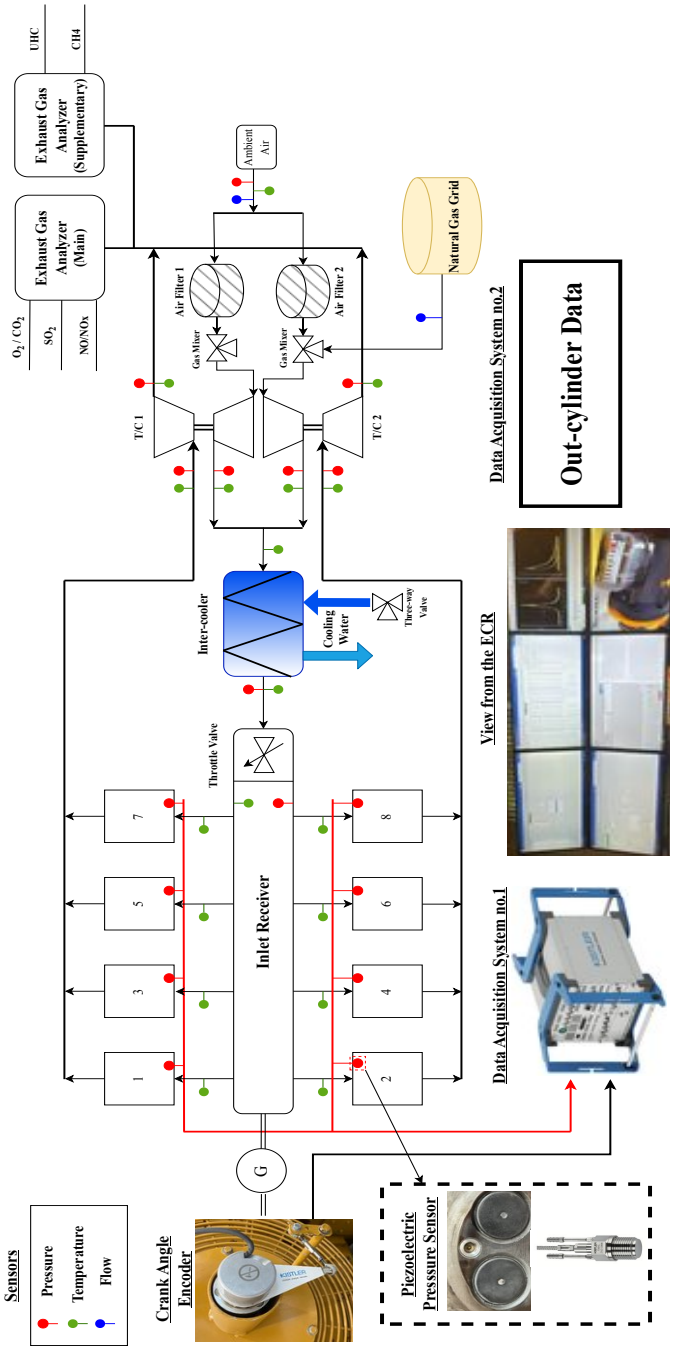

Figure 3.4: Schematic diagram of the experimental apparatus

Table 3.2: Main constituents in the NG and properties

Methane [Vol. %]	80.8
Ethane [Vol. %]	3.18
Propane [Vol. %]	0.71
Nitrogen [Vol. %]	13.1
CO_2 [Vol. %]	1.69
Density at 25 °C [kg/m^3]	0.77
Lower calorific value [MJ/kg]	38.12
Wobbe-index [MJ/m^2]	39.94
Methane number [-]	83

and total UHC emissions. This experimental campaign involves 26 operating points, including load, air excess ratio (λ), spark timing (ST) and intake air temperature sweeps, as shown in Table 3.4. Insights from recent optical access studies with LBSI engines are used to inform a phase-resolved analysis of combustion behavior, distinguishing the employed combustion diagnostic analysis. Pressure traces were recorded for the same cylinders over 400 consecutive cycles at each operating point and load levels were kept consistent for the sweeps with the preceding study in order to facilitate meaningful comparisons if required.

The difference in the number of recorded cycles between the two experimental campaigns arises from a statistical analysis conducted to determine the optimal number of cycles required to obtain a representative pressure trace for heat release rate (HRR) analysis, which is strongly influenced by the specific engine characteristics [270]. To establish this number, this research applied the method proposed by Maurya [271] by conducting an additional measurement campaign involving numerous consecutive cycles at several operating conditions indicated that averaging over 400 cycles can provide a suitable balance between data processing efficiency and accuracy. Fig. 3.5 shows the maximum standard deviation observed of one operating condition for different averaging number across all cylinders. This deviation on the y-axis represents the maximum difference between the minimum and maximum standard deviation in the envelope during combustion, as illustrated in the sub-figure within Fig. 3.5. A subplot in the figure demonstrates the variation in the pressure envelope when using a different number of averaged cycles for cylinder 7. All cylinders exhibit a maximum standard deviation below 1 bar, with 400 as the averaging number.

Additionally, the estimated values of key parameters, such as air excess ratio, emissions metrics, and heat release characteristics, are crucial for both diagnostic analysis and subsequent modeling studies, including computational fluid dynamics simulations. To ensure reliability in these parameters up to a certain confidence interval, this research adopts the uncertainty quantification methodology proposed by Gainey et al.[272] over the uncertainties of the measured parameters. Section A.4 provides more details regarding the methodology followed to quantify the uncertainties in combustion and performance characteristics in the LBSI engine testbed.

Table 3.3: Engine test conditions for stability analysis (EC I)

Sweep	Case	Gen. Power [kWe]	Fuel flow [m3/h]	Air Excess Ratio [-]	Spark Timing [° bTDC]
Load	1	100	54.49	1.35	20
	2	200	81.45	1.53	20
	3	300	108.33	1.55	20
	4	400	137.08	1.56	20
	5	450	151.08	1.57	20
Equivalence Ratio	6	200	80.17	1.24	20
	7	200	80.31	1.37	20
	8	200	81.14	1.44	20
	9	200	81.47	1.47	20
	10	200	84.95	1.59	20
	11	200	89.67	1.65	20
	12	200	95.09	1.71	20
	13	200	102.52	1.87	20
Spark Timing	14	200	87.58	1.53	16
	15	200	84.82	1.53	18
	16	200	81.54	1.54	22
	17	200	80.38	1.54	24
	18	200	79.46	1.53	26

3.3 STABILITY ANALYSIS

High cycle-to-cycle variation (CCV) and knocking present persistent limitation to efficiency and power density in HD SI engines [20]. Fig. 3.6 illustrates the typical constraints induced by knocking and poor combustion performance across air excess ratios and load [273]. Therefore, while a common strategy to mitigate knocking and enhance emission performance of these engines is to dilute the mixture, i.e., LBSI concept, it comes in the expense of exacerbating combustion behavior to a point of very low efficiency levels and elevated emissions of unburned hydrocarbons (UHC) [164]. Slower flame speeds due to dilution, along with greater flame travel distances in larger bores of HD engines, significantly narrows the engine's stable operating range [41, 274]. Since LBSI engines are primarily designed to operate under lean mixtures, it is first important to examine their stability before addressing combustion dynamics extensively. This section investigates in-cylinder pressure traces from multiple consecutive cycles to evaluate CCV and their influence on performance characteristics in the LBSI engine testbed fueled by NG. By further analyzing the effects of air excess ratio and spark timing, the objective is to identify the stability zones of a typical LBSI engine and to establish a stability threshold which can serve as a reference for the subsequent analysis.

Fig. 3.7 shows the pressure traces at 400 kWe, with Fig. 3.8 also presenting the corresponding mass-fraction-burned (MFB) trajectories for the same operating point.

Table 3.4: Engine test conditions for combustion characteristics (EC II)

Sweep	Case	Gen. Power [kWe]	Fuel flow [m3/h]	Air Excess ratio [-]	MAP [bar]	MAT [K]	ST [°bTDC]
Load	1	101	55.23	1.43	0.703	312.6	20
	2	200	83.82	1.57	1.118	312.0	20
	3	300	111.16	1.60	1.483	311.4	20
	4	400	138.99	1.58	1.858	310.4	20
	5	432	148.24	1.57	1.989	310.2	20
Air excess ratio	6	201	79.96	1.25	0.911	311.3	20
	7	200	80.11	1.38	0.979	314.7	20
	8	200	80.97	1.45	1.025	312.1	20
	9	200	81.92	1.50	1.060	312.3	20
	10	200	85.16	1.59	1.155	311.8	20
	11	200	89.70	1.65	1.254	312.3	20
	12	200	96.44	1.71	1.376	313.4	20
	13	200	100.26	1.77	1.430	311.6	20
Spark timing	14	200	79.30	1.53	1.048	312.0	26
	15	200	80.33	1.54	1.071	314.6	24
	16	200	81.49	1.54	1.085	314.2	22
	17	200	83.44	1.53	1.102	312.2	19
	18	200	84.77	1.53	1.121	312.5	18
	19	200	86.24	1.53	1.145	313.8	17
Intake Temperature	20	200	84.45	1.60	1.193	335.9	20
	21	200	83.68	1.57	1.159	330.8	20
	22	200	83.49	1.56	1.146	327.0	20
	23	200	83.09	1.55	1.122	320.6	20
	24	200	82.88	1.53	1.101	314.6	20
	25	200	82.39	1.51	1.074	308.2	20
	26	200	82.26	1.50	1.064	305.4	20

The engine operates with minor positive valve overlap, and limited scavenging effectiveness leads to retention of residuals. Higher residual gas ratios at lean operation are expected to reduce CCV by boosting flame propagation since they decrease the enleanment and increase intake temperatures. The cycles highlighted in red correspond to the lowest IMEP. While these might be mistaken for partial-burn cycles when viewed solely on the pressure-volume diagram, the heat release analysis reveal that they are instead characterized by markedly delayed combustion phasing. This late phasing reduces thermodynamic efficiency and work output [275]. Consequently, these are designated as late-burning cycles rather than partial burns, since their total MFB at end of combustion remains above the 90% threshold used in this chapter to classify partial burning. Further details on the partial burning and stability methodology are provided in Section A.5 and [234]. A higher incidence of late-burning cycles at a given operating point deteriorates efficiency and elevates carbon monoxide (CO) and unburned hydrocarbon (UHC) emissions due to lower

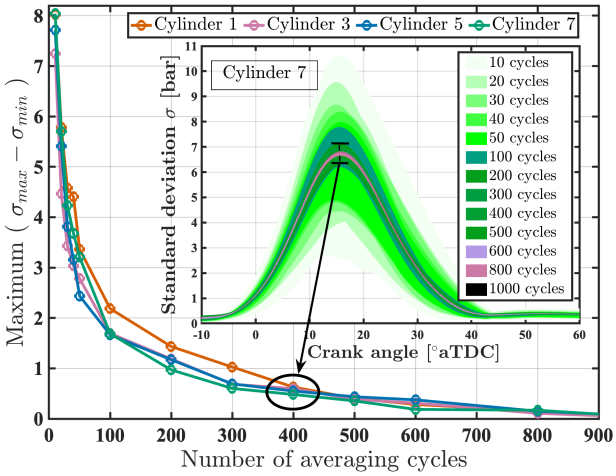

Figure 3.5: Pressure standard deviation vs. averaging cycles

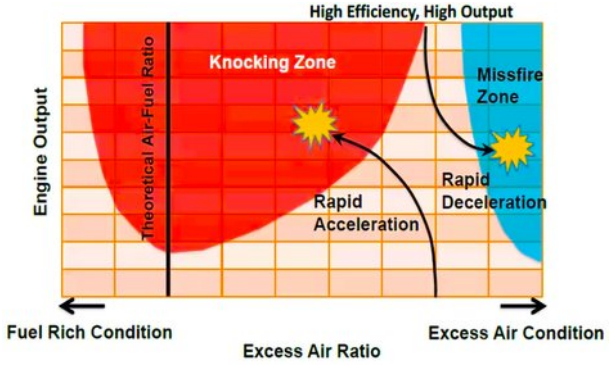

Figure 3.6: Knock and combustion-stability limits in flame-propagation concepts [273]

combustion temperatures. This trend is corroborated by exhaust-species analysis discussed in Section 3.4, where more resolved speciation enables a more reliable assessment of combustion efficiency.

Defining stability zones requires linking cyclic variation to performance. Fig. 3.9 demonstrates a strong inverse relationship between BTE and COV_{IMEP} across the dilution sweep. Since CCV in this campaign appeared less sensitive to ignition timing, the λ sweep was used to delineate stability regimes. Guided by the CCV behavior along the partial burning methodology, this research establishes two thresholds that divide engine stability into three zones:

1. **Stable Combustion Zone:** Characterized by very low levels of COV_{IMEP} and high levels of BTE, indicating an efficient engine operation.

2. **Transition Zone:** Marked by an increase in late-burning cycles, suggesting the onset of combustion instability.

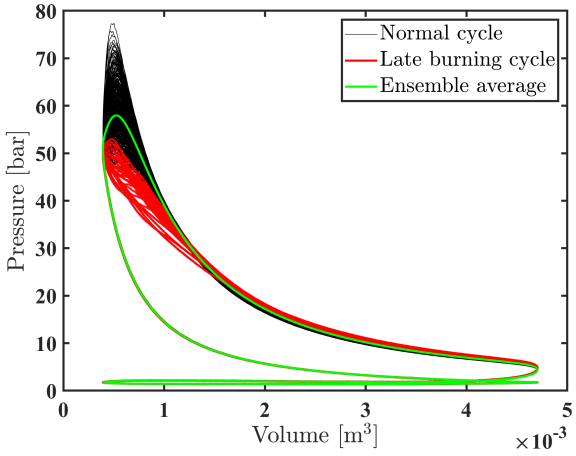

Figure 3.7: p-V diagram at 400 kWe (cycle variation)

3. **Poor Combustion Zone:** Defined by the occurrence of partial-burning cycles, which significantly deteriorate efficiency and stability.

In this dataset, the shift from $\lambda \approx 1.53$ to 1.59 marks entry into the transition zone, evidenced by intensified late burning and simultaneous significant slope changes: COV_{IMEP} rise more steeply while BTE falls more steeply. A further increase from $\lambda \approx 1.59$ to 1.65 introduces the first partial-burning cycles, establishing the second threshold as it further reinforces the increasing and decreasing slopes in COV_{IMEP} and BTE, respectively. Consistent with SI practice, the transition boundary coincides with COV_{IMEP} exceeding about 3%, while fully unstable operation with partial burns appears near 6% in this engine. In the leanest case, COV_{IMEP} peaked around 14% without, however, exhibiting any misfiring cycle.

3.4 EXPLORING THE IMPACT OF BOWL-IN AND SQUISH COMBUSTION ON ENGINE PERFORMANCE

The distinct flow field generated by diesel-derived bowl-in piston geometries in NG SI engines induces high turbulence that enables lean-burn operation at adequate burn rates. Beyond turbulence, the squish region produces a characteristic two-stage combustion sequence: an initial, rapid burn concentrated in the bowl, followed by a slower flame propagation phase in the squish. This dual-phase behavior contrasts with conventional SI chambers with flat pistons and pent-roof cylinder heads, where combustion is typically captured by a single main propagation phase [248, 276]. This behavior makes this LBSI concept highly sensitive to combustion phasing due to the existence of the second later combustion stage [277]. The fuel distribution across the two combustion stages influences the combustion stability and overall performance of the engine [278]. For instance, the typical effect of advancing ignition timing in the combustion phasing on efficiency and emissions can differ from that of conventional engines [20]. Advanced spark timing can deteriorate combustion and emissions

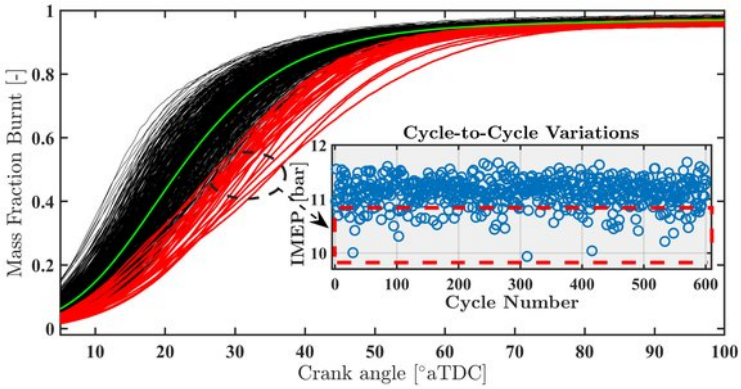

Figure 3.8: Mass fraction burnt variation at 400 kWe load

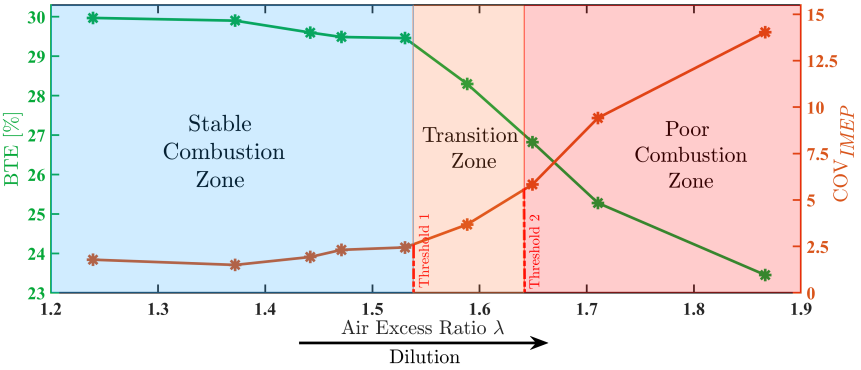

Figure 3.9: Combustion stability zones

performance in this engine type due to unfavorable conditions for the second squish combustion phase [279, 280]. A rise in the amount of fuel combusting in this phase can therefore overturn the benefit of the fast first combustion stage and result in reduced overall efficiency, leading to elevated UHC emissions [281]. Moreover, the combination of higher turbulence and prolonged combustion promote heat transfer processes in the cylinder and can therefore deteriorate engine efficiency even further. Limited studies have explored the interplay between distinct combustion phases and emissions—particularly methane and total UHC—which are of growing environmental concern. Methane slip, in particular, is now recognized as a critical challenge for marine gas engines [282, 283], but available data for large-scale SI concepts remain limited [283].

This section aims at addressing these gaps by analyzing new multi-cylinder experimental data (EC II) and phase-resolved combustion analysis from a 500 kWe NG LBSI marine engine featuring diesel-based geometry with a flat cylinder head and a hemispherical bowl-in piston. It examines the relationship between distinct combustion phases—bowl-in and squish—and both efficiency and emissions,

including methane, to better understand the fundamentals of this process in larger-scale multicylinder engines. The influence of key parameters—air excess ratio, spark timing, and intake air temperature—on combustion stages, efficiency, and emissions is systematically explored. The main objective is to provide deeper insights into the combustion and emissions performance of the diesel-adaptable LBSI concept for marine applications and to explore potential optimization strategies. Ultimately, these findings can support the marine sector's transition from petroleum-based fuels toward less carbon-intensive alternatives, such as methanol or ammonia, by focusing on the research and development of such dedicated engine conversion strategies for emerging sustainable fuels.

3.4.1 *Combustion staging methodology for LBSI engines*

The distinct combustion behavior of this engine strategy, combined with the research's focus on understanding the influence of combustion phasing on engine performance, necessitates a well-defined methodology for characterizing combustion phasing. Fig. 3.10 illustrates the implemented combustion staging framework, highlighting the defined combustion phases through various curves, including the aHRR profile and the in-cylinder pressure signal. While conventional SI engines typically employ CA05 or CA10 to quantify ignition lag or kernel development phase, recent studies suggest CA01 may be more accurate for representing the start of combustion [241, 279]. Nevertheless, given the inherent uncertainties in early combustion detection, this chapter will adhere to CA10 as the threshold to marking the flame development phase end, and thus the start of the bowl-in stage. CA10 is selected over CA05 for two main reasons: 1) CA10 is widely used as the indicator for the start of the combustion in conventional SI engines, which aligns with the start of the main bowl-in combustion phase in this LBSI concept; and 2) CA10 is less sensitive to aHRR signal noise and better centered with the first inflection point in the aHRR profile [235].

The transitional point between bowl-in and squish combustion phases follows the established methodology of Liu et al. [279] indicated by the second inflection point in the aHRR profile in Fig. 3.10, i.e., root of the second derivative of the aHRR curve. The use of the second aHRR inflection point to denote combustion phasing transition is based on correlations established in prior optical diagnostic studies of similar chamber geometries. While this approach provides a practical framework for phase identification in such engine strategies, the absence of in-cylinder visualization in the current testbed limits the correct establishment of such transition points and represents an approximation due to potential overlap between combustion stages. CA95 is finally used to identify the end of the squish combustion phase. Three distinct combustion phases are, consequently, defined:

1. **Phase I (Flame development):** Spanning from ST to CA10, including ignition lag.

2. **Phase II (Bowl-in combustion):** Extending from CA10 to the second aHRR inflection point, characterizing the rapid flame propagation stage within the bowl region.

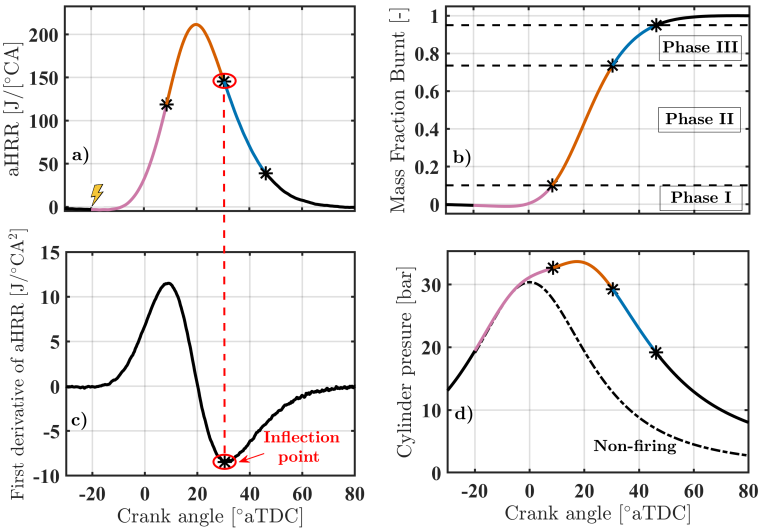

Figure 3.10: Definition of combustion phases for the converted NG-SI used in this dissertation

3. **Phase III (Squish combustion):** Covering the interval from Phase II conclusion to CA95, defining the slower flame propagation within the squish region.

Combustion duration (CD) is, therefore, quantified as the interval CA10-CA95. It should be noted that the MFB obtained using this methodology is correlated with the cumulated aHRR rather than the gHRR to avoid uncertainties associated with the heat transfer model.

3.4.2 *Combustion characteristics*

There were no indications of knock at any of the operating points tested during this experimental campaign. The primary challenge for these LBSI concepts remains combustion stability [262]. The lean capabilities of this engine technology also highlight its potential over conventional SI to utilize high specific heats in the chamber to improve efficiency closer to that of diesel engines.

Fig. 3.11 illustrates CCV of both in-pressure and heat release across all cylinders at 200 kWe nominal load, including the variations for the mean cylinder. All individual cylinders demonstrate good and relatively similar combustion stability, with COV values lower than 3%. It is evident that a number of individual cycles show delayed combustion phasing, which is expected in this type of LBSI engines. However, none of the average heat release profiles across the cylinders display such a distinct late combustion phase, with all average profiles coinciding well, indicating consistent combustion phasing across the cylinders. Cylinder 7, which experiences the fewest late-burning individual cycles, exhibits the highest work output and the lowest COV. Although the reduced occurrence of late burning may contribute to the slightly better

efficiency observed in cylinder 7, it is challenging to draw definitive conclusions due to the influence of gas path dynamics, which leads to different boundary conditions for each individual cylinder. As expected, Fig. 3.11(e) shows that the mean cylinder exhibits lower COV levels; notably, it also lacks a prominent late combustion phase across all cycles. This could be attributed to the fact that, at least for this operating point, the engine rarely encounters more than one cylinder exhibiting significantly delayed combustion simultaneously, resulting in effective averaging and balancing across the cylinders.

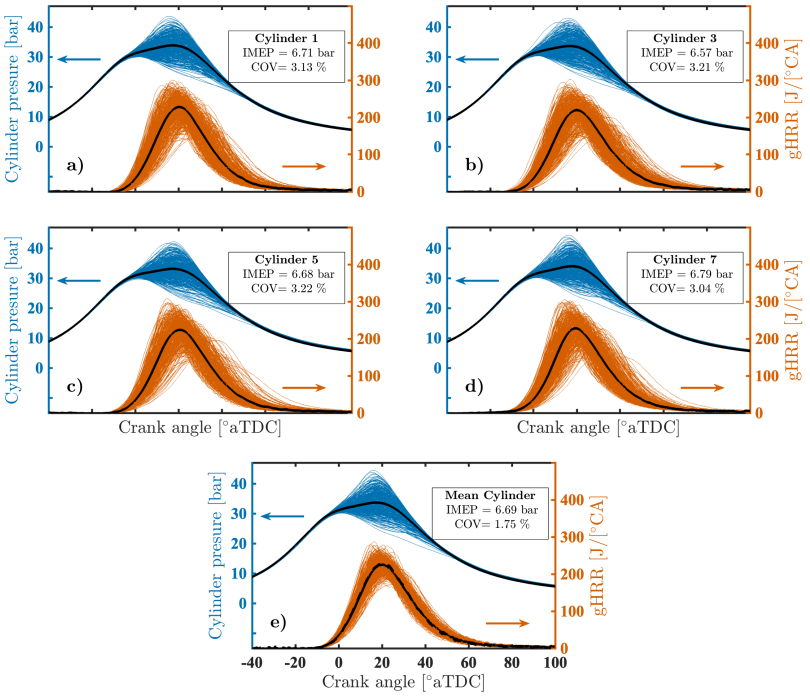

Figure 3.11: Cycle variation in pressure and HRR at 200 kWe (EC II)

Therefore, although the average HRRs demonstrate that late combustion is non-consistent across both cycles and cylinders, it is evident that relying solely on average values, either a mean cycle or a mean cylinder, can hide the real combustion profile that might occur in some cycles or cylinders. Nevertheless, average profiles still offer valuable insights into the overall combustion characteristics of the engine. While this chapter primarily focuses on comparing the mean heat release profile of the mean cylinder across different operating points, individual profiles should be analyzed when necessary to provide a more detailed understanding.

Combustion characteristics can vary significantly across different load points, especially in throttle-valve controlled systems like this particular concept. Fig. 3.12 presents in-cylinder pressure, heat release, bulk gas temperature, and mass fraction burnt across the load sweep. As expected, both pressure and heat release increase with load, with combustion phasing remaining consistent across most load points,

except for the lowest load of 100 kWe, which shows advanced combustion. The MFB plot in Fig. 3.12(c) demonstrates this advancement at the lowest load, which can be attributed to greater flame propagation speeds resulting from richer mixtures used as nominal conditions at this load to address low-load combustion stability challenges [244].

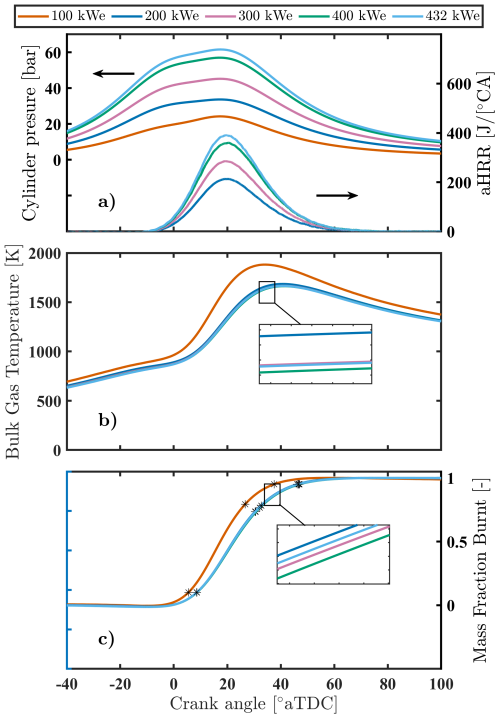

Figure 3.12: Load effects on combustion characteristics

These low-load richer mixtures also lead to the highest bulk gas temperatures in the cylinder, as seen in Fig. 3.12(b), which can be confirmed by out-cylinder temperature measurements across all cylinders and the manifold. This subsequently results in advanced phasing for the whole combustion process and all individual defined combustion stages at 100 kWe load. Fig. 3.12(c) highlights the transition points between the defined combustion stages. The consistent advancement of both bowl-in and squish combustion stages contrasts with the anticipated trend of squish combustion deterioration observed with advanced combustion phasing in converted SI engines. However, at least 20% of the fuel combusted during the slower squish combustion stage across the lean operating load points. Minimizing this phenomenon is crucial, as it significantly impacts both thermodynamic and combustion efficiency in these engine concepts. Additionally, the phase markers indicate consistent combustion phasing across all load points operating under similar dilution levels, with the exception of a slight delay in the combustion duration at the lowest load of 200 kWe.

3.4.3 *Performance and emissions characteristics*

Conducting a comprehensive combustion analysis of multicylinder engines necessitates a thorough examination of the energy balance. This aspect is critical for the current engine concept, as it can provide insights into how distinct combustion stages influence overall energy distribution. Analyzing the energy share at the baseline load points is important to better understand the effects of different parameters and combustion stages on overall engine performance. In this research, the energy balance for the representative mean cylinder is analyzed across all operating points. A Sankey diagram, as illustrated in Fig. 3.13 for the 200 kWe operating load point, offers a visual representation of this energy balance and its key components. Fuel slip in the exhaust, heat transfer through the combustion chamber boundaries, energy in the exhaust gases, pumping, and friction losses are the typical components of energy losses in a reciprocating ICE.

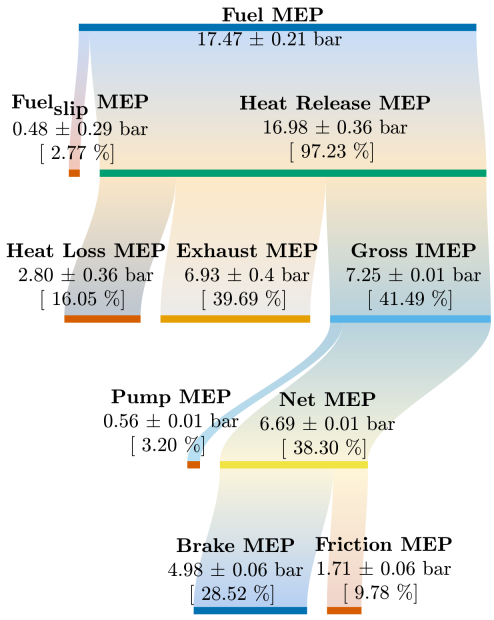

Figure 3.13: Sankey diagram of energy balance at 200 kWe (mean cylinder)

Fig. 3.14 collects the key fuel energy components across operating points and presents the energy distribution for the tested load sweep. Friction decreases with increasing load, while the relative share of friction losses in relation to the fuel energy input also diminishes, since the engine speed remains constant. Pumping losses follow a similar trend, decreasing at higher loads, which is typical for such throttle valve-controlled engines, particularly those equipped with a turbocharging system which are more efficient at higher loads, utilizing some exhaust gas energy to lower pumping losses. A decreasing pattern is also observed for heat losses from the combustion chamber boundaries as load increases. The higher level of

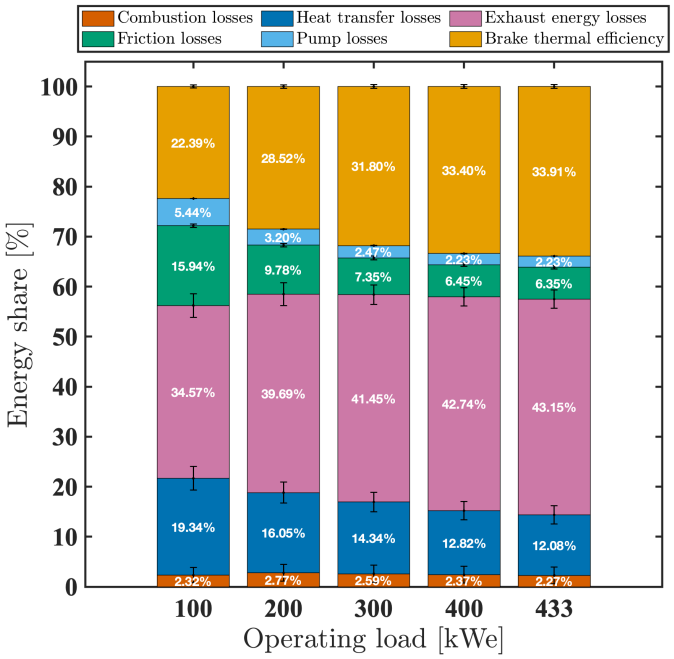

Figure 3.14: Load effects on energy share

heat losses at the lowest load can be attributed to the higher bulk gas temperature. Although bulk gas temperatures are relatively higher at the highest load, as shown in the zoomed section of Fig. 3.12(b), leading to greater cumulative heat transfer, the relative heat transfer losses decrease when compared to the increasing energy input. This trend was also supported by the calibrated heat loss model coefficient C_0 [235]. Exhaust gas losses, on the other hand, increase at higher loads due to the greater enthalpy associated with the increased mass flow rates and temperature of exhaust gases due to later combustion phasing.

Methane emissions remain one of the main challenges in such engine concepts due to both its impact on both the environment and the engine performance. In this experiment, energy losses due to unburned fuel, or fuel slip, remain fairly constant across all operating points, ranging from 2.26% to 2.76% $\pm$1.67%, with the lower fuel slip occurring at the highest load point. The slightly better combustion performance might be attributed to a better combination of thermal conditions and oxygen quantity for the conversion of the fuel. However, drawing definitive conclusions regarding the load effect is challenging when considering the associated uncertainty levels. Additionally, the relatively consistent levels of fuel slip across all loads can be attributed to trapped fuel in the crevices, while throttling and the controlled air excess ratio across loads are also expected to play a role. Consequently, these trends in energy distribution result in a typical increase in overall engine efficiency as the load increases Specifically, BTE increases 22.39% $\pm$0.33% at the lowest load point (100 kWe) to 33.91% $\pm$0.36% at the highest load point (432 kWe).

Fig. 3.15 illustrates the emission characteristics of the engine across the tested load sweep. Among the emissions considered, NO_x is the only regulated emission for maritime engines by the International Maritime Organization (IMO) [284], while methane regulations are still under development [283]. The rated amount of the IMO Tier III standards NO_x emissions for this engine is 2.08 g/kWh, which would correspond to the weighted average over a standardized test cycle, e.g., D2 for marine generator sets. This research presents NO_x values for each individual load point tested and indicate this Tier III standard for reference. To this end, it should be noted that direct comparison of single-point emissions to the Tier III standard may be misleading when the compliance of the engine is assessed. When considering the weighted average of the tested operating points across the load sweep, this engine meets Tier III NO_x requirements under nominal conditions. However, at the lowest load, NO_x emissions reached 2.79 $\pm$0.19% g/kWh, exceeding the single-point Tier III value, while all other tested loads remained below the standard.

The elevated NO_x at the lowest load is attributed to the use of a relatively richer mixture, which increases combustion temperatures, as reflected in Fig. 3.12(b). Low loads, while enriched, also resulted in the poorest combustion efficiency and the highest emissions of CO, CH_4, and total UHC. Clearly, this cannot be interpreted as a mixture richness' effect. The deliberate throttling strategy limits the tendency toward lean and unstable combustion at low loads, thereby reducing the poor combustion penalty of light-load operation. This demonstrates the effectiveness of lean-burn operation for controlling NO_x. Across the remaining load points, NO_x emissions remained relatively stable but showed a slight upward trend with increasing load from 200 to 432 kWe. Since combustion phasing, air excess ratio, and bulk gas temperatures were similar across this range, the observed increase is likely due to higher in-cylinder pressures and consequently densities at elevated loads, resulting in increased oxygen and nitrogen density, which can promote additional NO_x formation.

Although slight variations in air excess ratio were present across load points, the effect of load on emissions is clear: increasing load improves combustion efficiency, albeit with a modest rise in NO_x formation. Methane slip aligned well with the expected range for LBSI marine engines [283]. Among current marine engine strategies using natural gas, LBSI engines—most commonly with pre-chamber designs [285]—and low-pressure dual-fuel (LPDF) engines are prominent. Notably, the open-chamber LBSI configuration employed here, despite its simplicity, achieves methane emission levels comparable to more advanced pre-chamber SI engines. This finding is significant for retrofitting existing diesel engines to SI operation, where design simplicity and cost-effectiveness are priorities. At high loads (400 and 432 kWe), methane emissions were recorded 3.21 $\pm$0.13% and 3.01 $\pm$0.12% g/kWh, respectively, which falls within the typical 3-5 g/kWh range for pre-chamber LBSI engines and the broader 3-10 g/kWh range for LPDF engines [283]. At lower loads (100, 200, and 300 kWe), methane emissions ranged from 3.69 $\pm$0.15% to 4.59 $\pm$0.20% g/kWh, again within the anticipated 3.3-7.2 g/kWh range, and well below the much higher values occasionally reported for these engine types at very low loads. These results highlight the capability of open-chamber lean-burn engines to achieve low NO_x with acceptable combustion performance and methane slip at low loads.

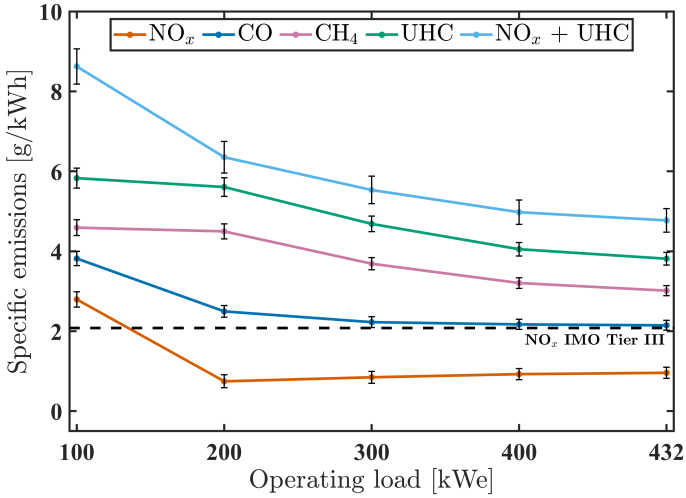

Figure 3.15: Load effects on emissions

Furthermore, the sum of of UHC and NO_x emissions—a metric often referenced in emissions legislation for non-road applications [245, 286] but not yet implemented in marine regulations—also exhibits a clear decreasing trend with increasing load. Future regulatory frameworks should incorporate holistic assessment methods that enable fair comparison of different engine strategies, including LBSI and DF engines, and consider not only NO_x and methane but also relevant pollutants such as soot, which is particularly relevant for diesel and DF engines. Such comprehensive evaluations will be essential for appropriately assessing and encouraging the adoption of alternative fuel engine concepts in the maritime sector, including simplified retrofitting solutions based on single-fuel LBSI strategies.

3.4.4 *Air excess ratio effects*

The high-turbulence induced by the distinct combustion chamber geometry offers advantages over conventional SI engines due to its ability to operate with high levels of dilution. This capability can simultaneously reduce NO_x emissions due to lower temperatures while enhancing combustion efficiency, i.e., lower CO and UHC emissions, due to greater oxygen availability. However, there is a threshold beyond which excessive dilution leads to very low temperatures, negatively impacting combustion efficiency, as discussed in Section 3.3. The distribution of fuel burned across the different combustion stages influences the overall combustion efficiency and emissions characteristics. During EC II, the air excess ratio was swept from 1.25 to 1.77 at constant engine speed, generator load, and spark timing.

Fig. 3.16 illustrates the mass fraction burnt across the operating points during the air excess ratio sweep, with Table 3.5 presenting the quantified combustion characteristics of the defined combustion stages. As the engine increases fuel mass flow to compensate the apparent decrease in IMEP with leaner mixtures, it also

increases the air mass flow to maintain the requested air excess ratio, which results in greater mass flow through the engine and slight changes in boundary conditions. These adjustments introduce some complexities when comparing performance across different air excess ratios. The same considerations apply to all parametric sweeps similarly conducted. However, adjustments do not diminish the research's ability to derive valuable insights into the impact of different parameters, such as dilution, on combustion characteristics and engine performance.

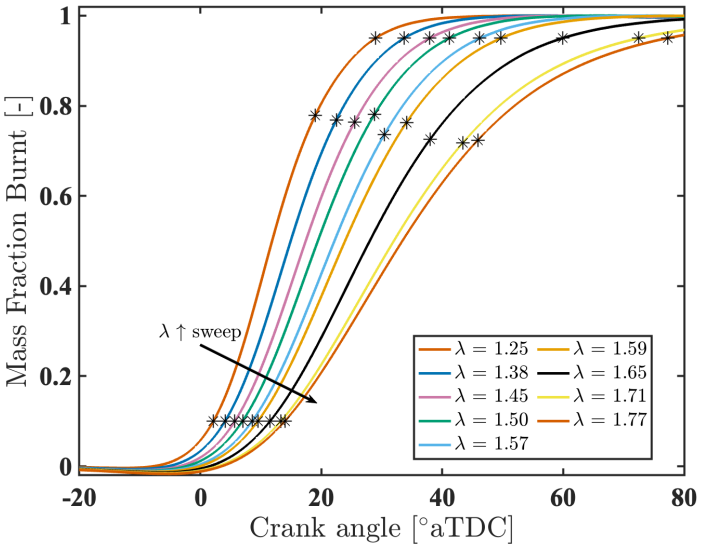

Figure 3.16: Air excess ratio effects on MFB

An extension in combustion duration is evident across all defined combustion phases during the dilution sweep, consistent with trends observed in conventional SI engines, due to reduced flame speed associated with leaner mixtures. Flame development phase I consistently increased across the sweep from 23.1 to 31.2°CA, as it is strongly influenced by laminar flame speed, a property highly sensitive to air-to-fuel ratios. The observed duration of flame development was longer than that reported in experiments with combustion chambers of similar geometric characteristics [245]. This can be attributed to the lower methane ratio in the used NG, as well as potential differences in ignition system configurations. Regarding the main combustion phase, the flame propagated more rapidly during both main combustion phases (Phases II and III) in richer mixtures, contrary to the anticipated slowing effect expected due to the larger surface-to-volume ratio in the squish region, as observed in previous experimental studies, e.g., in [280]. Diluting the mixture from λ of 1.25 to 1.77 increased the duration of Phase II from 16.9°CA to 31.9°CA, representing an increase of 89%, and Phase III from 10°CA to 31.4°CA, an increase of 214%. Combustion duration, therefore, showed a clear increasing trending with leaner mixtures, increasing from 26.9°CA at λ of 1.25 to 63.3°CA at λ of 1.77. This trend in overall combustion phasing and duration, including

Table 3.5: Combustion characteristics by stage across air excess ratio sweep

Air excess λ [-]	Flame Development Phase I [°CA]	Bowl-in Phase II			Squish Phase III			CD [°CA]
		CAD [°CA]	Fuel burnt [%]	Average temperature [K]	CAD [°CA]	Fuel burnt [%]	Average temperature [K]	
1.25	23.1	16.9	67.9%	1520	10	17.2%	2000	26.9
1.38	24.6	18.4	66.8%	1455	11.2	18.1%	1882	29.6
1.45	26.2	19.8	66.4%	1404	12.4	18.6%	1793	32.2
1.5	27.4	21.8	68.0%	1388	12.4	16.9%	1744	34.2
1.57	29.1	21.8	63.5%	1324	15.8	21.4%	1669	37.6
1.59	29.3	24.6	66.3%	1315	15.6	18.7%	1626	40.2
1.65	31.1	26.5	62.6%	1250	21.9	22.4%	1528	48.4
1.71	31	30.1	61.8%	1203	29.1	23.2%	1434	59.2
1.77	31.2	31.9	62.3%	1180	31.4	22.6%	1388	63.3

the individual squish combustion phase, demonstrates that enriching the mixture clearly outweighs the expected negative impact of the larger surface-to-volume ratio on the flame propagation in the squish region. The higher squish height in this engine's combustion chamber compared to the previous studies could explain the diminished effect of the surface-to-volume ratio on the flame speed in the squish region. The use of highly diluted and lower methane number NG in the experiments also plays a role in moderating flame propagation and extending it during the expansion phase. This results in flame propagating through the squish region at a later stage, where the surface-to-volume effect decreases. Interestingly, the sensitivity of the main combustion phase to air excess ratio in this engine is significantly higher than what is typically expected for a hemispherical piston bowl [245]. This is likely attributed to the distinct combustion chamber geometry in this setup, differing from this typical hemispherical shape featuring characteristics intermediate between a turbine bowl and a hemispherical design, with an extended squish area.

The amount of fuel burned across the two stages appears less sensitive to the dilution sweep tested compared to their phasing. While the trend is clear for the fuel distribution in the two phases from the richest to the leanest mixture, this trend is not consistent in the intermediate air excess ratios tested. A slight increase in the amount of fuel burned during the rapid combustion stage is even observed at some intermediate λ values compared to the richest mixture. It is difficult, however, to conclude that more fuel is actually consumed within the bowl for these leaner mixtures. Slower combustion rates associated with leaner mixtures can lead to greater overlap between the two distinct combustion stages, potentially causing a larger portion of the squish combustion heat release to be classified as part of the Phase II under the current methodology. Section 3.5 further elaborates on this matter. Nevertheless, it is clear that enriching in-cylinder mixture consistently improves combustion conditions for both phases. Richer mixtures, characterized by lower heat capacities, lead to more fuel being combusted faster, closer to TDC, and at higher temperatures, resulting in higher combustion and thermodynamic efficiency.

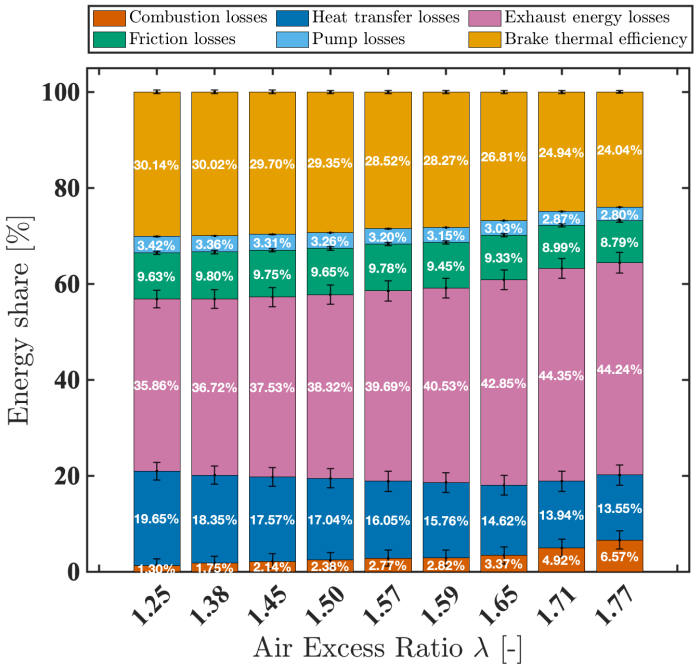

Figure 3.17: Air excess ratio effects on energy share

The efficiency improvements are corroborated by Fig. 3.17, which demonstrates a consistent improvement in combustion efficiency along the dilution sweep, as the fuel slip energy share decreased from 6.57% $\pm$1.95% at the leanest mixture to 1.30% $\pm$1.30% at the richest. Brake thermal efficiency followed a similar trend increasing by 25% across the whole enrichment sweep, despite the anticipated increase in heat losses, as friction and pumping losses remaining relatively constant across all tested air excess ratios. The improvement in efficiency could be anticipated even before conducting the energy analysis, as the engine's controller compensates for the lower IMEP in the cylinders by increasing fuel input to maintain the generator load. The lower IMEP is caused by the decrease in thermodynamic efficiency from the more delayed combustion phasing.

Concerning emissions, Fig. 3.18 shows an inverse relationship between NO_x and UHC emissions, with enrichment lowering UHC but elevating NO_x, and leaning doing the opposite. At the three richest settings, NO_x exceeded the IMO Tier III limit despite achieving the lowest CH_4, total UHC, and CO levels. Within approximately $\lambda \approx 1.50 - 1.60$, the response to dilution is less sensitive, offering a relatively stable trade-off between NO_x and combustion efficiency. This is corroborated by the sum of NO_x and UHC minimized in this band. Beyond this range, additional enrichment leads to a sharp rise in NO_x, whereas further leaning past this band induces significant combustion inefficiency leading to elevated UHC. The observed sensitivities and the optimal air excess ratio band are consistent with prior experiments comparing different combustion chambers for gas engines [245]. Consequently, for this load

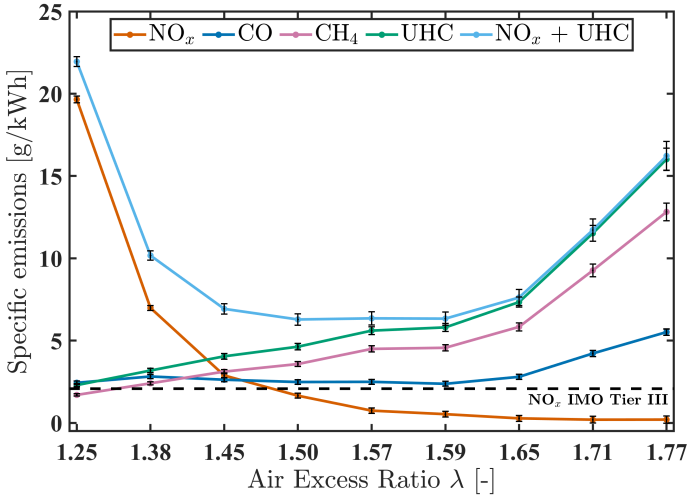

Figure 3.18: Air excess ratio effects on emissions

point, λ between 1.45 and 1.60 provides a relatively good balance between efficiency and NO_x, maintaining the sum of NO_x and UHC emissions below 6.5 g/kWh. However, in light of the stability analysis in Section 3.3, operating above $\lambda \approx 1.53$ falls into the transition zone, with an increasing prevalence of late-burning cycles. The concurrent rise in CH_4 and UHC confirms the influence of late burning on emission formation. Therefore, the practical operating window narrows to approximately $\lambda = 1.45 - 1.53$ at this condition. Although other boundary conditions with different control parameters (e.g., load, speed, ignition timing) may shift the exact optimal ranges for control parameters, the analysis clearly illustrates how narrow these ranges typically are for LBSI concepts to satisfy emissions requirements like NO_x Tier III while sustaining robust combustion and high efficiency. Additionally, given the importance of methane emissions, these trends reinforce the need for comprehensive standards that consider multiple pollutants jointly in marine engines.

3.4.5 *Spark timing effects*

Spark timing has always been a critical input parameter for controlling combustion phasing, efficiency, and emissions in SI engines. For this specific engine concept, spark timing is expected to have a distinct impact compared to conventional SI engines, influencing the different combustion phases and, consequently, overall engine performance. This subsection examines the effect of ignition timing on combustion characteristics and engine performance under constant engine speed, generator load, and air excess ratio.

Fig. 3.19 illustrates the mass fraction burned across the operating points during the spark timing sweep, with Table 3.6 quantifying the associated combustion characteristics. Unlike the effect of air excess ratio, spark timing sweep showed varying impacts across the defined combustion phases. Delayed spark timing clearly delayed

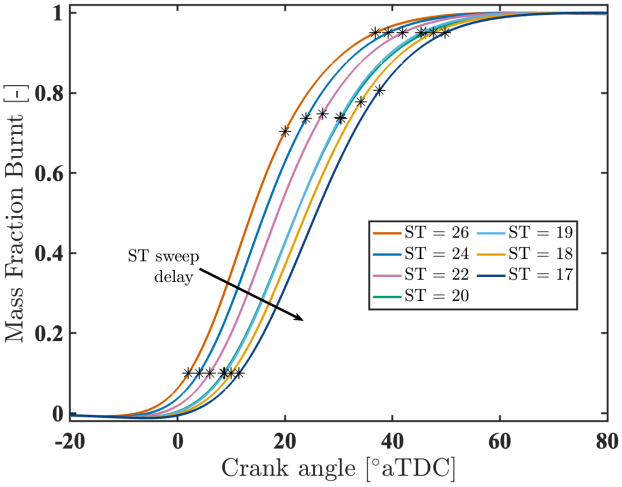

Figure 3.19: Spark timing effects on MFB

flame development and bowl-in phases, aligning with the anticipated behavior in conventional SI engines. The main combustion phase and total combustion duration exhibited a clear and consistent increase with delayed spark timing, rising from 18°CA to 26.2°CA and 34.8°CA to 38.4°CA, respectively. On the other hand, the squish combustion phase (Phase III) displayed an opposite trend advancing from 16.8°CA to 12.2°CA. Notably, the operating point with spark timing at 20°CA bTDC appears as a slight outlier in most observed trends, likely due to a slightly higher air excess ratio at this point. The offsetting effect of delayed spark timing on the total combustion duration by the enhanced squish phase is corroborated by Fig. 3.19, demonstrating a diminishing phase difference between different spark timing configurations in the squish phase. This behavior aligns with observations from previous optical studies of this type of SI strategy, highlighting minimal improvements in the squish region due to the counteracting higher surface-to-volume ratios with phasing advancements. While this effect can reduce or even reverse the benefits of spark timing advancement, as reported in earlier experimental studies, the slower squish combustion stage in this engine does not negate the benefits of spark advance. Advancing spark timing shifts most of combustion closer to TDC, enabling more fuel to be burned under thermodynamically favorable conditions, as evidenced by the CA50 advancement from 27.4 to 15.6 °CA aTDC during the ignition timing sweep, enhancing the pressure exerted during the early stage of the power stroke. The observed increase in the mass fraction burned during the rapid combustion phase (Phase II) with delayed spark timing, rising from 60.5% to 70.8%, likely suggests that delayed ignition prolongs combustion within the bowl-in and squish phases. This overlap complicates the attribution of fuel burned to each phase, as some of the heat release classified as bowl-in may in fact occur during the early squish phase period. Consequently, the redistribution of fuel burning between phases is not always clearly distinguished, and definitive trends are difficult to

establish based on pressure-derived data. Despite these complexities, the overall trend remains that later spark timing delayed overall combustion phasing, thereby deteriorating efficiency.

Table 3.6: Combustion characteristics by stage across ignition timing sweep

Spark timing ST [°CA bTDC]	Flame Development Phase I [°CA]	Bowl-in Phase II			Squish Phase III			CD [°CA]
		CAD [°CA]	Fuel burnt [%]	Average temperature [K]	CAD [°CA]	Fuel burnt [%]	Average temperature [K]	
26	22	18	60.5%	1361	16.8	24.6%	1691.4	34.8
24	24.5	19.9	63.5%	1376	15.3	21.4%	1675.6	35.2
22	26.2	21	64.7%	1362	14.9	20.2%	1661.3	35.9
20	29.1	21.8	63.5%	1335	15.8	21.4%	1620.3	37.6
19	28.9	21.5	63.8%	1331	15	21.1%	1646.0	36.5
18	29.6	24.1	67.9%	1335	13.5	17.2%	1639.7	37.6
17	31.8	26.2	70.8%	1348	12.2	14.3%	1624.1	38.4

Fig. 3.20 corroborates these phasing improvements illustrating the performance trend across the spark timing sweep. Despite the improvement in overall thermal efficiency of the engine, a 10% increase across the spark timing advancement sweep, there appears a consistent increase in combustion efficiency, rising from 97.14% at 26°CA bTDC to 97.62% $\pm$1.63% at 17°CA bTDC. It is challenging, however, to draw definitive conclusions regarding methane emissions improvement with spark timing delay with such minor differences, considering the varying mass flows and the inherent uncertainties in the measurement system. It is evident that spark timing influences combustion efficiency differently than air excess ratio. Within the range tested, spark timing demonstrated limited impact, with the generally anticipated benefits of advanced timing, even potentially deteriorating combustion efficiency. This behavior highlights the differences between this homogeneous LBSI strategy and conventional/pre-chamber SI systems. In conventional SI engines with flat piston geometries, advancing spark timing typically improves combustion efficiency by shifting combustion closer to TDC and more favorable thermodynamic conditions (until knock limit), as the absence of a squish phase eliminates sensitivity to late-stage flame propagation. The closer to TDC combustion, therefore, maximizes the pressure exerted on the piston during the power stroke. In contrast, pre-chamber SI systems, even when using similar chamber geometries as this LBSI concept, can mitigate squish region limitations through charge stratification. In such concept, fuel-richer mixtures near the spark plug enhance ignition energy transfer to the charge in the main chamber, while also reducing the amount of fuel present in the squish region. Given the critical importance of methane emissions in gas engines, these findings underscore the need for careful consideration of combustion phasing in the design and control strategies for such SI concepts.

Similar to the increasing λ trend, delayed spark timing led to higher exhaust gas energy share. This can be attributed to more delayed combustion phasing in both sweeps that result in hotter exhaust gases. This, in turn, slightly reduced pumping losses because of greater turbocharging power. Heat transfer processes exhibited minimal sensitivity, with a slight decrease observed as spark timing was

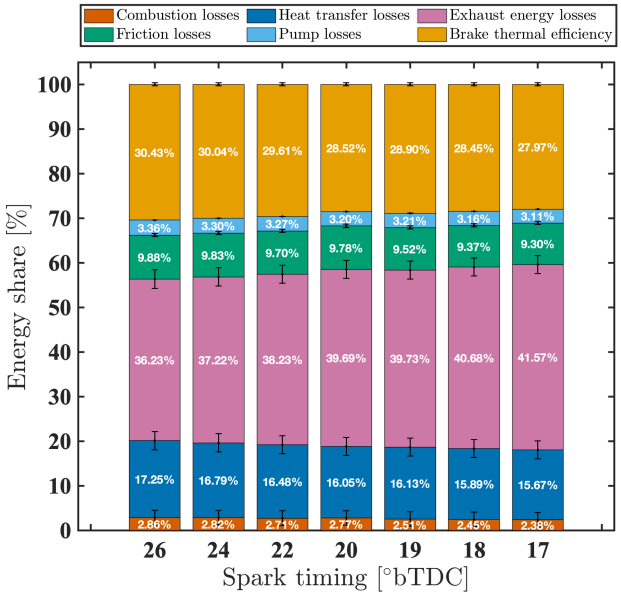

Figure 3.20: Spark timing effects on energy share

delayed due to lower maximum bulk gas temperatures. Therefore, although it is challenging to clearly determine the effect of spark timing in the engine performance characteristics, including combustion efficiency, due to different mass flows, the lower fuel slip energy share under these conditions suggest that delayed spark timing might slightly improve squish combustion phase, thereby improving overall combustion efficiency.

Fig. 3.21 illustrates the emissions characteristics across the spark timing sweep. All measured emissions decreased with delayed spark timing, with hydrocarbon related emissions aligning with the earlier discussion on improved combustion efficiency. This further highlights the distinct, and different from the conventional SI, sensitivity of this strategy to spark timing. Methane emissions decreased from 4.25 $\pm$0.23 to 3.84 $\pm$0.20 g/kWh, CO from 2.56 $\pm$0.14 to 2.18 $\pm$0.15 g/kWh, and total UHC emissions from 5.42 $\pm$0.18 to 4.92 $\pm$0.16 g/kWh. Additionally, all tested spark timings met the IMO Tier III standards for NO_x emissions except the most advanced setting at 26°CA bTDC. Delaying spark timing consistently reduced NO_x levels from 2.37 $\pm$0.15 to 0.59 $\pm$0.16 g/kWh, which can be attributed to the lower temperatures during the main combustion phases, as shown in Table 3.6. The critical metric of the sum of NO_x and UHC emissions clearly decreases with more delayed ignition timing. Interestingly, while the most advanced spark timing settings led to more advanced combustion phasing and higher brake thermal efficiency, they did not improve combustion efficiency but instead caused a decline. Therefore, an increase in BTE does not necessarily indicate improved combustion performance in these SI engines. This can be attributed to the deterioration of the squish phase at

advanced spark timings and the high sensitivity of combustion performance to this phase in such engines.

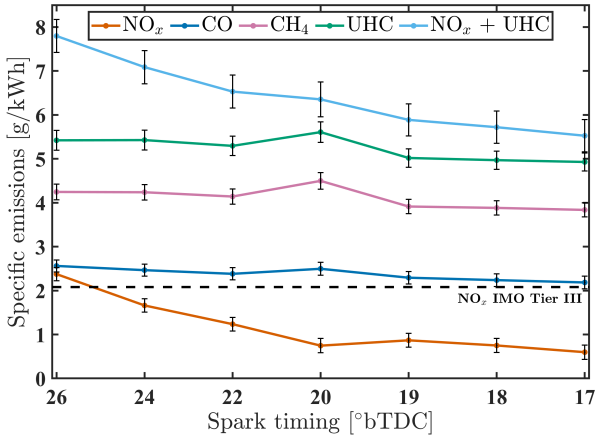

Figure 3.21: Spark timing effects on emissions

These results demonstrate that while richer mixtures enhanced combustion efficiency, advanced spark timing did not yield the same benefits in the squish phase. Despite both the most advanced spark timing (ST = 26°CA bTDC) and richest mixture ($\lambda \approx 1.25$) configurations resulting in flame reaching the squish region at similar timing, richer mixtures achieve superior flame propagation, with squish combustion phasing differing by over 10°CA between the two cases. This discrepancy arises from the limited effectiveness of turbulent kinetic energy (TKE) in the squish region, where flame's surface-to-volume ratio dominates over turbulence effects. Advanced spark timing enhances flame propagation in the bowl-in region, even under lean mixtures, by leveraging favorable thermodynamic conditions near TDC and elevated TKE induced by the combustion chamber geometry. While TKE partially compensates for lower laminar burning velocities under lean mixtures in the bowl-in region, its influence due to piston position diminishes in the squish region. Here, flame surface area becomes the critical factor. Richer (closer to stoichiometric) mixtures induce higher laminar burning velocities, develop larger flame surface areas, and enhance turbulence-aided flame speeds, enabling them to overcome the squish region's constraints more effectively than spark timing adjustments. Consequently, the interplay between the two control parameters is also expected to be very important for the optimization of combustion efficiency, and thus the UHC emissions including methane. Given the concerns surrounding methane, these findings underscore the need for a Design-of-Experiment (DOE) approach to systematically evaluate interactions between control parameters and optimize this SI engine concept [287].

3.4.6 *Phasing and engine performance*

Following the assessment of individual trends with both dilution and ignition timing (for the intake air temperature effects, the reader is referred to [235]), it is important to isolate the influence of combustion phasing metrics on key performance indicators across all tested operating points. Fig. 3.22 presents the trends of several engine performance metrics as functions of the inflection point—approximating the end of the bowl-in and the start of the squish phase—and the fuel burnt into ratio across these two phases. It should be noted that this figure is intended to illustrate general trends among various engine performance indicators, rather than to provide predictive relationships, since it is based on a limited number of discrete operating conditions.

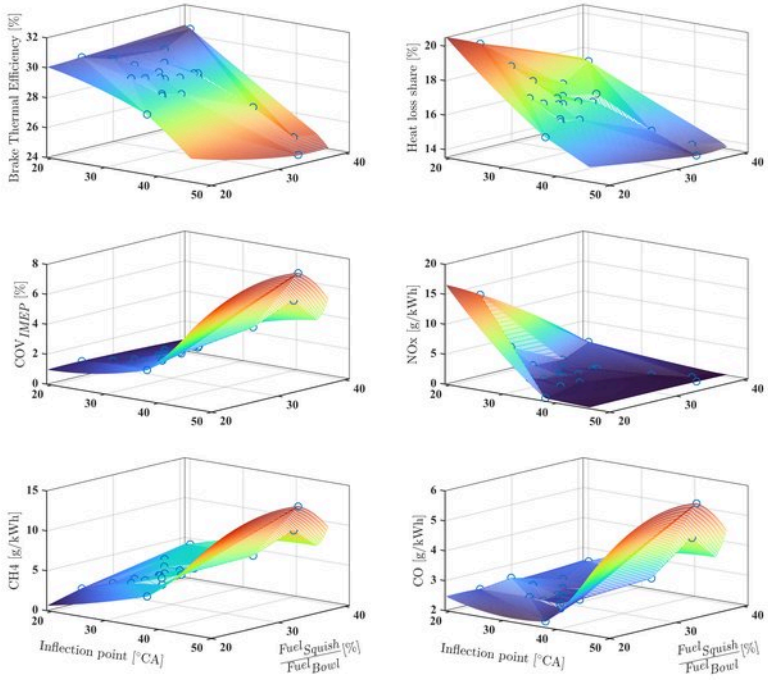

Figure 3.22: Fuel-burn ratio and inflection point vs. performance indicators

The summarized results clearly indicate that the inflection is a more critical influencing factor than the fuel burnt ratio for all performance indicators. This observation aligns with previous findings, as no distinct trend was found in fuel distribution across the two main combustion phases. This might be attributed to the overlapping phenomenon between the two stages. However, a certain influence can be observed, with lower fuel squish-to-bowl ratio leading to better combustion performance decreasing methane emissions while increasing heat losses and NO_x emissions. The effects in COV and BTE are less clear. On the contrary, the impact of the inflection point on all six performance indicators is quite clearer.

Advancing combustion in the squish region—characterized by an earlier inflection point—significantly enhances engine performance by reducing COV, increasing BTE, including combustion efficiency improvement. This led to lower methane and CO emissions at the expense of increased heat losses and NO_x emissions. The observed peak in heat losses and NO_x emissions at the minimum inflection point suggests that most of the fuel is consumed during Phase II, closer to TDC, resulting in elevated in-cylinder temperatures. This explains why COV, methane, and CO emissions reach their lower values under these conditions.

3.5 MULTI-STAGE WIEBE MODELING FOR COMBUSTION CHARACTERIZATION

To assist the combustion analysis for LBSI combustion, this research also develops a thermodynamic model employing multi-stage Wiebe formulations to simulate closed in-cylinder processes in the Caterpillar engine. This can be justified by the fact that beyond the provision of a computationally efficient thermodynamic tool, Wiebe functions can offer additional qualitative insights into the multi-stage combustion behavior in these engines. The parametric approach of simulating combustion with Wiebe may offer further guidance into the optimization of the performance and emissions across varying operating conditions. To this end, this modeling approach is coupled and developed alongside the experimental study of Section 3.4, with Chapter B providing the main information of the modeling development framework.

3.5.1 *Wiebe model development*

Previous studies have shown that standard single-Wiebe models cannot adequately capture the combustion profiles in this type of SI technology [288]. For example, advanced spark timing can lead to "dual-peak" HRR profiles due to slower flame propagation within squish regions, requiring a multiple-stage Wiebe formulation [289]. In such cases, even two-stage Wiebe formulations may prove insufficient, necessitating a third stage to capture late burning phenomena.

However, this "dual-peak" phenomenon was not observed in any tested operating condition for this particular NG-fueled LBSI engine, including the most advanced ignition timing and richest mixture cases [236]. This absence may be attributed to specific clearance volume characteristics influencing squish heights during expansion phases. Three alternative Wiebe formulations are explored in this dissertation:

- **Wiebe single mode**, using the straightforward single-stage Wiebe function for the whole combustion process, expressed in Eq. (B.1).
- **Wiebe double mode**, employing the double-stage Wiebe function, expressed in Eq. (B.3).
- **Wiebe double split mode**, employing the modified multi-stage Wiebe function, expressed in Eq. (B.4).

Fig. 3.23 provides a comparison between experimental results and simulated reaction rate, as well as the cumulative profiles obtained using the three discussed

Wiebe formulations at a nominal load point of 200 kWe. Table B.1 summarizes the quantified information of these calibrated Wiebe modes. Although previous studies with similar SI concepts concluded that single-stage Wiebe functions are generally inadequate for accurately capturing NG-SI engine combustion profiles [290, 291], this research finds that a single-Wiebe formulation can approximate to some extent the reaction rate profile. However, as it fails at effectively capturing the combustion rate, it is rejected for the subsequent analysis.

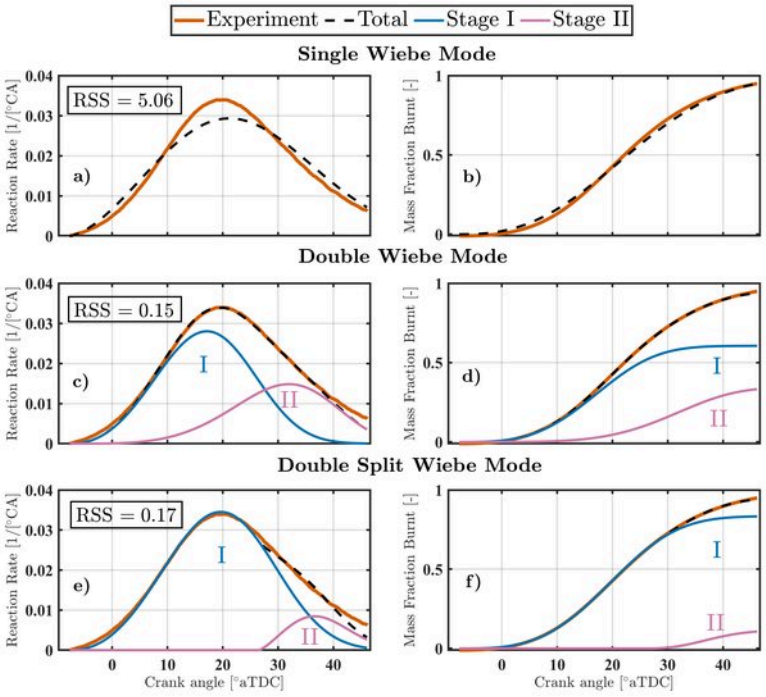

Figure 3.23: Simulated reaction rates and cumulative profiles for the three Wiebe modes at 200 kWe(EC II)

Regarding double-stage formulations, both conventional double-Wiebe and double-split Wiebe models effectively capture reaction rate and cumulative profiles throughout the combustion period. Minor discrepancies exist primarily during very early and late combustion phases; nevertheless, these phases have limited influence on critical thermodynamic properties such as in-cylinder pressure predictions. All models share an identical SOC, derived from the experimental analysis in Section 3.4, while it also provides the initial value for the SOC of the second squish combustion phase in the split version of double-Wiebe. Among the double-stage formulations evaluated, the conventional double-mode exhibits slightly higher accuracy than the double-split, achieving an RSS value of 0.15. The calibration routine yielded different parameter values between the two double-stage models. For instance, regarding the weight factors, although both models started from identical initial values, the calibrated values diverged in opposite directions within their defined

optimization ranges. The divergence is primarily attributed to differences in the SOC parameter assigned to each model. Specifically, in the conventional double-Wiebe formulation, the second combustion phase begins simultaneously with the first. Consequently, this formulation produces some reaction rate even at an early stage, despite representing the squish combustion phase, which is not physically expected to have started yet. This requirement leads to a reduction in the calibrated weight factor relative to its initial experimental estimate. However, this adjustment appears relatively minor as it is able to capture an expected significant overlap between the two combustion phases.

In contrast, for the split double-Wiebe formulation—where the second combustion phase initiates distinctly later—the optimization algorithm significantly reduced its weight factor magnitude to maintain a relatively smooth transition at the onset of this phase. Despite this effort, a slight abruptness in the heat release profile emerges at this transition point, an artifact not observed in the experimentally determined heat release. Clearly, these calibrating differences among the weight factors influence all other parameters. In spite of these inconsistencies, there is an insight derived from squish combustion phasing during the two double-Wiebe calibrations. The calibrated SOC in the split version of Wiebe aligned closely with the inflection point determined in the experimental analysis. In the conventional double-Wiebe, this appears in the vicinity of the reaction rate peak of the second phase, i.e., around 30°CA bTDC. This timing may correspond to the flame's entry into the squish region during expansion, which assumption aligns closely with previous experimental studies that correlated heat release rate profiles with optical observations [248].

To assist this discussion, Fig. 3.24 illustrates the combustion chamber at the initiation of combustion and the estimated point at which the flame is expected to reach the squish region according to this assumption. The discussion is particularly important when determining which Wiebe formulation to implement as the combustion rate model. While employing the split version and its associated second-phase SOC parameters may offer an intriguing insight into combustion phasing [290], its initiation point typically introduces some discontinuity in the overall heat release shape. If such abrupt heat release profiles had been experimentally observed, the split formulation would indeed be more appropriate for clearly distinguishing these combustion phases. Additionally, introducing another calibration parameter inherently increases uncertainty and sensitivity within the model. This complexity comes in addition to existing uncertainties associated with other critical parameters like the weight factors of each stage, none of which can be independently validated through available experimental data in this engine. Fig. B.3 confirms this added complexity, showing that while the conventional double-Wiebe has less parameters it leads to lower residual sum of squares (RSS) than the split version for the majority of the operating points used for calibration. Following the parsimony principle the simpler model is more appropriate [287]. To this end, the conventional double Wiebe is chosen to be applied as the combustion rate model to the cylinder model.

3.5.2 *Impact of dilution and ignition timing on Wiebe stages*

In addition to simulating the combustion process, the Wiebe modeling approach may offer insightful illustrations into the behavior of defined combustion stages,

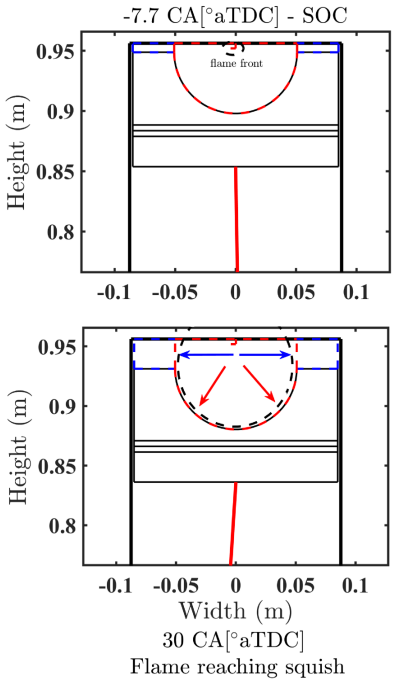

Figure 3.24: Circular flame reaching the squish region

including their sensitivity to operating parameters. Fig. 3.25 illustrates the reaction rates of distinct stages I and II, as modeled by the double-Wiebe formulation, across the dilution sweep in EC II. Richer mixtures lead to a more advanced and pronounced reaction rate profile for Stage I, which represents combustion occurring primarily within the bowl region. The weight factors consistently increase for Stage I and decrease for Stage II as the mixture becomes richer, aligning with the expected physical behavior of this engine configuration. Referring to the combustion chamber depicted in Fig. 3.24, it becomes evident that the squish-to-bowl volume ratio increases during the expansion stroke. This adds to the fact that as combustion further extends into the expansion phase, pressures from combustion will push more unburned mixture toward the periphery of the combustion chamber and subsequently the squish region. Consequently, as combustion advances closer to TDC, a larger proportion is expected to combust within the bowl region rather than the squish region.

To better illustrate this dilution effect demonstrated by the Wiebe model, Fig. 3.26 compares reaction rate profiles for the richest and leanest mixtures tested. Enriching the mixture reduces overlap between the two combustion stages, aligning with expectations given that richer mixtures combust more fuel within the bowl region. This observations is consistent with previous studies indicating that control parameters advancing combustion phasing typically reduce stage overlap [290]. As leaner mixtures are employed, reaction rate profiles for both stages also widen and exhibit

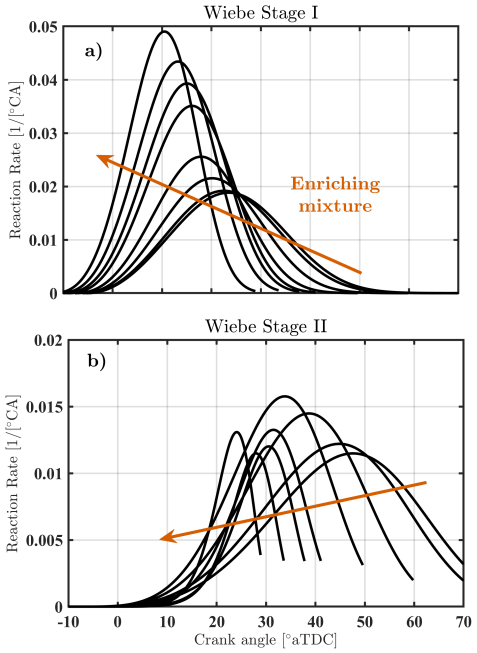

Figure 3.25: Reaction rate profiles modeled by double-Wiebe across dilution

decreasing kurtosis, clearly demonstrating the influence of higher air excess ratios on flame propagation speed.

Similar to dilution sweep, Fig. 3.27 compares reaction rate profiles for the most advanced and most retarded spark timing configurations. As expected when comparing these two extreme cases, both stages clearly advance with earlier ignition timing. Specifically, the peak reaction rate of Stage I advances from 20.5°CA aTDC to 10.6°CA aTDC, while the peak in Stage II advances from 35.8°CA aTDC to 27.4°CA aTDC. Interestingly, while peak reaction rate increases for Stage I, the reaction rate peak of Stage II actually decreases from 0.015/°CA to 0.013/°CA, aligning with the observations in Section 3.4. This highlights the distinct sensitivity of the second combustion stage within the squish region to operating parameters such as ignition timing. To conclude, the Wiebe-based analysis confirms the different influence between ignition timing and dilution in the two stages, as discussed in Section 3.4.6.

3.5.3 *Applying the closed in-cylinder process thermodynamic modeling*

Following the development and evaluation of the combustion models utilizing Wiebe functions, this section discusses the application of the double-Wiebe combustion model in the thermodynamic cylinder model. The primary aim is to evaluate the cylinder's model accuracy in capturing in-cylinder processes by comparing the simulated pressure profiles with experimental measurements. The thermodynamic cylinder model captured the overall pressure trends [236]. The cylinder model

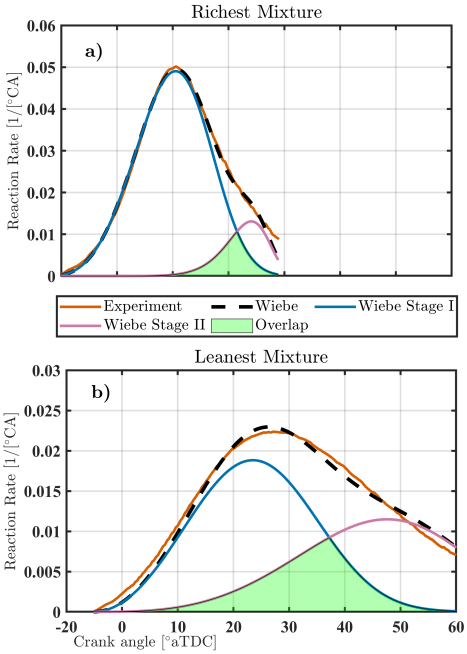

Figure 3.26: Stage overlap across the dilution sweep

consistently derived undervalues for pressure relative to the measured ones, and consequently piston work translated into MEP. This can be attributed to minor deviations in the initial stage of the reaction rate modeled by the Wiebe functions, as seen in Fig. 3.23(c). Despite the capability of this modeling approach to capture the closed in-cylinder processes, future studies should focus on establishing correlations for various model parameters across the engine's operating map, as well as validating the model using an additional independent experimental dataset. This can further expand and complete this modeling framework illustrated in Fig. B.1 to provide a fast closed in-cylinder process thermodynamic simulation tool that encapsulates the distinct combustion characteristics of LBSI engines.

3.6 CONCLUSIONS AND RECOMMENDATIONS

In summary, this chapter presented a comprehensive experimental investigation of a multi-cylinder marine-scale lean-burn spark ignition (LBSI) engine, encompassing a stability analysis and a unique characterization of its dual-phase combustion behavior (bowl-in and squish combustion). The research results discussed in this chapter address the second research question (**RQ2**) concerning the distinct combustion behavior and overall engine performance of marine LBSI engines, utilizing an experimental marine testbed fueled by natural gas (NG). This NG-fueled setup serves as a proxy to gain insights for future methanol operation in dedicated mono-fuel

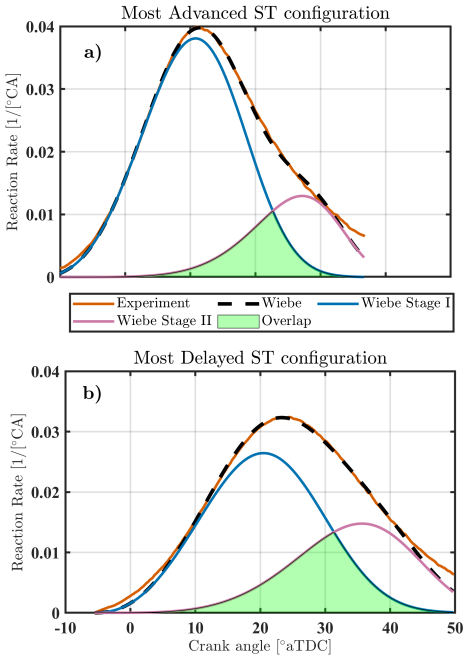

Figure 3.27: Stage overlap across the ignition timing sweep

marine engines, which is the ultimate goal of this chapter. The key conclusions from the experimental and analytical work are as follows:

EFFICIENT OPERATING REGION

Performance analysis revealed a specific range of air excess ratio at given operating conditions—considering other control parameters such as load and ignition timing—that offers a good compromise between NO_x emissions and combustion efficiency. These findings also corroborate the identified combustion stability regions across a tested dilution sweep. Although variations in control parameters (e.g., load, speed, ignition timing) may shift the exact optimal ranges, the analysis demonstrates that these operating windows are typically narrow for LBSI concepts in order to maintain the necessary trade-offs among constraints such as NO_x emissions and combustion robustness.

MULTI-STAGE COMBUSTION BEHAVIOR AND ENGINE PERFORMANCE

The analysis of the distinct combustion phases induced by the characteristic combustion chamber geometry in LBSI engines confirmed a two-stage combustion sequence: an initial rapid bowl-in burn followed by a slower flame propagation. This multi-stage behavior critically impacts engine efficiency and emissions. Notably, advancing spark timing—commonly advantageous in conventional SI engines—was

shown to have minimal or even adverse effects on combustion efficiency due to its impact on the squish phase. Nevertheless, advancing combustion phasing through ignition timing or mixture enrichment consistently enhance stability and thermal efficiency, albeit at the expense of increased NO_x emissions and wall heat transfer losses. The complex interplay of key control parameters—spark timing, air excess ratio, and intake charge temperature—strongly governs combustion characteristics and thus engine efficiency and emissions. This distinct sensitivity underscores the necessity for systematic DOE campaigns to elucidate parameter interactions and optimize operating ranges.

MODELING FRAMEWORK AND FUTURE WORK

This chapter demonstrated that the multi-stage Wiebe function-based thermodynamic model offers a simple yet accurate simulation tool for closed in-cylinder processes in marine LBSI engines. Nonetheless, further improvements demand validation across broader engine operating maps and independent datasets. Extending this modeling framework can enable fast, reliable in-cylinder process simulations that capture the distinct two-phase combustion behavior inherent in these engines.

METHANOL-FUELED LBSI MARINE ENGINES

Although this chapter used NG, the investigated LBSI concept operates under premixed flame propagation in the same bowl-squish geometry intended for future methanol operation. Therefore, the identified two-stage combustion behavior and the qualitative relationship between squish-entry phasing and engine performance are expected to remain valid as concept-based insights. However, methanol operation will differ from NG operation due to the distinct physical and chemical characteristics. Because of the liquid state of methanol, it is expected to be injected via multi-point PFI. The cooling effect during the evaporation of methanol will increase the sensitivity to intake thermodynamic conditions and mixture preparation, while together with its burning characteristics under lean mixtures can narrow the stable dilution window relative to NG. These fuel-specific differences are expected to shift optimal air management requirements, alter turbocharger boundary-conditions interactions in such a multi-cylinder engine configuration, and change emissions behavior. For these reasons, the primary value of the present chapter for methanol is the diagnostic framework and the phasing-based interpretation, while quantitative operating limits need to be established experimentally on methanol. A more in-depth discussion of the anticipated differences between the two fuels within the LBSI concept is provided in Section 6.3.

4

COMBUSTION MODE ANALYSIS IN PRDF MARINE ENGINES[1]

The great tragedy of science,
the slaying of a beautiful hypothesis by an ugly fact.

— Thomas Henry Huxley

This chapter addresses the third research question (**RQ3**), introduced in Chapter 1 and further elaborated in Section 2.1 and Section 2.2, which provided foundational insights into methanol PRDF operation, while identifying key knowledge gaps. Building on these findings, the present chapter advances understanding of combustion and performance characteristics specific to methanol PRDF engines—a field that remains comparatively underexplored. To accomplish this, it leverages a marine-scale single-cylinder research engine, specifically configured for methanol PRDF combustion and develops a systematic framework to characterize the distinct combustion behavior beyond conventional trend-based analysis.

This chapter is organized as follows. Section 4.1 revisits the background of the PRDF combustion strategy, referring to the more foundational discussion in Section 2.1. Section 4.2 details the experimental setup and test conditions, with Section 4.3 outlining the data analysis strategy, with special emphasis on the combustion staging methodology developed to address the unique combustion characteristics and knocking phenomena encountered in PRDF operation. Building upon these foundations and employing the developed methodologies, the following subsections present and discuss the results from the experimental study on the methanol PRDF single-cylinder engine. In Section 4.4, this research conducts preliminary comparative assessment of DO versus methanol dual-fuel operation, highlighting fundamental changes in combustion and engine behavior upon transitioning to methanol. This research places particular emphasis on the value of qualitative assessment and systematic characterization of HRR profile morphologies in PRDF engines. Accordingly, Section 4.5 performs an in-depth exploration by examining HRR profile shapes, their underlying mechanisms, and establishes quantitative metrics to classify combustion modes under methanol operation. Section 4.6 then explores the effects of varying MEFs at two high-load points, to better understand the trends in combustion stability and phasing, and their impact on efficiency and emissions

1 This chapter is partly reproduced from Kiouranakis et al. [35]

across a range of high MEFs. By incorporating intake air temperature adjustments within the MEF sweep at the highest load, this chapter also partly addresses **RQ3** by providing insights into the influence of critical boundary conditions on methanol PRDF combustion behavior. Finally, Section 4.7 synthesizes the primary findings and offers key recommendations for future research and practical applications.

4.1 INTRODUCTION

In DF engine concept, combustion of the LRF, such as methanol, is enabled by the reactivity and ignition control provided by the HRF, typically diesel [21]. This synergy between fuels enables ignition and combustion control, making DF strategies suitable for HD applications. While alternative DF concepts, such as RCCI and DDFS, have demonstrated great potential in achieving high efficiency levels and further reduce NOx emissions, their challenges in combustion controllability have restricted their commercial adoption [105]. Two primary DF combustion strategies have demonstrated the ability to effectively utilize the reactivity synergy between LRFs and and HRFs, while maintaining controllability, and have dominated engine research and development: DFDC and PRDF.

Because achieving the highest possible methanol utilization is a key objective in DF engine development, most practical applications—particularly in large marine engines—have prioritized the DFDC concept [22, 292]. For these large-bore engines, for which space and design constraints are less restrictive for the selected injection strategy, DFDC provides a viable pathway for methanol utilization, leveraging its robust diffusion-driven combustion mechanism. However, for a wide range of engine sizes, such as high-speed four-stroke marine and locomotive engines, DFDC presents significant challenges. These engines often face spatial constraints in the cylinder head that complicate the integration of additional injection systems necessary for DFDC operation. The high-pressure fuel system required for injecting methanol further limits its applicability as a diesel engine retrofitting option. This limitation underscores the importance of PRDF strategies as a more practical and flexible solution for methanol utilization across an extended spectrum of engine sizes. As such, PRDF represents a critical area of research for expanding methanol's role as a sustainable fuel in HD powertrains.

However, the PRDF combustion strategy faces challenges due to the complex interaction of multiple combustion mechanisms [293]. Combustion proceeds through an initial premixed pilot-fuel phase, with partial entrainment of methanol, followed by the combustion of remaining methanol-air mixture. This latter stage may occur either through premixed autoignition [133] or via multiple turbulent flame fronts propagating through the mixture [134]. Beyond shifting CDC from a mixing-controlled to a premixed regime, methanol also modifies the dynamics of the pilot combustion [135, 136, 175]. This is critical, as the pilot combustion governs the ignition characteristics of the subsequent methanol-air charge. These interactions are highly sensitive to the LRF–to–HRF ratio and load, which influence the resulting combustion regime [34]. The resulting interplay strongly impacts abnormal combustion propensity, and consequently efficiency and emissions. When methanol is used as the LRF, its pronounced charge-cooling effect is expected to further alter ignition and flame propagation compared to gaseous LRFs such as methane,

underscoring the need for more insights into methanol PRDF combustion. A more detailed background on the PRDF concept and the role of methanol is provided in Section 2.1.

Chapter 2 suggested that experimental studies on methanol PRDF engines, particularly at higher MEFs, remain limited, with most research constrained to moderate MEFs due to combustion challenges. This scarcity is especially pronounced for large-bore HD engines. Cung et al. [294] investigated methanol PRDF strategy in a HD single-cylinder engine with a bore size of 131 mm. This study revealed that knock challenges limit MEF to 49.4% under high-load operation of 23.5 gIMEP and 1200 rpm. Dierickx et al. [161] demonstrated stable operation at the highest MEF of 84% in a six-cylinder high-speed marine engine with a bore size of 108 mm using single-point injection strategy. Zhao et al. [119] retrofitted a single-cylinder diesel engine setup with a bore size of 100 mm to explore the effect of the injection timing of both high-pressure directly injected methanol and diesel fuel on the combustion mode. When the combustion mode shifted to premixed with early methanol injection configurations, MEF was limited to 50%. Overall, methanol PRDF applications barely achieve MEF greater than 80% [22, 34]. However, recent experiments have demonstrated the feasibility of attaining these higher MEFs, even in large-bore engines (bore $>$ 130 mm). For example, Splitter et al. [295] reported feasible maximum MEFs greater than 75% across the full operating load range at 1800 rpm in a 145 mm bore single-cylinder engine using the methanol PRDF concept. Similarly, Stenzel et al. [296] conducted single-cylinder experiments with an even larger bore (175 mm), while both studies demonstrated the challenges associated with combustion stability during the transition from diesel-only (DO) to methanol PRDF operation and the associated MEF limitations.. Both research efforts reported successful optimization strategies to overcome the MEF constraints, demonstrating how altering boundary conditions, such as charge pressure, temperature, and injection timing, can improve combustion performance and extend the attainable MEFs in large-bore engines. Among various optimization variables, pilot injection timing consistently emerges as a critical parameter for ensuring stable operation and increasing MEF limits.

Despite these advances, this chapter underscores three remaining key research gaps in this field. First, there is a lack of detailed investigation into the transition from DO to methanol PRDF operation at high MEFs. Second, systematic analyses of heat release behavior and conceptual mode classification remain scarce for large-bore PRDF engines, hindering comprehensive understanding of the underlying combustion mechanisms, their interactions, and their implications for engine performance. This gap is especially critical for methanol-fueled engines, as methanol's unique thermophysical properties greatly influence combustion dynamics. Third, an analytical methodology that can assess and quantify combustion characteristics specific to the distinct behavior in methanol PRDF concepts is lacking. Consequently, the operational behavior of large-bore methanol PRDF engines remains poorly understood, a shortcoming that significantly impedes efforts to achieve high MEFs while maintaining diesel-like performance.

This chapter addresses these research gaps through an experimental investigation on a marine-scale single-cylinder engine featuring a 170 mm bore and a high-pressure methanol PFI system. The elevated injection pressure is designed to enhance methanol evaporation, thereby mitigating combustion challenges typically

associated with poor evaporation and mixing, and ultimately expanding the feasible MEF range in PRDF engines. This experimental research demonstrates two MEF operating regimes that appear during the transition from diesel to methanol operation, and provides results in the high-MEF region constrained by poor combustion performance. Beyond the novelty of the experimental setup and campaign, this chapter delivers a systematic and in-depth analysis of combustion characteristics and engine performance in methanol-fueled PRDF operation.

4.2 EXPERIMENTAL SETUP AND CAMPAIGN

4.2.1 *Apparatus*

Experimental investigations were conducted using a single-cylinder research diesel engine featuring a modular design. A schematic of the engine test bed is presented in Fig. 4.1. The engine features a compression ratio of 14:1, with bore and stroke measuring 170 mm and 180 mm, respectively, resulting in a total displacement of approximately 4.1 L. Key specifications, as well as the properties of the fuels used, are summarized in Table 4.1.

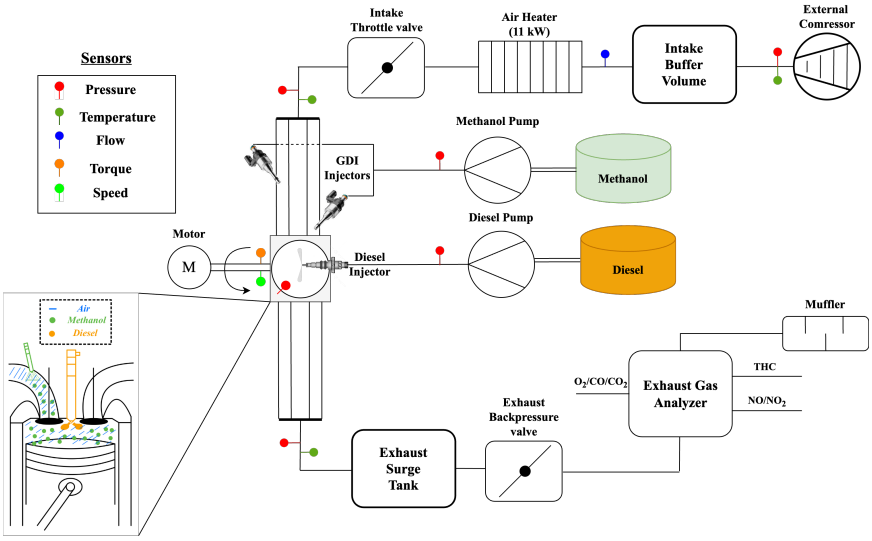

Figure 4.1: Schematic diagram of the single-cylinder test setup

The diesel fuel system comprises a centrally located injector mounted on the cylinder head, supplied by a mechanical inline pump. The injector nozzle opening pressure is 340 bar. For methanol delivery, a dual-port fuel injection system was implemented to enhance mixture formation controllability. This system utilizes two Bosch HDEV 5.2 injectors, each targeting one of the intake runners. The selection of two Gasoline Direct Injection (GDI) injectors instead of normal PFI injectors was done to improve methanol's atomization and reach high MEFs. A stainless steel plunger pump, with a 150 bar pressure capability, supplies methanol to the

Table 4.1: Engine and fuel specifications

Parameter	Specification
Engine	
Type	1-cyl 4-stroke CI
Bore x Stroke [mm]	170 x 180
Displacement [L]	4.1
Piston bowl shape	ω
Number of valves	4
Compression Ratio [-]	14:1
Fuels	
Diesel type	EN590
Diesel LHV [MJ/kg]	42.7
Diesel HC ratio	1.88:1
Methanol type	ISO 6583 Grade A
Methanol LHV [MJ/kg]	19.9

injectors. The flow rates of both diesel and methanol were measured using Coriolis mass flow meters, enabling accurate monitoring of fuel consumption and the MEF during the experiments. Surge tanks on both the intake and exhaust sides dampen pressure fluctuations inherent to single-cylinder engine operation. An 11 kWe electric heater is installed in the engine setup to provide additional control over the intake air temperature, a critical factor affecting methanol evaporation and combustion efficiency.

4.2.2 *Operating test conditions*

This chapter employs the third experimental campaign (EC III) of this dissertation to investigate two high-load points tested during a D2 test cycle on the engine at 1500 rpm, corresponding to torques of 300 Nm and 420 Nm. These operating points represent gross indicated mean effective pressures (gIMEPs) of approximately 11 and 15 bar, respectively, and serve as the primary load conditions for the analysis. Initial tests were conducted under diesel-only (DO) operation to establish a baseline for comparison, after which methanol was incrementally introduced. Although diesel injection activation was kept constant across all operating conditions, the actual start of injection could fluctuate slightly due to variations in in-cylinder pressure affecting needle valve opening. Intake conditions during the MEF sweeps were kept constant within each sweep but were slightly increased relative to DO operation. The intake temperature rose from 298 K in DO operation to 333 K at 300 N m and 323 K at 420 N m under methanol operation. Table 4.2 summarizes the experimental operating points, including the temperature (T_{IVC}) and pressure (p_{IVC}) at inlet valve closure (IVC), which represent the trapped charge boundary conditions at the start of compression for each test. These parameters provide insight into the small variations in thermodynamic conditions across the various cases. Therefore, this experimental study primarily assesses the control parameters of load and MEF. To evaluate load effects on combustion characteristics, MEF sweeps were performed

Table 4.2: Experimental test conditions for combustion mode analysis (EC III)

Mode	gIMEP [bar]	Diesel flow [grams/cycle]	Methanol flow [grams/cycle]	MEF [%]	Air Excess ratio [-]	T_{IVC} [K]	p_{IVC} [bar]
Diesel only	2.83	0.06	0	0	6.04	326	1.37
	11.09	0.22	0	0	2.85	348	2.38
	14.95	0.30	0	0	2.59	348	2.90
Methanol DF [11 bar]	10.64	0.087	0.284	62	2.35	346	1.90
	10.13	0.079	0.284	64	2.45	346	1.91
	10.55	0.078	0.301	66	2.37	342	1.89
	10.50	0.070	0.320	69	2.37	339	1.88
	10.66	0.063	0.344	73	2.33	337	1.87
	10.57	0.057	0.364	76	2.29	337	1.87
	10.54	0.050	0.390	79	2.26	332	1.85
	10.74	0.045	0.409	82	2.22	329	1.84
	10.66	0.040	0.425	84	2.20	328	1.84
	10.71	0.035	0.451	86	2.14	325	1.83
Methanol DF [15 bar]	15.18	0.071	0.535	79	2.58	329	2.90
	15.24	0.067	0.547	80	2.56	330	2.90
	15.23	0.063	0.554	81	2.56	329	2.89
	15.15	0.060	0.564	82	2.56	327	2.88
	15.16	0.055	0.574	84	2.56	328	2.88
	15.17	0.048	0.598	86	2.52	325	2.85
	15.13	0.040	0.626	88	2.48	323	2.84
	15.08	0.033	0.622	90	2.55	327	2.87
	14.98	0.023	0.595	93	2.72	340	2.95

at both high-load conditions. At 11 bar gIMEP, MEF was varied from 62% to 86%, while at 15 bar gIMEP, the sweep ranged from 79% to 93%. The upper and lower limits of the MEF sweeps were determined by elevated cyclic variations and the onset of excessive knocking, respectively, with the operational constraints further elaborated in Section 4.5.

4.3 DATA ANALYSIS METHODOLOGY FOR PREMIXED DUAL-FUEL OPERATION

This section outlines the data analysis methodology applied in the context of the methanol PRDF experiments. To avoid redundancy with the array of combustion and performance metrics, detailed in Chapter A, the focus here is limited to the principal additional parameters and analytic procedures specific to DF operation.

4.3.1 *Performance*

In DF systems, defining air excess ratio is complex due to the differing stoichiometric requirements of the fuels and the stratified nature of the pilot injection, which deviates from the more uniform mixture in conventional spark ignition engines. To address this, three air excess ratio definitions are employed, each aiming to capture different aspects of the combustion process. Global air excess ratio λ_{global}, providing

an overall measure of mixture richness, considering both fuels relative to the total air supply:

$$\lambda_{\text{global}} = \frac{\dot{m}_{\text{air}}}{(\dot{m}_{\text{m}} + \dot{m}_{\text{d}}) \cdot (\text{MMF} \cdot \text{AFR}_{\text{stoich,m}} + (1 - \text{MMF}) \cdot \text{AFR}_{\text{stoich,d}})} \tag{4.1}$$

where $\dot{m}_{\text{air}}$ is the mass flow rate of air, and $\text{AFR}_{\text{st,i}}$ is the stoichiometric air-to-fuel ratio for each fuel. Methanol air excess ratio $\lambda_{\text{methanol}}$, approximating the premixed charge conditions for flame propagation, focusing solely on methanol and air:

$$\lambda_{\text{m}} = \frac{\dot{m}_{\text{air}}}{\dot{m}_{\text{m}} \cdot \text{AFR}_{\text{st,m}}} \tag{4.2}$$

Defining an air excess ratio specifically for diesel combustion is challenging due to the high degree of stratification. This research employs the simplistic approach of oxygen reservation by methanol to define a single metric for diesel air excess ratio:

$$\lambda_{\text{d}} = \frac{\dot{m}_{\text{air}} - \text{AFR}_{\text{st,m}} \cdot \dot{m}_{\text{m}}}{\dot{m}_{\text{d}} \cdot \text{AFR}_{\text{st,d}}} \tag{4.3}$$

4.3.2 *Combustion phasing*

To quantify and analyze combustion characteristics in the PRDF concept, this research employs suitable metrics for its unique behavior, moving beyond traditional combustion parameters. A primary objective is quantifying transition between distinct combustion phases. Li et al. [231] divided the HRR profile in two segments by identifying a tangency point in the HRR signal, which they used to assess the effects of the defined stages in the vibration levels of a methanol-fueled PRDF engine. For combustion phasing analysis, this research adopts metrics validated in optical investigations of PRDF combustion that correlated HRR profile markers with physical combustion transitions, as illustrated by Fig. 4.2. Following the approach of Ahmad et al. [132, 297], the local maxima of the HRR profile are employed to divide the overall combustion process into:

1. **Delay phase (Ignition delay):** Spanning from start of injection (θ_{SOI}) to the first local maxima (θ_1), i.e., start of combustion (SOC).
2. **Combustion Phase I (Pilot combustion):** Extending from SOC to the second local maxima (θ_2), dominated by diesel premixed autoignition (Stage I).
3. **Combustion Phase II (Methanol combustion):** Covering the interval from (θ_2) to θ_{EOC} (matching CA90), encompassing methanol combustion via autoignition (Stage II) or flame propagation (Stage III).

SOI is defined as the moment when the fuel pressure in the injector line reaches the needle opening threshold, indicating the onset of needle lift and the beginning of fuel injection. Combustion duration (CD) is defined as the interval θ_1-θ_{EOC}. A key distinction from the study of Ahmad et al. on methane PRDF combustion lies in the characteristics of the observed HRR profiles, which reflect differences in the staging of underlying combustion mechanisms. Whereas Ahmad et al.'s optical analysis revealed a clear separation of all combustion stages—producing multi-peak

second derivatives—this research consistently observes clear two-peak HRR profiles. This outcome is attributed to the delay and separated combustion of methanol relative to the initial diesel premixed combustion, resulting in significant overlap between the combustion mechanisms associated with methanol [129]. This overlap, which was not observed with the methane PRDF concept, may be attributed to the distinct charge-cooling effect of methanol. Here, the first local maximum remains the mark for diesel premixed autoignition and SOC, while the second signifies methanol combustion initiation—whether through premixed autoignition or flame propagation.

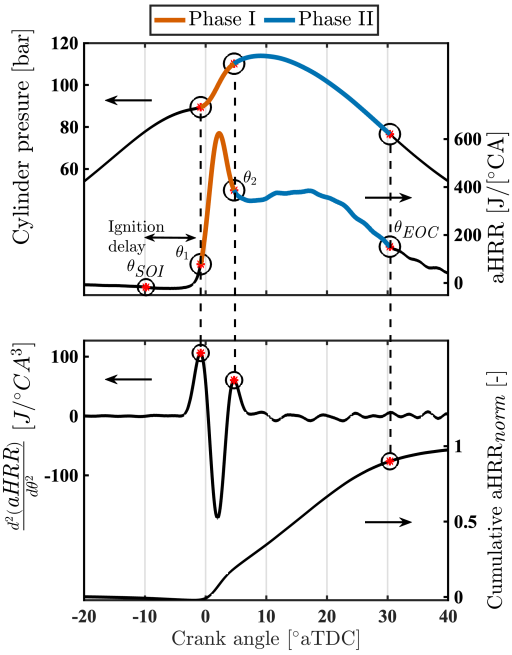

Figure 4.2: Combustion phasing methodology

Following the description of the quantitative analysis of combustion characteristics here and the qualitative analysis in Section 2.1.2, it is necessary to clarify the terminology to avoid ambiguity, as the terms *combustion stages* and *phases* are used extensively in the discussion of results. As depicted in Fig. 2.6, the quantitative combustion methodology cannot resolve the defined three combustion stages. Therefore, for the remainder of this thesis, the term *combustion stages* refers to the mode-informed qualitative analysis, while *combustion phases* refers to the two-phase (diesel and methanol) division obtained from the quantitative analysis. In short, combustion phases capture quantitative trends, whereas combustion staging provides complementary qualitative insights into underlying mechanisms that are not clearly distinguished by the quantitative approach.

4.3.3 *Knocking*

This work uses two complementary metrics to assess knocking in PRDF combustion: the maximum pressure rise rate (PRR_{max}) and the maximum amplitude of pressure oscillations (MAPO), as determined by Eq. (4.4) and Eq. (4.5), respectively:

$$\mathrm{PRR} = \max\left(\frac{dp_{\mathrm{filt}}}{d\theta}\right) \tag{4.4}$$

$$\mathrm{MAPO} = \max\left(\left|p_{\mathrm{filt,freq}}\right|_{\theta_0+w}^{\theta_0}\right) \tag{4.5}$$

where p is the raw pressure, p_{filt} the filtered pressure with Savitzky–Golay filter, $p_{\mathrm{filt,freq}}$ is the high-pass filtered pressure, θ is the crank angle, and w is the filtering crank angle window. PRR_{max}, calculated as the steepest slope of the in-cylinder pressure trace, serves as an indicator of the severity of rapid premixed combustion of the pilot diesel (diesel-knock), which is particularly relevant given methanol's sensitivity to IDs. MAPO is employed to quantify the high-frequency pressure fluctuations associated with knock phenomena, including both diesel and end-gas knock. For its calculation, the in-cylinder pressure signal is filtered using a bandpass filter (p_{filt}), with a frequency range of 2 to 20 kHz. In this large-bore engine, knock-related ringing is mainly associated with transverse acoustic modes of the in-cylinder gas. Using typical in-cylinder conditions close to TDC to estimate the speed of sound c and the bore B as the length scale, the resonant frequency of the lowest circumferential mode (1,0) can be approximated as $f \approx \frac{\rho \cdot c}{\pi \cdot B}$, which for the engine yields about 2.5 kHz [298]. The lower cutoff of the band-bass filter was therefore set to 2 kHz to safely retain this mode while suppressing the slower and regular flame propagation combustion, while the upper limit of 20 kHz is well below the measurement system's Nyquist frequency (45 kHz), ensuring accurate signal representation without introducing high-frequency noise [299, 300]. The crank angle window for knock analysis (w) begins at the start of injection and spans 60 °CA.

Recognizing that pressure oscillations can originate from both rapid premixed diesel combustion and end-gas autoignition [301, 302], MAPO is quantified separately for the two main combustion Phases I and II. This approach allows for partial distinction between pressure fluctuations arising from the initial diesel-driven combustion and those associated with methanol combustion in the second stage during the bulk flame propagation. This methodology reflects the dual-knock nature inherent to PRDF operation, as discussed in Section 2.1. As this dissertation does not include dedicated knock limit testing, these metrics are used to compare relative knock intensity between operating points, thereby supporting the broader analysis of combustion modes.

4.4 DIESEL-ONLY TO METHANOL DUAL-FUEL OPERATION

Before examining the effects of methanol addition in the behavior of the diesel engine under PRDF strategy, it is beneficial for the analysis to first compare DO operation—at both minimal and full fueling rates—with DF operation at a representative MEF. This approach enables a clearer distinction between the primary effects of methanol

addition on combustion behavior and conventional diesel operation, as well as the main differences between DO and methanol PRDF operation.

4.4.1 *Combustion characteristics*

At low loads, operation with a minimal amount of diesel results in combustion dominated by a single premixed autoignition phase. As the diesel quantity increases with higher loads, combustion transitions to a two-stage process, as illustrated in Fig. 4.3. The combination of larger diesel quantities—requiring longer injection durations—and potentially shorter IDs due to a higher thermal state of the combustion chamber components and increased cylinder pressure during injection, results in a reduced premixed phase magnitude. This leads to the majority of diesel fuel combusting during the subsequent diffusion phase. In DF operation at high loads and high MEF, the combustion behavior of diesel is expected to closely resemble that observed in the low diesel quantity case (2.8 bar gIMEP), with the addition of methanol modifying the process. To clearly illustrate this effect, Fig. 4.4 compares heat release profiles for DO and two DF cases, all employing the same pilot diesel quantity of approximately 63 mg/cycle.

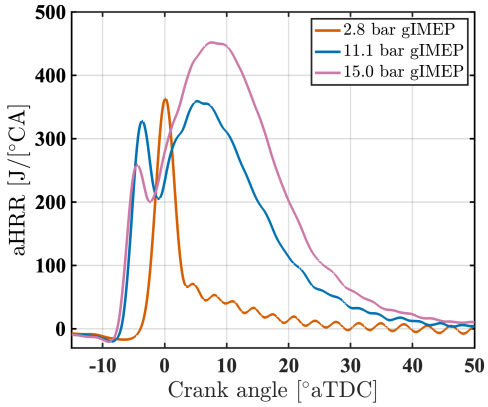

Figure 4.3: DO combustion HRR profiles

For the lower methanol quantity case (a), the introduction of methanol extends the ID by about 1.8 °CA, resulting in a more intense premixed combustion phase. This is reflected in the maximum HRR (HRR_{max}), which nearly doubles from 363 to 693 J/°CA. In the higher methanol quantity case (b), although a similar combustion pattern is observed, the ID extension is somewhat shorter—around 1.1 °CA—despite the greater cooling effect expected from the increased methanol mass. This counterintuitive result can be attributed to the higher pressures and global air excess ratio at the higher load (increasing from 2.33 to 2.56), which enhance shear forces on the pilot jet, as well as the higher thermal states of chamber components at higher loads, ultimately improving atomization of the pilot diesel.

Despite the shorter ID in the higher methanol case, the magnitude of the first premixed combustion phase is slightly greater, with HRR_{max} reaching approximately

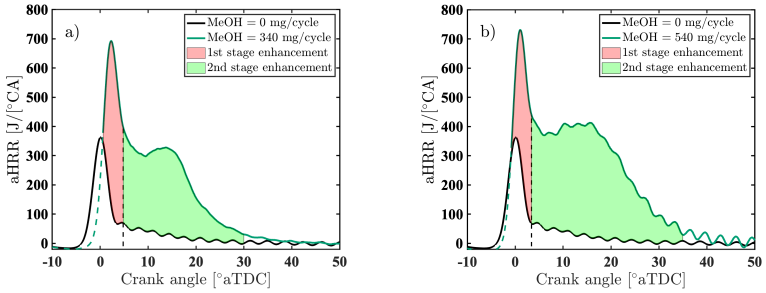

(a) MEF = 72% at 10.7 bar gIMEP **(b)** MEF = 80% at 15.2 bar gIMEP

Figure 4.4: DO to PRDF mode under the same amount of pilot diesel

728 J/°CA. This is due to the larger amount of methanol that is expected to co-combust with pilot diesel, either entrained or simultaneously in the vicinity of the flame, which enhances the energy released in the initial combustion stage. Additionally, in both DF cases, the extended ID relative to DO operation allows for more thorough mixing of diesel with air, promoting combustion under less fuel-rich conditions. Consequently, the majority of diesel fuel is expected to complete its energy release by the end of the first combustion stage [132], as indicated by the black dashed line. These combined effects lead to an intensified first premixed combustion stage, as highlighted by the red shaded region. Quantitatively, methanol addition increases the heat released in the first phase by 100% and 111% in the two DF cases compared to DO, respectively. Notably, the influence of methanol on the pilot's premixed diesel stage in the PRDF concept is substantially more pronounced than that observed with other LRFs, such as natural gas, which typically do not induce such significant changes in ID of diesel [293].

The analysis now shifts to a direct comparison between methanol DF and DO operation at the same high load, in order to clearly distinguish the principal characteristics of a diesel engine under methanol operation. Fig. 4.5 presents the HRR profiles and bulk gas temperatures for both DO and methanol DF cases at high load (15 bar gIMEP). Under DO operation, the combination of elevated thermodynamic conditions and higher injection pressures—required to deliver the necessary diesel quantity—results in the shortest IDs observed across the tested load range. This leads to a relatively weak premixed diesel combustion phase, with the majority of fuel burning during the subsequent mixing-controlled stage. In contrast, the introduction of methanol under the DF mode displaces a portion of the intake air and cools the cylinder charge, resulting in an ID increase from 4.4 °CA in the DO case to 9.3 °CA. This prolonged ID enhances the premixed combustion stage, increasing the fraction of total fuel burned in this phase from 10% to 23%.

Comparing the second combustion stages, flame propagation in the methanol DF case proceeds more rapidly than the diffusion phase in DO operation, with durations of 22.2 and 26.6 °CA, respectively. As a result, the overall combustion duration is reduced under methanol operation (27.7 °CA) compared to DO (31.9 °CA). However, this metric does not fully account for the longer ID observed in the methanol case, and thus does not completely capture the shift in combustion phasing. Indeed, the

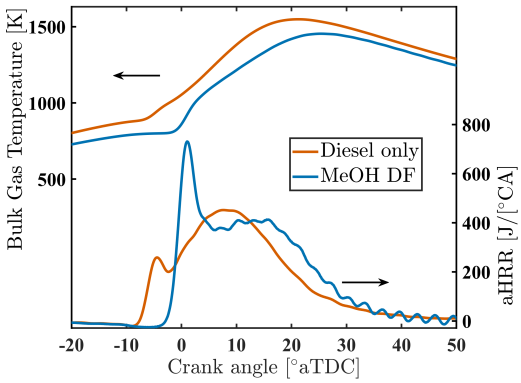

Figure 4.5: Bulk gas temperature and HRR in DO and PRDF combustion at 15 bar gIMEP

phasing itself is more advanced in the DO case, with the center of heat release (CA50) occurring at 9.6 °CA aTDC compared to 11.8 °CA aTDC for methanol DF operation. Despite the more pronounced and faster premixed combustion stage in the methanol DF case, DO operation yields higher bulk gas temperatures through the combustion window.

The intensified premixed autoignition in the methanol DF mode results in significantly higher pressure rise rates (PRRs). Fig. 4.6 illustrates the differences in cyclic in-cylinder pressures, including the high-frequency variations revealed by bandpass filtering. The stronger premixed phase in the DF case leads to substantially higher PRRs for each individual cycle, with PRR_{max} nearly doubling from 4.24 bar/°CA in DO to 7.22 bar/°CA in DF operation. The MAPO metric further highlights the highly fluctuating pressure signal characteristic of methanol DF combustion, increasing from 3.4 bar in DO to 9.6 bar in DF operation. Note that the maximum values of the knocking metrics represent the highest values observed across the 50 consecutive cycles recorded for each operating point. Transitioning from DO to methanol DF operation thus produces a significant rise in both PRR_{max} and MAPO, underscoring a greater propensity for combustion knock and less stable combustion. Both rapid premixed diesel combustion and end-gas autoignition contribute to the observed pressure oscillations, resulting in more intense high-pressure waves and stronger knock-like events. This trend toward elevated combustion instability under methanol operation is also reflected in the increased COV_{gIMEP}, which rises from 0.6% in DO to 2.5% in DF mode. The heightened instability underscores the sensitivity of DF operation to abnormal combustion phenomena, highlighting the critical importance of controlling parameters such as ignition timing and air excess ratio to maintain stable engine performance.

4.4.2 *Performance and emissions characteristics*

A comprehensive evaluation of engine performance between DO and methanol DF operation requires quantifying how the input fuel energy is distributed among useful work and various loss mechanisms. The Sankey diagrams in Fig. 4.7 illustrate

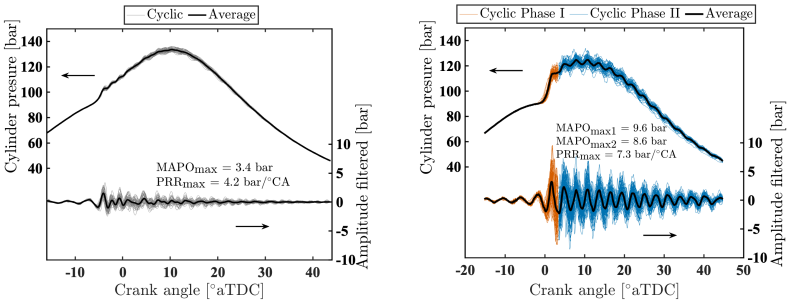

(a) DO at 15.0 bar gIMEP **(b)** DF with MEF = 80% at 15.2 bar gIMEP

Figure 4.6: Raw and filtered pressure in DO and PRDF modes at high load

the energy balance for both modes at high load. Despite both cases achieving similar work output (approximately 15 bar gIMEP), the total fuel energy input is notably higher—by about 12%—in methanol DF operation. This increased requirement arises from the inherent challenges of the methanol PRDF concept, primarily reflected in lower combustion efficiency. Three main factors contribute to this efficiency gap: 1) lower specific heat ratios, in-cylinder temperatures, and leaner mixtures, which weaken flame propagation (mirroring issues in lean SI engines), 2) potential wall wetting effects that can cause methanol to adhere to cylinder surfaces and crevices, and 3) absorption of methanol into oil layers. In this experimental campaign, the latter two factors are considered negligible, as high injection pressures promote effective methanol atomization and evaporation, and lube oil analysis revealed nil methanol contamination below the detection limit of the measurement device. Consequently, the dominant cause of combustion inefficiency is attributed to the relatively low in-cylinder temperatures and high air excess ratios ($\lambda = 2.6$ in this reference case), resulting in 11.8% combustion losses under methanol DF operation.

Interestingly, while the gross heat release is comparable between the two cases, methanol DF operation delivers slightly more work to the piston, despite less favorable combustion phasing compared to DO. This highlights methanol's potential to improve heat efficiency in diesel engines by significantly reducing heat transfer losses, while the slightly decreased thermodynamic efficiency can be further enhanced by advancing combustion phasing through boundary condition adjustments [303]. Ultimately, methanol DF operation fundamentally reconfigures the energy balance within this engine, altering the distribution of input fuel energy. Overall, the gain in the sum of heat and thermodynamic efficiencies—reflecting improved conversion of released fuel energy into piston work—underscores the promise of high-efficiency methanol operation in PRDF engines.

The transition from DO to methanol DF operation also leads to pronounced changes in the diesel engine's emissions profile, as summarized in the comparative bar chart of Fig. 4.8. As anticipated from the increased combustion inefficiency, methanol DF operation is characterized by a substantial increase in both CO and UHC emissions relative to DO operation. Specifically for this comparative case, CO emissions rise from 0.2 to 15.9 g/kWh, while UHC increases from 98 to 4868 ppm. As both emissions are indicators of low combustion efficiency, this trend

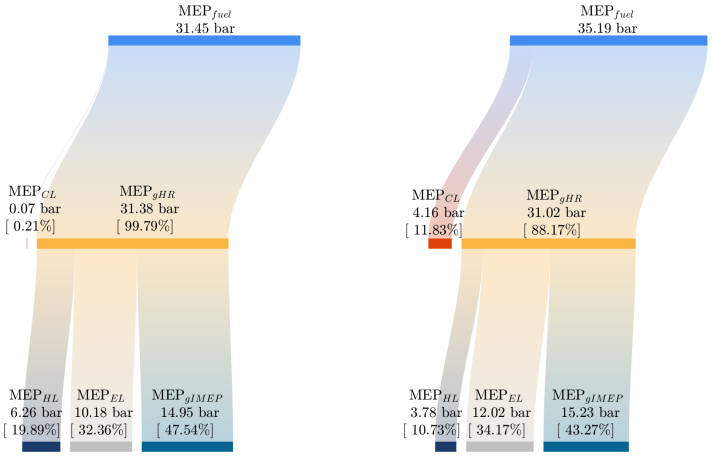

(a) DO at 15.0 bar gIMEP **(b)** DF with MEF = 80% at 15.2 bar gIMEP

Figure 4.7: Sankey diagram of energy balance for DO and PRDF operation at high load

clearly demonstrates the bottleneck of the PRDF concept with poorer combustion performance.

In contrast, methanol DF mode yields a clear reduction in ISCO$_2$ emissions, decreasing from 554 g/kWh in DO mode to 479 g/kWh under DF operation. While a reduction in CO_2 emissions was expected due to methanol's higher hydrogen-to-carbon ratio compared to diesel, the observed decrease of approximately 13.5% exceeds what would be anticipated solely from this ratio. To isolate the effect of the hydrogen-to-carbon ratio, an estimated perfect combustion in methanol DF operation would yield around 534 g/kWh, corresponding to a reduction of approximately 6%. The greater observed decrease in CO_2 emissions is also influenced by the concurrent increase in CO and UHC, as a fraction of the fuel's carbon remains partially oxidized and is emitted as CO or UHC rather than fully converted to CO_2.

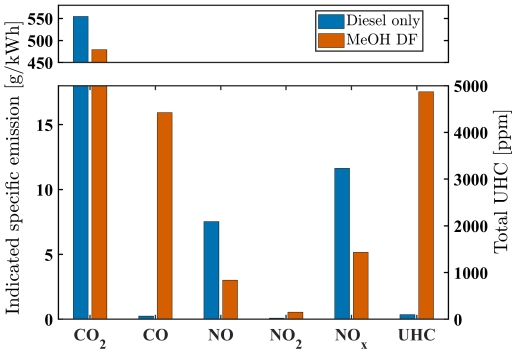

Figure 4.8: Emissions characteristics in DO and PRDF operation at high load

A notable benefit of methanol use is the marked decrease in NO_x emissions. The combination of methanol's charge cooling effect and the more homogeneous combustion environment it fosters contribute to lower peak combustion temperatures, thereby suppressing thermal NO_x formation [304]. In the present study, NO_x emissions are reduced from 11.6 g/kWh in DO operation to 5.2 g/kWh in the DF case. However, since combustion phasing is known to influence NO_x formation, the observed decrease cannot be attributed solely to changes in combustion regimes with methanol. A clearer comparison would require adjusting boundary conditions to align combustion phasing more closely with DO operation. Moreover, the decrease in total NO_x is accompanied by an increase in NO_2 emissions, which rise from 0.1 to 0.55 g/kWh. Note that NO_x emissions are quantified based on the molecular weight of NO_2, which explains the discrepancies when comparing the sum of NO and NO_2 to the total reported NO_x values.

The observed increase in NO_2 emissions under methanol PRDF operation has also been reported in previous experimental studies and its interpretation requires insights from mechanistic investigations on NO_2 formation [34, 305]. To decouple the effect of methanol's cooling effect from the inherent PRDF combustion behavior, it is interesting to explore the trends with another LRF. Li et al. [306] performed a numerical analysis on a natural gas PRDF engine and found that most NO_2 forms during late post-combustion oxidation of the remaining premixed fuel-air mixture. This occurs predominantly in the end-gas region of the squish area, where local conditions favor low temperature reactions and the abundance of HO_2 radicals promotes the conversion of NO to NO_2 through the $NO + HO_2 \rightarrow NO_2 + OH$ pathway [307]. The cooling effect of methanol is expected to enhance these low temperature regions, thereby further intensifying NO_2 formation relative to other LRFs.

Overall, the shift to methanol PRDF operation fundamentally alters the emission landscape of the diesel engine. Although this transition offers a reduction in CO_2 and NO_x emissions, it presents a clear trade-off in the form of increased CO, UHC, and NO_2. The wide high-MEF sweeps—including the points compared with DO—are used diagnostically to reveal knock and combustion deterioration challenges, rather than defining applied setpoints. A viable concept will select MEF within an application-specific region that balances knock propensity, desired diesel displacement, NO_x levels, and overall efficiency. These observations reinforce the need to optimize combustion control to utilize the benefits of methanol operation while minimizing its drawbacks. In practice, this may lead to compromises on the maximum MEFs so that gains in emissions, i.e., lower global warming impact, are not offset by excessive efficiency penalties. Accordingly, managing boundary conditions, such as pilot injection timing and air excess ratio, will be central to enabling smooth transitions from DO to methanol PRDF and to robust transient and steady-state operation.

4.5 COMBUSTION MODE ANALYSIS IN METHANOL DUAL-FUEL MODE

The combustion dynamics in PRDF engines are governed by the interplay of multiple mechanisms, resulting in distinct HRR profiles. This complex behavior, inherent to the PRDF strategy regardless of fuel, is further influenced by variations in fuel

properties (e.g., methanol's chemical and thermophysical properties) and operating conditions (e.g., load or speed), which dictate the evolution of combustion phasing and heat release characteristics. This subsection develops a systematic analysis of combustion modes in methanol PRDF, integrating both qualitative observations and quantitative assessments, to elucidate the underlying combustion mechanisms and their trends.

4.5.1 *Qualitative evaluation*

Li et al. [139] identified three primary HRR profiles (h-, m-, and n-shape) in a natural gas PRDF engine at low loads and discussed their distinct combustion processes. Similarly, Lee et al. [308] reported analogous profiles through different operation boundary conditions in gasoline PRDF combustion. For instance, the h-shape profile observed by Li et al. at high natural gas ratios featured a strong premixed combustion stage followed by attenuated flame propagation, whereas Lee et al.'s Mode 1 of a similar shape occurred at low gasoline ratios exhibiting conventional diesel-like characteristics. A core contribution of this dissertation is to expand this qualitative approach, apply it to methanol PRDF data, and ultimately offer a systematic characterization framework for HRR profile morphologies.

In conventional diesel operation, HRR profiles transition from single- to double-peak patterns as load increases, as seen in Fig. 4.3. Low loads exhibit dominant premixed combustion with a minimal diffusion phase, while higher loads with increasing fuel mass intensify mixing-controlled combustion phase, yielding a distinct secondary peak. Transitioning to methanol PRDF operation is expected to fundamentally alter this behavior. At very low MEFs, methanol combusts passively during the diesel diffusion phase, thus retaining conventional diesel combustion characteristics, i.e., non-premixed diffusion combustion dominance. As MEF increases, methanol increasingly influences the in-cylinder processes by: 1) extending ID due to its charge-cooling effect, which strengthens the pilot combustion (Stage I), and 2) weakening the diesel diffusion phase as more diesel is consumed in Stage I and a greater portion is replaced by methanol, which primarily combusts via premixed flame propagation (Stage III). Under the lean conditions typical of diesel engines, premixed autoignition of methanol becomes difficult. During this MEF increase, these effects eventually reach critical points: 1) the prolonged ID leads to excessive PRR, risking mechanical integrity and degrading combustion stability, and 2) the reduced augmentation of methanol combustion by diesel diffusion, combined with very lean methanol-air mixtures, further deteriorates combustion stability and reduces combustion efficiency, resulting in high levels of UHC and CO emissions. This combination of mechanical (diesel knock) and emissions-related (poor combustion) challenges requires imposing limits on MEF to prevent excessive component stresses and to control the emission of methanol and formaldehydes. This limits the MEF to below an average of 50% for most loads in this study, consistent with the findings of Stenzel et al. [296].

Notably, this experimental campaign identified two distinct MEF operational regions rather than the commonly reported single knock-limited range. Beyond the initial limited window, higher MEFs can re-stabilize combustion and improve efficiency by enriching the methanol-air mixture and enhancing Stage II/III, while

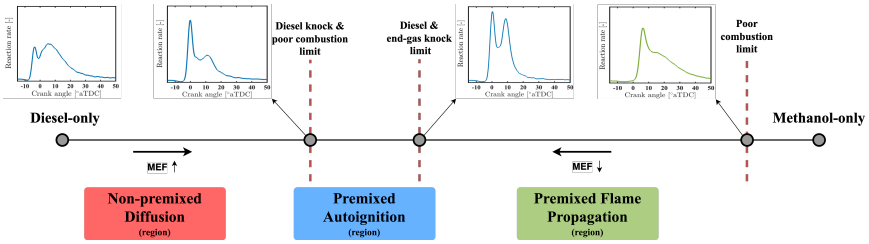

Figure 4.9: MEF operating regions at high loads

inhibiting further enhancement of Stage I by reducing diesel's contribution. This region is restricted by a diesel and primarily end-gas knocking at the lower bound, while it is ultimately bounded at the upper end by renewed instability and poor combustion efficiency, as diesel ignition energy becomes insufficient and combustion phasing is delayed extensively. Clearly, with a common rail injection system, advancing diesel injection timing would be the primary control strategy to counteract this combustion delay. Therefore, the upper and lower MEF limits are determined by different instability mechanisms rather than knock alone, with Fig. 4.9 qualitatively illustrating these ranges across the MEF sweeps. The subsequent analysis focuses on the high-MEF region.

This chapter assesses the combustion profiles across the operating points explored in this experimental campaign, i.e., two high-load MEF sweeps, 11 and 15 bar gIMEP. Analysis of heat release profiles revealed and defined three distinct combustion modes (I-III) based on their unique HRR shapes, and thus the underlying combustion mechanisms. Fig. 4.10 illustrates the profiles of HRR and pressure across the defined combustion modes. These modes are classified based on their dominant combustion mechanism, building upon characterization systems [129, 139, 308] and several optical experimental studies with the PRDF concept [129, 132, 138, 293].

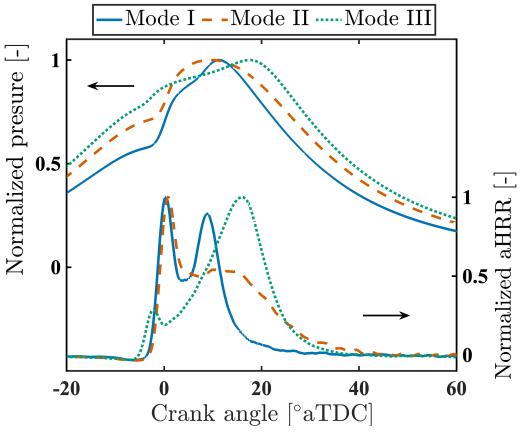

Figure 4.10: Defined combustion modes across operating points

Combustion **Mode I** emerged at the lowest MEF boundary (62%) during the 11 bar gIMEP operation, exhibiting an m-shaped HRR profile with two distinct peaks of comparable magnitude and duration. This peak similarity indicates a common combustion mechanism: premixed autoignition, consistent with the knocking-restricted lower MEF limit. The reduced knocking intensity—compared to levels below the operational threshold—stems from phased separation of both fuels' autoignition event due to delayed methanol-air combustion phasing [129]. This dual-peak profile and the absence of a single-peak HCCI-like profile may also be attributed to the highly lean methanol-air mixtures across the MEF sweeps in this experimental campaign. Optical studies have demonstrated that leaner mixtures tend to reduce the overlap between the premixed autoignition stages of the LRF and diesel [132]. Analogous profiles have been observed in prior PRDF experiments with methanol [184, 304], as well as with gasoline [308] and natural gas [139, 309]. Fig. 4.11 illustrates this mode within the conceptual DF framework, employed in this thesis and illustrated in Fig. 2.6, showcasing the Stages I and II as the dominant heat release mechanisms.

At elevated MEFs, methanol's intensified cooling effect further suppresses premixed autoignition, maintaining a pronounced premixed diesel combustion Stage I despite reduced diesel quantities, while attenuating the secondary combustion phase. The sustained premixed phase arises from prolonged ID, which increases diesel participation in initial combustion and entrained methanol. Conversely, the weakened secondary phase results from the lower reactivity of methanol due to lower temperatures resulting in increased heat release via premixed flame propagation—a comparatively slower mechanism than autoignition. These dynamics define Combustion **Mode II**, exhibiting an h-shaped dual-peak HRR profile with a sharp initial peak and attenuated secondary phase. While premixed Stage I resembles that of Mode I, Stage II is substantially weakened, shifting heat release toward Stage III as depicted in Fig. 4.11. This mode appeared at all MEFs except the lowest under the 11 bar gIMEP load conditions and low-to-intermediate MEFs at 15 bar gIMEP load.

Conversely, high-load operation at peak MEFs (90-93%) produced Combustion **Mode III**, exhibiting an n-shaped profile with a dominant second peak. Minimal pilot quantities and IDs diminished premixed diesel autoignition (Stage I), while turbulent flame propagation (Stage III) dominated heat release—aligning with MPDF strategies [146], as depicted in Fig. 4.11. Reaching high MEFs at high loads required enhancing charge reactivity to promote faster flame propagation and stabilize combustion stability. This was achieved by increasing intake air temperature, which shortened the pilot diesel ignition delay and improved combustion phasing, while methanol's cooling effect and knock resistance enabled knock-free flame propagation. To avoid confusion, this morphology fundamentally differs from n-shapes reported by Li et al. [139] and Lee et al. [308], which reflect HCCI-like autoignition rather than flame propagation dominance.

The hypothesis that the attenuated combustion Phase II observed in Mode II arises from a transition in dominant combustion mechanism—from premixed autoignition (Stage II) to flame propagation (Stage III)—can be substantiated by knocking intensity analysis. Fig. 4.12 displays both raw and bandpass-filtered in-cylinder pressure traces at 11 bar gIMEP for operating points representative of Mode I (62% MEF) and Mode II (86% MEF). The pressure trace analysis demonstrates that Mode I exhibits substantially more persistent and intense pressure oscillations—indicative of knock—

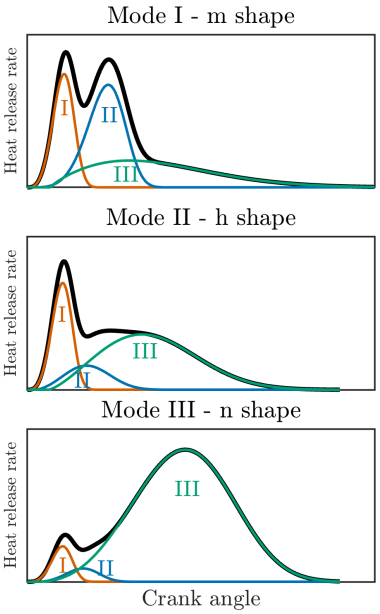

Figure 4.11: Conceptual model for the three defined combustion modes

compared to Mode II. In the Mode II case, a minor premixed autoignition likely occurs near the jets, corresponding to the weakened Stage II. By contrast, Mode I exhibits a stronger Stage II, anticipated to originate near the jets and gradually develop into bulk premixed autoignition [310]. This aligns Mode I more closely with the PREMIER combustion strategy commonly used to promote higher reactivity and controlled end-gas premixed autoignition. Quantitatively, the MAPO in Phase I reaches 12.1 bar at 62% MEF, in clear contrast to 2.1 bar at 86% MEF. For Phase II, this difference persists, with MAPO maxima of 14.2 bar and 2.4 bar, respectively. These pronounced differences confirm that knocking is considerably more significant in Mode I. The greater magnitude of premixed autoignition in Phase I at lower MEF (PRRmax of 7.7 versus 2.95 bar/°CA at the highest MEF) induces stronger in-cylinder pressure fluctuations, which may also propagate and intensify MAPO levels in the subsequent combustion Phase II. The sustained and even increasing pressure fluctuations that extend beyond the end of Phase I further showcase the presence of elevated end-gas autoignition reactivity in Mode I.

4.5.2 *Quantitative evaluation*

Qualitative analysis of heat release profiles in methanol PRDF combustion revealed distinct morphologies corresponding to varying combustion dynamics. To complement this phenomenological assessment, quantitative characterization of HRR profile evolution is essential for robust combustion mode classification. Comparable approaches have been employed in other studies, ranging from quantifying symmetry and magnitude ratios in a natural gas PRDF engine [139] to tracking the

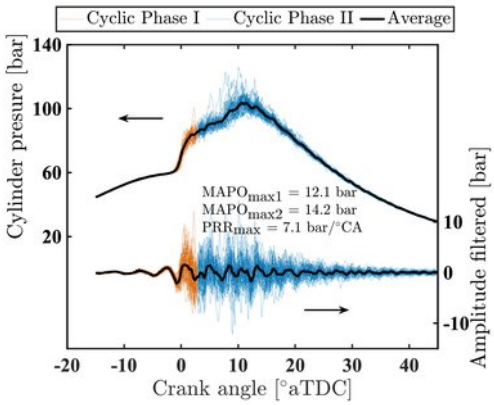

(a) Combustion mode I (MEF 62% at 11 bar gIMEP)

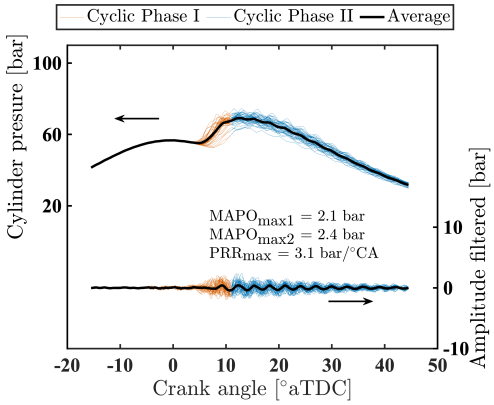

(b) Combustion mode II (MEF 86% at 11 bar gIMEP)

Figure 4.12: Raw and filtered pressure for Modes I and II at 11 bar gIMEP

transition from a two- to a single-stage heat release profile in a diesel-ethanol RCCI engine [311].

This research introduces two metrics to systematically characterize HRR profiles in methanol PRDF combustion: the **Combustion Mechanism Index (CMI)** and the **Phase Magnitude Ratio (PMR)**. The CMI quantifies the fraction of the duration from SOC to the peak of Phase I to the overall combustion duration:

$$\mathrm{CMI} = \frac{\mathrm{CA}_{\mathrm{PHRR1}} - \mathrm{CA}_{\mathrm{SOC}}}{\mathrm{CA}_{\mathrm{EOC}} - \mathrm{CA}_{\mathrm{SOC}}} \cdot 100\% \tag{4.6}$$

where $\mathrm{CA}_{\mathrm{PHRR1}}$, $\mathrm{CA}_{\mathrm{SOC}}$, $\mathrm{CA}_{\mathrm{EOC}}$ represent crank angles of the first peak heat release rate, start of combustion, and end of combustion, respectively. Since the first phase in PRDF engines always occurs via premixed autoignition, the CMI expresses the extent to which premixed autoignition dominates the subsequent combustion process. Lower CMI values indicate a relatively longer second phase and greater phase separation, whereas higher CMI values suggest more similar mechanisms

between the two phases, with a faster second phase and a more homogeneous profile. The PMR characterizes the relative intensity of Phase I to Phase II:

$$\mathrm{PMR} = \frac{\mathrm{PHRR1}}{\mathrm{HRR60}} \cdot 100\% \tag{4.7}$$

where PHRR1 represents the first peak in HRR and HRR60 denotes HRR at CA60. The metric was initially calculated with HRR50, but CA50 does not correlate very well with Phase II, limiting its ability to represent the second phase. HRR60 consistently aligned with the actual second-phase peak across all operating modes, making it a more representative choice. PMR values above 100% indicate Phase I dominance, whereas values below 100% reflect Phase II dominance.

Fig. 4.13 illustrates how the proposed metrics capture profile-shaping characteristics across the three combustion modes. Mode I shows the highest CMI (18.7%), reflecting reduced phase separation (I/II) due to similar combustion rates between phases, which also enhances HRR symmetry. Its moderate PMR above 100% (109.0%) indicates comparable peak magnitudes of the two stages. Mode II exhibits a lower CMI (11.6%) as the flame propagation mechanism prolongs Phase II, creating greater temporal separation between diesel (Phase I) and methanol combustion (Phase II). The elevated PMR (180.5%) reflects the h-shaped profile's dominant first peak, in which intense diesel premixed autoignition (Stage I) overshadows the attenuated methanol combustion phase, primarily via Stage III. This transition from autoignition to flame propagation alters both temporal distribution and magnitude balance, as captured by the metrics. Mode III shows the lowest CMI (10.9%) and PMR (27.1%), indicating stronger temporal asymmetry and clear Phase II dominance. The inverse relationship (PMR<100%) arises when HRR60 exceeds PHRR1, signifying MPDF combustion with flame propagation generating higher HRR than the initial autoignition of the small pilot diesel. This corresponds to the n-shaped profile observed at extreme MEFs and maximum load, which, as it will be discussed later, required increased intake air temperature to make such high-MEF operation feasible.

Mapping HRR profiles with the combined CMI and PMR metrics establishes a quantitative link between profile shape and underlying combustion behavior, offering a systematic method for combustion mode identification. Fig. 4.14 shows all operating points from this campaign plotted in the CMI-PMR domain, color-coded by combustion mode, including the DO baseline at 11 and 15 bar gIMEP. Dashed arrows indicate shaping transitions along the two MEF sweeps and the simultaneous intake air temperature increase at the highest load and MEFs.

This visualization reveals four possible regimes, defined by thresholds in the two metrics. The horizontal threshold at PMR = 100% separates first- and second-phase dominance. PMR above 100% indicate a stronger Phase I, typical of Modes I and II, whereas PMR below 100% reflects Phase II dominance, as in Mode III. Concerning DO cases, low-load DO would typically lie above 100% PMR because of the Phase I dominance, while higher load DO shifts below 100% PMR due to a stronger diffusion phase.

The vertical threshold, set at CMI $\approx$ 15% , further differentiates regimes by combustion mechanism. Higher CMI values indicate more symmetric profiles with phases more evenly distributed between SOC, PHRR1, and EOC, as in Mode I. Low CMI values, approaching 0%, reflect greater temporal separation between

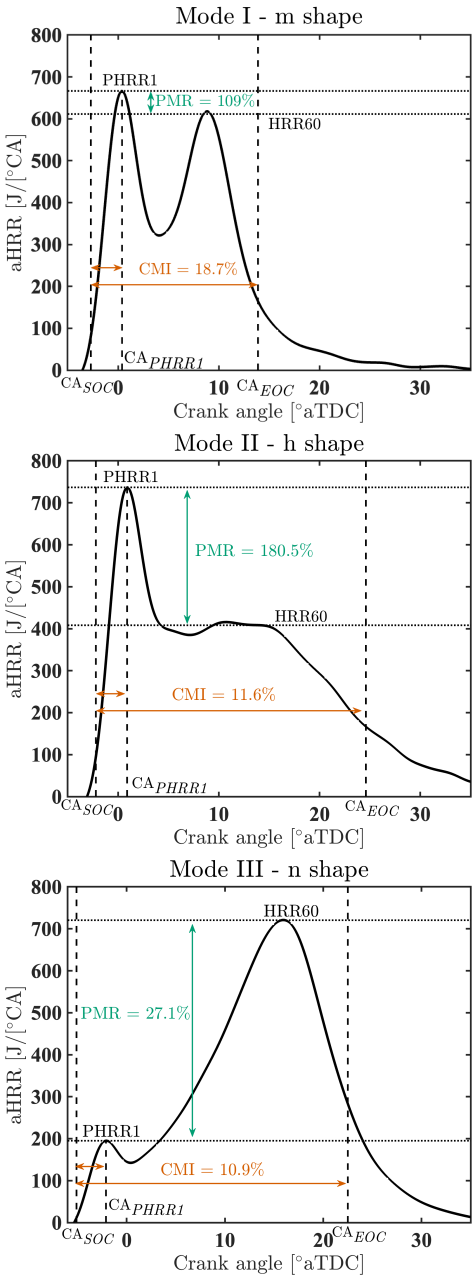

Figure 4.13: Shaping characterization methodology using CMI and PMR metrics

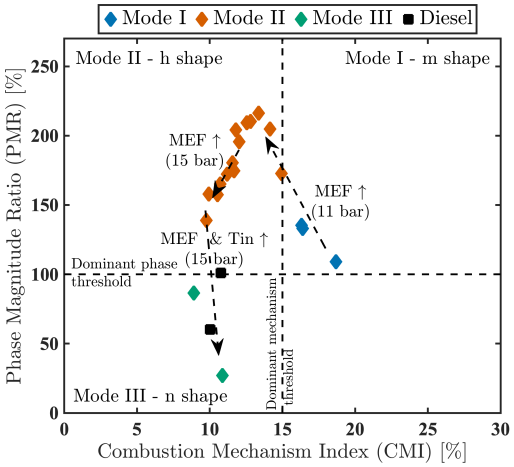

Figure 4.14: Heat release profile mapping based on CMI and PMR metrics

combustion phases, typical of flame-propagation-dominated Modes II and III. The 15% threshold was approximately chosen, acknowledging the limits of pressure-based HRR evaluation. More refined thresholds could be derived from optical diagnostics, detailed knock analysis, or chemical kinetics-based modeling.

Within this framework, three quadrants are populated experimentally:

- Quadrant I (CMI $>$ 15%, PMR $>$ 100%): Mode I (m-shape).
- Quadrant II (CMI $<$ 15%, PMR $>$ 100%): Mode II (h-shape).
- Quadrant III (CMI $<$ 15%, PMR $<$ 100%): Mode III (n-shape).

Quadrant IV (CMI $>$ 15%, PMR $<$ 100%), representing strong methanol autoignition similar to Mode I but with Phase II dominance, was not realized experimentally in this experimental campaign. Such a regime could likely be achieved under higher reactivity conditions. However, these conditions must be carefully controlled, as they drive the engine closer to knock, as seen in the closest case that approached 100% PMR. In theory, CMI exceeding 30% together with PMR near 100% would indicate an RCCI-like homogeneous autoignition regime.

4.6 IMPACT OF MEF ON COMBUSTION AND ENGINE PERFORMANCE

Following the direct comparison between DO and methanol DF operation and combustion mode analysis, this subsection systematically explores the effects of varying MEF at the two high-load points (around 11 and 15 bar gIMEP). By examining both load points in parallel, the discussion aims at providing direct insights into load-dependent characteristics together with the methanol effect, due to the influence of different boundary conditions such as air excess ratio and in-cylinder temperatures. Fig. 4.15 illustrates the effects of varying MEF at the two high-load points tested.

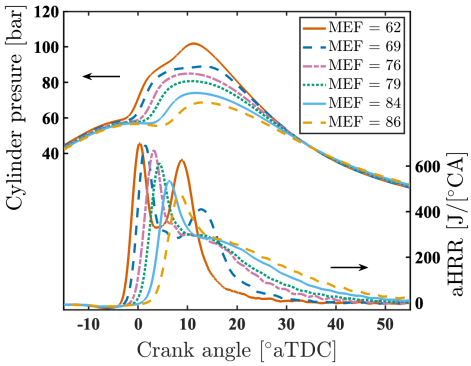

(a) 11 bar gIMEP

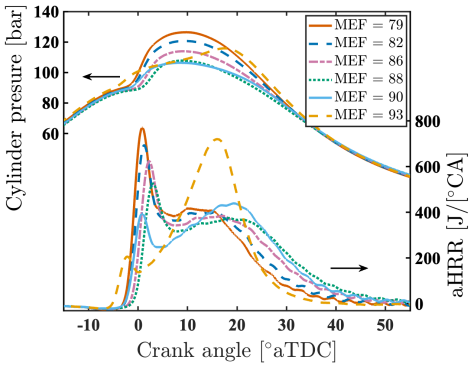

(b) 15 bar gIMEP

Figure 4.15: MEF effects on pressure and aHRR at high loads

4.6.1 *Combustion phasing and duration*

At the 11 bar gIMEP load point, the evolution of heat release profile with incremental increases in MEF becomes particularly evident, building on the combustion mode analysis presented earlier. As MEF increases, the characteristic m-shaped profile of combustion Mode I transitions progressively toward the h-shaped profile associated with combustion Mode II. This shift is primarily driven by the enhanced charge cooling effect of methanol, which delays ignition, as reflected in the steady increase in ID from 8.8 to 14.4 °CA across the MEF sweep relative to 5.3 °CA in DO, as shown in Fig. 4.16. Interestingly, the extended ID does not result in a more pronounced Phase I. Instead, the premixed phase only marginally lengthens—from 5.5 °CA at the minimum MEF to 6.5 °CA at the maximum—and its intensity diminishes, as indicated by a decrease in the HRR_{max} from 685 to 476 J/°CA. This attenuation can be attributed to the later phasing of combustion after TDC, which makes the thermodynamic conditions, pressure and temperature, less favorable for methanol autoignition alongside diesel in Stages I/II. The increased displacement of air with higher MEF further deteriorates the mixing quality of diesel and air during the

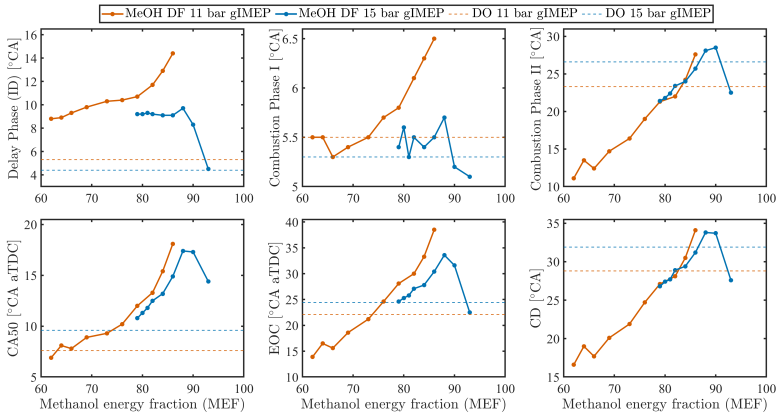

Figure 4.16: MEF effects on phasing and duration

ID period. As a result, the less intense premixed combustion during Phase I leads to a correspondingly weaker and more prolonged Phase II, as the duration of the methanol-air combustion phase increases from 11.1 to 27.6 °CA. Both CA50 and EOC are delayed with increasing MEF, with the combustion duration at the highest MEF being more than twice that at the lowest MEF.

Interestingly, for MEF values below 82%, the combustion duration is actually shorter than in the DO baseline at the same load, despite a longer ID and a slightly more retarded CA50. This effect is primarily due to a more pronounced Phase II, which is significantly shorter than the mixing-controlled second phase in DO operation. For example, at a minimum MEF of 62%, Phase II lasts about 11.1 °CA, compared to 23.3 °CA for the diffusion phase in DO mode. These observations underscore the nuanced sensitivity of combustion phasing metrics in PRDF strategies. Notably, the most advanced CA50 does not always correspond to the fastest overall combustion, as variations in the behavior of the second phase can lead to extended combustion durations. Therefore, it is essential to consider both combustion duration and additional phasing metrics, such as CA60, for a comprehensive evaluation of PRDF combustion and its comparison with DO operation. Additionally, at minimum MEF, all combustion phasing characteristics—including CA50—are more optimal than in the DO case, counterbalancing the overall ignition delay in methanol PRDF operation.

At 15 bar gIMEP, the evolution of the heat release profile reveals a distinctly different trend from that observed at the lower load point of 11 bar gIMEP. As the MEF increases, the initial response mirrors the lower load case; ID becomes longer with combustion phasing gradually deteriorating. However, a critical transition occurs once MEF exceeds 88%. Beyond this MEF, ID decreases sharply, leading to a more advanced Phase I of combustion—an effect most pronounced at the higher MEFs (90% and 93%). This abrupt change in ignition profoundly impacts the subsequent combustion dynamics. The primary driver of this ignition phenomenon was a targeted adjustment in intake air temperature, from 323 K at MEF below 88% to 333 K and 353 K at 90% and 93% MEF, respectively. This was implemented to briefly

assess the stability enhancement at these higher MEFs with an adjustment in such an operating control parameter. The temperature increase improved in-cylinder thermal conditions at the time of diesel injection, gradually advancing combustion phasing and improving efficiency. Consequently, less fuel was required for both methanol and diesel to maintain the target load, resulting in a reduced methanol cooling effect that further supported phasing advancement and a subsequent increase in air excess ratio from 2.48 to a peak of 2.72. These combined boundary condition changes ultimately reduced ID and overall improved combustion performance. While this research focuses on MEF effects under nominally constant boundaries, the observed improvements from this temperature adjustment underscore the value of simple parameter optimization in methanol PRDF engines.

The observed shift in ID at the highest load, deriving from adjustments in boundary conditions, fundamentally changes the subsequent combustion dynamics and results in a clear improvement in overall combustion performance. At 93% MEF, methanol DF operation achieves IDs comparable to those of the DO mode, yet with key distinction in combustion phasing and heat release propagation. Despite similar IDs, CA50 remains more advanced in DO mode, occurring in 9.6 °CA aTDC versus 14.4 °CA aTDC for methanol operation. However, it is in the latter half of the heat release process in which methanol DF's distinct combustion mode becomes more evident. In methanol DF conditions with 93% MEF, combustion Phase II is notably faster, with its duration decreasing from 26.6 °CA in DO to 22.5 °CA. This acceleration in the latter combustion phase enables the entire combustion event in methanol operation to finish earlier, as reflected in a more advanced EOC, 22.5 °CA aTDC relative to 24.4 °CA in DO. The changing behavior is attributed to the fundamental difference between the combustion regimes of the two strategies in their second combustion phase. At 93% MEF, methanol DF operation tends toward a MPDF regime, dominated by premixed bulk turbulent flame propagation, whereas the DO case remains characterized by mixing-controlled combustion phase. The formation and development of flame kernels take longer to initiate than the onset of mixing-controlled combustion in DO, resulting in initially slower heat releases in the DF mode. Yet, once these flame kernels are established and a bulk turbulent flame propagation is initiated, combustion rate is higher than that of diffusion-limited combustion under DO, enabling the second combustion phase in methanol DF to overtake the first phase and ultimately produce a shorter total combustion duration, decreasing it to 27.6 °CA from 31.9 °CA under DO.

Comparing the operating points across the MEF sweep reveals how shortening the ID and advancing flame initiation toward TDC fundamentally enhance combustion performance, mirroring the behavior in SI engines. Even though the ignition energy from the pilot jet diminishes at the highest MEF—as evidenced by the reduction in HRR_{max} from 736 J/°CA at 79% MEF to 195 J/°CA at 93% MEF—the advancement of ignition timing creates more favorable thermodynamic conditions near TDC. This better phasing supports more robust flame propagation, underscoring that, in this regime, combustion performance is more sensitive to ignition timing of the pilot fuel than to its absolute energy—a trend also well-aligned with knowledge from SI engines [264, 312]. Moreover, the performance of flame propagation observed at a global air excess ratio of 2.72 highlights the strong capability of multi-point pilot-induced flames to sustain efficient combustion under very lean conditions.

This stands in contrast to conventional lean-burn SI engines, which typically cannot operate stably at λ greater than 1.6, particularly in large HD applications [235, 245].

4.6.2 *Combustion stability and engine performance*

The intricate balance between combustion phasing, stability, and engine performance is critical in PRDF operations. Advancing combustion closer to TDC is typically desired to maximize thermal efficiency, yet it often escalates knocking propensity, challenging engine stability and its mechanical integrity. Given this interdependency, it is essential to assess a variety of combustion metrics, including peak PRR (PRR_{max}), peak pressure (P_{max}), MAPO and COV_{gIMEP} to better characterize engine response.

Fig. 4.17 illustrates how these key indicators vary across the MEF sweeps at both analyzed load points. To provide deeper insights into the combustion process, an additional metric is illustrated: the ratio of the heat released during Phase I to the total heat release (HR_I), offering quantitative information of the relative intensity of the premixed combustion phase. As expected from combustion phasing results, HR_I is more pronounced during methanol DF operation compared to DO due to the increased IDs, except the two highest MEF at 15 bar gIMEP load point. However, the trend of HR_I is decreasing with increasing MEF despite the increased IDs, as it drops from 33.1% to 26.5% and from 25% to 6.2% across the two MEF sweeps of 11 and 15 bar gIMEP load points. This can be attributed to the less favorable thermodynamic conditions when premixed Phase I occurs farther away from TDC, resulting in less methanol combusting alongside diesel. The lower premixed air excess ratio due to increasing MEF also deteriorates the mixing of diesel and air during ID. The resulting weaker and delayed Phase I results in the apparent lower peak pressure and PRR. At 11 bar gIMEP load point, P_{max} consistently decreases from 102 to 69 bar, with PRR_{max} dropping from 7.05 to 3.14 bar/°CA, even below the 4.54 bar/°CA in DO operation. The same decreasing trend is observed for both pressure metrics at the higher load, yet after the transition at 88% MEF, both starts rising again. While peak pressures under methanol operation remain well below the peak pressure levels of DO due to the relatively delayed combustion phasing, peak PRRs are typically well above the DO baseline which is attributed to the observation of more concentrated combustion of fuel in less time for methanol DF.

Knock intensity emerges as a key parameter when transitioning from DO to methanol PRDF operation, primarily due to enhanced reactivity of the end-gas mixture during combustion. Knocking levels are higher across most MEFs investigated, with the most severe knock occurring at the lower end of the MEF range, a factor that ultimately constrained the minimum MEF limit during experimental campaign. As the MEF increases, the MAPO during both Phase I and II systematically declines, reflecting reduced knocking severity. This trend is attributed to the greater methanol-induced charge cooling, which lowers end-gas reactivity and knock propensity. At the highest MEFs studied, the MAPO for Phase I even drops below the DO baseline. Specifically, at 11 bar gIMEP, MAPO reduction is linked to delayed combustion phasing, despite enhanced HR_I, while at 15 bar gIMEP, the decrease is due to a less intense Phase I, despite combustion timing closely matching that of DO operation.

Apart from knocking, increased reliance on flame propagation as the dominant combustion mechanism at higher MEFs makes the in-cylinder processes inherently

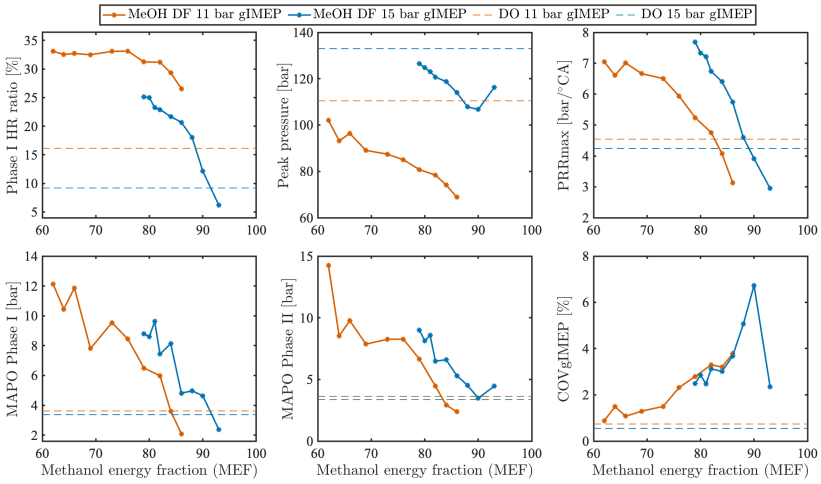

Figure 4.17: MEF effects on combustion characteristics and stability

more sensitive to cycle-to-cycle variations, particularly under lean operating conditions. This sensitivity is evidenced by the rising trend of the COV_{gIMEP} as MEF increases. For instance, at 11 bar gIMEP, as the combustion mechanism shifts from premixed autoignition to slower flame propagation, MAPO declines but COV_{gIMEP} rises significantly—from 0.87% at 62% MEF to 3.78% at 86% MEF—surpassing the DO baseline of 0.74%. Such deterioration in combustion stability serves as a precursor to lower efficiencies and increased UHC emissions. It is important to note that a COV_{IMEP} threshold of 3% is typically regarded as a practical upper limit for acceptable stability in flame propagation regimes such as lean-burn SI engines [234, 242]. For the lower load (11 bar gIMEP), this limit is surpassed after 79% MEF, indicating a transition to rough engine operation, while at higher load (15 bar gIMEP) exceeds this threshold after 82% MEF. However, the transition to the MPDF-type of combustion under the maximum MEF (93%) and its combustion phasing improvements achieve acceptable COV_{IMEP} of 2.35%; though it still remains considerably above the DO baseline value of 0.55%. The effect of combustion phasing and stability on performance across the MEF sweeps, including the behavior at the highest MEFs and the maximum load, is confirmed through the analysis of energy balance, as depicted in Fig. 4.18.

For both 11 and 15 bar gIMEP load points, the overall energy balance shifts similarly with increasing MEF, except for the distinct transition observed after 88% at high load due to increased intake temperature. Across the MEF sweep, gross indicated thermal efficiency (gITE) declines with increasing MEF, primarily due to deteriorating combustion phasing that occurs farther from TDC. This delayed and prolonged combustion is responsible for the observed increase in exhaust energy losses throughout the sweeps. Conversely, elevated MEFs enhance cooling, consistently reducing heat transfer losses relative to DO operation (approximately 20%). At 11 bar gIMEP, heat transfer losses decrease substantially—from 15.60%

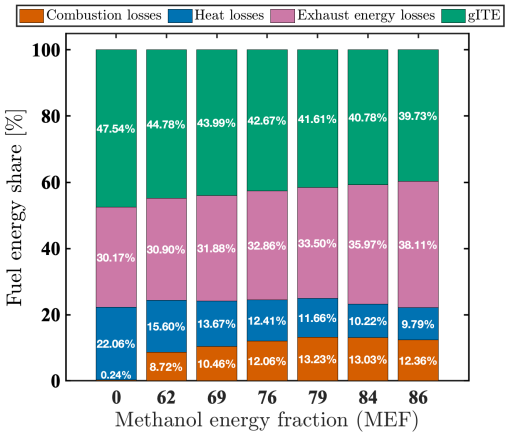

(a) 11 bar gIMEP

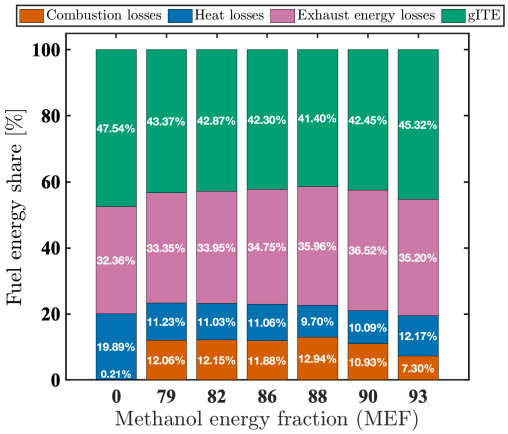

(b) 15 bar gIMEP

Figure 4.18: MEF effects on energy balance

at 62% MEF to 9.79% at 86% MEF. A similar trend is evident at 15 bar gIMEP; however, beyond 88% MEF, heat transfer losses begin to rise again, peaking at 12.17% at 93% MEF due to higher air temperature which counteracts methanol's cooling effect. Overall, the net decrease in heat-transfer losses at elevated MEF is linked to several coupled effects: methanol's cooling effect that lowers the bulk gas temperature, a progressive combustion transition from mixing-controlled to premixed flame propagation that reduces localized high-temperature zones, and changes in overall combustion duration. All these three factors together modify the temperature gradients within the combustion chamber, and thus the cumulative wall heat transfer. The combustion phasing switch after 88% at high load leads to recovery in performance: gITE and combustion efficiency reach their maximums of 45.32% and 92.70% at 93% MEF, respectively. These remain, however, below those of DO operation (47.54% and 98.79%). Notably, even at the optimal combustion

phasing at 93% MEF, exhaust losses stay elevated compared to other MEFs and DO operation. This is attributed to the absence of most premixed autoignition in the overall combustion process at the highest MEFs, which shifts a larger fraction of fuel to burn during the later expansion phase, thereby reducing thermodynamic efficiency.

4.6.3 *Emissions characteristics*

Fig. 4.19 presents the engine-out emissions profiles for NO, NO_2, CO, and UHC across the two MEF sweeps. NO emissions were significantly reduced compared to DO operation at all tested MEF levels for both load sweeps. This reduction was less pronounced at the lower end of the MEF range at 11 bar gIMEP, owing to diminished charge-cooling from lower methanol quantities and more advanced combustion phasing near TDC. At 11 bar gIMEP, ISNO emissions steadily decreased from 5.88 to 2.10 g/kWh as MEF increased, considerably lower than the DO baseline of 7.53 g/kWh. At 15 bar gIMEP, the benefit is even more substantial due to higher achieved MEFs, with ISNO emissions falling to as low as 1.07 g/kWh under methanol DF operation (compared to 7.53 g/kWh for DO). As anticipated, NO_2 emissions are higher at all MEF conditions relative to the DO baseline. Increasing MEF, however, resulted in lower levels of NO_2, which can be attributed to the lower levels of NO, which reduces the NO density in the end-gas region during the end combustion phase.

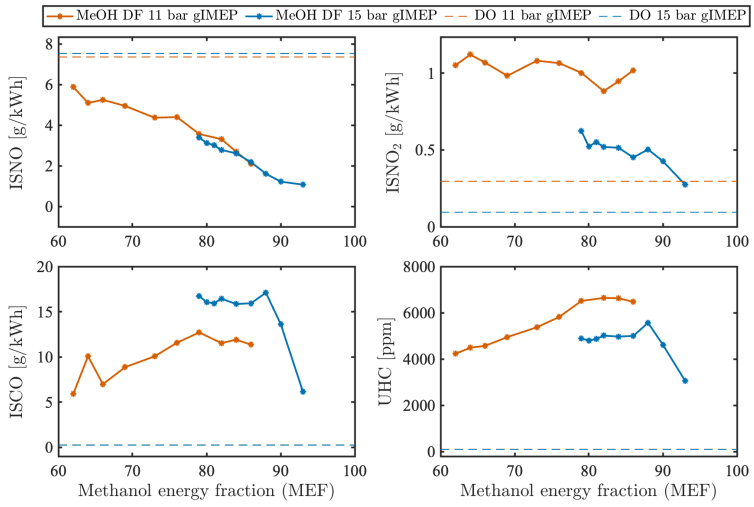

Figure 4.19: MEF effects on emissions

The cooling effect of methanol and the increased reliance on flame propagation in PRDF mode generally produces a clear trade-off between NO_x and partial combustion products, i.e., higher CO and UHC emissions. For all MEFs assessed, CO and UHC levels far exceeded those of DO operation (with DO baselines at 0.23 g/kWH for CO and 97 ppm for UHC). At 11 bar gIMEP, ISCO rose from 5.88 to

11.35 g/kWh, and UHC values increased from 4228 to 6472 ppm with rising MEF. At 15 bar gIMEP, these emissions remained at relatively similar levels across the sweep, except a slight rise at 88% MEF. However, beyond 88% MEF, a remarkable drop occurs: ISCO falls from 17.1 to 6.14 g/kWh at 93% MEF, with UHC also decreasing from 5567 ppm to 3061 ppm.

In summary, higher MEF in PRDF tends to lower NO emissions by reducing in-cylinder temperatures and diffusion combustion, but this benefit is offset by higher CO, UHC, and NO_2. Raising the intake air temperature at 93% MEF markedly improved emissions and overall performance, showing the strong influence of boundary conditions. Careful control of intake temperature can enhance PRDF performance, reduce pilot-fuel demand, and improve both emissions and efficiency. In practice, the objective remains to maximize MEF, but only within a feasible operating window defined by efficiency, emissions targets, and combustion constraints like knock and stability. The expected important role of different boundary conditions—such as air excess ratio and retained residual gases—on the performance of methanol PRDF engines and their potential to enable this high-MEF operation is examined in Chapter 5.

4.7 CONCLUSIONS AND RECOMMENDATIONS

In summary, this chapter presented the results of an experimental investigation on a large-bore single-cylinder marine engine operating under the methanol premixed dual-fuel (PRDF) strategy at high methanol energy fractions (MEFs). By integrating qualitative and quantitative analytical frameworks, the research provides new insights into combustion mechanisms and phasing at play, and their relationships to overall engine performance. The results and discussions presented herein aimed to address the third research question (**RQ3**), demonstrating how a systematic analytical approach can reveal dominant combustion modes and deepen understanding of combustion behavior in methanol PRDF engines.

The diesel-only (DO) to methanol dual-fuel (DF) transition fundamentally alters the energy balance. Heat transfer losses were nearly halved in methanol mode compared to DO, and although thermodynamic efficiency was slightly compromised, methanol operation enhanced the conversion of released fuel energy into work output. Nevertheless, the main barrier to maintain or even further improve the overall thermal efficiency of diesel engines with methanol remains the high combustion losses, as combustion efficiency dropped from 99.8% (DO) to 92.7% (PRDF) at the highest MEF and load tested. Two distinct MEF operational windows were identified during the employed experimental campaign (EC III): the first limited to lower MEFs by excessive pressure rise and combustion instability, and the second bounded at higher MEFs by a renewed onset of instability and deteriorating combustion efficiency. Qualitative analysis of heat release rate (HRR) profiles revealed three distinct combustion modes: i) m-shape (Mode I)—a dual peak profile dominated by premixed autoignition for both fuels, ii) h-shape (Mode II)—a pronounced pilot autoignition followed by attenuated flame propagation, and iii) n-shape (Mode III)—dominated by turbulent bulk flame propagation at the highest MEFs and increasing air temperatures. Combustion performance was found to be more sensitive to pilot ignition timing than to total ignition energy, mirroring

SI engine behavior; at 15 bar gIMEP, shortening ID from 9.2 to 4.4 °CA (79–93% MEF) increased combustion efficiency from 87.9% to 92.7% and gross indicated thermal efficiency from 43.4% to 45.3%. All methanol DF operating points resulted in lower NO_x emissions compared to DO (ISNO reduced from 7.53 g/kWh to as low as 1.07 g/kWh at peak MEF). This came at the cost of higher NO_2/NO ratios and substantial increases in CO and UHC emissions, yet these trade-offs diminished at the highest MEF which achieved the best overall performance and emissions balance. Notably, the observed boost in combustion efficiency at 93% MEF with increased intake temperature indicates a promising path to reduce combustion losses without raising heat transfer or NOx emissions. This is particularly important for existing diesel engines with mechanically driven injection systems, in which minimal modifications are sought in retrofitting scenarios. This highlights the scope for detailed parametric studies on such control parameters to further optimize methanol PRDF performance.

Given these findings, several recommendations emerge for future research and practice. First, the developed CMI-PMR methodology provides a practical tool for diagnosing and optimizing combustion regimes in methanol PRDF engines, but its classification robustness would benefit from validation and extension using more sophisticated data—including optical diagnostics and detailed chemical kinetics simulations. Second, a deeper understanding of several boundary conditions—such as mixture temperature, air excess ratio, and residual gas masses—seems crucial for methanol PRDF engines. Better understanding of how these boundary conditions can enhance methanol PRDF engine performance can unlock the potential of methanol in a wide range of engine sizes and enhance the efforts for its integration as a sustainable marine fuel.

Ultimately, this chapter advanced the understanding of high-MEF methanol PRDF combustion, clarified its distinct operating modes, and introduced robust frameworks for combustion classification. The established methodologies can be extended using broader operating ranges to enhance diagnostic and optimization strategies, supporting continued development of methanol-fueled heavy-duty powertrains and advancing the adoption of renewable fuels.

5

IMPACT OF BOUNDARY CONDITIONS ON METHANOL PRDF ENGINE PERFORMANCE[1]

Failure is unimportant.
It takes courage to make a fool of yourself.

— Charlie Chaplin

This chapter addresses the fourth and final research question (**RQ4**), introduced in Chapter 1 and further developed in Section 2.3. Given the scarcity of detailed experimental investigations on how design and operating parameters influence combustion and overall performance in methanol PRDF engines, this study extends and applies the analytical framework developed in Chapter 4 to a broader parametric exploration. To this end, the fourth and final experimental campaign (EC IV) of this research conducted parametric sweeps to isolate the effects of selected control parameters—each manipulating distinct boundary conditions—and to examine their influence under high-MEF, high-load operation. These sweeps include variations in intake and exhaust pressure, in addition to the intake air temperature effect discussed in Chapter 4.

This chapter is structured as follows. Section 5.1 revisits the literature on parametric exploration in methanol PRDF engines. Section 5.2 presents the operating conditions of EC IV tested for the analysis of this chapter. The impacts of the retrofit-friendly control levers—intake and exhaust pressure—on combustion and engine performance characteristics are discussed in Section 5.3 and Section 5.4, respectively. Section 5.5 then applies the combustion mode map classification of Section 4.5.2 to the parametric dataset. Finally, Section 5.6 summarizes the findings and provides key conclusions and recommendations derived from the parametric exploration.

5.1 INTRODUCTION

Methanol PRDF engines face persistent challenges with reduced combustion efficiency and knock at high MEFs [300, 314]. Successful diesel-to-PRDF conversion requires careful control of in-cylinder conditions—temperature, volume, pressure,

1 This chapter is partly reproduced from Kiouranakis et al. [313]

and equivalence ratio—to secure stable combustion. Intrusive hardware modifications may be employed, such as geometric compression ratio changes [315], variable compression ratio technologies [316–319], variable valve actuation [320], or exhaust gas recirculation [321, 322]. Domínguez et al. [323] employed a single-cylinder research diesel engine incorporating several adjustable control variables, including EGR, to study methanol PRDF operation. Utilizing methanol's cooling effect and high EGR rates, they demonstrated that faster and highly-premixed combustion can be achieved compared to diesel baseline, resulting in significantly lower NO_x and soot emissions. However, PRDF high-load operation was restricted to 60% MEF due to elevated pressure rise rates deriving from the premixed combustion. In a subsequent study by the authors [315], the piston crown was replaced by one with geometrically similar but smaller bowl to assess the impact of increasing CR on the performance of the engine. Increasing CR from 16 to 18 and lowering EGR decreased ID of diesel and improved combustion stability. The combustion stability improvement contributed to the increase of maximum MEF at 82%, with the main combustion mechanism shifting to flame propagation in the unburned methanol-air mixture. However, this transition increased CD and resulted in lower ITE compared to DO baseline and the lower CR and MEF PRDF operating points.

PRDF combustion remains anchored in diesel injection strategy, because timing, quantity, and characteristics of diesel injection continue to dictate ignition behavior, heat release phasing, and overall combustion behavior. Wang et al. [229] emphasized the key role of pilot injection timing in their efforts to improve combustion performance under part loads in a methanol PRDF engine. Advancing pilot injection, together with higher intake temperatures, increased thermal efficiency beyond that of diesel at 60% MEF. Similarly, Li et al. [231], using a six-cylinder HD engine, showed that advancing injection timing or increasing injection pressure significantly improves combustion stability and thermal efficiency. Moreover, Yang et al. [324] used numerical simulations to explore the effects of several injection parameters, such as pressure and angle, confirming that delayed injection timing deteriorates combustion and overall efficiency, whereas increased injection angle and pressure enhance them. Srna et al. [135, 136] conducted fundamental methane-diesel PRDF combustion studies, showing that pilot injection dynamics critically influence the interaction between pilot and methane combustion, which is corroborated by similar optical access studies of methanol-diesel PRDF combustion [129]. The methane-fueled studies also demonstrated that transitioning from DO to PRDF makes combustion more coupled with in-cylinder boundary conditions such as temperature, oxygen density, and equivalence ratios.

When diesel engines are converted to PRDF operation, precise control of boundary conditions becomes essential to ensure robust operation across the engine map and to enable flexible switching between DO and PRDF modes [129]. However, many existing diesel engines employ conventional, mechanically-controlled injection systems that limit direct manipulation of injection parameters such as timing. In such cases, the importance of retrofit-friendly control levers is amplified. Adjustments to intake or exhaust pressure through throttling, as well as modulation of intake air temperature using charge air cooling [325] or heating [326], offer practical means to influence boundary conditions and combustion behavior without requiring fundamental changes to core engine hardware. Experimental investigations have already

demonstrated the impact of these measures. For example, raising intake air temperature has shown its ability to mitigate methanol's strong charge cooling and enhance both ignition and combustion stability in PRDF engines, at both low [109] and high loads [155, 191, 327]. The performance gains observed with intake air temperature adjustments during the MEF sweep in Section 4.6 further underscore the critical role of this control parameter in optimizing methanol utilization within the PRDF concept. Conversely, Dierickx et al. [230] reported only marginal improvements in combustion performance at low loads with elevated intake air temperatures, which, according to the authors, may not justify the complexity and cost of implementing an intake air temperature control system. While DF concepts aim at minimizing the diesel dependence, most experimental studies are limited to low MEFs, as they face knock challenges. This has resulted in the majority of parametric explorations to adopt strategies which reduce in-cylinder mixture reactivity to extend these relatively low MEF limits [314]. Dierickx et al. [230] applied EGR and reduced intake pressure, while Guan et al. [158] used EGR and intake air cooling to suppress MEF limitations caused by high pressure gradients at high loads. In a similar way, the study of Cung et al. [294] delayed the combustion phasing using the control levers of pilot injection timing and EGR to increase the maximum MEF at high loads.

However, recent evidence from experimental studies in large-bore methanol PRDF engines [295, 296] challenges this knock-centric paradigm. These findings indicate that, in large-bore engines operating under medium to high load and high MEF conditions, performance limitations arise primarily from poor combustion rather than knock. Section 4.5 discussed the two observed MEF regions found under methanol PRDF operation, each bounded by a different mechanism: a low-MEF region limited by knock and incomplete combustion, and a high MEF region at which poor combustion performance becomes the dominant limitation. This revised understanding indicates that strategies should prioritize charge reactivity to enable stable and efficient high-MEF operation in methanol PRDF engines. The fact that different combustion mechanisms constrain high-MEF operation at varying load conditions has led to ambiguity regarding the influence of operating parameters on methanol PRDF engine performance. Consequently, this ambiguity and overall scarcity of studies under high-MEF PRDF operation—particularly in large-bore engines—restricts our understanding of marine-scale methanol PRDF systems, which operate under distinct regimes characterized by lower speeds and higher power outputs.

To address these gaps, this chapter investigates how key boundary conditions—air excess ratio and residual gas (RG) mass—influence the combustion behavior of methanol in PRDF engines. Employing the analytical framework of Section 4.5, the aim is to better understand how retrofit-friendly parameters affect ignition dynamics, combustion development, efficiency, and emissions at high MEFs. Although optimization toward maximum MEF with high efficiency and low emissions is beyond the scope of this thesis, this chapter provides mechanistic insights into the influence of individual control parameters. Such understanding informs future optimization strategies and promotes a retrofit-oriented pathway for higher methanol utilization in methanol-fueled PRDF marine engines.

5.2 OPERATING TEST CONDITIONS

This chapter employs the final experimental campaign EC IV of this dissertation, extending the methanol PRDF dataset (EC III) by means of key control parameters: intake and exhaust pressure. The experiments were performed on the same single-cylinder marine research engine setup at 1500 rpm (see Fig. 4.1), using the thermodynamic analysis framework developed in Chapter 4. The discrete actuator levels and corresponding operating points are summarized in Table 5.1.

Table 5.1: Experimental test conditions for parametric pressure boundary conditions exploration (EC IV)

Sweep	p_{intake} [bar]	$p_{exhaust}$ [bar]	$\Delta p_{scavenge}$ [kPa]	gIMEP [bar]	Diesel flow [g/cycle]	MeOH flow [g/cycle]	MEF [%]	λ_{global} [-]	T_{IVC} [K]	p_{IVC} [bar]
Intake pressure	1.80	1.80	0.7	15.26	0.061	0.538	81	1.91	327	2.09
	1.85	1.85	-0.2	15.30	0.061	0.538	81	1.97	326	2.15
	1.90	1.89	-0.7	15.28	0.060	0.538	81	2.03	327	2.20
	1.95	1.95	0.5	15.28	0.060	0.537	81	2.09	328	2.27
	2.00	2.00	0.2	15.27	0.060	0.539	82	2.15	328	2.34
	2.05	2.04	-1.2	15.40	0.061	0.539	81	2.20	329	2.41
	2.10	2.11	0.4	15.35	0.060	0.542	82	2.25	329	2.47
	2.16	2.16	-0.1	15.36	0.061	0.542	82	2.30	332	2.54
	2.21	2.22	0.3	15.45	0.062	0.544	81	2.34	331	2.60
	2.27	2.27	-0.2	15.23	0.062	0.545	81	2.40	331	2.66
	2.31	2.32	0.4	15.40	0.063	0.547	81	2.44	331	2.74
	2.37	2.39	1.2	15.39	0.063	0.551	81	2.48	330	2.79
	2.53	2.54	1.1	15.36	0.063	0.565	81	2.60	332	2.99
	2.59	2.58	-5.4	15.34	0.063	0.570	82	2.62	332	3.06
Exhaust pressure	2.22	2.21	-1.1	14.47	0.026	0.602	92	2.46	324	2.61
	2.22	2.32	9.9	14.74	0.027	0.602	92	2.45	325	2.61
	2.21	2.44	23.2	14.65	0.026	0.602	92	2.45	325	2.60
	2.22	2.52	30.7	14.76	0.027	0.602	92	2.44	327	2.61
	2.21	2.60	39.0	14.99	0.028	0.602	92	2.43	327	2.61
	2.21	2.70	50.0	14.85	0.027	0.601	92	2.44	327	2.61
	2.23	2.80	58.3	15.10	0.028	0.600	92	2.43	329	2.62
	2.22	2.90	69.0	15.04	0.027	0.602	92	2.43	328	2.62

To assess the effect of boost and global dilution on combustion behavior and overall engine performance, intake pressure was varied from 1.8 to 2.6 bar while maintaining constant engine speed, MEF (82%), and pilot start of injection (SOI $\approx$ 11°CA bTDC). Because the boost changes the trapped charge, the sweep induces slight changes in torque, with the operating window remaining centered around high-load point of approximately 15.30 bar gIMEP, ranging from 15.23 to 15.45 bar. Exhaust pressure was adjusted to follow a constant intake-exhaust scavenging pressure differential $\Delta p = p_{exhaust} - p_{intake}$, which also affects retained residual gases (RG). To further isolate the role of RG, a separate exhaust-pressure sweep was conducted from 2.21 to 2.90 bar at 92% MEF, with a SOI of 15°CA bTDC, and an average load of 14.80 bar gIMEP, ranging from 14.47 to 15.10 bar. Injection timing adjustments were carried out by modifying the pump's angular position relative to the engine camshaft. This sweep was also performed at 1500 rpm, with an intake temperature of 318 K (slightly lower than the 323 K used in the intake-pressure sweep). The differences in boundary conditions between the two pressure sweeps

stem from their involvement within a broader experimental campaign methodology; however, these variations do not affect the overarching objective of isolating the influence of the targeted boundary conditions on engine performance.

5.3 AIR EXCESS RATIO

Adjusting the air excess ratio (λ) is the principal boundary condition manipulation along the intake pressure adjustment. In this study, intake pressure sweep results from the compressor speed adjustment alone, with intake throttling used only when pressures below the compressor's minimum air flow capability are required. Intake pressure adjustment inherently modifies several interrelated in-cylinder boundary conditions, which together influence combustion dynamics over the closed in-cylinder process period. Fig. 5.1 illustrates how progressively increased boost pressure drives changes in multiple boundary parameters, including various defined air excess ratios (λ), temperature and pressure at inlet valve closure (IVC) (T_{IVC} and p_{IVC}), specific heat ratio during compression (γ_{comp}), and trapped masses. RG represents the amount of hot exhaust gases retained from the previous cycle, estimated using the Mirsky method as discussed in Section A.3 [328].

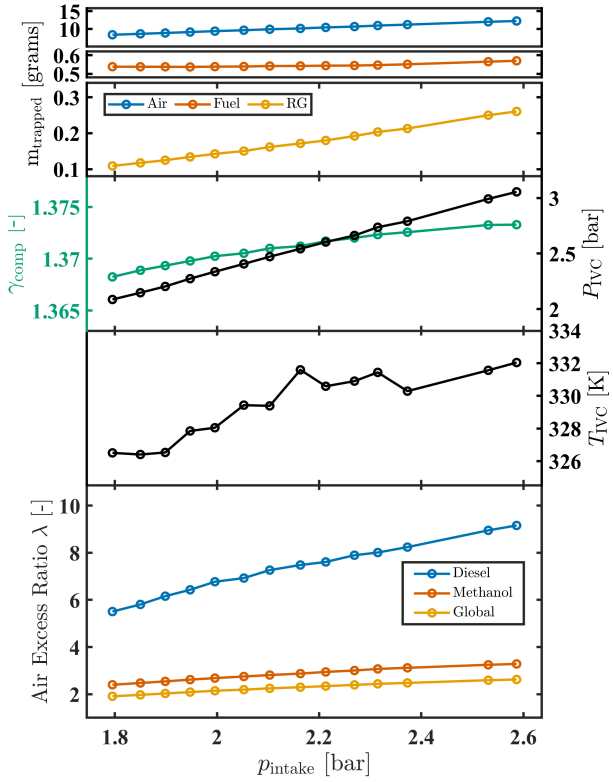

Figure 5.1: Intake pressure sweep conditions

Enhancing the scavenging efficiency with increased intake pressure would decrease retained RG masses at EVC. However, the exhaust pressure was simultaneously adjusted throughout the sweep to ensure nearly constant scavenging pressure differential $\Delta p_{\text{scavenge}} = p_{\text{exhaust}} - p_{\text{intake}}$, as seen in Table 5.1. As a result, the increasing exhaust pressure, together with increasing inertia due to elevated gas densities, during the intake pressure rise increases the total trapped RG mass from 0.11 to 0.26 grams over the full sweep. Intake charge temperature rose across the boost sweep, reflecting the higher enthalpy associated with increased air mass, further offsetting methanol's cooling effect. Despite elevated in-cylinder temperatures, the specific heat ratio γ_{comp} also rose, driven by the composition change and the higher specific heat associated with the increased air fraction in the charge. All air excess ratio definitions λ—global, methanol, and diesel-specific—demonstrate an increasing trend with intake pressure, deriving from greater air masses trapped in the cylinder. However, the diesel air excess ratio shows a markedly higher sensitivity to intake pressure variations. The diesel-specific air excess ratio responds more sharply to changes in intake oxygen density, arising from the pronounced difference in stoichiometric air-to-fuel ratios ($\text{AFR}_{\text{stoich.}}$) between diesel and methanol. This heightened sensitivity crucially influences the pilot fuel's ignition characteristics, and since PRDF combustion dynamics are highly sensitive to ignition delay (ID), the oxygen availability to diesel is expected to play a critical role in the overall combustion behavior.

Fig. 5.2 illustrates how increasing intake pressure affects the aHRR and in-cylinder pressure profiles. As intake pressure rises, the ID shortens, leading to earlier combustion phasing and elevated in-cylinder pressures throughout the sweep. The

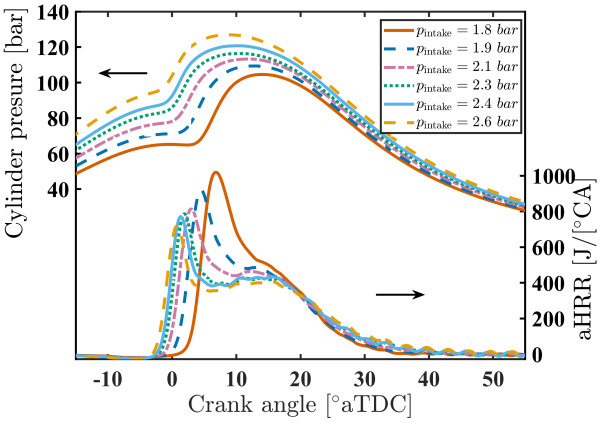

Figure 5.2: Intake pressure effects on pressure and aHRR

lower ID leads to the first part of combustion closer to TDC leading to the observed increase in peak pressure across the sweep from 105 to 127 bar. This reduction in ID results from several boundary condition changes:

- Elevated intake valve closure temperatures T_{IVC} and overall thermal state.
- Increased λ_{d}, boosting the oxygen density for the pilot and enhancing mixing.

- Higher in-cylinder pressures during injection due to increased intake valve closure pressures p_{IVC} and specific heat ratio ($\gamma_{\mathrm{comp.}}$).

Fig. 5.3 shows the effects of intake pressure on combustion phasing metrics, quantifying the decreasing trend of ID from 13.9 to 9.1°CA. The reader is referred to Section 4.3 for a reminder of the definitions of combustion phasing and staging. This shortens Phase I from 6.9 to 5.3°CA, but overall combustion phasing is delayed, as evidenced by later CA50 and EOC values due to the prolongation of Phase II from 12 to 23.6°CA. With increasing intake pressure, the HRR profile becomes less symmetric, as Phases I and II separate further. The less compact heat release profile at higher intake pressure results in lower pressure rise rate (PRR) that drops from 7.9 to 7.1 bar/°CA across the sweep. Additionally, the slower combustion phasing deteriorates combustion stability with $\mathrm{COV}_{\mathrm{gIMEP}}$ rising from 1.1% to 3.2%.

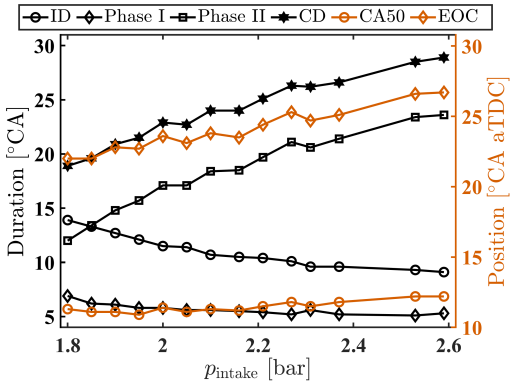

Figure 5.3: Intake pressure effects on combustion phasing and duration

At the lowest intake pressure, the longer ID causes most of diesel to burn in Stage I, while more methanol combusts either entrained within the pilot fuel (Stage I) or via premixed autoignition near the jets (Stage II). Lower air excess ratios at these conditions also increase reactivity during flame propagation combustion Stage III, pulling its phasing closer to the first two stages. Fig. 5.4 summarizes this evolution: Stage I is delayed and grows slightly due to more entrained methanol, Stage II strengthens, and Stage III accelerates, yet with less fuel left to burn. Together these effects improve overall combustion phasing despite the later ignition, and yield the HRR profile observed at lower intake pressures.

Fig. 5.5 depicts the impact of intake pressure on the energy balance. Section 4.4 underscored that delayed combustion phasing and poor combustion performance remain the main barrier to achieving diesel-like efficiency in methanol PRDF operation—a challenge that becomes even more difficult to overcome when diesel injection timing cannot be readily adjusted, as in this testbed. Combustion efficiency is highly sensitive to intake pressure and its influence on boundary conditions, especially air excess ratio, increasing from 87.7% at 2.6 bar to 92.7% at 1.8 bar. This improvement at lower intake pressures is attributed to faster flame propagation under richer conditions, resulting in a more compact heat release and a reduced proportion of fuel burning during the second combustion phase. Interestingly, des-

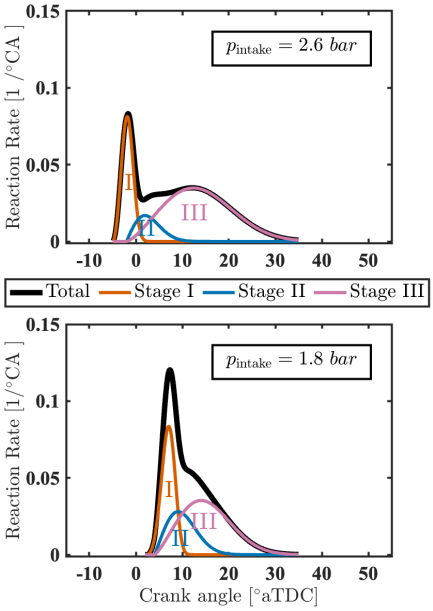

Figure 5.4: Conceptual model for the two extreme points of the intake pressure sweep

pite the enhanced combustion efficiency at lower intake pressure, heat loss remains nearly constant with a slight increase from 11% to 11.5%. A shorter combustion duration, advanced phasing, and reduced pressure levels are the primary factors contributing to heat loss increase offset resulting from the higher temperatures associated with richer combustion under the lower intake pressure conditions. This heat loss effect suggests that enriching the mixture with lower intake pressure offers potential to improve combustion efficiency providing space for further improvement through intake temperature increase or advanced pilot injection. This room for further parametric adjustments can also help decrease the exhaust energy losses that derive from the delayed combustion phasing at lower intake pressures. However, such parametric adjustments that advance combustion phasing should be implemented cautiously, as they may elevate knocking propensity. Overall, gross indicated thermal efficiency (gITE) clearly improved from 42.6% at the highest pressure to 44.7% at the lowest, demonstrating the potential of intake pressure manipulation to enhance combustion and performance. A comprehensive assessment in a multi-cylinder context, accounting for gas dynamics and pumping losses, is still necessary to draw more holistic conclusions regarding performance improvements.

Fig. 5.6 shows the effect of intake pressure on the emission characteristics. In line with the combustion efficiency trends, both UHC and CO emissions generally increase with intake pressure. However, unlike the combustion-loss trend, UHC emissions exhibit a non-monotonic behavior—decreasing from 4,430 ppm at 1.8 bar to 4,162 ppm at 2.1 bar, before rapidly rising to 5,221 ppm at 2.6 bar. This apparent inconsistency arises from the different bases of these two quantities.

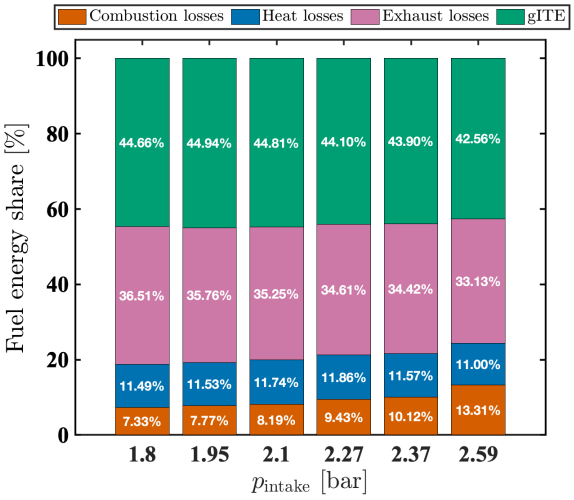

Figure 5.5: Intake pressure effects on energy balance

UHC concentration represents the ratio of unburned hydrocarbon molecules to the total exhaust gas molecules, making it dependent on the total exhaust mass flow. Combustion efficiency, on the other hand, reflects only the ratio of released energy to the total fuel energy supplied. As intake pressure increases, the air excess ratio and total exhaust flow rise, partially offsetting the effect of higher unburned fuel on UHC concentration. Thus, while higher combustion efficiency tends to lower UHC emissions, the concurrent decrease in exhaust gas flow can mask this effect, particularly at lower intake pressure where combustion efficiency improvements were more modest.

NO and NO_2 exhibit opposite trends to CO and UHC, consistently decreasing with increasing intake pressure. Specifically, NO drops from 5.38 to 2.70 g/kWh, reflecting the lower combustion temperatures associated with leaner mixtures at higher intake pressures. NO_2 also declines from 1.51 to 0.79 g/kWh across the sweep. This NO_2 behavior can be attributed to the three main factors that favor its rise: 1) density of methanol in the end-gas which can support late combustion oxidation and provide the hydroperoxyl HO_2 radical, 2) NO density coming from the pilot combustion phase, and 3) suitable temperature levels that support the conversion of NO to NO_2 [306]. Methanol density remains at similar levels during the intake pressure sweep. The similar levels of methanol quantity in the end gas and the higher end-gas temperature with lower intake pressure, thus HO_2 density, promote the conversion rate of NO to NO_2. Richer combustion of methanol alongside the pilot fuel also results in higher local temperatures, increasing NO formation. Together, these effects promote the reaction $NO + HO_2 \rightarrow NO_2 + OH$, thereby increasing NO_2 at lower intake pressures.

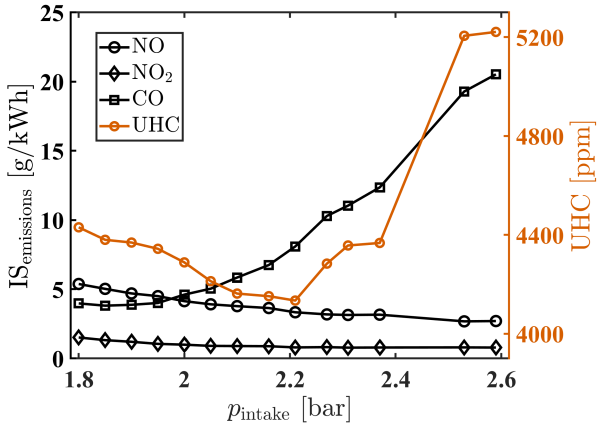

Figure 5.6: Intake pressure effects on emission characteristics

5.4 RESIDUAL GAS

This section discusses the results from the exhaust pressure sweep which influences the scavenging pressure differential. Compared to the intake pressure sweep, the impact on RG mass was slightly weaker, with trapped RG increasing from 0.18 to 0.21 g. However, unlike the intake cases, most other boundary conditions remained nearly constant. This configuration was intentionally designed to isolate the influence of residual gas on combustion as a strategy to increase the in-cylinder temperature by retaining more hot RG and provide ignition/combustion assistance. As shown in Fig. 5.7, RG mass exhibits an increasing trend with rising exhaust pressure, while air mass decreases marginally due to the reduced scavenging efficiency and more trapped RG. T_{IVC} rose from 324 to 328 K across the sweep. Other boundary conditions like air excess ratios and p_{IVC} are not displayed explicitly in Fig. 5.7 due to their nearly constant values, conserving space.

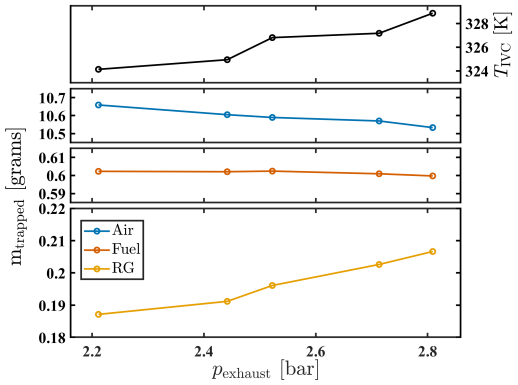

Figure 5.7: Exhaust pressure effects on trapped masses

Fig. 5.8 depicts the effect of exhaust pressure on the aHRR and bulk gas temperature profiles. Two main differences emerge compared to the intake pressure cases: 1) combustion behavior is notably less sensitive to exhaust pressure variations, as anticipated from the smaller impact on boundary conditions; and 2) the baseline HRR profile across the sweep differs distinctly from that of the intake pressure sweep. The HRR differences stem primarily from two factors: the distinct MEFs (81% for intake and 92% for exhaust) and the more advanced injection timing used during the exhaust pressure sweep. To aid the comparison, Fig. 5.9 presents two rep-

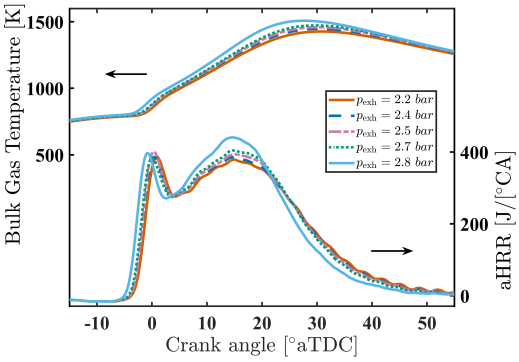

Figure 5.8: Exhaust pressure effects on bulk gas temperature and aHRR

resentative HRR profiles from the two pressure sweeps which share most boundary conditions: the base intake pressure case of 2.21 bar and the base exhaust pressure case of 2.20 bar. Both operate at comparable load levels and exhibit a minimized

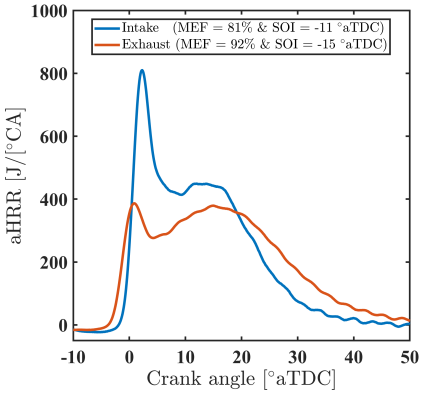

Figure 5.9: Heat-release profiles for intake- and exhaust-pressure sweeps

scavenging pressure differential between intake and exhaust. However, the intake pressure case shows a stronger premixed combustion Phase I followed by a weaker Phase II, whereas the exhaust pressure case exhibits a less pronounced Phase I and a prolonged Phase II which consumes most of the fuel. In the exhaust-pressure case,

the higher MEF weakens the pilot's ignition energy, which—combined with the advanced injection timing that counterbalances a further ID rise—leads to ID reduction, advancing the pilot combustion phasing and enhancing the flame-propagation characteristics of the methanol–air mixture. Overall, despite these distinctions between the two baseline cases, they do not obscure the main objective of this chapter: to isolate and elucidate the influence of specific boundary conditions on methanol PRDF combustion behavior.

The increased presence of hot RG enhanced ignition and combustion dynamics by shortening ID and advancing the heat release profile, as corroborated by the combustion phasing metrics in Fig. 5.10. The ID decreased from 12.2 to 10.9°CA, leading to slightly shorter Phase I (from 6.2 to 5.9°CA) and earlier onset of Phase II (from 3.5 to 1.8°CA aTDC). Higher bulk gas temperatures across the sweep further accelerated combustion, shortening Phase II from 28.6 to 26°CA and advancing both CA50 (from 15.8 to 13.9 °CA aTDC) and EOC (from 34.8 to 27.8 °CA aTDC). While the associated reduction in oxygen availability at higher exhaust pressure is expected to prolong ID, the concurrent rise in thermal state due to more hot residual gases dominates the response, resulting in an overall ID reduction. This behavior corroborates the study of Srna et al [135, 136] which demonstrates that, in PRDF mode with methane, the sensitivity of the pilot ID to thermal state increases compared to DO mode, while its sensitivity to oxygen density decreases. The stronger sensitivity of EOC compared to CA50 highlights the additional influence of hot RG mass and elevated mixture temperature on the ignition advancement of Phase II combustion, which promoted faster flame propagation through the methanol-air mixture. Overall, the total CD decreased from 34.8 to 31.9°CA.

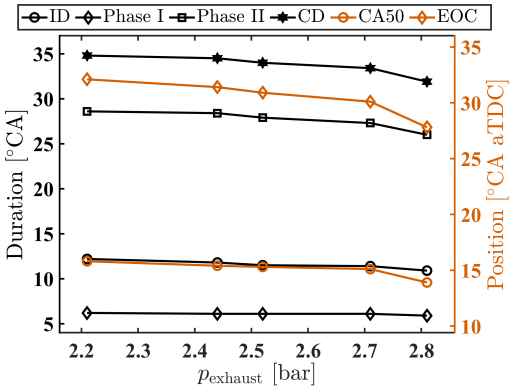

Figure 5.10: Exhaust pressure effects on combustion phasing and duration

Fig. 5.11 shows the effects of exhaust pressure on the energy balance. Despite the relatively minor impact of exhaust pressure on the HRR profile, the energy balance shows a strong sensitivity of combustion behavior to the increased mass of hot RGs. The combustion efficiency trend reflects the combustion enhancement trend observed in the HRR profiles, rising from 87.34% at the baseline exhaust pressure condition of 2.2 bar to 92.41% at that of 2.81 bar. This confirms that the higher bulk gas temperatures resulting from the trapped hot RGs substantially improved

methanol oxidation, particularly under Phase II which is the main contributing factor to incomplete combustion products. This trend is similar to the enhancing effects of intake air temperature observed in Section 4.6. This improvement comes at the expense of slightly higher heat losses, which increased from 7.7% to 10.8%, while exhaust losses remain nearly constant around 37% across the sweep. However, the overall combustion enhancement outweighed the rise in heat losses, leading to an improvement in gITE from 42.7% to 44.5%.

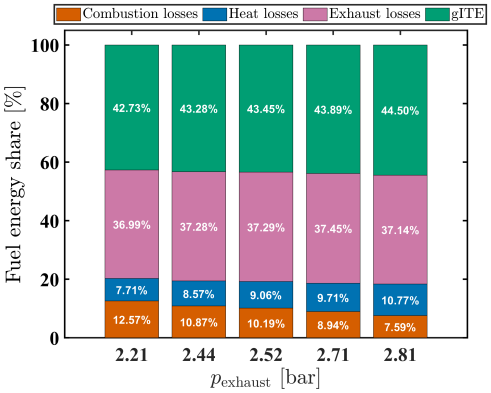

Figure 5.11: Exhaust pressure effects on energy balance

The combustion improvements are further corroborated by the consistent decrease in UHC emissions, which dropped from 5,720 to 3,499 ppm, as shown in Fig. 5.12. CO emissions followed a similar, though less pronounced, decline from 12.25 to 7.00 g/kWh. The smaller reduction in CO compared to UHC emissions can be attributed

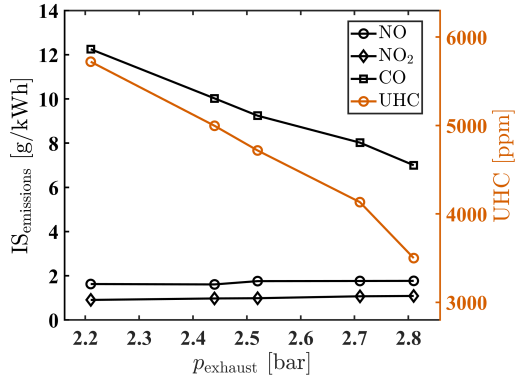

Figure 5.12: Exhaust pressure effects on emission characteristics

to the interplay between improved combustion efficiency—which lowers UHC emissions—and the tendency for increased intermediate CO formation with more fuel undergoing partial oxidation before its final conversion to CO_2. Interestingly, despite a 40% rise in heat losses across the increasing exhaust pressure sweep, NO emissions increased moderately by about 9% (from 1.63 to 1.77 g/kWh), while NO_2

rose more substantially by 20% (from 0.91 to 1.09 g/kWh). The more modest rise in NO can be linked to reduced oxygen density with higher residual gas content and higher end-gas temperatures which promote more of the formed NO to convert to NO_2 at the later combustion phasing, as discussed earlier for the intake pressure sweep.

5.5 COMBUSTION MODE MAP

Section 4.5 identified three distinct combustion modes through qualitative heat release analysis, each characterized by a specific HRR profile linked to the underlying combustion mechanisms. To support this analysis, two quantitative descriptors—the combustion mechanism index (CMI) and phase magnitude ratio (PMR)—were introduced to offer a morphological assessment of the HRR profiles. These metrics enabled systematic mapping and further classification of combustion behavior based on HRR shapes. To extend this framework, the present section quantifies the CMI and PMR metrics for the HRR profiles obtained from the employed parametric sweeps, thereby populating the CMI-PMR map. Fig. 5.13 illustrates the distribution of the HRR profiles across all operating conditions explored in this dissertation, including the MEF sweeps of Section 4.6 and subsequent sweeps of this chapter.

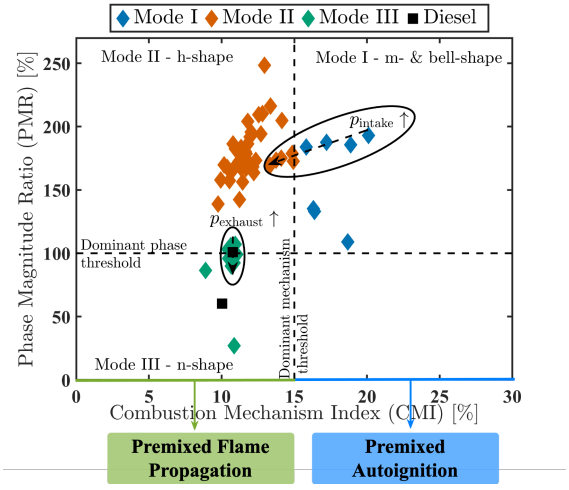

Figure 5.13: CMI-PMR combustion-mode map

Across the intake pressure sweep, the HRR profile progressively transitions from a single-peak, quasi-bell-shaped form, to the previously identified double-peak, h-shape profile. This evolution arises from the increasing separation between the diesel and methanol combustion phases, leading to a less homogeneous combustion process. At lower intake pressures, the longer ID and the higher reactivity of the methanol-air mixture promote methanol combustion through premixed autoignition within Stages I and II, respectively. This behavior aligns with the CMI-PMR trends, wherein the lowest-pressure operating points fall within the Mode I quadrant,

indicating an increasing dominance of premixed autoignition, consistent with the characteristics of the m-shaped profiles discussed in Section 4.5.2.

However, the bell-shaped profile occupies a distinct region within the quadrant. Despite the elevated CMI metric, its PMR values remain elevated, higher than those associated with the m-shaped profiles. Although both profile types reflect a strong contribution of premixed autoignition to methanol combustion, the underlying source of this autoignition differs, resulting in their distinct HRR shapes and PMR magnitudes. For the bell-shaped profiles, the intensified premixed autoignition primarily originates from the longer ID at low intake pressure, which leads to a larger portion of methanol to undergo Stage I autoignition alongside the pilot diesel. In contrast, the premixed autoignition that characterizes the m-shaped profiles arises predominantly from an intensified Stage II process, clearly separated from the pilot diesel combustion of Stage I. Overall, the chosen CMI threshold of 15% effectively indicates the transition from premixed flame propagation toward an enhanced premixed autoignition as the governing methanol combustion.

For the exhaust pressure sweep, the influence on combustion morphology is comparatively weaker. Adjustments in exhaust pressure introduce only minor variations in the PMR metric, indicating a modest strengthening of Phase II relative to Phase I, with CMI remaining nearly constant. The corresponding operating points cluster near the boundary between Modes II and III quadrants of the combustion mode map. Moreover, these points are situated away from the mechanism-transition threshold and exhibit n-shaped HRR profiles, a characteristic of flame propagation-dominated combustion in the methanol-air mixture. On the whole, the integrated CMI-PMR analysis across all operating points underscores that boundary conditions beyond pilot injection timing—such as air excess ratio, intake temperature, and trapped residual gases—influence and can govern the balance between premixed autoignition and flame propagation mechanisms, dictating the combustion behavior and resulting heat release characteristics.

To link heat release morphology to engine-level outcomes, Fig. 5.14 maps four key performance indicators—combustion efficiency, heat losses, gITE, and $ISNO_x$—in the CMI-PMR plane. Note that the lower-right quadrant (Mode IV) is not populated by experimental points; hence, contouring in that region should not be over-interpreted. Nevertheless, the dominant trends are clear. Combustion efficiency is lowest in Mode II, where h-shaped HRR profiles prevail. This is consistent with the mechanism translated by the CMI-PMR analysis: a pronounced separation between Phase I and the comparatively slow Phase II that deteriorates overall burn completeness. As CMI increases, signaling a shift toward stronger methanol premixed autoignition, combustion efficiency rises, with the highest values found in Mode I. Importantly, n-shaped profiles (Mode III) also deliver high combustion efficiency at more elevated MEF compared to Mode I cases. This enhanced combustion performance within a premixed flame propagation regime is achieved by tuning certain boundary conditions like intake temperatures to strengthen combustion Phase II.

Heat losses follow a broadly opposing trend to combustion efficiency; yet within Mode I there is a systematic difference between m-shaped and bell-shaped curves. The m-shaped Mode I points exhibit higher heat losses than the bell-shaped Mode I points, primarily attributed to their lower MEF ($\approx$ 62% versus $\approx$ 81%) and the reduced cooling effect, thereby increasing bulk gas temperatures and wall heat

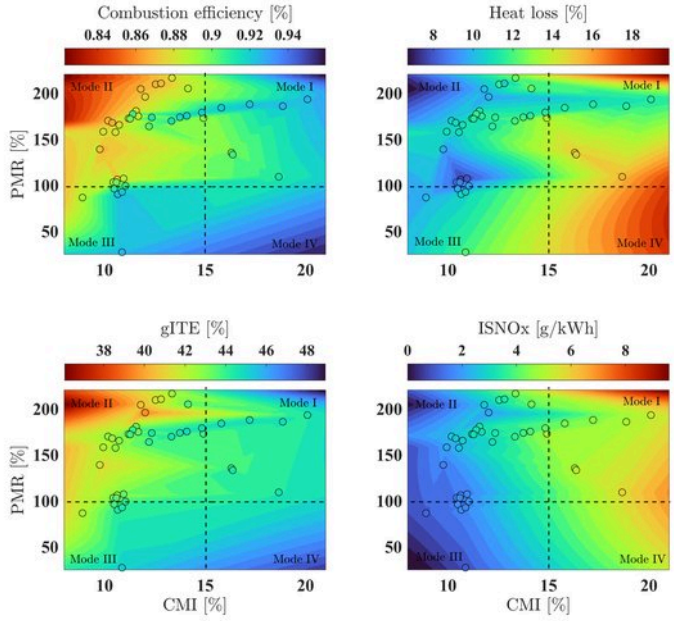

Figure 5.14: Contours of key performance indicators over the CMI-PMR map

transfer. Interestingly, gITE tracks changes in combustion efficiency more strongly than changes in heat losses, yielding clear efficiency improvements in both Mode I and Mode III conditions. By contrast, the NO_x map shows a pronounced CMI-driven increase: transitioning from flame propagation-dominated to premixed autoignition-dominated combustion advances phasing toward TDC and elevates in-cylinder temperatures which, together with typically lower MEFs using these cases, results in increased NO_x formation. These results confirm that the CMI-PMR metrics not only classify combustion physics but also can summarize and clarify the direction of performance-emissions trade-offs, thereby offering an effective tool for boundary-condition tuning and control.

5.6 CONCLUSIONS AND RECOMMENDATIONS

This chapter examined the isolated effects of intake and exhaust pressure conditions on the combustion dynamics and performance of a retrofitted single-cylinder, marine-scale methanol premixed dual-fuel (PRDF) engine operating at high load and high methanol energy fractions (MEFs). Building on the dual analytical framework developed in Section 4.5, this chapter extends the understanding of how retrofit-friendly control levers influence combustion behavior in these methanol PRDF engines. The aim was to isolate specific boundary conditions, such as air excess ratio and residual gas (RG) mass, to provide insights applicable to control and op-

timization strategies of these engines. The main conclusions and recommendations are as follows:

- Intake pressure manipulation proved to be an effective strategy for enhancing combustion efficiency through air excess ratio control. Richer mixtures enabled significantly higher combustion efficiency, from 87.7% to 92.7% across the employed sweep, with only marginal increases in heat losses. This provides room for further improvements through complementary adjustments such as increasing intake air temperature or advancing pilot injection timing.

- NO_2 emissions increased at lower intake pressure with richer mixtures, attributed to higher concentration of HO_2 radicals in the unburned zone combined with higher NO species coming from the combustion zone.

- Although exhaust pressure adjustments demonstrated weaker influence on the HRR profile compared to intake pressure, they yielded a comparable improvement in combustion efficiency. The increase in trapped hot RGs promoted methanol combustion, particularly in the region away from the jets during the flame propagation stage (Stage III). This highlights that RG management, which can be accomplished with alternative control strategies such as exhaust gas recirculation (EGR) and variable geometry turbine (VGT), is a promising strategy to enhance combustion quality.

- Quantitative HRR morphology mapping across the two pressure sweeps revealed stronger sensitivity of the HRR profile to intake pressure. Increasing intake pressure induced a transition from a single-peak (bell-shaped) to a double-peak (h-shaped) profile, reflecting a shift in dominant combustion mechanisms from premixed autoignition to flame propagation.

- The CMI-PMR map further demonstrates its capability to bridge combustion phenomena through heat release morphology to engine-level performance indicators. This mapping framework can be a very effective tool for boundary-condition tuning and combustion control, providing a lever for steering combustion toward desirable efficiency-emissions trade-off.

Overall, this chapter underscores the potential of retrofit-friendly levers—such as intake and exhaust pressure control—to enhance combustion stability and efficiency in methanol PRDF engines at high MEFs and high loads. While optimization is not the focus of this dissertation, the findings provide a strong foundation for future design-of-experiment (DOE) studies and control strategies aimed at improving performance and expanding the stable operating range of methanol-fueled PRDF systems.

6

SYNTHESIS

Our scientific power has outrun our spiritual power.
We have guided missiles and misguided men.

— Martin Luther King, Jr.

This chapter synthesizes the main conclusions, recommendations, and reflections of the dissertation, emphasizing how the findings from this research collectively address the overarching objective of *developing an experimentally based thermodynamic analysis framework for premixed methanol combustion in marine engines*. This objective stemmed from the limited understanding of methanol combustion behavior in premixed marine engines. This research therefore sets out to build experimentally based thermodynamic analysis frameworks that clarify how premixed methanol concepts behave in marine engines, and what this implies for deploying methanol as a sustainable shipping fuel. Two premixed pathways were investigated: mono-fuel lean-burn spark ignition (LBSI) and premixed dual-fuel (PRDF) compression ignition. Each pathway was studied with a diagnostic framework that links in-cylinder pressure-based combustion analysis to efficiency and emissions, applying one-factor-at-a-time experimental campaign methodology to isolate the influence of distinct boundary conditions. This experimental work utilized two representative marine engine platforms: a multi-cylinder marine LBSI engine operated on natural-gas, and a marine-scale single-cylinder research engine operated in methanol PRDF mode. The developed frameworks systematically characterize combustion processes and their sensitivity to several boundary conditions, laying the foundation for future design-of-experiment (DOE)-based optimization studies.

This chapter is structured as follows. Section 6.1 summarizes the results from each research chapter and highlights the key contributions in relation to the specific research questions addressed therein. Section 6.2 presents recommendations for future research, and Section 6.3 provides three overarching reflections on methanol premixed combustion strategies. Lastly, Section 6.4 provides details on the raw data and analytical scripts used throughout this research.

6.1 CONCLUSIONS

This section formulates the main conclusions of this PhD research, from an extensive literature review and conceptual classification of methanol combustion strategies, to the development of combustion-informed diagnostic frameworks for premixed methanol marine engines and their application to representative testbed platforms. The literature review established that, despite rapidly growing interest in alternative fuels like methanol, the maritime field faces challenges with inconsistencies in terminologies regarding injection, ignition, and combustion strategies for methanol-fueled engines. To resolve these ambiguities with engine strategies, this thesis organized methanol engine concepts according to certain degrees of freedom like injection and ignition strategies. The developed classification framework linked the several potential pathways determined by variations in these design variables to their corresponding combustion mechanism.

Beyond establishing this classification, the dissertation synthesized the main experimental findings across methanol engine technologies and identified persistent knowledge gaps. While methanol's suitability for alternative mono-fuel strategies like SI and partially premixed compression ignition (PPCI) is recognized, few studies explore such concepts, especially in marine engines. This scarcity of information is also seen across most engine concepts, including the limitation of insights into high-MEF PRDF operation. Moreover, the impact of several boundary conditions on combustion and overall performance of methanol PRDF engines was highlighted in the literature review. These identified gaps directly motivated the subsequent experimental and analytical work of this research.

Employing a multi-cylinder LBSI marine engine testbed operated on natural-gas, this work developed a pressure-based, combustion-informed thermodynamic analysis to capture both distinct combustion behavior and whole-engine performance in a unified framework. The analysis confirmed a two-stage combustion behavior, with an initial fast bowl-in stage followed by a slower squish one, and showed how the phasing of the transition between these stages governs the trade-off between efficiency, stability, and NO_x emissions. Advancing the squish-entry point improved combustion stability and both combustion and brake thermal efficiency, yet at the expense of increased heat losses and NO_x formation, illustrating the narrow operating window of such LBSI concepts. The associated multi-stage Wiebe modeling also underscored that this approach is not merely a fast and effective thermodynamic simulation tool, but that it is useful to quantify combustion progress when incorporated in the developed framework. Overall, this part of the work established a general methodology for the LBSI concept in diesel-derived combustion chambers, that is readily transferable to methanol operation.

For PRDF combustion engines, this research utilized a single-cylinder marine engine to explore high-MEF operation. The employed experimental campaigns showed that methanol PRDF operation is possible but constrained by two distinct mechanisms: knock at intermediate MEFs and deteriorating combustion efficiency with high CO and UHC emissions at the highest MEFs. A combined qualitative-quantitative combustion analysis identified three characteristic heat-release morphologies, i.e., m-, h-, and n-shaped, each associated with different balances between pilot ignition followed by premixed autoignition and flame propagation of the methanol-air mix-

ture. By introducing combustion mechanism index (CMI) and phase magnitude ratio (PMR) as heat release shape indicators, the work demonstrated that the morphology evolution can be monitored and linked to the underlying combustion mechanisms. This CMI-PMR framework provides a clear link between combustion phenomena, as expressed through heat release morphology, and engine-level performance indicators, ultimately serving as an effective tool for boundary-condition tuning and combustion control. A threshold for CMI was also defined to capture the associated transition across the two main combustion modes of the methanol-air mixture. The quantitative analysis showed that combustion phasing and stability strongly depend on MEF, and that overall combustion performance is more sensitive to pilot ignition timing than to ignition energy, mirroring conventional SI engine behavior. Moreover, all methanol PRDF operating points achieved lower NO_x emissions than diesel-only (DO) baseline operation, but at the expense of higher NO_2/NO ratios and substantial increases in CO and UHC emissions.

Following the exploration of MEF impact on combustion characteristics and overall performance of methanol PRDF operation, this research focused on key control parameters, specifically ones that can be easily adapted for engine retrofits. The parametric exploration of intake temperature, as well as intake and exhaust pressure further emphasized the central role of boundary conditions in enabling high-MEF and high-load PRDF operation. The observed boost in combustion efficiency at 93% MEF with increased intake temperature demonstrated that the inherent high-load penalty associated with combustion losses can be mitigated without compromising heat transfer or NO_x emissions. A similar increase in heat losses was also avoided when intake pressure was reduced, which significantly improved combustion efficiency, primarily through the air excess ratio reduction. Moreover, higher exhaust pressures enhanced flame propagation in the methanol-air mixture by retaining more hot residual gases in the cylinder. The expansion of the developed morphology analysis revealed that increasing intake pressure moves heat release profiles from a bell-shaped toward h-shaped forms. This also indicated a change in the dominant mechanism from premixed autoignition to flame propagation, accompanied by balance changes in efficiency and emissions. The key conclusion from these parametric studies was that relatively simple, retrofit-friendly control levers in the air and exhaust path can be used to improve methanol PRDF combustion, even when injection control is limited, e.g., for engines with mechanically controlled fuel injection.

Taken together, three overarching conclusions emerge. First, premixed methanol engines should be designed and controlled based on an understanding of their underlying combustion mechanisms and boundary condition sensitivities, rather than solely through conventional engine calibration logic. Second, combustion-informed pressure-based heat release analysis is the most effective general-purpose diagnostic methodology, especially for multi-cylinder engines, because it relates detailed combustion behavior to whole-engine performance. Third, heat release qualitative exploration is critical for diagnostic analysis of the more complex methanol combustion in PRDF engines, as they can better inform performance and control optimization studies.

6.2 RECOMMENDATIONS FOR FUTURE RESEARCH

Based on the research conducted within this dissertation, the main recommendations are summarized as follows:

- **Enhancement of the classification framework:**

  The unified classification framework developed in Chapter 2 should be further expanded to include insights from other low-reactivity fuels (LRFs) (e.g., methane, ethanol, and ammonia). Integrating information from a broader range of fuels would enable the formulation of a more holistic framework for the emerging LRFs, facilitating easier cross-fuel comparisons across the various combustion strategies.

- **Applications and advancement of the thermodynamic framework for methanol LBSI operation:**

  The combustion-informed thermodynamic framework developed using the natural-gas fueled LBSI engine should be applied to future methanol-fueled experiments on that engine to compare the combustion and overall engine behavior between the two high-octane fuels on this engine. This comparative application would deepen the understanding of methanol combustion characteristics and provide further validation of the framework's transferability to other fuels.

- **Completion of the holistic combustion analysis through broader Wiebe calibration:**

  Future work should extend the multi-stage Wiebe modeling approach coupled with the experimental studies on the LBSI engine to establish correlations for the full operating map and validate the model with additional independent datasets. Such work will help improve operating-point dependency and enable the development of a fast, combustion-informed simulation tool suitable for predictive analysis of methanol LBSI engines.

- **Adoption of design of experiments for LBSI operation:**

  Beyond one-factor-at-a-time parametric studies, future investigation should employ statistically designed experiments to explore the interaction between spark timing and air-excess ratio. This would provide deeper insights into their coupled influence on combustion phasing, stability, and overall engine performance, ultimately supporting optimization of LBSI operation for alternative fuels like methanol.

- **Extension of the methanol PRDF classification framework and hypotheses' validation:**

  The morphology-based framework proposed in Chapter 4 should be further refined by coupling pressure-based heat release analysis with optical diagnostics for methanol PRDF operation. Such integration would allow validation of the combustion mechanisms hypothesized in this work and a more precise identification of transition thresholds. Further, the expansion of the framework to a wider range of operating conditions is recommended, including early diesel

injection timings leading toward RCCI-type operation. This would establish a more holistic classification of methanol PRDF combustion.

- **Adoption of design of experiments for PRDF studies:**

  Given that the present studies followed the one-factor-at-a-time methodology to isolate physical effects, future work should employ multi-parameter DOE approaches to systematically explore the interactions between boundary conditions on a multi-cylinder engine configuration. This will allow a more comprehensive mapping of the operating envelope and optimization of the retrofitting strategies, while it will also strengthen the understanding of methanol PRDF engine behavior under realistic variable and interrelated boundary conditions.

Collectively, these recommendations outline the next steps toward advancing the understanding and practical deployment of methanol-fueled premixed combustion in marine engines. By extending the developed frameworks, validating the proposed mechanisms through coupled diagnostics, and employing experimental designs, future research can move from isolated parametric observations toward comprehensive, predictive, and optimization-oriented methodologies. These efforts will contribute to realizing efficient, stable, and sustainable methanol operation in both retrofitted and next-generation marine engines.

6.3 REFLECTIONS

The purpose of this section is to step back from the preceding results-centered discussion and synthesize three overarching reflections derived from this doctoral research: i) the extent to which insights beyond the established analytical framework transfer natural-gas to methanol LBSI operation, ii) a comparative assessment of mono-fuel LBSI and PRDF as premixed combustion pathways for methanol, and iii) the positioning of premixed combustion concepts within the broader landscape of methanol engine strategies for marine applications.

METHANOL-FUELED LBSI MARINE ENGINES

Although the present work uses natural-gas as a fuel, the LBSI engine operates under the premixed flame-propagation regime in the same bowl-squish geometry that will be used for methanol. Consequently, the two-stage bowl-in/squish combustion behavior and its qualitative impact on engine performance, i.e., the phasing of the transition point and fuel ratio combusting across the two stages, are expected to show strong similarities under methanol operation. However, key differences exist in thermophysical and combustion properties between methanol and natural-gas, primarily composed of methane, which will alter certain combustion and overall engine performance characteristics.

First, methanol is expected to be introduced as a liquid via multi-point PFI, requiring evaporation in the intake port and cylinder, which will reduce homogeneity and increase sensitivity to intake air temperature relative to natural-gas. This impacts local temperatures and equivalence ratios, and thus flame propagation

dynamics in both bowl and squish regions. Together with methanol's lower laminar burning velocity under lean conditions compared with methane, these effects are expected to narrow the stability window, a trend already indicated by previous natural-gas-methanol comparisons on this engine platform.

Second, methanol's lower heating value results in slightly lower total stoichiometric air demand relative to natural-gas, despite its significantly lower stoichiometric air-fuel ratio stemming from its oxygen content. Thus, at the same air excess ratio levels, the engine would likely require slightly less air flow. However, in practice, the lower flame speeds of methanol at lean conditions and its additional charge-cooling effect are expected to require operation at lower air excess ratios to maintain acceptable combustion stability, thereby calling for stricter requirements on air management and intake temperature control. Differences in boundary conditions and exhaust properties are also expected to alter turbocharger dynamics and its interplay with the in-cylinder processes, underscoring the need for dedicated methanol experiments.

Finally, methanol's oxidation chemistry and thermophysical behavior are expected to shift the emissions picture: lower in-cylinder temperatures may reduce NO_x formation, but increase the risk of incomplete combustion products such as CO and UHC. Alongside unburned methanol, formaldehyde will require particular attention in future methanol LBSI studies because the methanol's oxidation path is always through formaldehyde. It should be noted that the open-chamber LBSI concept explored in this research is not expected to become the dominant architecture for future dedicated methanol marine engines, but rather to serve as an easier and retrofit-friendly route toward mono-fuel SI operation on existing diesel platforms. For the next-generation dedicated methanol marine engines, more advanced lean-burn SI concepts—particularly pre-chamber SI architectures that can extend lean limits and robustness—are likely to take over as the primary mono-fuel solutions.

MONO-FUEL LBSI VS. PRDF

Both mono-fuel LBSI and PRDF pursue methanol use through premixed combustion, for which the methanol-air mixture is compressed and an ignition source initiates the combustion which is intended to be largely governed by flame propagation. This shared premixed premise makes both concepts attractive not only for new engine designs, but also for retrofitting existing diesel platforms, for which minimizing engine modifications is often an important requirement. However, there is a key distinction between the two concepts related to the ignition source: LBSI relies on a spark-ignited flame kernel, whereas PRDF uses a high-reactivity fuel to initiate combustion of the premixed methanol-air mixture.

From a sustainability and integration perspective, LBSI is conceptually appealing because it eliminates diesel dependency and its additional fuel supply system. In retrofitting scenarios, however, LBSI operation would require more hardware modifications to the existing diesel engine architecture, such as replacing the entire fuel injection system with an ignition-based one and lowering compression ratio, and would also lose the capability for diesel-only operation. This loss of flexibility often becomes a critical challenge to the short-term adoption of this single-fuel LBSI strategy. On top of that, the LBSI technology also faces operating robustness

challenges due to knock and poor combustion efficiencies to a greater extent than PRDF. These differences are rooted in the distinct ignition characteristics of the two premixed concepts. In PRDF, the pilot effectively provides multi-point ignition of the methanol-air mixture, which tends to improve burn rate and combustion-stability margins relative to a spark-initiated flame front, especially under very lean mixtures or operating conditions with little margin for acceptable cycle-to-cycle variability. This is consistent with the typically leaner mixtures at which PRDF can operate efficiently relative to LBSI. Furthermore, beyond knock, highly boosted or high CR premixed SI can also be limited by ignition robustness because required spark breakdown voltage increases with higher pressures; whereas PRDF is free of this electrical constraint. At the same time, the PRDF pathway retains pilot-related trade-offs: soot is reduced relative to diesel-only but not eliminated as long as the pilot fuel remains, and the achievable reduction in NO_x strongly depends on the attainable methanol energy fraction (MEF). Nevertheless, for both concepts, the main emission trade-off shifts from soot-NO_x of diesel engines to NO_x-incomplete combustion products (CO/UHC), and needs careful management.

A further important distinction emerges when load control is considered. Conventional diesel engines employ qualitative load control by varying injected fuel quantity at unthrottled air flow. On the other hand, LBSI adopts the typical SI approach of quantitative control via throttle valve or similar control measures. On the contrary, the PRDF strategy tends to continue diesel-like qualitative control philosophy. At high loads, replacing a large part of directly injected diesel with methanol nearly eliminates the diesel diffusion combustion fraction, replacing it with methanol premixed flame propagation. If favorable thermodynamic conditions are established, this flame propagation can improve thermal efficiency, especially by accelerating the second combustion phase. This makes overall combustion more sensitive to boundary conditions than in the corresponding diesel-only operation.

At low loads, this sensitivity becomes even more critical. Combustion in diesel engines shifts from primarily diffusion to mostly premixed autoignition at lower loads, retaining their operating robustness across loads. However, in PRDF operation at low loads, methanol's combustion shifts from the more effective premixed autoignition to flame propagation, which is highly sensitive to boundary conditions. Under the even leaner and colder conditions of lower loads, exacerbated by the cooling effect of methanol, flame propagation is weakened considerably resulting in restriction to very low MEFs. Consequently, to maintain high efficiencies and high MEFs in PRDF, boundary conditions need to be actively controlled in a quantitative way that resembles SI practice, through throttle valves, waste-gate control, or variable-geometry turbines, especially when pilot injection timing control is limited. Despite this increased need for boundary-condition control in both premixed concepts, PRDF offers additional flexibility beyond preserving diesel-only operability.

The PRDF strategy introduces an additional control dimension through MEF, for which this dissertation has demonstrated its strong impact on combustion mode, stability, and emissions. This is fundamentally different from LBSI, where the main ignition control lever is spark timing, whereas in PRDF, the quantity of pilot fuel, which determines ignition energy, plays a crucial role. This becomes especially important when ignition energy manipulation is combined with modern common rail technology where ignition timing can also be manipulated. The relatively narrow

stable operating range of premixed concepts, and especially of LBSI, is expected to make them more suitable for applications with comparatively modest and slowly varying load fluctuations, such as on-board power generation, than for highly dynamic propulsion profiles.

Taken together, PRDF appears to be the most pragmatic near-term transition route for converting existing diesel engines to methanol operation because it can retain diesel-only operability, robustness levels closer to those of the baseline diesel engine, and achieve higher power density. In contrast, full defossilization ultimately requires either transitioning to mono-fuel LBSI concepts that eliminate the pilot altogether, or adopting sustainable pilot fuels, such as biodiesel, within the PRDF strategy.

PREMIXED CONCEPTS IN THE METHANOL MARINE ENGINE LANDSCAPE

The comparison above becomes more meaningful when viewed in the broader landscape of methanol engines for marine applications, where the suitability of a given concept is application- and scale-dependent rather than universally optimal. Although premixed combustion concepts are not new to marine engines—notably in lean-burn natural-gas dual-fuel engines—their adoption has been constrained by limitations in power density and operating robustness due to knock and combustion instability challenges. In contrast, diesel engine technology, founded on mixing-controlled combustion, satisfies these requirements and has therefore dominated across a wider range of applications, with the primary distinction being the engine cycle, i.e., two- versus four-stroke designs.

When natural-gas was introduced as an alternative marine fuel, primarily for large two-stroke marine engines, the PRDF concept initially emerged as the main adoption pathway. However, persistent challenges with unburned fuel motivated a transition toward dual-fuel diffusion combustion (DFDC) concepts for methane and, more recently, for alternative fuels such as methanol. A similar development trajectory was pursued for medium-speed four-stroke engines, where DFDC concepts could be accommodated through sufficient cylinder head space or advanced injection systems. In both cases, the underlying drivers are power density and operating robustness. DFDC retains diesel-like controllability while enabling high diesel substitution ratios and effectively suppressing the incomplete combustion of the LRF. As a result, for engine sizes above a certain threshold—including medium-speed four-stroke and low-speed two-stroke engines—research and development efforts have largely moved away from premixed concepts.

As bore size decreases toward the high-speed four-stroke segment, which dominates many marine auxiliary and smaller propulsion applications, DFDC becomes increasingly challenging due to tighter cylinder head constraints. In this size range, premixed concepts such as LBSI and PRDF regain strategic relevance by offering more feasible retrofit pathways with fewer intrusive mechanical modifications. Similar considerations apply to new engine designs, where significant departures from existing combustion chamber architectures are typically avoided. Moreover, if careful boundary conditions management can address the combustion-efficiency challenges, they can even offer a better option regarding NO_x reduction as they shift combustion away from diffusion-dominated behavior. These segments of the

shipping sector—where methanol is often considered particularly suitable compared to emerging alternatives such as ammonia and hydrogen due to its liquid state and lower handling and safety complexity—also tend to rely on high-speed engines, in which premixed combustion concepts can be more readily implemented. Moreover, for large ocean-going vessels, premixed methanol concepts can complement DFDC engines, as they offer simpler engine architectures for gensets, and via SI technologies, the potential for further reduction in overall diesel reliance.

Ultimately, beyond performance and emissions, durability and long-term robustness are likely to be decisive factors in the practical adoption of premixed methanol strategies. In this sense, this dissertation does not advocate a single universally optimal concept. Instead, it provides experimentally grounded diagnostic frameworks that render combustion mechanisms and their performance implications more transparent—an essential prerequisite for control development and retrofit-oriented optimization within the relevant engine-size range.

6.4 SUPPLEMENTARY DATA AVAILABILITY

The datasets and analytical scripts developed and utilized throughout this dissertation are made publicly available to ensure transparency and reproducibility of the presented results. Table 6.1 summarizes the corresponding digital object identifiers (DOIs) for the primary datasets and analytical scripts referenced in this work.

Table 6.1: Supplementary data

Related Chapter	DOI
Chapter 3	https://doi.org/10.4121/b652d737-e6cd-4f9b-91b9-8c400e6dc72b.v1
Chapter 4 & Chapter 5	https://doi.org/10.4121/9bcf4ce5-942d-4fd1-819d-3ede4baced6a

A

DATA ANALYSIS METHODOLOGY

This PhD research involves performance, stability, and combustion diagnostic analyses, all implemented within the MATLAB and Simulink environment [329]. This appendix outlines the key elements of the raw data analysis methodology developed during the PhD research, with the overarching aim of ensuring the transparency, reliability, and validity of the processed data used to characterize engine testbeds' behavior. Particular emphasis is placed on the treatment of in-cylinder pressure data, including pegging and filtering procedures. These were primarily developed for the multi-cylinder LBSI testbed used in EC I and II (Chapter 3), located at the engine laboratory of the Netherlands Defense Academy in Den Helder. This testbed was established for scientific engine research, and equipped with an extensive sensor array to support detailed combustion investigations. By contrast, the single-cylinder facility, located at the facilities of TNO in Helmond, used in EC III and IV (Chapter 4 & Chapter 5) already employed a well-established in-house pressure analysis methodology, and therefore required no additional development for this work. Nevertheless, regular discussions and exchanges with TNO provided valuable insights into ongoing developing methodology at the NLDA lab.

A.1 IN-CYLINDER PRESSURE DATA

In-cylinder pressure measurement represents one of the most fundamental diagnostic tools in reciprocating ICE research and development [164]. Testbed environments range from highly advanced single-cylinder facilities equipped with dedicated optical-access combustion analysis systems to large-scale production-line evaluations, such as shop tests for marine engines [330, 331]. Across this spectrum, in-cylinder pressure data are consistently employed, as they provide direct access to the combustion process and enable the evaluation of key phenomena, including cycle-to-cycle variability and combustion phasing. Beyond their diagnostic value, pressure traces can play different roles depending on the application. In experimental research, they can provide the basis for exploring advanced combustion concepts and can guide more specialized investigations. For multi-cylinder engines

they remain indispensable for optimization studies [332], while in commercial applications they increasingly become the basis of control strategies to meet various efficiency and emissions requirements [333].

Therefore, critical reflection is necessary when employing such pressure-based diagnostics, ranging from diagnostic analysis to thermodynamic models' calibration [334]. Errors introduced through measurement, signal conditioning, or data processing can propagate through subsequent diagnostic procedures, and be amplified in derived quantities. If not carefully designed, erroneous processed data can result in misleading interpretations and misdirect further research efforts [269]. For these reasons, ensuring the reliability of the processed in-cylinder pressure data is a prerequisite for robust experimental analysis and forms the foundation of the methodological approach applied in this PhD research.

Piezoelectric transducers, paired with charge amplifiers, have become the primary sensing technology for capturing in-cylinder pressure data in ICEs, due to their high accuracy, frequency response, durability, and robustness [268, 335, 336]. These characteristics make them ideally suited for detailed combustion diagnostic investigations. Accurate analysis of in-cylinder pressure traces requires, however, a series of data processing steps prior to engine performance evaluation. The four main preprocessing stages are:

1. Crank angle phasing (TDC determination)—the reference of the pressure trace to the correct timing [337, 338].
2. Absolute pressure correction (pegging)—the calibration of the pressure trace to the correct absolute value [269, 339, 340].
3. Ensemble-averaging—the statistical smoothing of cycle-to-cycle variations to obtain a representative trend [271].
4. Filtering—the removal of high-frequency noise or other artifacts from the pressure signal [270, 341].

These steps are fundamental to ensuring that the resulting pressure signal can accurately represent the in-cylinder process under a certain operating condition, and thus enable a reliable heat release analysis. Fig. A.1 illustrates the overall data processing analysis implemented in this research. Pegging and TDC determination procedures are discussed below, while the ensemble averaging methodology was described in Section 3.2.2.

Regarding filtering strategies, distinct approaches were adopted on the two engine platforms. For EC I and II, involving the LBSI engine, the pressure traces exhibited low levels of fluctuation and the employed combustion staging analysis is relatively insensitive to minor signal noise, resulting in the use of a straightforward mean value algorithm. In contrast, for EC III and IV, which included both DO and MeOH PRDF operational regimes, the pressure signal exhibited great noise, while its developed staging methodology is very sensitive to the filtering procedure. To address this, a more sophisticated filtering technique was implemented: pressure signals across 50 consecutive cycles were processed using a first-order Savitzky-Golay filter with 2.7°CA frame length. This filtering strategy is chosen to avoid over-smoothing, keep the non-physical heat release rate at low levels, and be able to separate the two main combustion stages in both diesel-only (DO) and DF modes [341]. o

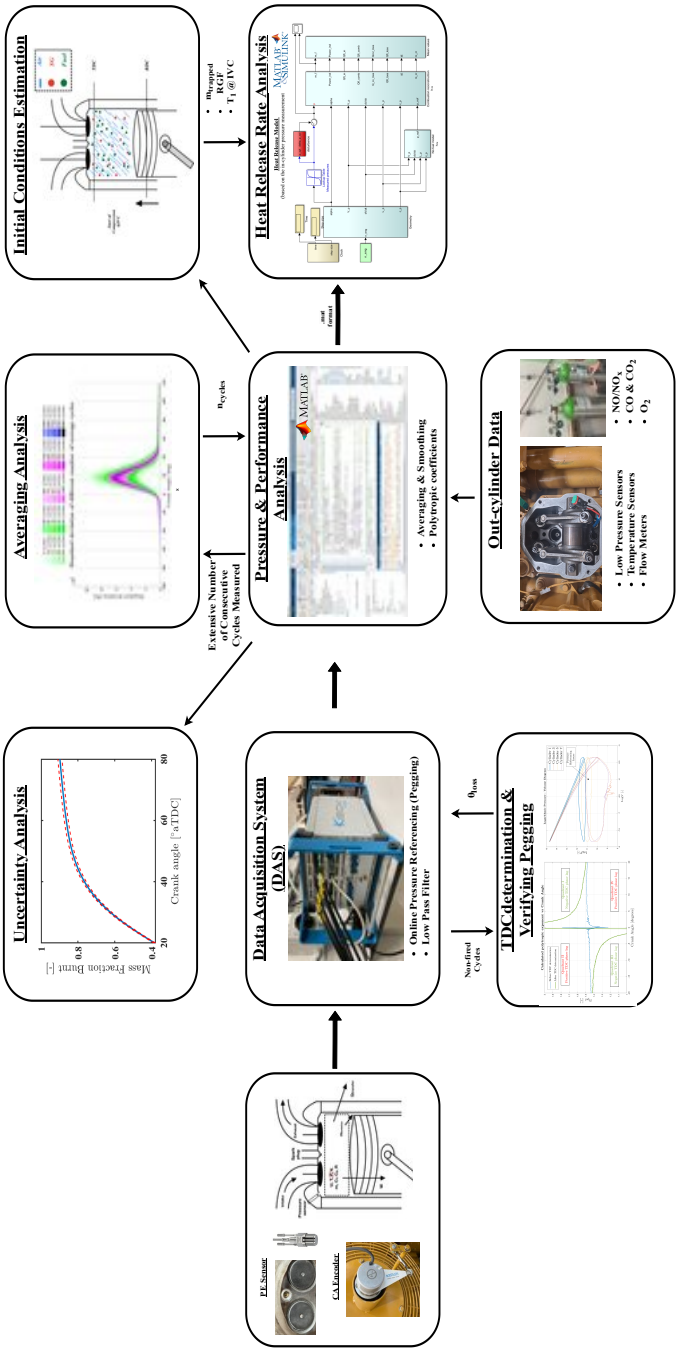

Figure A.1: Data-processing workflow scheme

ABSOLUTE PRESSURE CORRECTION

Piezoelectric pressure transducers inherently measure only dynamic changes in pressure, not the absolute pressure itself, necessitating their periodic referencing (pegging) to a known and reliable absolute pressure. Erroneous pegging can propagate to inaccurate estimates of bulk gas temperature and combustion phasing metrics, including the correct identification of start or end of combustion. Randolph comprehensively reviewed several pegging methods used to prepare pressure trace for combustion analysis. Four main approaches are distinguished:

1. Inlet bottom dead center reference: the in-cylinder pressure is "grounded" using the intake manifold pressure, typically measured by a low-frequency sensor.
2. Exhaust back pressure reference: the pressure signal is referenced using the exhaust manifold pressure during the exhaust stroke.
3. Two-point fixed polytropic coefficient method: this method utilizes the near-polytropic nature of compression in ICEs using two points on the compression stroke and an assumed polytropic coefficient to calculate the absolute pressure offset.
4. Three-point variable polytropic coefficient method: this alternative version of the polytropic-based method avoids using an assumed polytropic coefficient, but instead uses another pressure point instead.

This thesis adopts the two-point fixed polytropic coefficient method. This choice reflects both its practical robustness and the challenges with the alternative options. The intake and exhaust pegging methods are complicated by pressure oscillations in the multi-cylinder V8 engine during gas exchange, making it difficult to reliably select appropriate reference points. The three-point variable polytropic method is highly susceptible to pressure signal noise diminishing its robustness. In implementation, the two-point polytropic method is automatically applied on cyclic basis by the KiBox data acquisition system used in both EC I and II. Pegging reference points were chosen at 65° and 100°CA bTDC, with a polytropic coefficient of 1.33 [339]. An offline verification was also performed to ensure the reliability of the derived pressure traces [269, 340].

TDC DETERMINATION

Another critical aspect of pressure signal processing is its accurate phasing with the crank angle signal. This process involves two primary stages: first, aligning the mechanical TDC to 0°CA, and second, applying a thermodynamic loss angle correction to account for the fact that maximum pressure occurs before geometric TDC due to heat transfer. Accurate TDC determination is essential, since any phasing errors can lead to significant deviations in pressure-volume analysis, affecting cylinder work (IMEP) and, consequently, overall engine efficiency and emission metrics. While the most precise method for TDC identification involves dedicated hardware, such as TDC sensors, implementing such systems is often impractical in complex multi-cylinder engine testbeds [342].

This work adopts in-cylinder pressure-based TDC determination methods. The initial estimation used the technique proposed by Sta s [343], which identifies TDC based on characteristic inflection points in compression and expansion curves of a motored (non-firing) pressure trace. Although direct acquisition of motored pressure data was infeasible for the current engine, a cycle is captured after an inducing misfiring to reach near-motoring conditions. This strategy yielded thermodynamic loss angle corrections in the range of 0.3-0.6°CA for the four in-line cylinders measured during EC I and II. To further corroborate these findings, a coupling analysis adapted from Tazerout et al. [344, 345] was performed. This resulted in refined thermodynamic loss angles between 0.4 and 0.8°CA across the tested cylinders. The validity of these corrections was subsequently verified through an additional offline crank-angle resolved polytropic approach recommended by by Douaud and Eyzat [337]. This strategy method, in conjunction with the expected thermodynamic loss angle range typically ranging between 0.4 and 1°CA, provided further confidence of accurate phasing. Although the loss angle was observed to slightly vary among cylinders, an averaged value of 0.6°CA was ultimately used in all experiments for consistency in the KiBox DAS, which requires a single global input for TDC referencing.

A.2 ENGINE AND COMBUSTION PERFORMANCE PARAMETERS

Cycle-to-cycle variation (CCV) is analyzed through the coefficient of variation (COV) for IMEP, defined by Eq. (A.1), with the mean value and standard deviation being given by Eq. A.2 and Eq. A.3, respectively.

$$\mathrm{COV}_x = \frac{\sigma_x}{\mu_x} \cdot 100\% \tag{A.1}$$

$$\mu_x = \frac{\sum_{i=1}^{N_{\mathrm{cycles}}} x_i}{N_{\mathrm{cycles}}} \tag{A.2}$$

$$\sigma_x = \sqrt{\frac{\sum_{i=1}^{N_{\mathrm{cycles}}} (x_i - \mu_x)^2}{N_{\mathrm{cycles}}}} \tag{A.3}$$

where x is the corresponding variable under the statistic analysis, and N_{cycles} is the amount of consecutive cycles that the mean an standard deviation are computed across.

Combustion efficiency is estimated through an energy balance accounting for exhaust constituents, using:

$$\eta_{\mathrm{c}} = \left(1 - \frac{1 + \lambda \cdot \mathrm{AFR}_{\mathrm{stoich.}} \cdot \sum_{i=1}^{n_{\mathrm{UHC}}} y_i \cdot Q_{\mathrm{HV,i}}}{\mathrm{LHV}_{\mathrm{fuel}}}\right) \cdot 100\% \tag{A.4}$$

where λ is the air excess ratio, $\mathrm{AFR}_{\mathrm{stoich.}}$ is the stoichiometric air-to-fuel ratio for the NG, with y_i and $Q_{\mathrm{HV,i}}$ being the mass fraction and lower heating value of the corresponding species in the exhaust.

To analyze the efficiency of the engine and better analyze the fuel energy components, this study uses the relative engine performance measure of mean effective

pressure (MEP) to quantify the key energy balance components (EBCs) [20], using Eq. A.5.

$$\mathrm{MEP}_{\mathrm{EBC}_i} = \frac{\mathrm{EBC}_i}{V_{\mathrm{displacement}}} \tag{A.5}$$

where $V_{\mathrm{displacement}}$ is the displaced cylinder volume and EBC_i is the individual energy component. These components will be used to analyze the energy share paths deriving from the fuel energy and presented in the Sankey diagram of Fig. 3.13, using an adapted version of the sankey plot script created by Liu [346]. Fuel slip energy or combustion losses are calculated based on the fuel energy input and combustion efficiency, while heat transfer is determined from the calibrated heat transfer model at EVO, which is also used for the estimation of the gross heat release rate (gHRR). Gross indicated mean effective pressure (IMEP), as well as pump and net MEPs, are computed directly from the cylinder pressure traces. Brake MEP is estimated using the measured generated electric power and the know generator efficiency. Exhaust and friction losses are then quantified by closing the energy balance for gHRR and net IMEP, respectively. The resulting MEPs are used to determine the fuel's energy share paths.

Brake thermal efficiency (BTE) is calculated based on the measured generator power ($P_{\mathrm{generator}}$) in kWe, the generator efficiency $n_{\mathrm{generator}}$ and the mass consumption rates of NG ($\dot{m}_{\mathrm{NG}}$) in kg/s, using:

$$\mathrm{BTE} = \frac{P_{\mathrm{generator}}}{\eta_{\mathrm{generator}} \cdot \dot{m}_{\mathrm{NG}} \cdot \mathrm{LHV}_{\mathrm{NG}}} \cdot 100\% \tag{A.6}$$

Regarding emissions, this thesis normalizes the concentration of measured gaseous emissions, including NO_x, CO, CH_4 and total UHC, in the exhaust gases in flow rates of the corresponding pollutant per unit brake power output, using Eq. A.7. Specific NO_x emissions are calculated as the total weighted NO_2 in accordance with IMO standards [347].

$$Emission_{\mathrm{specific}} = \frac{\dot{m}_{\mathrm{emission}}}{P_{\mathrm{brake}}} \tag{A.7}$$

Note that for the single-cylinder setup and the experimental campaigns *EC III* and *EC IV*, emissions indices are normalized by gross power output, expressed as:

$$P_{\mathrm{gross,ind}} = \frac{\int_{\theta=-180}^{\theta=180} p_i(\theta) \cdot dV_i(\theta) \cdot n_{\mathrm{eng}}}{k \cdot 60} \tag{A.8}$$

where θ denotes crank angle, p_i and V_i the instantaneous pressure and volume, n_{eng} the engine speed in rpm, and k the number of revolutions per power cycle. UHC emissions for these two campaigns are quantified in ppm due to the challenges to determine the composition of UHC emissions with FID of the corresponding setup.

A.3 HEAT RELEASE ANALYSIS

The used heat release model is a zero-dimensional, single-zone thermodynamic model based on the first law of thermodynamics for a closed system during the non-flow period (inlet valve closing (IVC) to exhaust valve opening (EVO)) [20]. An

example of its calculations is Eq. A.9 that calculates the gHRR, with both crevice and blow-by losses being neglected [348].

$$gHRR = aHRR + \dot{Q}_{\text{loss}} = m \cdot c_v(\theta) \cdot \frac{dT(\theta)}{d\theta} + p(\theta) \cdot \frac{dV(\theta)}{d\theta} + \dot{Q}_{\text{loss}} \tag{A.9}$$

where $aHRR$ is the apparent HRR, m is the trapped in-cylinder mass, c_v is the mixture's specific heat at constant volume, T is the estimated bulk gas temperature calculated by the ideal gas law, p is the measured in-cylinder pressure, V is the measured in-cylinder volume, θ the crank angle degree, and $\dot{Q}_{\text{loss}}$ is the estimated heat transfer rate through the cylinder boundaries.

The heat release model assumes perfect homogeneity of the gases in the combustion chamber, with air, fuel and stoichiometric gases as constituents. For the multi-cylinder setup of *EC I & II*, the single point injection of natural gas (upstream of the compressor) and its gaseous state, combined with the engine speed (1500 rpm), ensure ample mixing time for fuel and air [349]. This minimizes local mixture variations, allowing the effects of control parameters like air excess ratio and spark timing to be interpreted in the context of a well-mixed charge. While for the single-cylinder setup of *EC III & IV* local mixture variations are expected to be higher, the dual-high-pressure PFI system enhances evaporation and mixing of methanol reducing those mixture variations. To this end, perfect homogeneity was assumed in all cases. Stoichiometric gases are modeled as the products from stoichiometric combustion of the fuel.

To estimate trapped conditions at IVC position, the residual gas (RG), i.e., the retained exhaust gases at the end of gas exchange process, two methods are used for the two experimental setups, thus the two groups of experimental campaigns. For the multi-cylinder testbed and *EC I & II*, in-cylinder mass is first estimated using the ideal gas law at the inlet valve opening (IVO) condition, with its temperature approximated as the measured exhaust outlet temperature [20, 350]. While this approach is applied for HRR calculation of the mean cylinder and cycle, the cyclic HRR analysis employs the Fitzgerald method to estimate the cyclic RG fraction [351]. The temperature at IVC is then calculated based on the mixing between the inducted and RG masses, with the temperature of the inducted mass being estimated from the measured temperature at the intake runner, considering heat pickup from the intake valves and ports. For the single-cylinder testbed and *EC III & IV*, the residual gas mass is estimated using a simplified Mirsky approach, assuming isentropic expansion of the residual gases between exhaust valve opening (EVO) and the end of gas exchange [328]. In this work, the inlet valve opening (IVO) is taken to mark the end of gas exchange, as it occurs slightly earlier than exhaust valve closing (EVC), and the small residual loss during overlap is neglected [352]. The total trapped mass is then determined by summing the estimated residual mass and the measured inducted one, with the temperature at IVC being calculated from the ideal gas law.

The thermodynamic properties of the species, including specific heat ratios and enthalpies, are calculated based on the in-cylinder gas dynamic composition and temperature via power series [353]. The pressure signal used for each operating condition was derived from the ensemble-average for 400 consecutive cycles across all in-line cylinders, minimizing errors related to variation in gas path dynamics in

multi-cylinder configurations. Heat transfer was modeled using the Woschni correlation using Eq. A.10 to estimate the convective heat transfer coefficient h_{woschni} [354], and total heat loss deriving from Eq. A.11. Since heat transfer depends on specific engine and operation conditions, the estimated combustion efficiency at each operating point was used to calibrate the heat loss model [355], as illustrated in Fig. A.2. For the *EC II*, a flame ionization detector (FID), Thermo-FID PT84 analyzer, was used to capture methane emissions and estimate combustion efficiency. However, the same methodology is less reliable for the methanol experiments conducted in *EC III & IV*. In these cases, FID measurements obtained with the Horiba MEXA-ONE system are subject to increased uncertainty due to the inherently low sensitivity of FID to oxygenated chemical species such as methanol. To correct this lower sensitivity to methanol, a response factor of 0.63 was used to the raw measurements. Nevertheless, for both fuels, methane and methanol were considered the only unburned fuel species, respectively, and together with measured CO emissions, were used to determine combustion efficiency using Eq. (A.4). After estimating the gHRR with the calibrated heat losses, the cumulative mass fraction burnt is calculated using Eq. A.12.

$$h_{\text{woschni}} = C_0 \cdot \frac{1}{D_b^{0.214}} \frac{p^{0.786}}{T^{0.525}} \cdot \left[(2.28 + 0.308 \cdot \text{SR}) \cdot c_m + 0.00324 \cdot \frac{p - p_0}{p_1} \frac{V_S}{V_1} \cdot T_1\right]^{0.786} \tag{A.10}$$

where C_0 is the calibrating parameter, D_b is the bore diameter, SR is the swirl ratio, c_m is the mean piston speed, p_0 is the motoring pressure, V_S the stroke volume, and p_1, V_1, and T_1 are the pressure, volume and temperature at IVC, respectively.

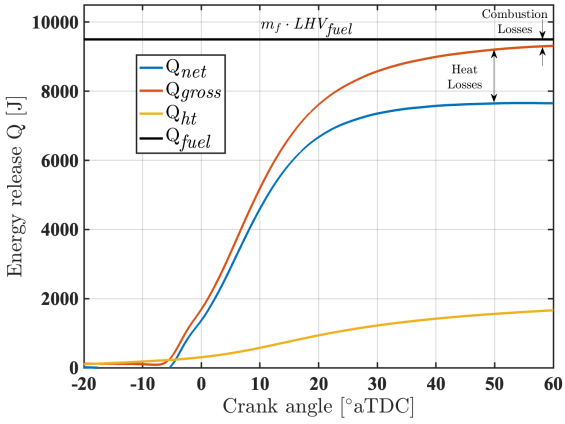

Figure A.2: Cumulative energies illustrating calibration

$$\dot{Q}_{\text{loss}} = A_{\text{wall}} \cdot h_{\text{woschni}} \cdot (T - T_{\text{wall}}) \tag{A.11}$$

where A_{wall} and T_{wall} are the surface are and temperature of the wall, respectively, comprising cylinder head and wall, and piston crown.

$$MFB = \frac{\int_{ST}^{EVO} \frac{gHRR}{LHV(\theta)} d\theta}{m_{\text{fuel,trapped}}} \tag{A.12}$$

where LHV's temperature dependence is considered. The crank angle corresponding to x% of MFB, referred to as CAx, was determined to characterize different combustion phases.

A.4 UNCERTAINTY QUANTIFICATION

In experimental studies, where measurements of key properties form the basis of analysis, quantifying measurement uncertainty is essential. This is particularly critical when the measurements feed into subsequent calculations used to derive performance indicators that characterize system behavior. In combustion diagnostics, for instance, multiple measured variables are combined to estimate quantities such as heat release rates and thermal efficiency. Since these estimates rely on a sequence of calculations, the uncertainties of individual measurements propagate through the analysis, directly influencing the confidence in the resulting performance metrics. According to the guide of uncertainty in measurement (GUM) [356], there are two primary ways to evaluate uncertainties: 1) statistical Type A [357]; and 2) non-statistical Type B like Monte Carlo approach [358]. Given the empirical nature of the Monte Carlo approach ad its requirement for extensive trails to ensure convergence, this work adopts the statistical methodology described by Gainey et al. [272], centered on combustion diagnostics in reciprocating ICEs. It should be noted that the present uncertainty analysis is solely applied to the experimental studies of the LB-SI multi-cylinder engine. The reason to not use it for the experimental analysis of the single-cylinder engine was that that analysis was more centered on the overall trends' direction and the associated qualitative combustion mode analysis. For subsequent optimization- and quantitative-oriented studies, a similarly detailed uncertainty analysis needs to be employed.

BACKGROUND ON UNCERTAINTY

Measurement errors fall into two categories: systematic (repeatable) and stochastic (random). Systematic errors are typically characterized by instrument manufacturers, arising from linearity, hysteresis and repeatability limitations, with stochastic errors being unpredictable environmental factors. The standard uncertainty of a measured variable x is the square root of its variance σ_x^2, which is commonly expanded—multiplied by a coverage factor of 2—to represent a 95% confidence interval. In this dissertation and the uncertainties related to the EC I and II of the marine LBSI engine, a 95% confidence level is assumed for all measurement instruments, and the corresponding expanded uncertainty is denoted as Δx.

The statistical framework for propagating uncertainties derives from the following equation (for dependent variable $z = ax + by$:

$$\sigma_z^2 = a^2 \cdot \sigma_x^2 + b^2 \cdot \sigma_y^2 + 2 \cdot a \cdot b \cdot \sigma_{xy} \tag{A.13}$$

where a and b are constants, and σ_{xy} the covariance between x and y. For more general functions $z = f(x, y)$ where the relative uncertainty in the variables is small, a first-order Taylor series expansion yields the approximate uncertainty:

$$\Delta z \approx \partial z_x \cdot \Delta x + \partial z_y \cdot \Delta y \tag{A.14}$$

where the partial derivatives represent the sensitivity coefficients of z to changes in the independent variables. Extending to n variables, the expanded uncertainty expression is:

$$\sigma_z^2 = \sum_{i=1}^{n} \partial z_{x_i}^2 \cdot \sigma_{x_i}^2 + 2 \cdot \sum_{i=1}^{n-1} \sum_{j=i+1}^{n} \partial z_{x_i} \cdot \partial z_{x_j} \cdot \sigma_{x_i x_j}^2 \tag{A.15}$$

The first term represents the root sum squared (RSS) method for uncorrelated input variables, whereas the second term accounts for covariances between input pairs. Covariance may be neglected when inputs are statistically independent and steady-state operating conditions are studied, which is the case for the present work. In this context, the RSS formulation provides a valid approach for uncertainty propagation in research.

UNCERTAINTY PROPAGATION METHODOLOGY

To support the systematic quantification and propagation of measurement uncertainty, this work utilizes the uncertainty tree visualization technique proposed by Longtin [359]. As illustrated in Fig. A.3, this method graphically traces how uncertainties arising at the instrument level (the "ground") propagate upward through derived quantities at higher levels. Each branch of the tree originates from the instrumental or measurement uncertainties associated with the data acquisition system (DAS), with base values being determined by the manufacturers' specifications for each sensor. The principal measurement instruments utilized for the marine LBSI engine in EC I and II are summarized in Table A.1. For certain critical variables, where direct manufacturer data is unavailable or infeasible to acquire, literature values or empirically reasoned estimates are applied. For example, the compression ratio (ϵ) uncertainty is conservatively taken as ±0.4, while the phasing uncertainty in crank angle (θ) is set at ±0.2 °CA.

Table A.1: Main measurement instruments of the DAS

Instrument	Sensor type	Unit	Accuracy
Exhaust pressure	JUMO dTRANS p30	bar	± 0.5%FS
Natural gas flow meter	Bronkhorst F-106Cl	m^3/h	± 1%FS
Cylinder pressure	Kistler 7061C non-cooled	bar	± 0.5%FS
Exhaust gas analyzer	Horiba PG-350	ppm	± 2%FS
Exhaust gas analyzer	Thermo-FID PT84/LT	mg/m^3	± 4%FS
Intake-Exhaust temperature	K-type thermocouple	K	± 0.4%FS

Red rhombi in Fig. A.3 denote calculations nodes, where uncertainties are compounded and propagated according to analytical relationships. Green rectangles indicate the quantified uncertainties at each stage of the process. For clarity and brevity, only the initial uncertainty propagation trees are illustrated. These initial

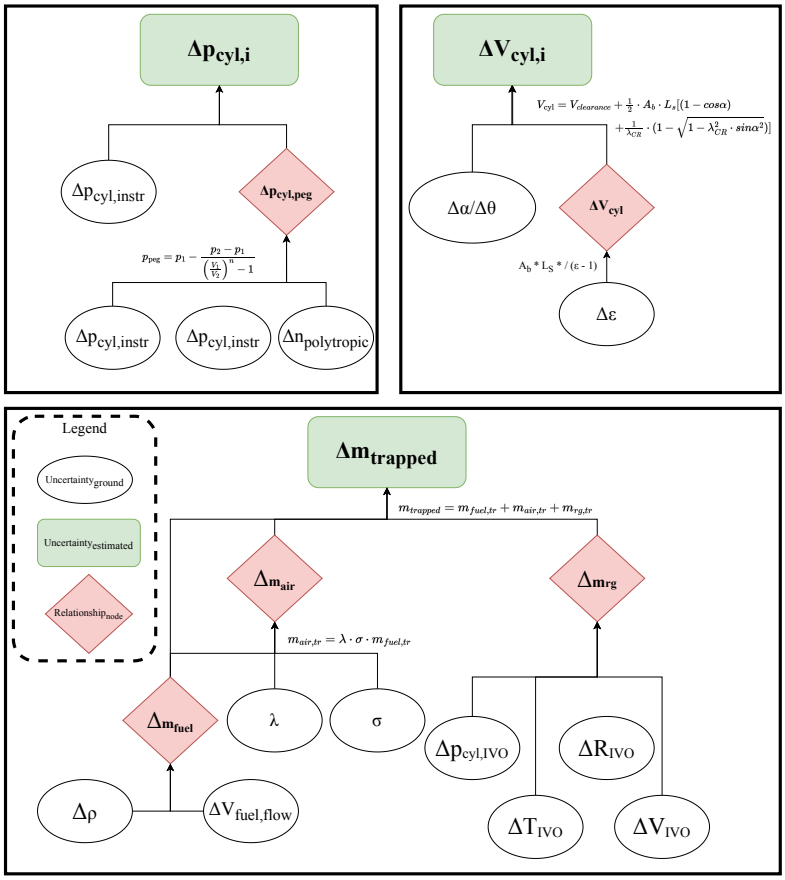

Figure A.3: Uncertainty propagation tree

uncertainties are then propagated through higher-order analysis—such as heat release calculations. For more detailed tree structures, readers are referred to the cited literature. Note that where sensitivity coefficients, i.e., partial derivatives, appear negligible, they are removed from the propagation chain, as discussed in [272].

Uncertainty propagation is conducted on a cycle-by-cycle and cylinder-by-cylinder basis across the entire dataset of the multicylinder LBSI engine, followed by ensemble-averaging to estimate the final uncertainty bounds for the cycle-averaged engine metrics. The conservative approach using the mean cyclic uncertainty is applied to estimate the final uncertainty in ensemble-averaged values. Fig. A.4 depicts the ensemble-average MFB along the.

A.5 STABILITY ANALYSIS METHODOLOGY

Identifying misfires or cycles with partial burning, as well as better understanding the conditions that influence these occurrences, is crucial for both online and offline

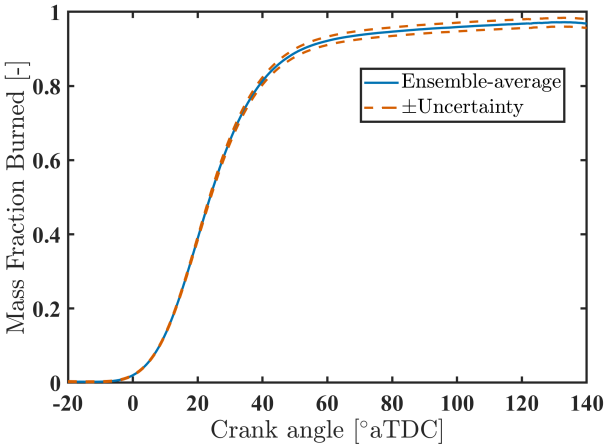

Figure A.4: Estimated uncertainty in the ensemble-average MFB

diagnostics and the subsequent optimization of engine performance. While cyclic variations are inherent in the operation of ICEs, establishing necessary acceptable limits for these variations is essential. Exceeding these limits can deteriorate engine operation, resulting in low efficiency, increased emissions of UHC, and potentially leading to highly unbalanced engine loading, as well as the risk of strong "rebound" that could damage the engine [360]. Realizing the transition zones between stable operating regime and unstable with many partial burns or even misfires is of paramount importance [361]. This enhances the understanding of the impact of various parameters such as ST and λ, and navigate the optimization efforts for the trade-offs between the various emissions like NO_x and UHC with engine efficiency.

A misfire cycle is commonly defined as a cycle in which no fuel was combusted, resulting in negative IMEP. On the other hand, consensus on the definitions of partial burning is lacking. Some studies have set their thresholds for partial burning cycles at 50% MFB [362], while others consider cycles with less than 90% [363, 364]. Additionally, the COV [20, 365, 366] and standard deviation [364] of IMEP have been utilized as the metrics to identify partial burning. This research considers partial burning cycles the ones that exhibit MFB below 90%, as found for the operating point with air excess ratio of 1.57 illustrated in Fig. A.5. Using this threshold for individual cycles, this research determines partial burning operating points as the ones that include at least one partial burning cycle [367].

Besides the partial burning recognition through the heat release analysis, the various statistical metrics for the various performance parameters need to be assessed. This research aimed to use either the COV or σ as metrics to assess parameters related to combustion stability. Since COV is directly proportional to σ, as per Eq. (A.1), correlation is expected between these parameters, as shown by the impact of λ on both parameters for IMEP [234]. Consequently, COV is selected over σ due to its ability to better compare the degree of variation among data series of different scale.

To better understand CCV along with its impact on engine performance, it is essential to analyze key performance parameters like IMEP across numerous con-

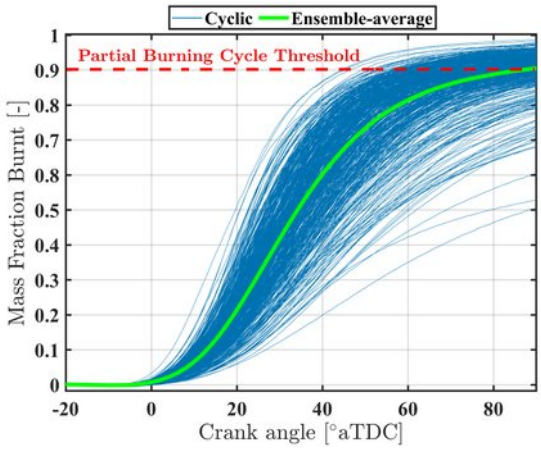

Figure A.5: Partial-burn threshold (90% MFB)

secutive cycles. Fig. A.6 presents the COV of pressure-related parameters including IMEP and some combustion parameters from *EC I*. Parameters that depend on a single point in the combustion process, such as P_{max}, $CA_{P_{max}}$, HRR_{max}, and CA50, exhibit higher COV values. Conversely, the more holistic parameters of IMEP, which broadly reflects the closed in-cylinder cycle, demonstrates the lowest levels of COV.

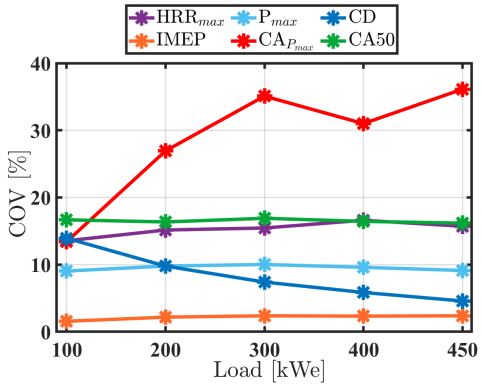

Figure A.6: COV for combustion and performance parameters across load points

The COV of $CA_{P_{max}}$ appears to be the most sensitive among all assessed parameters. The $COV_{HRR_{max}}$ rises with the increasing load, likely due to more intense combustion at higher loads. The lowest values of COV for both CD and CA50 are observed at the highest load of 450 kWe, indicating a more consistent combustion at higher loads due to higher temperatures. Notably, the medium load of 300 kWe shows slightly higher COV_{CA50} at 16.9% compared to 16.6% at the lowest 100 kWe load, contradicting the expected trend of decreasing COV with increased load, as it also appears in CD. This is likely due to the use of richer mixtures at the lower load point, which shows that the dilution level used in this range outweighed the load

effect. However, CA50 variation is relatively consistent in the whole operating load range.

This research selects COV_{IMEP} as the main metric for assessing combustion stability. The selection of IMEP over other parameters was influenced by several considerations:

- Simplicity: IMEP does not require HRR calculations, making it a straightforward choice.
- Consistency: P_{max} variations were found relatively inconsistent when higher CCV were observed. For instance, during the λ sweep, opposite trends were identified between the COV of P_{max} and that of IMEP and $CA_{P_{max}}$ [234].
- Holistic assessment: IMEP provides a holistic view of the closed cycle, thereby preferred over $CA_{P_{max}}$.

B

THERMODYNAMIC MODELING WORKFLOW

The development and application of thermodynamic engine cycle simulations have been fundamental in engine research for decades [368]. Zero-dimensional (0D) modeling stands out as the most straightforward approach for simulating the closed in-cylinder process in internal combustion engines (ICEs). This method offers notable advantages in terms of computational efficiency and predictive capability, especially when high-quality experimental data is available for calibration and validation. This study employs this 0D thermodynamic modeling approach, coupled with experimental studies, to simulate the closed in-cylinder processes of a marine NG-SI engine. The modeling framework is developed within the environment of MATLAB and Simulink [329].

B.1 WIEBE COMBUSTION MODELING

To simulate the combustion process, 0D models often rely on empirical or semi-empirical sub-models calibrated using heat release data. One of the most widely used semi-empirical combustion modeling approaches is the application of the Wiebe formula, an analytical function that can effectively represent the rate of combustion [369, 370]. By employing single or multiple Wiebe functions, the Wiebe modeling approach has demonstrated its versatility in accurately capturing a wide range of combustion profiles—from the simple flame propagation mechanism typical of SI engines [291] to two-stage diesel combustion [371] and three-stage combustion processes observed in premixed dual-fuel engines [131].

The conventional standard Wiebe functions for mass fraction burnt and rate of fuel combustion, typically used for combustion profiles in SI engines, are expressed as, respectively:

$$X_b(\theta) = 1 - \exp\left[-a\left(\frac{\theta - \theta_{\mathrm{SOC}}}{\Delta\theta_{\mathrm{CD}}}\right)^{m+1}\right] \tag{B.1}$$

$$\frac{dX_b(\theta)}{d\theta} = \frac{a \cdot m}{\Delta\theta_{\mathrm{CD}}}\left(\frac{\theta - \theta_{\mathrm{SOC}}}{\Delta\theta_{\mathrm{CD}}}\right)^{m} \exp\left[-a\left(\frac{\theta - \theta_{\mathrm{SOC}}}{\Delta\theta_{\mathrm{CD}}}\right)^{m+1}\right] \tag{B.2}$$

where $X_b(\theta)$ is the mass fraction burned, θ is the crank angle, θ_{SOC} is the crank angle at the start of combustion (SOC), $\Delta\theta_{CD}$ is the combustion duration, a is the efficiency parameter, m is the shape factor.

While the standard Wiebe function can accurately represent the combustion mechanism in conventional SI engines, it lacks the capability to simulate combustion profiles in alternative ICE technologies, such as diesel and dual-fuel engines. This limitation arises when the combustion process deviates from a single-stage mechanism, as is typically observed in SI engines, where a flame propagates at a relatively constant rate through the chamber until extinguished as the flame front approaches the chamber walls. A notable example is the distinct combustion behavior observed in converted SI engines, which, in contrast to conventional SI, exhibits a two-stage combustion profile, as illustrated in Fig. 3.10. To capture multi-stage combustion mechanisms, the combination of multiple Wiebe functions can be employed, expressed as:

$$X_b(\theta) = \sum_{i=1}^{n} \beta_i \left(1 - \exp\left[-a\left(\frac{\theta - \theta_{SOC}}{\Delta\theta_{CD,i}}\right)^{m_i+1}\right]\right) \tag{B.3}$$

where β_i is the fraction of the fuel that burns during the i-th stage, and n is the number of Wiebe function used that simulate the different combustion phases. The β_i or weight factor offers a tool for manipulating multi-stage combustion processes.

In addition to the multi-stage formulation of the Wiebe combustion model, alternative uses and adaptations of the Wiebe parameters have resulted in diverse formulations and approaches for simulating combustion profiles. For instance, the conventional multi-stage Wiebe formulation, as expressed in Eq. (B.3), assumes similar SOC for all stages. However, distinct combustion phases in specific engine technologies can lead to abrupt peaks in HRR profiles that are not adequately captured by this assumption. To address this limitation, modified multi-Wiebe formulations have been developed that define each combustion stage that features distinct SOC, providing with a more flexible framework for such complex and non-uniform behaviors, expressed as:

$$X_b(\theta) = \sum_{i=1}^{n} H_i(\theta - \theta_{SOC,i})\,\beta_i \left(1 - \exp\left[-a_i\left(\frac{\theta - \theta_{SOC,i}}{\Delta\theta_{CD,i}}\right)^{m_i+1}\right]\right) \tag{B.4}$$

where the H_i is the Heaviside step function which is introduced to ensure the estimation of the function at the corresponding combustion phase.

This study utilizes combustion data from the *EC II* of this thesis to determine the optimal set of parameters for the Wiebe functions. Fig. B.1 illustrates the methodology and primary inputs used in building the model. Combustion phasing characteristics, such as the SOC and initial weight factors for multi-stage formulations, are employed as inputs for calibrating the Wiebe model parameters.

This study uses a least-square-based optimization approach to solve the resulting non-linear calibration problem [236, 372]. Specifically, the MATLAB optimization toolbox function *lsqcurvefit* is utilized to determine the optimal set of Wiebe parameters. To enhance the accuracy of combustion profile representation near TDC, primarily during the early expansion phase, an additional weighting function is applied within the crank-angle interval from -10 to 40 °CA aTDC. The primary

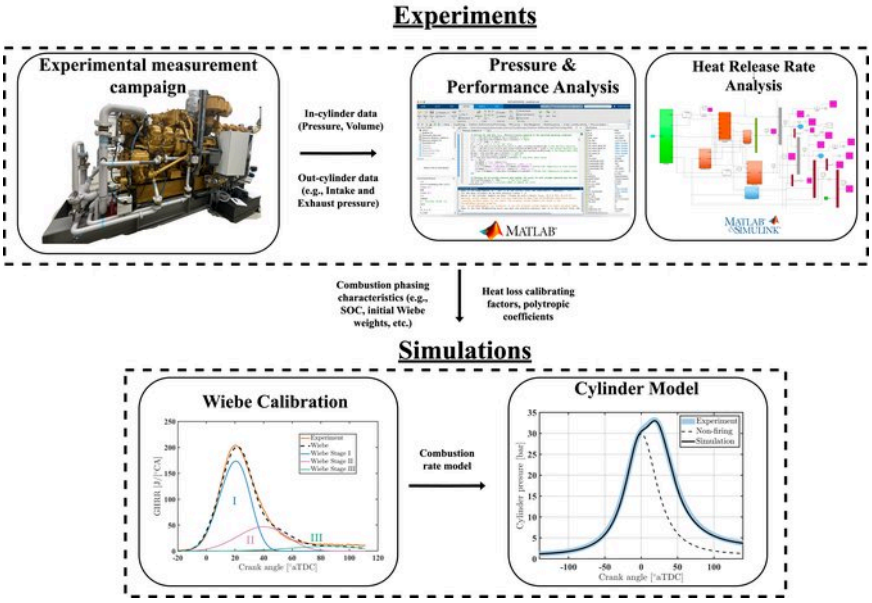

Figure B.1: Thermodynamic modeling workflow

parameter influencing the reaction rate profile in the Wiebe model is the shape factor m_i. However, when multi-Wiebe formulation is used with adjustable combustion duration of each stage, $\Delta\theta_{CD,i}$ parameter also influences the shape of the heat release profile. Fig. B.2 illustrates how variations in these key parameters affect the reaction rate and cumulative reaction rate profiles. While combustion efficiency a_i parameter can also influence the reaction rate profile, it is assumed relatively constant at 95% [288]. Additionally, when employing modified multi-stage Wiebe formulations, calibration includes adjusting weight factors for each combustion stage and defining SOC points for each stage. The initial parameterization for Wiebe parameters is derived from Section 3.4, with general knowledge of physical insight guiding the selection of appropriate parameter ranges within the optimization algorithm.

B.2 CLOSED IN-CYLINDER PROCESS MODELING

The developed combustion model is integrated into a closed oD single-zone thermodynamic in-cylinder model. This closed cylinder model is formulated based on the solution of the ordinary differential equation derived from the first law of thermodynamics, coupled with the gas law, expressed as:

$$\frac{dT}{d\theta} = \frac{\frac{dX_b(\theta)}{d\theta}\, m_{\text{fuel,net}}\, LHV_{\text{fuel}}(\theta)\, \eta_{\text{comb-p}} - \frac{dV(\theta)}{d\theta}}{m_{\text{trapped}}\, c_v(\theta)} \tag{B.5}$$

where T is the temperature, X_b is the mass fraction burnt from the Wiebe model, $m_{\text{fuel,net}}$ is the injected fuel mass, LHV_{fuel} is the lower heating value of the fuel, p is the pressure deriving from the gas law, $V(\theta)$ is the cylinder volume, m_{fuel} is

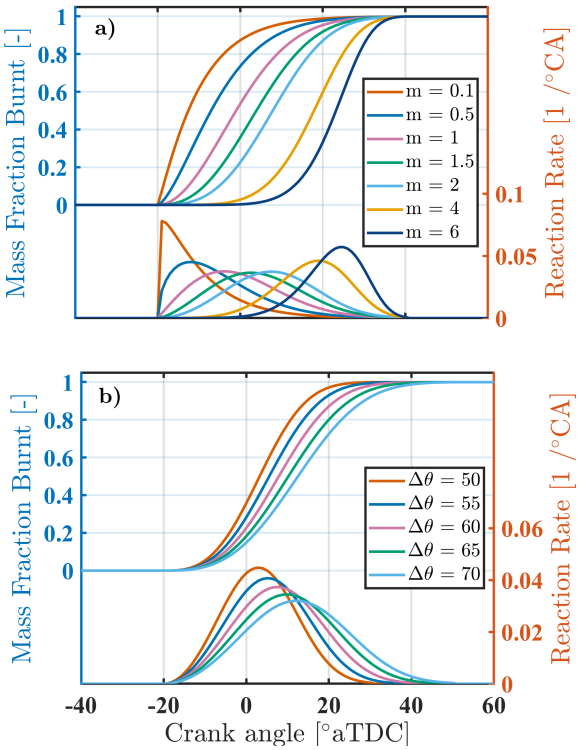

Figure B.2: Sensitivity of MFB and HRR to main Wiebe parameters

the total trapped mass including residual gas mass fractions, c_V is the mixture's specific heat at constant volume as derived from power series depending on both temperature and mixture's composition. Note that the $m_{\text{fuel,net}}$ is utilized because the methodology is based on the apparent heat release data. To determine this net fuel mass, an estimation of the heat transfer needs to be performed to convert the measured apparent into a gross heat release, thereby connecting the experimentally measured trapped fuel mass to its net value via a heat transfer model. In the same way as with the heat release model, heat transfer is modeled using Woschni correlation, as discussed in Section A.3.

Once heat transfer model is calibrated, the net mass fuel is estimated from equation:

$$m_{\text{fuel,net}} = \frac{\text{aHRR}_{\text{cumulative}}}{\text{gHRR}_{\text{cumulative}}} \tag{B.6}$$

The thermodynamic model is then employed during the combustion process, ranging from experimentally estimated SOC to EOC. For non-combusting phases within the closed in-cylinder process—compression prior to SOC and expansion after EOC—polytropic functions are utilized. Polytropic coefficients of 1.35 and 1.26 are applied consistently across all operating points for compression and expansion.

The residual sum of squares (RSS) is used to evaluate the accuracy of the models, expressed as:

$$RSS = \sum_{i=1}^{n} \hat{\varepsilon}_i^2 = \sum_{i=1}^{n} \left(f_{\text{model}}(x_{\text{exp}}, m, \dots) - y_{\text{exp}} \right)^2 \tag{B.7}$$

where $\hat{\varepsilon}_i$ is the error term and f_{model} is the corresponding model used.

B.3 ADDITIONAL FIGURES AND TABLES RELATED TO WIEBE CALIBRATION

This section provides some additional figures and tables assisting the discussions in Section 3.5.

Table B.1: Calibrated Wiebe parameters at 200 kWe

Wiebe-Mode	**Parameters**				**RSS**
	β	m	$\Delta\theta$	θ	
Single	1	1.56	53.9	-7.7	5.06
Double	0.61	2.31	38.6	-7.7	0.15
	0.34	3.78	52.5	-7.7	
Double split	0.83	2.27	42.9	-7.7	0.17
	0.12	1.3	20.8	20.8	

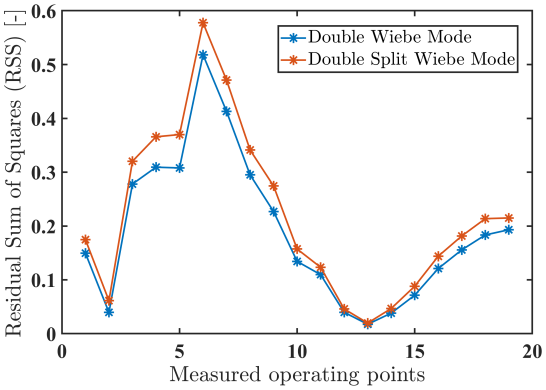

Figure B.3: Residual sum of squares for the double-Wiebe models at different operating points

BIBLIOGRAPHY

[1] Joseph D. Ortiz and Roland Jackson. 'Understanding Eunice Foote's 1856 experiments: heat absorption by atmospheric gases'. *Notes and Records: the Royal Society Journal of the History of Science* (2022). DOI: 10.1098/rsnr.2020.0031.

[2] Eunice Foote. 'Circumstances Affecting the Heat of the Sun's Rays'. *The American Journal of Science and Arts* (1856). URL: https://www.davidmorrow.net/eunice-foote.

[3] Tamara S. Ledley et al. 'Climate change and greenhouse gases'. *Eos, Transactions American Geophysical Union* (1999). DOI: 10.1029/99EO00325.

[4] Mikalai Filonchyk et al. 'Greenhouse gases emissions and global climate change: Examining the influence of CO2, CH4, and N2O'. *Science of The Total Environment* (2024). DOI: 10.1016/j.scitotenv.2024.173359.

[5] Hannah Ritchie and Pablo Rosado. *Energy Mix*. Tech. rep. Our World in Data, 2024. URL: https://ourworldindata.org/energy-mix.

[6] European Commission. Joint Research Centre. *Alternative fuels for marine and inland waterways An exploratory study*. JRC Technical Reports. LU: Joint Research Centre, 2016. URL: https://data.europa.eu/doi/10.2790/227559.

[7] International Chamber of Shipping. *Fuelling the Fourth Propulsion Revolution*. Tech. rep. 2022. URL: https://www.ics-shipping.org/publication/fuelling-the-fourth-propulsion-revolution-an-opportunity-for-all-full-report/.

[8] Gautam Kalghatgi. 'Is it really the end of internal combustion engines and petroleum in transport?' *Applied Energy* (2018). DOI: 10.1016/j.apenergy.2018.05.076.

[9] Vaclav Smil. *Numbers don't lie: 71 stories to help us understand the modern world*. [New York, New York]: Penguin Books, 2021.

[10] R D Reitz et al. 'IJER editorial: The future of the internal combustion engine'. *International Journal of Engine Research* (2020). DOI: 10.1177/1468087419877990.

[11] Sebastian Verhelst et al. 'Methanol as a fuel for internal combustion engines'. *Progress in Energy and Combustion Science* (2019). DOI: 10.1016/j.pecs.2018.10.001.

[12] Martin Svanberg et al. 'Renewable methanol as a fuel for the shipping industry'. *Renewable and Sustainable Energy Reviews* (2018). DOI: 10.1016/j.rser.2018.06.058.

[13] Nathan Gray et al. 'Decarbonising ships, planes and trucks'. *Advances in Applied Energy* (2021). DOI: 10.1016/j.adapen.2021.100008.

[14] Katie Tartaglia et al. *Transportation Electrification Beyond Light Duty*. Tech. rep. 2017. DOI: 10.2172/1413627.

[15] Joanne Ellis. *SPIRETH - End of Project Report*. Tech. rep. Sweden: SSPA, 2014. URL: http://www.dendanskemaritimefond.dk/wp-content/uploads/2016/02/Final-report-SPIRETH-Energy-Transport-20140228-1.pdf.

[16] Sebastian Verhelst and Thomas Wallner. 'Hydrogen-fueled internal combustion engines'. *Progress in Energy and Combustion Science* (2009). DOI: 10.1016/j.pecs.2009.08.001.

[17] Walter Cornelius, L. William Huellmantel and Harry R. Mitchell. 'Ammonia as an Engine Fuel'. Detroit, Michigan, United States, 1965. DOI: 10.4271/650052.

[18] Cinzia Tornatore et al. 'Ammonia as Green Fuel in Internal Combustion Engines'. *Frontiers in Mechanical Engineering* 8 (July 2022), p. 944201. DOI: 10.3389/fmech.2022.944201.

[19] Senthil Krishnan Mahendar, Anders Erlandsson and Ludvig Adlercreutz. 'Challenges for Spark Ignition Engines in Heavy Duty Application: a Review'. 2018. DOI: 10.4271/2018-01-0907.

[20] John B. Heywood. *Internal combustion engine fundamentals*. Second edition. New York: McGraw-Hill Education, 2018. ISBN: 978-1-260-11610-6.

[21] Ghazi A. Karim. *Dual-Fuel Diesel Engines*. CRC Press, 2015. ISBN: 978-0-429-06976-5. DOI: 10.1201/b18163.

[22] Konstantinos I. Kiouranakis, Peter De Vos and Rinze Geertsma. 'Methanol as a Fuel in Shipping: Review and Outlook to ICE Research Within MENENS'. Series Title: Lecture Notes in Mobility. Springer, 2025. ISBN: 978-3-031-89443-5. DOI: 10.1007/978-3-031-89444-2_106.

[23] Thomas Stenhede. *Effship a project for sustainable shipping WP2 Present and future maritime fuels*. Tech. rep. Gothenburg: SSPA, 2013.

[24] Andreas Schmid et al. 'Fuel Flexible Injection System - How to Handle a Fuel Spectrum from Diesel-like Fuels to Alcohols'. Vancouver, 2019.

[25] Joanne Ellis et al. 'Deliverable D6.2 Final Report – Summary of the SUMMETH Project Activities and Results' (2018).

[26] Magnus Svensson, Martin Tuner and Sebastian Verhelst. 'Investigation of Combustion Characteristics of a Fuel Blend Consisting of Methanol and Ignition Improver, Compared to Diesel Fuel and Pure Methanol'. Detroit, Michigan, United States, 2024. DOI: 10.4271/2024-01-2122.

[27] B. Ramne et al. *GreenPilot - Pilot Boat with Minimal Environmental Impact*. Tech. rep. v. 20181128. 2018.

[28] Jiang Yuqi and Yan Ping. 'Experimental Study on the Conversion of Marine Diesel Engine to Methanol Engine Fuel'. *30th CIMAC World Congress*. Busan, Korea, 2023.

[29] Scott Curran et al. 'The future of ship engines: Renewable fuels and enabling technologies for decarbonization'. *International Journal of Engine Research* (2023). DOI: 10.1177/14680874231187954.

[30] Jeroen Dierickx et al. 'Strategies for introducing methanol as an alternative fuel for shipping'. Apr. 2018.

[31] Yi-Hao Pu et al. 'The FASTWATER Demonstrator: Retrofitting a Harbor Tug Boat to Methanol/Marine Gas Oil Dual-Fuel Operation' (2023). Publisher: Elsevier BV. DOI: 10.1016/j.trpro.2023.11.554.

[32] Anren Yao and Chunde Yao. 'Study of Diesel/Methanol Dual Fuel Combustion in CI Engines and Its Practice in China'. *International Journal of Automotive Manufacturing and Materials* (2023). DOI: 10.53941/ijamm0201002.

[33] J. Harmsen. *Green Maritime Methanol. Towards a zero emission shipping industry*. Tech. rep. TNO 2021 P10262. 2021. URL: http://resolver.tudelft.nl/uuid:0542ccdc-00fc-4229-a39f-401688d3ee03.

[34] Konstantinos I. Kiouranakis et al. 'Methanol for heavy-duty internal combustion engines: Review of experimental studies and combustion strategies'. *Renewable and Sustainable Energy Reviews* (2025). DOI: 10.1016/j.rser.2025.115529.

[35] Konstantinos I. Kiouranakis et al. 'Combustion mode analysis of a large-bore methanol premixed dual-fuel engine with high methanol energy fractions'. *Energy Conversion and Management: X* (2025). DOI: 10.1016/j.ecmx.2025.101417.

[36] A. McIlroy et al. *Basic Research Needs for Clean and Efficient Combustion of 21st Century Transportation Fuels*. Tech. rep. 2006. DOI: 10.2172/935428.

[37] J. Vancoillie et al. 'The potential of methanol as a fuel for flex-fuel and dedicated spark-ignition engines'. *Applied Energy* (2013). DOI: 10.1016/j.apenergy.2012.05.065.

[38] A Das and H C Watson. 'Development of a natural gas spark ignition engine for optimum performance'. *Proceedings of the Institution of Mechanical Engineers, Part D: Journal of Automobile Engineering* (1997). DOI: 10.1243/0954407971526506.

[39] Changchun Xu et al. 'Effect on the performance and emissions of methanol/diesel dual-fuel engine with different methanol injection positions'. *Fuel* (2022). DOI: 10.1016/j.fuel.2021.121868.

[40] Zhifang Chen et al. 'The impact of methanol injecting position on cylinder-to-cylinder variation in a diesel methanol dual fuel engine'. *Fuel* (2017). DOI: 10.1016/j.fuel.2016.11.072.

[41] Harsh Sapra et al. 'Hydrogen-natural gas combustion in a marine lean-burn SI engine: A comparitive analysis of Seiliger and double Wiebe function-based zero–dimensional modelling'. *Energy Conversion and Management* (2020). DOI: 10.1016/j.enconman.2020.112494.

[42] T. Sathish Kumar and B. Ashok. 'Critical review on combustion phenomena of low carbon alcohols in SI engine with its challenges and future directions'. *Renewable and Sustainable Energy Reviews* (2021). DOI: 10.1016/j.rser.2021.111702.

[43] Shrey Trivedi and R. S. Cant. 'Turbulence Intensity and Length Scale Effects on Premixed Turbulent Flame Propagation'. *Flow, Turbulence and Combustion* (2022). DOI: 10.1007/s10494-021-00315-5.

[44] Manuel Alejandro Echeverri Marquez et al. 'A Pathway to Ultra-Lean IC Engine Combustion: The Narrow Throat Pre-chamber'. *Engines and Fuels for Future Transport*. Ed. by Gautam Kalghatgi et al. Springer, 2022.

[45] Yi-Hao Pu et al. 'Renewable Methanol as a Fuel for Heavy-Duty Engines: A Review of Technologies Enabling Single-Fuel Solutions'. *Energies* (2024). DOI: 10.3390/en17071719.

[46] Jun Li et al. 'Effect of injection and ignition timings on performance and emissions from a spark-ignition engine fueled with methanol'. *Fuel* (2010). DOI: 10.1016/j.fuel.2010.06.038.

[47] Lijia Zhong et al. 'Experimental observation of the combustion characteristics of methanol/air by turbulent jet ignition'. *30th CIMAC World Congress*. Busan, June 2023.

[48] Xianyin Leng et al. 'A preliminary numerical study on the use of methanol as a Mono-Fuel for a large bore marine engine'. *Fuel* (2022). DOI: 10.1016/j.fuel.2021.122309.

[49] Vilmar AEsoy et al. 'LNG-Fuelled Engines and Fuel Systems for Medium-Speed Engines in Maritime Applications'. SAE Technical Paper. 2011. DOI: 10.4271/2011-01-1998.

[50] T. Humerfelt et al. 'Development of The Rolls-Royce C26: 33 Marine Gas Engine Series'. *26th CIMAC World Congress*. 2010.

[51] J. Hélie and A. Trouvé. 'Turbulent flame propagation in partially premixed combustion'. *Symposium (International) on Combustion* (1998). DOI: 10.1016/S0082-0784(98)80486-4.

[52] Y. Iwamoto et al. 'Development of Gasoline Direct Injection Engine'. 1997. DOI: 10.4271/970541.

[53] Martin Wissink and Rolf D. Reitz. 'Direct Dual Fuel Stratification, a Path to Combine the Benefits of RCCI and PPC'. *SAE International Journal of Engines* (2015). DOI: 10.4271/2015-01-0856.

[54] Zhiyong Li et al. 'To achieve high methanol substitution ratio and clean combustion on a diesel/methanol dual fuel engine: A comparison of diesel methanol compound combustion (DMCC) and direct dual fuel stratification (DDFS) strategies'. *Fuel* (2021). DOI: 10.1016/j.fuel.2021.121466.

[55] Yaopeng Li et al. 'Multiple-objective optimization of methanol/diesel dual-fuel engine at low loads'. *Fuel* (2020). DOI: 10.1016/j.fuel.2019.116673.

[56] Ulugbek Azimov and Nobuyuki Kawahar. 'Combustion and Exhaust Emission Characteristics of Diesel Micro-Pilot Ignited Dual-Fuel Engine'. *Diesel Engine - Combustion, Emissions and Condition Monitoring*. InTech, 2013. ISBN: 978-953-51-1120-7. DOI: 10.5772/54613.

[57] Sam Shamun et al. 'Experimental investigation of methanol compression ignition in a high compression ratio HD engine using a Box-Behnken design'. *Fuel* (2017). DOI: 10.1016/j.fuel.2017.08.039.

[58] Thomas W. Ryan et al. 'Combustion and Emissions Characteristics of Minimally Processed Methanol in a Diesel Engine Without Ignition Assist'. 1994. DOI: 10.4271/940326.

[59] Antonio García et al. 'Parametric evaluation of neat methanol combustion in a light-duty compression ignition engine'. *Fuel Processing Technology* (2023). DOI: 10.1016/j.fuproc.2023.107850.

[60] B.G. Richards. 'Methanol-Fueled Caterpillar 3406 Engine Experience in On-Highway Trucks'. 1990. DOI: 10.4271/902160.

[61] Stanley P. Miller. 'DDC's Production 6V-92TA Methanol Bus Engine'. 1991. DOI: 10.4271/911631.

[62] Yu Zhang et al. 'Mixing-Controlled Combustion of Conventional and Higher Reactivity Gasolines in a Multi-Cylinder Heavy-Duty Compression Ignition Engine'. 2017. DOI: 10.4271/2017-01-0696.

[63] Brian Gainey et al. 'Mixing controlled compression ignition with methanol: An experimental study of injection and EGR strategy'. *International Journal of Engine Research* (2023). DOI: 10.1177/14680874221105161.

[64] Richard Samson, Anne-Gaëlle Morin and Fabrice Foucher. 'Effects of the Combustion Enhancer Containing Alkyl Nitrate (CEN) to Methanol in a Direct-Injection Compression Ignition (DICI) Engine'. Greenville, South Carolina, United States, 2023. DOI: 10.4271/2023-01-1619.

[65] Rasmus F. Cordtz et al. 'Combustion of Methanol Blended with a Fuel Additive in a CI Engine'. *MTZ worldwide* (2021). DOI: 10.1007/s38313-021-0703-6.

[66] Magnus Svensson et al. 'The development and certification of a single fuel high speed marine CI engine on methanol'. *30th CIMAC World Congress*. 2023.

[67] Päivi T. Aakko-Saksa et al. 'Renewable Methanol with Ignition Improver Additive for Diesel Engines'. *Energy & Fuels* (2020). DOI: 10.1021/acs.energyfuels.9b02654.

[68] Peng Wang et al. 'Combustion characteristics of methanol engine applying TJI-HPDI with optimized pre-chamber nozzle structure under different injection and spark strategy'. *Energy* (2024). DOI: 10.1016/j.energy.2024.133503. (Visited on 16/02/2025).

[69] Gernot Kammel et al. 'Simulation Based Predesign and Experimental Validation of a Prechamber Ignited HPDI Gas Combustion Concept'. 2019. DOI: 10.4271/2019-01-0259.

[70] M. Krishnamoorthi et al. 'A review on low temperature combustion engines'. *Renewable and Sustainable Energy Reviews* (2019). DOI: 10.1016/j.rser.2019.109404.

[71] Shigeru Onishi et al. 'Active Thermo-Atmosphere Combustion (ATAC) - A New Combustion Process for Internal Combustion Engines'. 1979. DOI: 10.4271/790501.

[72] Masaaki Noguchi et al. 'A Study on Gasoline Engine Combustion by Observation of Intermediate Reactive Products during Combustion'. SAE Technical Paper. 1979. DOI: 10.4271/790840.

[73] Paul M. Najt and David E. Foster. 'Compression-Ignited Homogeneous Charge Combustion'. 1983. DOI: 10.4271/830264.

[74] R. H. Thring. 'Homogeneous-Charge Compression-Ignition (HCCI) Engines'. 1989. DOI: 10.4271/892068.

[75] Allen W. (Bill) Gray and Thomas W. Ryan. 'Homogeneous Charge Compression Ignition (HCCI) of Diesel Fuel'. 1997. DOI: 10.4271/971676.

[76] Ayat Gharehghani. 'Load limits of an HCCI engine fueled with natural gas, ethanol, and methanol'. *Fuel* (2019). DOI: 10.1016/j.fuel.2018.11.066.

[77] Tomohiro Kanda et al. 'PCCI Operation with Early Injection of Conventional Diesel Fuel'. 2005. DOI: 10.4271/2005-01-0378.

[78] W. L. Hardy and Rolf D. Reitz. 'A Study of the Effects of High EGR, High Equivalence Ratio, and Mixing Time on Emissions Levels in a Heavy-Duty Diesel Engine for PCCI Combustion'. 2006. DOI: 10.4271/2006-01-0026.

[79] Ryo Hasegawa and Hiromichi Yanagihara. 'HCCI Combustion in DI Diesel Engine'. 2003. DOI: 10.4271/2003-01-0745.

[80] Sanghoon Kook and Choongsik Bae. 'Combustion Control Using Two-Stage Diesel Fuel Injection in a Single-Cylinder PCCI Engine'. 2004. DOI: 10.4271/2004-01-0938.

[81] Pop-Paul Ewphun et al. 'Investigation on Premixed Charge Compression Ignition Combustion Control Using Multi Pulse Ultrahigh Pressure Injection'. 2019. DOI: 10.4271/2019-01-1155.

[82] Pop-Paul Ewphun et al. 'Combustion Characteristic of Offset Orifice Nozzle under Multi Pulse Ultrahigh Pressure Injection and PCCI Combustion Conditions'. *SAE International Journal of Advances and Current Practices in Mobility* (2020). DOI: 10.4271/2019-32-0522.

[83] Mateusz Pucilowski et al. 'Effect of Start of Injection on the Combustion Characteristics in a Heavy-Duty DICI Engine Running on Methanol'. 2017. DOI: 10.4271/2017-01-0560.

[84] Burak Zincir et al. 'Investigation of Effects of Intake Temperature on Low Load Limitations of Methanol Partially Premixed Combustion'. *Energy & Fuels* (2019). DOI: 10.1021/acs.energyfuels.9b00660.

[85] Vittorio Manente et al. 'Effects of Ethanol and Different Type of Gasoline Fuels on Partially Premixed Combustion from Low to High Load'. 2010. DOI: 10.4271/2010-01-0871.

[86] Keiichi Okude et al. 'Premixed Compression Ignition (PCI) Combustion for Simultaneous Reduction of NOx and Soot in Diesel Engine'. 2004. DOI: 10.4271/2004-01-1907.

[87] Fan Zhang et al. 'Investigation into Light Duty Dieseline Fuelled Partially-Premixed Compression Ignition Engine'. *SAE International Journal of Engines* (2011). DOI: 10.4271/2011-01-1411.

[88] Adam B. Dempsey et al. 'Comparison of Low Temperature Combustion Strategies for Advanced Compression Ignition Engines with a Focus on Controllability'. *Combustion Science and Technology* (2014). DOI: 10.1080/00102202.2013.858137.

[89] John Gandolfo, Benjamin Lawler and Brian Gainey. 'An Experimental Comparison of Methanol Combustion Strategies: Spark Ignition Versus Compression Ignition'. *ASME ICE Forward Conference*. San Antonio, Texas, USA, 2024.

[90] H. Persson et al. 'Investigation of the Early Flame Development in Spark Assisted HCCI Combustion Using High Speed Chemiluminescence Imaging'. 2007. DOI: 10.4271/2007-01-0212.

[91] Xiaona Li et al. 'Effect of air and gas dilution on combustion and emission characteristics in alcohol-gasoline fueled SACI engine'. *Energy Conversion and Management* (2024). DOI: 10.1016/j.enconman.2024.118631.

[92] Ambarish Datta and Bijan Kumar Mandal. 'Impact of alcohol addition to diesel on the performance combustion and emissions of a compression ignition engine'. *Applied Thermal Engineering* (2016). DOI: 10.1016/j.applthermaleng.2015.12.047.

[93] R.G. Van De Ketterij et al. 'Impact of methanol on the combustion process an experimental study' (2020). Publisher: Ministry of Defense, Netherlands. DOI: 10.13140/RG.2.2.17619.20000.

[94] Ahmed I. EL-Seesy et al. 'Improvement of the combustion, emission, and stability features of diesel-methanol blends using n-decanol as cosolvent'. *Scientific Reports* (2022). DOI: 10.1038/s41598-022-20326-0.

[95] Mohit Raj Saxena, Rakesh Kumar Maurya and Prashant Mishra. 'Assessment of performance, combustion and emissions characteristics of methanol-diesel dual-fuel compression ignition engine'. *Journal of Traffic and Transportation Engineering* (2021). DOI: 10.1016/j.jtte.2021.02.003.

[96] Jon Van Gerpen. 'Cetane number testing of biodiesel'. *liquid fuel and industrial products from renewable resources*. American Society of Agricultural Engineers, 1996.

[97] Michael E. Karpuk and Scott W. Cowley. 'On Board Dimethyl Ether Generation to Assist Methanol Engine Cold Starting'. Portland, Oregon, United States, 1988. DOI: 10.4271/881678.

[98] David L. Horstman, Duane L. Abata and Jason M. Keith. 'On-Site DME Generation from Methanol for Pilot Injection in CI Engines'. Pittsburgh, Pennsylvania, United States, 2003. DOI: 10.4271/2003-01-3198.

[99] Zunqing Zheng et al. 'Experimental Study on HCCI Combustion of Dimethyl Ether(DME)/Methanol Dual Fuel'. Tampa, Florida, United States, 2004. DOI: 10.4271/2004-01-2993.

[100] Rodica A. Baranescu. 'Fumigation of Alcohols in a Multicylinder Diesel Engine-Evaluation of Potential'. 1986. DOI: 10.4271/860308.

[101] M. Alperstein, W. B. Swim and P. H. Schweitzer. '*Fumigation kills smoke - - improves diesel performance*'. 1958. DOI: 10.4271/580058.

[102] K.. R. Houser et al. 'Methanol Fumigation of a Light Duty Automotive Diesel Engine'. 1980. DOI: 10.4271/801379.

[103] E. Eugene Ecklund et al. 'State-of-the-Art Report on the Use of Alcohols in Diesel Engines'. 1984. DOI: 10.4271/840118.

[104] Jakob Coulier and Sebastian Verhelst. 'Using alcohol fuels in dual fuel operation of compression ignition engines: a review'. *28th CIMAC World Congress*. Helsinki, Finland, 2016.

[105] Rolf D. Reitz and Ganesh Duraisamy. 'Review of high efficiency and clean reactivity controlled compression ignition (RCCI) combustion in internal combustion engines'. *Progress in Energy and Combustion Science* (2015). DOI: 10.1016/j.pecs.2014.05.003.

[106] Derek E. Nieman et al. 'Methods of Improving Combustion Efficiency in a High-Efficiency, Lean Burn Dual-Fuel Heavy-Duty Engine'. 2019. DOI: 10.4271/2019-01-0032.

[107] Hyunwook Park et al. 'Comparative evaluation of conventional dual fuel, early pilot, and reactivity-controlled compression ignition modes in a natural gas-diesel dual-fuel engine'. *Energy* (2023). DOI: 10.1016/j.energy.2023.126769.

[108] Jian Wang, Luteng Chen and Jinke Chen. 'Experimental investigation on combustion and emission characteristics of diesel methanol dual fuel (DMDF) engine at various altitudes'. *Energy & Environment* (2024). DOI: 10.1177/0958305X221130140.

[109] Khanh Cung et al. 'Improved Combustion Efficiency in Methanol/Renewable Diesel Dual Fuel Combustion by Advanced Injection Timing and Increased Intake Temperature'. Greenville, South Carolina, United States, 2023. DOI: 10.4271/2023-01-1641.

[110] Khanh Cung et al. 'Engine-out Gaseous Emissions in a Diesel Engine using Methanol as a Low-carbon Fuel under Dual-fuel Operation'. 2024. DOI: 10.4271/2024-01-2364.

[111] Chunde Yao et al. 'Effect of Diesel/methanol compound combustion on Diesel engine combustion and emissions'. *Energy Conversion and Management* (2008). DOI: 10.1016/j.enconman.2007.11.007.

[112] Z.H. Zhang et al. 'Experimental investigation on regulated and unregulated emissions of a diesel/methanol compound combustion engine with and without diesel oxidation catalyst'. *Science of The Total Environment* (2010). DOI: 10.1016/j.scitotenv.2009.10.060.

[113] Hui Wang et al. 'Investigation to meet China II emission legislation for marine diesel engine with diesel methanol compound combustion technology'. *Journal of Environmental Sciences* (2020). DOI: 10.1016/j.jes.2020.04.017.

[114] Yabin Dong et al. 'High-pressure direct injection of methanol and pilot diesel: A non-premixed dual-fuel engine concept'. *Fuel* (2020). DOI: 10.1016/j.fuel.2020.117932.

[115] Yang Wang et al. 'Study on the performance of diesel-methanol diffusion combustion with dual-direct injection system on a high-speed light-duty engine'. *Fuel* (2022). DOI: 10.1016/j.fuel.2022.123414.

[116] Michael Saccullo, Timothy Benham and Ingemar Denbratt. 'Dual Fuel Methanol and Diesel Direct Injection HD Single Cylinder Engine Tests'. 2018. DOI: 10.4271/2018-01-0259.

[117] Le Ning et al. 'A comparative study on the combustion and emissions of a non-road common rail diesel engine fueled with primary alcohol fuels (methanol, ethanol, and n-butanol)/diesel dual fuel'. *Fuel* (2020). DOI: 10.1016/j.fuel.2020.117034.

[118] Xiaojun Yin et al. 'A comparative study on operating range and combustion characteristics of methanol/diesel dual direct injection engine with different methanol injection timings'. *Fuel* (2023). DOI: 10.1016/j.fuel.2022.126646.

[119] Yifan Zhao, Xinyu Liu and Sanghoon Kook. 'Combustion Mode Evaluation of a Methanol–Diesel Dual Direct Injection Engine with a Control of Injection Timing and Energy Substitution Ratio'. *SAE International Journal of Engines* (2024). DOI: 10.4271/03-18-01-0002.

[120] Zhiyong Li et al. 'Effect of injection strategy on a diesel/methanol dual-fuel direct-injection engine'. *Applied Thermal Engineering* (2021). DOI: 10.1016/j.applthermaleng.2021.116691.

[121] Yong Yang et al. 'Performance of large-bore methanol/diesel dual direct injection engine applying asymmetrical diesel nozzle strategies'. *Applied Thermal Engineering* (2024). DOI: 10.1016/j.applthermaleng.2024.122674.

[122] Martin Wissink and Rolf Reitz. 'Exploring the Role of Reactivity Gradients in Direct Dual Fuel Stratification'. *SAE International Journal of Engines* (2016). DOI: 10.4271/2016-01-0774.

[123] Guan Huang et al. 'Effects of fuel injection strategies on combustion and emissions of intelligent charge compression ignition (ICCI) mode fueled with methanol and biodiesel'. *Fuel* (2020). DOI: 10.1016/j.fuel.2020.117851.

[124] Ian May et al. 'Reduction of Methane Slip Using Premixed Micro Pilot Combustion in a Heavy-Duty Natural Gas-Diesel Engine'. 2015. DOI: 10.4271/2015-01-1798.

[125] Qiang Zhang et al. 'Experimental and Numerical Study of Jet Controlled Compression Ignition on Combustion Phasing Control in Diesel Premixed Compression Ignition Systems'. *Energies* (2014). DOI: 10.3390/en7074519.

[126] Wuqiang Long et al. 'Effects of dual-direct injection parameters on performance of fuel Jet Controlled Compression Ignition mode on a high-speed light duty engine'. *Fuel* (2019). DOI: 10.1016/j.fuel.2018.08.043.

[127] Fuxing Wei et al. 'Visualization investigation of jet ignition ammonia-methanol by an ignition chamber fueled H2'. *Fuel* (2023). DOI: 10.1016/j.fuel.2023.128658.

[128] S Singh et al. 'Effect of pilot injection timing, pilot quantity and intake charge conditions on performance and emissions for an advanced low-pilot-ignited natural gas engine'. *International Journal of Engine Research* (2004). DOI: 10.1243/146808704323224231.

[129] Baodong Ma et al. 'Multiple combustion modes existing in the engine operating in diesel methanol dual fuel'. *Energy* (2021). DOI: 10.1016/j.energy.2021.121285.

[130] Ghazi A. Karim. 'A review of combustion processes in the dual fuel engine—The gas diesel engine'. *Progress in Energy and Combustion Science* (1980). DOI: 10.1016/0360-1285(80)90019-2.

[131] Shuonan Xu et al. 'A phenomenological combustion analysis of a dual-fuel natural-gas diesel engine'. *Proceedings of the Institution of Mechanical Engineers, Part D: Journal of Automobile Engineering* (2017). DOI: 10.1177/0954407016633337.

[132] Zeeshan Ahmad et al. 'A parametric investigation of diesel/methane dual-fuel combustion progression/stages in a heavy-duty optical engine'. *Applied Energy* (2019). DOI: 10.1016/j.apenergy.2019.04.187.

[133] Gaurav Bansal and Hong G. Im. 'Autoignition and front propagation in low temperature combustion engine environments'. *Combustion and Flame* (2011). DOI: 10.1016/j.combustflame.2011.03.019.

[134] G.P. Beretta, M. Rashidi and J.C. Keck. 'Turbulent flame propagation and combustion in spark ignition engines'. *Combustion and Flame* (1983). DOI: 10.1016/0010-2180(83)90135-9.

[135] Aleš Srna et al. 'Experimental investigation of pilot-fuel combustion in dual-fuel engines, Part 2'. *Fuel* (2019). DOI: 10.1016/j.fuel.2019.115766.

[136] Aleš Srna et al. 'Experimental investigation of pilot-fuel combustion in dual-fuel engines, Part 1'. *Fuel* (2019). DOI: 10.1016/j.fuel.2019.115642.

[137] A.M.L.M. Wagemakers and C.A.J. Leermakers. 'Review on the Effects of Dual-Fuel Operation, Using Diesel and Gaseous Fuels, on Emissions and Performance'. 2012. DOI: 10.4271/2012-01-0869.

[138] Minhoo Choi, Khawar Mohiuddin and Sungwook Park. 'Effects of methane ratio on MPDF (micro-pilot dual-fuel) combustion characteristic in a heavy-duty single cylinder engine'. *Scientific Reports* (2021). DOI: 10.1038/s41598-021-89161-z.

[139] Weifeng Li, Zhongchang Liu and Zhongshu Wang. 'Experimental and theoretical analysis of the combustion process at low loads of a diesel natural gas dual-fuel engine'. *Energy* (2016). DOI: 10.1016/j.energy.2015.11.052.

[140] Jesús Benajes et al. 'Gaseous emissions and particle size distribution of dual-mode dual-fuel diesel-gasoline concept from low to full load'. *Applied Thermal Engineering* (2017). DOI: 10.1016/j.applthermaleng.2017.04.005.

[141] M.S. Lounici et al. 'Knock characterization and development of a new knock indicator for dual-fuel engines'. *Energy* (2017). DOI: 10.1016/j.energy.2017.11.138.

[142] J. A. Eng. 'Characterization of Pressure Waves in HCCI Combustion'. 2002. DOI: 10.4271/2002-01-2859.

[143] Martin Wissink et al. 'Investigation of Pressure Oscillation Modes and Audible Noise in RCCI, HCCI, and CDC'. SAE Technical Paper. 2013. DOI: 10.4271/2013-01-1652.

[144] Jeremie Dernotte, John E. Dec and Chunsheng Ji. 'Investigation of the Sources of Combustion Noise in HCCI Engines'. *SAE International Journal of Engines* (2014). DOI: 10.4271/2014-01-1272.

[145] Rakesh Kumar Maurya and Mohit Raj Saxena. 'Characterization of ringing intensity in a hydrogen-fueled HCCI engine'. *International Journal of Hydrogen Energy* (2018). DOI: 10.1016/j.ijhydene.2018.03.194.

[146] U Azimov et al. 'Premixed mixture ignition in the end-gas region (PREMIER) combustion in a natural gas dual-fuel engine'. *International Journal of Engine Research* (2011). DOI: 10.1177/1468087411409664.

[147] Taku Imamoto, Nobuyuki Kawahara and Eiji Tomita. 'PREMIER combustion characteristics of a pilot fuel-ignited dual-fuel biogas engine with consideration of cycle-to-cycle variations'. *Fuel* (2022). DOI: 10.1016/j.fuel.2021.123049.

[148] Ulugbek Azimov et al. 'Effect of syngas composition on combustion and exhaust emission characteristics in a pilot-ignited dual-fuel engine operated in PREMIER combustion mode'. *International Journal of Hydrogen Energy* (2011). DOI: 10.1016/j.ijhydene.2011.04.192.

[149] R.G Papagiannakis and D.T Hountalas. 'Experimental investigation concerning the effect of natural gas percentage on performance and emissions of a DI dual fuel diesel engine'. *Applied Thermal Engineering* (2003). DOI: 10.1016/S1359-4311(02)00187-4.

[150] Meng-Choung Chiong et al. 'Challenges and opportunities of marine propulsion with alternative fuels'. *Renewable and Sustainable Energy Reviews* (2021). DOI: 10.1016/j.rser.2021.111397.

[151] Jerald A Caton. 'Maximum efficiencies for internal combustion engines: Thermodynamic limitations'. *International Journal of Engine Research* (2018). DOI: 10.1177/1468087417737700.

[152] Paul Breeze. 'Types of Reciprocating Engine'. *Piston Engine-Based Power Plants*. Elsevier, 2018. ISBN: 978-0-12-812904-3. DOI: 10.1016/B978-0-12-812904-3.00003-3.

[153] Yaoyuan Zhang et al. 'Application of methanol and optimization of mixture design over the full operating map in an intelligent charge compression ignition (ICCI) engine'. *Fuel Processing Technology* (2022). DOI: 10.1016/j.fuproc.2022.107345.

[154] Kasinath Panda and A. Ramesh. 'Diesel injection strategies for reducing emissions and enhancing the performance of a methanol based dual fuel stationary engine'. *Fuel* (2021). DOI: 10.1016/j.fuel.2020.119809.

[155] Wang Pan et al. 'The impact of intake air temperature on performance and exhaust emissions of a diesel methanol dual fuel engine'. *Fuel* (2015). DOI: 10.1016/j.fuel.2015.08.073.

[156] Wenhui Tao et al. 'The effect of diesel pilot injection strategy on combustion and emission characteristic of diesel/methanol dual fuel engine'. *Fuel* (2022). DOI: 10.1016/j.fuel.2022.124653.

[157] Ruben Tol. 'Combustion of diesel/methanol blends in a compression ignited engine' (2020). URL: https://repository.tudelft.nl/islandora/object/uuid%3A51d875d8-19cf-4397-8755-680de1cbc080.

[158] Wei Guan et al. 'Exploring the high load potential of diesel–methanol dual-fuel operation with Miller cycle, exhaust gas recirculation, and intake air cooling on a heavy-duty diesel engine'. *International Journal of Engine Research* (2021). DOI: 10.1177/1468087420926775.

[159] Le Ning et al. 'Parametric study on effects of methanol injection timing and methanol substitution percentage on combustion and emissions of methanol/diesel dual-fuel direct injection engine at full load'. *Fuel* (2020). DOI: 10.1016/j.fuel.2020.118424.

[160] Dhananjay Kumar, Hardikk Valera and Avinash Kumar Agarwal. 'Numerical Predictions of In-Cylinder Phenomenon in Methanol Fueled Locomotive Engine Using High Pressure Direct Injection Technique'. 2021. DOI: 10.4271/2021-01-0492.

[161] Jeroen Dierickx et al. 'Retrofitting a high-speed marine engine to dual-fuel methanol-diesel operation'. *Fuel Communications* (2021). DOI: 10.1016/j.jfueco.2021.100010.

[162] MAN Energy Solution. *The Methanol- fuelled MAN B&W LGIM Engine*. Tech. rep. 2016.

[163] J. Repo, M. Axelsson and V. Heir. 'Methanol combustion concept alternatives for new build and retrofit of 4-stroke medium speed engines'. *30th CIMAC World Congress*. Busan, Korea, 2023.

[164] Rakesh Kumar Maurya. *Reciprocating Engine Combustion Diagnostics: In-Cylinder Pressure Measurement and Analysis*. Mechanical Engineering Series. 2019. ISBN: 978-3-030-11954-6. DOI: 10.1007/978-3-030-11954-6.

[165] Lijiang Wei et al. 'Effects of methanol to diesel ratio and diesel injection timing on combustion, performance and emissions of a methanol port premixed diesel engine'. *Energy* (2016). DOI: 10.1016/j.energy.2015.12.020.

[166] M. Ghaderi Masouleh et al. 'Comparative study on chemical kinetic schemes for dual-fuel combustion of n-dodecane/methane blends'. *Fuel* (2017). DOI: 10.1016/j.fuel.2016.10.114.

[167] Hanjun Xu, Chunde Yao and Guanglan Xu. 'Chemical kinetic mechanism and a skeletal model for oxidation of n-heptane/methanol fuel blends'. *Fuel* (2012). DOI: 10.1016/j.fuel.2011.09.048.

[168] John E. Dec and Edward B. Coy. 'OH Radical Imaging in a DI Diesel Engine and the Structure of the Early Diffusion Flame'. Detroit, Michigan, United States, 1996. DOI: 10.4271/960831.

[169] John E. Dec. 'A Conceptual Model of DI Diesel Combustion Based on Laser-Sheet Imaging*'. Detroit, Michigan, United States, 1997. DOI: 10.4271/970873.

[170] Thomas Heinze and Thomas Schmidt. 'Fuel-Air Ratios in a Spray, Determined between Injection and Autoignition by Pulsed Spontaneous Raman Spectroscopy'. Baltimore, Maryland, United States, 1989. DOI: 10.4271/892102.

[171] Christoph Espey and John E. Dec. 'Diesel Engine Combustion Studies in a Newly Designed Optical-Access Engine Using High-Speed Visualization and 2-D Laser Imaging'. Detroit, Michigan, United States, 1993. DOI: 10.4271/930971.

[172] Christoph Espey et al. 'Quantitative 2-D Fuel Vapor Concentration Imaging in a Firing D.I. Diesel Engine Using Planar Laser-Induced Rayleigh Scattering*'. Detroit, Michigan, United States, 1994. DOI: 10.4271/940682.

[173] Rainer N. Dahms et al. 'Understanding the ignition mechanism of high-pressure spray flames'. *Proceedings of the Combustion Institute* (2017). DOI: 10.1016/j.proci.2016.08.023.

[174] Zenghui Yin et al. 'Visualization of combustion characteristic of diesel in premixed methanol–air mixture atmosphere of different ambient temperature in a constant volume chamber'. *Fuel* (2016). DOI: 10.1016/j.fuel.2016.02.030.

[175] Aleš Srna et al. 'Effect of methane on pilot-fuel auto-ignition in dual-fuel engines'. *Proceedings of the Combustion Institute* (2019). DOI: 10.1016/j.proci.2018.06.177.

[176] Heikki Kahila et al. 'Large-eddy simulation of dual-fuel ignition'. *Combustion and Flame* (2019). DOI: 10.1016/j.combustflame.2018.10.014.

[177] Zhiqin Jia and Ingemar Denbratt. 'Experimental investigation into the combustion characteristics of a methanol-Diesel heavy duty engine operated in RCCI mode'. *Fuel* (2018). DOI: 10.1016/j.fuel.2018.03.088.

[178] Jeroen Dierickx, Louis Sileghem and Sebastian Verhelst. 'Efficiency and Emissions of a High- Speed Marine Diesel Engine Converted to Dual-Fuel Operation with Methanol.pdf'. Vancouver, BC, Canada, 2019.

[179] Peng Geng et al. 'Reduction of PM emissions from a heavy-duty diesel engine with diesel/methanol dual fuel'. *Fuel* (2014). DOI: 10.1016/j.fuel.2014.01.056.

[180] Kjeld Aabo, Berit Hinnemann and et al. 'MAN B&W two-stroke methanol-powered engines for small and large container vessels in the A.P. Moller Maersk fleet - experience and new development'. *30th CIMAC World Congress*. Busan, Korea, 2023.

[181] Yongseok Lee, Gwanghyeon and et al. 'Development of carbon-neutral fuel engine: HiMSEN methanol engine'. *30th CIMAC World Congress*. Busan, Korea, 2023.

[182] Dennis L. Siebers and C. F. Edwards. 'Autoignition of Methanol and Ethanol Sprays under Diesel Engine Conditions'. 1987. DOI: 10.4271/870588.

[183] Guo Lijun, Li Huang and et al. 'The retrofit investigation of medium-speed marine engine using methanol as primary fuel'. *30th CIMAC World Congress*. Busan, Korea, 2023.

[184] Lijiang Wei et al. 'Combustion and emission characteristics of a turbocharged diesel engine using high premixed ratio of methanol and diesel fuel'. *Fuel* (2015). DOI: 10.1016/j.fuel.2014.09.070.

[185] Erik Fridell, Håkan Salberg and Kent Salo. 'Measurements of Emissions to Air from a Marine Engine Fueled by Methanol'. *Journal of Marine Science and Application* (2021). DOI: 10.1007/s11804-020-00150-6.

[186] Yi-Hao Pu et al. 'The FASTWATER demonstrator : retrofitting a pilot boat to methanol operation'. *Scaling Decarbonisation Solutions : Reducing Emissions by 2030, Proceedings*. 2022. URL: http://hdl.handle.net/1854/LU-01GT1J5WK77C40G7Z3HMTB5WGY.

[187] Brian Gainey and Benjamin Lawler. 'The role of alcohol biofuels in advanced combustion'. *Fuel* (2021). DOI: 10.1016/j.fuel.2020.118915.

[188] Jeroen Dierickx et al. 'Performance and emissions of a high-speed marine dual-fuel engine operating with methanol-water blends as a fuel'. *Fuel* (2023). DOI: 10.1016/j.fuel.2022.126349.

[189] Sipeng Zhu et al. 'A review of water injection applied on the internal combustion engine'. *Energy Conversion and Management* (2019). DOI: 10.1016/j.enconman.2019.01.042.

[190] Changchun Xu and Haengmuk Cho. 'Effect of Methanol/Water Mixed Fuel Compound Injection on Engine Combustion and Emissions'. *Energies* (2021). DOI: 10.3390/en14154491.

[191] Dhananjay Kumar et al. 'Experimental investigations of methanol fumigation via port fuel injection in preheated intake air in a single cylinder dual-fuel diesel engine'. *Fuel* (2022). DOI: 10.1016/j.fuel.2022.124340.

[192] W.J. Mclean et al. 'Direct Formation of NO_2 in Combustion Products'. *Studies in Environmental Science*. 1980. DOI: 10.1016/S0166-1116(08)71653-4.

[193] Yasushi Kodama et al. 'Environmental NO_2 Concentration and Exposure in Daily Life along Main Roads in Tokyo'. *Environmental Research* (2002). DOI: 10.1006/enrs.2002.4350.

[194] Chao Chen et al. 'Study of the characteristics of PM and the correlation of soot and smoke opacity on the diesel methanol dual fuel engine'. *Applied Thermal Engineering* (2019). DOI: 10.1016/j.applthermaleng.2018.11.062.

[195] C.H. Cheng et al. 'Experimental investigation on the performance, gaseous and particulate emissions of a methanol fumigated diesel engine'. *Science of The Total Environment* (2008). DOI: 10.1016/j.scitotenv.2007.08.041.

[196] Chunde Yao, Zhi Hui Zhang and Chun Shun Cheung. 'Emissions and oxidation characteristics of particulate from a diesel/methanol compound combustion engine'. *Neiranji Xuebao/Transactions of CSICE (Chinese Society for Internal Combustion Engines)* (2010).

[197] Chunde Yao, Wang Pan and Anren Yao. 'Methanol fumigation in compression-ignition engines'. *Fuel* (2017). DOI: 10.1016/j.fuel.2017.08.038.

[198] Wai K. Cheng et al. 'An Overview of Hydrocarbon Emissions Mechanisms in Spark-Ignition Engines'. 1993. DOI: 10.4271/932708.

[199] E.W. Kaiser, A.A. Adamczyk and G.A. Lavoie. 'The effect of oil layers on the hydrocarbon emissions generated during closed vessel combustion'. *Symposium (International) on Combustion* (1981). DOI: 10.1016/S0082-0784(81)80194-4.

[200] K. W. Aniolek and R. D. Wilk. 'Preflame Oxidation Characteristics of Methanol'. *Energy & Fuels* (1995). DOI: 10.1021/ef00051a002.

[201] John R Creighton. 'Dependence of CO emissions on the rate of product cooling'. *Combustion and Flame* (2000). DOI: 10.1016/S0010-2180(00)00160-7.

[202] Alain Lépinette et al. 'Reduced kinetics and coupling functions for calculating co and no emissions in gas-turbine combustion'. *Combustion Science and Technology* (2005). DOI: 10.1080/00102200590926923.

[203] David Cooper and Tomas Gustafsson. *Methodology for calculating emissions from ships*. 2004. URL: https://urn.kb.se/resolve?urn=urn:nbn:se:naturvardsverket:diva-7083.

[204] K. F. Hansen et al. 'The Influence of an Oxidation Catalytic Converter on the Chemical and Biological Characteristics of Diesel Exhaust Emissions'. 1994. DOI: 10.4271/940241.

[205] Kati Vaaraslahti et al. 'Effect of Oxidation Catalysts on Diesel Soot Particles'. *Environmental Science & Technology* (2006). DOI: 10.1021/es060615h.

[206] Greg Rideout, Morrie Kirshenblatt and Chandra Prakash. 'Emissions from Methanol, Ethanol, and Diesel Powered Urban Transit Buses'. 1994. DOI: 10.4271/942261.

[207] Ahmed Betül and Lukacs Emma. 'Oxidation Catalysts in Exhaust Aftertreatment Systems for Green-Methanol Engines'. PhD thesis. Chalmers University of Technology, 2024. URL: http://hdl.handle.net/20.500.12380/307774.

[208] Inderpal Singh et al. 'Experimental and Numerical Investigation of a Single-Cylinder Methanol Port-Fuel Injected Spark Ignition Engine for Heavy-Duty Applications'. SAE Technical Paper. 2024. DOI: 10.4271/2024-26-0072.

[209] Christian Wouters, Patrick Burkardt and Stefan Pischinger. 'Limits of compression ratio in spark-ignition combustion with methanol'. *International Journal of Engine Research* (2022). DOI: 10.1177/14680874211043390.

[210] Arne Güdden et al. 'An experimental study on methanol as a fuel in large bore high speed engine applications – Port fuel injected spark ignited combustion'. *Fuel* (2021). DOI: 10.1016/j.fuel.2021.121292.

[211] J. Bosklopper et al. 'Experimental study on a retrofitted marine size spark-ignition engine running on portinjected 100% methanol'. en. *INEC 2020, Delft* (2020).

[212] J.J. Bosklopper et al. 'Experimental and simulation-based investigation of the performance of a 100 % methanol port-injected spark-ignited engine'. MA thesis. TU Delft, 2020. URL: https://resolver.tudelft.nl/uuid:946dbdf6-ea99-4f57-8441-5a012e704d37.

[213] Zengqiang Zhu et al. 'Experimental evaluation of performance of heavy-duty SI pure methanol engine with EGR'. *Fuel* (2022). DOI: 10.1016/j.fuel.2022.124948.

[214] Lee Björnestrand. 'Efficiency and Emission Analysis of a Methanol Fuelled Direct Injection Spark Ignition Heavy Duty Engine'. MA thesis. 2017. URL: http://lup.lub.lu.se/student-papers/record/8907927.

[215] Senthil Krishnan Mahendar, Tara Larsson and Anders Christiansen Erlandsson. 'Alcohol lean burn in heavy duty engines'. *International Journal of Engine Research* (2021). DOI: 10.1177/1468087420972897.

[216] Christof Noehre et al. 'Characterization of Partially Premixed Combustion'. 2006. DOI: 10.4271/2006-01-3412.

[217] Sam Shamun et al. 'Exhaust PM Emissions Analysis of Alcohol Fueled Heavy-Duty Engine Utilizing PPC'. *SAE International Journal of Engines* (2016). DOI: 10.4271/2016-01-2288.

[218] Sam Shamun et al. 'Quantification and Analysis of the Charge Cooling Effect of Methanol in a Compression Ignition Engine Utilizing PPC Strategy'. *Volume 1: Large Bore Engines; Fuels; Advanced Combustion*. San Diego, California, USA, 2018. DOI: 10.1115/ICEF2018-9657.

[219] Burak Zincir, Cengiz Deniz and Martin Tunér. 'Investigation of environmental, operational and economic performance of methanol partially premixed combustion at slow speed operation of a marine engine'. *Journal of Cleaner Production* (2019). DOI: 10.1016/j.jclepro.2019.07.044.

[220] Erik Svensson, Martin Tuner and Sebastian Verhelst. 'Influence of Injection Strategies on Engine Efficiency for a Methanol PPC Engine'. *SAE International Journal of Advances and Current Practices in Mobility* (2019). DOI: 10.4271/2019-24-0116.

[221] Magnus Svensson, Martin Tuner and Sebastian Verhelst. 'Experimental Investigation of Pilot Injection Strategies to Aid Low Load Compression Ignition of Neat Methanol'. *SAE Technical Paper*. Detroit, Michigan, United States, 2024. DOI: 10.4271/2024-01-2119.

[222] Konstantinos-Marios Tsitsilonis and Gerasimos Theotokatos. 'A novel systematic methodology for ship propulsion engines energy management'. *Journal of Cleaner Production* (2018). DOI: 10.1016/j.jclepro.2018.08.154.

[223] Malcolm Latarche and C. Coulson Pounder. *Pounder's marine diesel engines and gas turbines*. Tenth edition. Oxford: Butterworth-Heinemann, 2021.

[224] Zhifang Chen et al. 'Study of cylinder-to-cylinder variation in a diesel engine fueled with diesel/methanol dual fuel'. *Fuel* (2016). DOI: 10.1016/j.fuel.2015.12.019.

[225] A. Uludogan, David E. Foster and Rolf D. Reitz. 'Modeling the Effect of Engine Speed on the Combustion Process and Emissions in a DI Diesel Engine'. 1996. DOI: 10.4271/962056.

[226] C. S. Cheung et al. 'Investigation on the Effect of Port-Injected Methanol on the Performance and Emissions of a Diesel Engine at Different Engine Speeds'. *Energy & Fuels* (2009). DOI: 10.1021/ef9005516.

[227] Bin Wang et al. 'To extend the operating range of high MSP with ultra-low emissions for DMDF unit pump engine'. *Fuel* (2018). DOI: 10.1016/j.fuel.2018.01.028.

[228] Xiaojun Yin et al. 'In-depth comparison of methanol port and direct injection strategies in a methanol/diesel dual fuel engine'. *Fuel Processing Technology* (2023). DOI: 10.1016/j.fuproc.2022.107607.

[229] Quangang Wang et al. 'Effect of intake pre-heating and injection timing on combustion and emission characteristics of a methanol fumigated diesel engine at part load'. *Fuel* (2015). DOI: 10.1016/j.fuel.2015.07.032.

[230] Jeroen Dierickx et al. 'Effect of Intake Conditions (Temperature, Pressure and EGR) on the Operation of a Dual-Fuel Marine Engine with Methanol'. 2023. DOI: 10.4271/2023-24-0046.

[231] Yangyang Li et al. 'Effects of rapid burning characteristics on the vibration of a common-rail diesel engine fueled with diesel–methanol dual-fuel'. *Fuel* (2016). DOI: 10.1016/j.fuel.2015.12.045.

[232] Junheng Liu, Anren Yao and Chunde Yao. 'Effects of diesel injection pressure on the performance and emissions of a HD common-rail diesel engine fueled with diesel/methanol dual fuel'. *Fuel* (2015). DOI: 10.1016/j.fuel.2014.09.109.

[233] Taizo Shimada, Takeshi Shoji and Yoshinaka Takeda. 'The Effect of Fuel injection Pressure on Diesel Engine Performance'. 1989. DOI: 10.4271/891919.

[234] Konstantinos I. Kiouranakis et al. 'Natural Gas for Marine Lean-Burn Spark Ignition Engines: A Combustion Stability Analysis'. *ASME 2024 ICE Forward Conference*. San Antonio, Texas, USA, 2024. DOI: 10.1115/ICEF2024-139218.

[235] Konstantinos I. Kiouranakis et al. 'Heat release behaviour in a natural gas lean-burn SI marine engine: Exploring the impact of bowl-in and squish combustion on performance and emissions'. *Applied Thermal Engineering* (2025). DOI: 10.1016/j.applthermaleng.2025.127509.

[236] Konstantinos Ioannis Kiouranakis et al. 'Using multi-stage Wiebe to characterize the combustion of a marine natural gas lean-burn SI engine'. *31st CIMAC World Congress*. Zurich, 2025. DOI: 10.5281/ZENODO.15193328.

[237] Christine Mounaïm-Rousselle et al. 'Operating Limits for Ammonia Fuel Spark-Ignition Engine'. *Energies* (2021). DOI: 10.3390/en14144141.

[238] Behdad Shadidi, Gholamhassan Najafi and Talal Yusaf. 'A Review of Hydrogen as a Fuel in Internal Combustion Engines'. *Energies* (2021). DOI: 10.3390/en14196209.

[239] Päivi T. Aakko-Saksa et al. 'Reduction in greenhouse gas and other emissions from ship engines'. *Progress in Energy and Combustion Science* (2023). DOI: 10.1016/j.pecs.2022.101055.

[240] Bengt Johansson and Krister Olsson. 'Combustion Chambers for Natural Gas SI Engines Part I'. 1995. DOI: 10.4271/950469.

[241] Jinlong Liu and Cosmin E. Dumitrescu. 'Flame development analysis in a diesel optical engine converted to spark ignition natural gas operation'. *Applied Energy* (2018). DOI: 10.1016/j.apenergy.2018.09.059.

[242] M. G. Kingston Jones and D. M. Heaton. 'Nebula Combustion System for Lean Burn Spark Ignited Gas Engines'. SAE Technical Paper. 1989. DOI: 10.4271/890211.

[243] Robert L. Evans. 'Lean-Burn Spark-Ignited Internal Combustion Engines'. *Lean Combustion*. 2008. DOI: 10.1016/B978-012370619-5.50005-4.

[244] Simon K. Chen and N. John Beck. 'Gas Engine Combustion Principles and Applications'. 2001, pp. 2001–01–2489. DOI: 10.4271/2001-01-2489.

[245] Krister Olsson and Bengt Johansson. 'Combustion Chambers for Natural Gas SI Engines Part 2'. 1995. DOI: 10.4271/950517.

[246] C. D. De Boer and D. W. Grigg. 'Gasoline Engine Combustion — The Nebula Combustion Chamber'. SAE Technical Paper. 1988. DOI: 10.4271/885148.

[247] Mahmut Kaplan. 'Influence of swirl, tumble and squish flows on combustion characteristics and emissions in internal combustion engine-review'. *International Journal of Automotive Engineering and Technologies* (2019). DOI: 10.18245/ijaet.558258.

[248] Jinlong Liu and Cosmin E. Dumitrescu. 'Combustion partitioning inside a natural gas spark ignition engine with a bowl-in-piston geometry'. *Energy Conversion and Management* (2019). DOI: 10.1016/j.enconman.2018.12.118.

[249] Patrik Einewall and Bengt Johansson. 'Combustion Chambers for Supercharged Natural Gas Engines'. SAE Technical Paper. 1997. DOI: 10.4271/970221.

[250] Jinlong Liu, Christopher J. Ulishney and Cosmin E. Dumitrescu. 'Experimental investigation of a heavy-duty natural gas engine performance operated at stoichiometric and lean operations'. *Energy Conversion and Management* (2021). DOI: 10.1016/j.enconman.2021.114401.

[251] Amir Sharafian, Paul Blomerus and Walter Mérida. 'Natural gas as a ship fuel'. *Energy Policy* (2019). DOI: 10.1016/j.enpol.2019.05.015.

[252] Patrick Lott and Olaf Deutschmann. 'Lean-Burn Natural Gas Engines'. *Emission Control Science and Technology* (2021). DOI: 10.1007/s40825-020-00176-w.

[253] Jinlong Liu, Christopher Ulishney and Cosmin Dumitrescu. 'Characterization of Cycle-by-Cycle Variations of an Optically Accessible Heavy-Duty Diesel Engine Retrofitted to Natural Gas Spark Ignition'. *SAE Technical Paper Series*. SAE Technical Paper. SAE International, 2021. DOI: 10.4271/2021-24-0045.

[254] P. Corbo et al. 'Comparison Between Lean-Burn and Stoichiometric Technologies for CNG Heavy-Duty Engines'. 1995. DOI: 10.4271/950057.

[255] Jinlong Liu and Cosmin Emil Dumitrescu. 'Limitations of Natural Gas Lean Burn Spark Ignition Engines Derived From Compression Ignition Engines'. *Journal of Energy Resources Technology* (2020). DOI: 10.1115/1.4047404.

[256] Carlos Eduardo Castilla Alvarez et al. 'A review of prechamber ignition systems as lean combustion technology for SI engines'. *Applied Thermal Engineering* (2018). DOI: 10.1016/j.applthermaleng.2017.08.118.

[257] Evgeniy Shapiro et al. 'Experimental and Numerical Analysis of Pre-Chamber Combustion Systems for Lean Burn Gas Engines'. 2019. DOI: 10.4271/2019-01-0260.

[258] Mehmet Cakir. 'Effect of Stratified Charge Combustion Chamber Design on Natural Gas Engine Performance'. *Energies* (2025). DOI: 10.3390/en18092187.

[259] Yohei Tsuji et al. 'Flexible Operation of Gas Engines for Grid Power Stability and Carbon Neutrality'. Zurich, 2025.

[260] Nathan Peters and Michael Bunce. 'Optimization of Pre-Chamber Design and Operation for Marine Future Fuels'. *31st CIMAC World Congress*. Zurich, 2025.

[261] Luis F. Alvarez and Cosmin E. Dumitrescu. 'Experimental Study of Ammonia Combustion in a Heavy-Duty Diesel Engine Converted to Spark Ignition Operation'. 2024. DOI: 10.4271/2024-01-2371.

[262] Xiongbo Duan et al. 'An experimental study the impact of the hydrogen enrichment on cycle-to-cycle variations of the large bore and lean burn natural gas spark-ignition engine'. *Fuel* (2020). DOI: 10.1016/j.fuel.2020.118868.

[263] Yangyang Li et al. 'Influences of the control parameters and spark plug configurations on the performance of a natural gas spark-ignition engine'. *Fuel* (2022). DOI: 10.1016/j.fuel.2022.124728.

[264] Zhongshu Wang et al. 'Impact of ignition energy on the combustion performance of an SI heavy-duty stoichiometric operation natural gas engine'. *Fuel* (2022). DOI: 10.1016/j.fuel.2021.122857.

[265] Penmatsa Sandeep Varma and Mayank Mittal. 'Investigations with bowl-in-piston (CI type) and flat-piston (SI type) geometries to study the engine characteristics of a CI engine retrofitted for SI operation with CNG fuel'. *Energy Conversion and Management* (2024). DOI: 10.1016/j.enconman.2024.118083.

[266] Fatih Aktas. 'Spark ignition timing effects on a converted diesel engine using natural gas' (2022). DOI: 10.1177/09544070221081671.

[267] Harsh D. Sapra et al. 'Experimental Investigations of Hydrogen-Natural Gas Engines for Maritime Applications'. 2018. DOI: 10.1115/ICEF2018-9615.

[268] David R. Lancaster, Roger B. Krieger and John H. Lienesch. 'Measurement and Analysis of Engine Pressure Data'. SAE Technical Paper. 1975. DOI: 10.4271/750026.

[269] Michael F. J. Brunt and Christopher R. Pond. 'Evaluation of Techniques for Absolute Cylinder Pressure Correction'. 1997. DOI: 10.4271/970036.

[270] F. Payri et al. 'Digital signal processing of in-cylinder pressure for combustion diagnosis of internal combustion engines'. *Mechanical Systems and Signal Processing* (2010). DOI: 10.1016/j.ymssp.2009.12.011.

[271] Rakesh Kumar Maurya. 'Estimation of optimum number of cycles for combustion analysis using measured in-cylinder pressure signal in conventional CI engine'. en. *Measurement* (2016). DOI: 10.1016/j.measurement.2016.07.065.

[272] Brian Gainey, Jon P. Longtin and Benjamin Lawler. 'A Guide to Uncertainty Quantification for Experimental Engine Research and Heat Release Analysis'. *SAE International Journal of Engines* (2019). DOI: 10.4271/03-12-05-0033.

[273] Ohashi Issei. *Dual-Fuel Marine Engine (Highly Reliable Environmentally Friendly Engine) Technical Review*. Tech. rep. YANMAR, 2015. URL: https://www.yanmar.com/global/about/technology/technical_review/2015/0727_2.html.

[274] Sadi Tavakoli et al. 'Modeling and analysis of performance and emissions of marine lean-burn natural gas engine propulsion in waves'. *Applied Energy* (2020). DOI: 10.1016/j.apenergy.2020.115904.

[275] Aydek Gökçe Erman, Paul Hellier and Nicos Ladommatos. 'The impact of ignition delay and further fuel properties on combustion and emissions in a compression ignition engine'. *Fuel* (2020). DOI: https://doi.org/10.1016/j.fuel.2019.116155.

[276] M. Reyes et al. 'Characterization of cycle-to-cycle variations in a natural gas spark ignition engine'. *Fuel* (2015). DOI: 10.1016/j.fuel.2014.09.121.

[277] G. A. Karim and I. Wierzba. 'Experimental and Analytical Studies of the Lean Operational Limits in Methane Fuelled Spark Ignition and Compression Ignition Engines'. SAE Technical Paper. 1989. DOI: 10.4271/891637.

[278] Cosmin E. Dumitrescu, Vishnu Padmanaban and Jinlong Liu. 'An Experimental Investigation of Early Flame Development in an Optical Spark Ignition Engine Fueled With Natural Gas'. *Journal of Engineering for Gas Turbines and Power* (2018). DOI: 10.1115/1.4039616.

[279] Jinlong Liu and Cosmin E. Dumitrescu. 'Analysis of two-stage natural-gas lean combustion inside a diesel geometry'. *Applied Thermal Engineering* (2019). DOI: 10.1016/j.applthermaleng.2019.114116.

[280] Jinlong Liu and Cosmin Emil Dumitrescu. 'Lean-Burn Characteristics of a Heavy-Duty Diesel Engine Retrofitted to Natural-Gas Spark Ignition'. *Journal of Engineering for Gas Turbines and Power* (2019). DOI: 10.1115/1.4042501.

[281] Jinlong Liu and Cosmin E. Dumitrescu. 'Methodology to separate the two burn stages of natural-gas lean premixed-combustion inside a diesel geometry'. *Energy Conversion and Management* (2019). DOI: 10.1016/j.enconman.2019.04.091.

[282] L.D. Danny Harvey. 'A guide to global warming potentials (GWPs)'. *Energy Policy* (1993). DOI: 10.1016/0301-4215(93)90205-T.

[283] Niina Kuittinen, Mikko Heikkilä and Kati Lehtoranta. *Review of methane slip from LNG marine engines*. Tech. rep. 2023.

[284] IMO. *International Maritime Organization*. 2024. URL: https://www.imo.org.

[285] Dag Stenersen and Ole Thonsta. *GHG and NOx emissions from gas fuelled engines: Mapping, verification, reduction technologies*. Tech. rep. SINTEF Ocean AS. URL: https://www.nho.no/siteassets/nox-fondet/rapporter/2018/methane-slip-from-gas-engines-mainreport-1492296.pdf.

[286] International Council On Clean Transportation. *European stage v non-road emission standars*. Tech. rep. 2016.

[287] Oivind Andersson. *Experiment!: Planning, Implementing and Interpreting*. John Wiley & Sons, 2012. ISBN: 978-1-118-31101-1.

[288] S Rousseau, B Lemoult and M Tazerout. 'Combustion characterization of natural gas in a lean burn spark-ignition engine'. *Journal of Automobile Engineering* (1999). DOI: 10.1243/0954407991527044.

[289] Jinlong Liu, Hemanth Kumar Bommisetty and Cosmin Emil Dumitrescu. 'Experimental Investigation of a Heavy-Duty Compression-Ignition Engine Retrofitted to Natural Gas Spark-Ignition Operation'. *Journal of Energy Resources Technology* (2019). Publisher: ASME International. DOI: 10.1115/1.4043749.

[290] Jinlong Liu, Christopher J. Ulishney and Cosmin Emil Dumitrescu. 'Effect of Spark Timing on the Combustion Stages Seen in a Heavy-Duty Compression-Ignition Engine Retrofitted to Natural Gas Spark-Ignition Operation'. *SAE International Journal of Engines* (2021). DOI: 10.4271/03-14-03-0020.

[291] Jinlong Liu and Cosmin E. Dumitrescu. 'Single and double Wiebe function combustion model for a heavy-duty diesel engine retrofitted to natural-gas spark-ignition'. *Applied Energy* (2019). DOI: 10.1016/j.apenergy.2019.04.098.

[292] Xiaojun Yin et al. 'Influence of methanol and diesel injection timings on the maximum methanol energy substitution ratio and performance of diesel/methanol dual-direct injection engine'. *Energy* (2025). DOI: 10.1016/j.energy.2025.134762.

[293] Zhongshu Wang et al. 'Combustion process decoupling of a diesel/natural gas dual-fuel engine at low loads'. *Fuel* (2018). DOI: 10.1016/j.fuel.2018.05.152.

[294] Khanh Duc Cung et al. 'Experimental study on engine and emissions performance of renewable diesel methanol dual fuel (RMDF) combustion'. *Fuel* (2024). DOI: 10.1016/j.fuel.2023.129664.

[295] Derek Splitter et al. 'Approach for high methanol substitution by energy with conventional and bio pilot fuels'. *31st CIMAC World Congress*. Zurich, 2025.

[296] Karsten Stenzel et al. 'Experimental investigations of a methanol dual-fuel combustion process for marine engines'. *31st CIMAC World Congress*. Zurich, 2025.

[297] Zeeshan Ahmad et al. 'An Optical Characterization of Dual-Fuel Combustion in a Heavy-Duty Diesel Engine'. SAE Technical Paper. 2018. DOI: 10.4271/2018-01-0252.

[298] Daniela Siano, Maria Antonietta Panza and Danilo D'Agostino. 'Knock Detection Based on MAPO Analysis, AR Model and Discrete Wavelet Transform Applied to the In-Cylinder Pressure Data'. *SAE International Journal of Engines* (2014). DOI: 10.4271/2014-01-2547.

[299] Andreas Vressner et al. 'Pressure Oscillations During Rapid HCCI Combustion'. 2003. DOI: 10.4271/2003-01-3217.

[300] Ward Suijs, Rik De Graeve and Sebastian Verhelst. 'An exploratory study of knock intensity in a large-bore heavy-duty methanol engine'. *Energy Conversion and Management* (2024). DOI: 10.1016/j.enconman.2024.118089.

[301] Rik D Meininger et al. 'Knock criteria for aviation diesel engines'. *International Journal of Engine Research* (2017). DOI: 10.1177/1468087416669882.

[302] David P. Lowe et al. 'Diesel Knock Combustion and its Detection Using Acoustic Emission' (2011). URL: https://www.ndt.net/article/jae/papers/29-078.pdf.

[303] Hans Klein Woud and Douwe Stapersma. *Design of propulsion and electric power generation systems*. London: Imarest, 2002. ISBN: 978-1-902536-47-7.

[304] Bin Wang et al. 'In-depth comparison between pure diesel and diesel methanol dual fuel combustion mode'. *Applied Energy* (2020). DOI: 10.1016/j.apenergy.2020.115664.

[305] Qiao Huang et al. 'Investigation of the mechanism behind the surge in nitrogen dioxide emissions in engines transitioning from pure diesel operation to methanol/diesel dual-fuel operation'. *Fuel Processing Technology* (2024). DOI: 10.1016/j.fuproc.2024.108131.

[306] Yu Li et al. 'A Numerical Investigation on NO2 Formation in a Natural Gas–Diesel Dual Fuel Engine'. *Journal of Engineering for Gas Turbines and Power* (2018). DOI: 10.1115/1.4039734.

[307] Han Lu et al. 'An investigation on the characteristics of and influence factors for NO2 formation in diesel/methanol dual fuel engine'. *Fuel* (2019). DOI: 10.1016/j.fuel.2018.08.061.

[308] Jeongwoo Lee et al. 'Classification of diesel and gasoline dual-fuel combustion modes by the analysis of heat release rate shapes in a compression ignition engine'. *Fuel* (2017). DOI: 10.1016/j.fuel.2017.07.067.

[309] Krisada Wannatong et al. 'Combustion and Knock Characteristics of Natural Gas Diesel Dual Fuel Engine'. 2007. DOI: 10.4271/2007-01-2047.

[310] Lei Zhou et al. 'Knock characteristics and combustion regime diagrams of multiple combustion modes based on experimental investigations'. *Applied Energy* (2018). DOI: 10.1016/j.apenergy.2018.07.102.

[311] Robbert Willems et al. 'Heat release rate shaping for optimal gross indicated efficiency in a heavy-duty RCCI engine fueled with E85 and diesel'. *Fuel* (2021). DOI: 10.1016/j.fuel.2020.119656.

[312] Xiao Zhang and Lin Chen. 'The Synergy Effect of Ignition Energy and Spark Plug Gap on Methane Lean Combustion with Addressing Initial Flame Formation and Cyclic Variation' (2023). DOI: 10.1021/acsomega.2c07897.

[313] Konstantinos I. Kiouranakis et al. 'Steering methanol premixed dual-fuel combustion with boundary conditions: Performance gains and mode shifts in a marine engine'. *Fuel* (2026). DOI: 10.1016/j.fuel.2026.139458.

[314] Quangang Wang et al. 'Investigation of operating range in a methanol fumigated diesel engine'. *Fuel* (2015). DOI: 10.1016/j.fuel.2014.09.067.

[315] Victor M. Dominguez et al. 'Role of the Compression Ratio in Dual-Fuel Compression Ignition Combustion with Hydrogen and Methanol'. *Energy & Fuels* (2024). DOI: 10.1021/acs.energyfuels.4c02741.

[316] D. T. Hountalas, T. C. Zannis and G. C. Mavropoulos. 'Potential Benefits in Heavy Duty Diesel Engine Performance and Emissions from the Use of Variable Compression Ratio'. 2006. DOI: 10.4271/2006-01-0081.

[317] Bhaskor J. Bora and Ujjwal K. Saha. 'Experimental evaluation of a rice bran biodiesel – biogas run dual fuel diesel engine at varying compression ratios'. *Renewable Energy* (2016). DOI: 10.1016/j.renene.2015.11.002.

[318] Mohit Raj Saxena and Rakesh Kumar Maurya. 'Effect of premixing ratio, injection timing and compression ratio on nano particle emissions from dual fuel non-road compression ignition engine fueled with gasoline/methanol (port injection) and diesel (direct injection)'. *Fuel* 203 (2017). DOI: 10.1016/j.fuel.2017.05.015.

[319] Marcel Ott et al. 'Compression without compromise: dynamic optimisation of combustion in dual-fuel engines with VCR'. *31st CIMAC World Congress*. Zurich, May 2025.

[320] R Modiyani et al. 'Effect of intake valve closure modulation on effective compression ratio and gas exchange in turbocharged multi-cylinder engines utilizing EGR'. *International Journal of Engine Research* (2011). DOI: 10.1177/1468087411415180.

[321] Taoyang Wu et al. 'Experimental study on ultra-low raw emissions in diesel/-methanol dual fuel engine based on dual-loop EGR'. *E3S Web of Conferences* (2022). Ed. by F. Yan et al. DOI: 10.1051/e3sconf/202236001037.

[322] Daanish S Tyrewala, David Rothamer and Jaal Ghandhi. 'Assessing the influence of EGR on diesel pilot ignition combustion with methane/hydrogen blends in a single-cylinder compression ignition engine'. *International Journal of Engine Research* (2025). DOI: 10.1177/14680874241305837.

[323] Víctor M. Domínguez et al. 'Hydrogen or hydrogen-derived methanol for dual-fuel compression-ignition combustion'. *Fuel* (2023). DOI: 10.1016/j.fuel.2022.126301.

[324] Dong Yang et al. 'Influence of critical parameters on combustion and emission characteristics of methanol/diesel dual fuel compression combustion engine'. *Fuel* 368 (2024). DOI: 10.1016/j.fuel.2024.131647.

[325] D. Di Battista, M. Di Bartolomeo and R. Cipollone. 'Flow and thermal management of engine intake air for fuel and emissions saving'. *Energy Conversion and Management* (2018). DOI: 10.1016/j.enconman.2018.07.074.

[326] Henrik Wasberg. 'Electrical heater for charge air conditioning on a research engine'. BSc Thesis. 2012. URL: https://www.theseus.fi/handle/10024/43450.

[327] Keshav S. Varde. 'Ignition Delay and Emissions Characteristics of a Methanol-Diesel Fueled Engine at Low Charge Temperatures'. 1992. DOI: 10.4271/920037.

[328] H. J. Yun and W. Mirsky. 'Schlieren-Streak Measurements of Instantaneous Exhaust Gas Velocities from a Spark-Ignition Engine'. Feb. 1974, p. 741015. DOI: 10.4271/741015.

[329] The MathWorks Inc. *MATLAB Version: 23.2.0 (R2023b)*. 2023.

[330] Ulf Aronsson. 'Processes in optical diesel engines'. Doctoral thesis. Lund University, 2011.

[331] V.T. Lamaris and D.T. Hountalas. 'A general purpose diagnostic technique for marine diesel engines – Application on the main propulsion and auxiliary diesel units of a marine vessel'. *Energy Conversion and Management* (2010). DOI: 10.1016/j.enconman.2009.10.031.

[332] Robbert Willems. 'Designed experiments for efficient engines'. Doctoral thesis. Technische Universiteit Eindhoven, 2020.

[333] Frank Willems et al. 'Cylinder Pressure-Based Control in Heavy-Duty EGR Diesel Engines Using a Virtual Heat Release and Emission Sensor'. 2010. DOI: 10.4271/2010-01-0564.

[334] Yeliana Yeliana et al. 'Estimation of double-Wiebe function parameters using least square method for burn durations of ethanol-gasoline blends in spark ignition engine over variable compression ratios and EGR levels'. *Applied Thermal Engineering* (2011). DOI: 10.1016/j.applthermaleng.2011.01.040.

[335] E. Rosseel, R. Sierens and R.S.G. Baert. 'Evaluating Piezo-electric Transducer Response to Thermal Shock from In-cylinder Pressure Data'. 1999. DOI: 10.4271/1999-01-0935.

[336] Dennis A. Soltis. 'Evaluation of Cylinder Pressure Transducer Accuracy based upon Mounting Style, Heat Shields, and Watercooling'. 2005. DOI: 10.4271/2005-01-3750.

[337] A. Douaud and P. Eyzat. 'DIGITAP-An On-Line Acquisition and Processing System for Instantaneous Engine Data-Applications'. 1977. DOI: 10.4271/770218.

[338] Ales Hribernik. 'Statistical Determination of Correlation Between Pressure and Crankshaft Angle During Indication of Combustion Engines'. 1998. DOI: 10.4271/982541.

[339] Andrew L. Randolph. 'Methods of Processing Cylinder-Pressure Transducer Signals to Maximize Data Accuracy'. 1990. DOI: 10.4271/900170.

[340] Weihua Sun et al. 'A Cylinder Pressure Correction Method Based on Calculated Polytropic Exponent'. SAE Technical Paper. 2017. DOI: 10.4271/2017-01-2252.

[341] K.S. Kim et al. *Optimization of In-Cylinder Pressure Filter for Engine Research*. Tech. rep. US Army Research Laboratory, 2017.

[342] David R Rogers. *Engine Combustion: Pressure Measurement and Analysis*. Warrendale, PA: SAE International, 2010. ISBN: 978-0-7680-3442-4. DOI: 10.4271/R-388.

[343] Marek J. Sta S. 'Thermodynamic Determination of T.D.C. in Piston Combustion Engines'. 1996. DOI: 10.4271/960610.

[344] M. Tazerout, O. Le Corre and S. Rousseau. 'TDC Determination in IC Engines Based on the Thermodynamic Analysis of the Temperature-Entropy Diagram'. 1999. DOI: 10.4271/1999-01-1489.

[345] M. Tazerout, O. Le Corre and P. Stouffs. 'Compression Ratio and TDC Calibrations Using Temperature - Entropy Diagram'. 1999. DOI: 10.4271/1999-01-3509.

[346] Zhaoxu Liu. *sankey plot*. 2025. URL: https://www.mathworks.com.

[347] International Maritime Organization. *MARPOL Annex VI and NTC 2008 with Guidelines for Implementation*. International Maritime Organization, 2023. ISBN: 978-92-801-1752-3. DOI: 10.62454/KD664E.

[348] D. Stapersma. *Diesel engines: A fundamental approach to performance analysis, turbocharging, combustion, emissions and heat transfer*. TU Delft, 2009. URL: https://books.google.gr/books?id=Bpq7nQEACAAJ.

[349] T. Yusaf et al. 'Effect of Compressed Natural Gas Mixing on the Engine Performance and Emissions'. *International Journal of Automotive and Mechanical Engineering* (2013). DOI: 10.15282/ijame.8.2013.29.0117.

[350] Hanseong Cho et al. 'Measurements and Modeling of Residual Gas Fraction in SI Engines'. SAE Technical Paper. 2001. DOI: 10.4271/2001-01-1910.

[351] Russell P. Fitzgerald et al. 'Determination of Cycle Temperatures and Residual Gas Fraction for HCCI Negative Valve Overlap Operation'. *SAE International Journal of Engines* (2010). DOI: 10.4271/2010-01-0343.

[352] Joachim Demuynck et al. 'Applying Design of Experiments to Determine the Effect of Gas Properties on In-Cylinder Heat Flux in a Motored SI Engine'. *SAE International Journal of Engines* (2012). DOI: 10.4271/2012-01-1209.

[353] A. Burcat, B. Ruscic and Chemistry. *Third millenium ideal gas and condensed phase thermochemical database for combustion (with update from active thermochemical tables)*. Tech. rep. 2005.

[354] G. Woschni. 'A Universally Applicable Equation for the Instantaneous Heat Transfer Coefficient in the Internal Combustion Engine'. SAE Technical Paper. 1967. DOI: 10.4271/670931.

[355] Yann G. Guezennec and Wajdi Hamama. 'Two-Zone Heat Release Analysis of Combustion Data and Calibration of Heat Transfer Correlation in an I. C. Engine'. SAE Technical Paper. 1999. DOI: 10.4271/1999-01-0218.

[356] Saudi Arabian Standards Organization. *GUIDE TO THE EXPRESSION OF UNCERTAINTY IN MEASUREMENT*. 1993. URL: http://chapon.arnaud.free.fr/documents/resources/stat/GUM.pdf.

[357] Guillaume Petitpas, Matthew J. McNenly and Russell A. Whitesides. 'A Framework for Quantifying Measurement Uncertainties and Uncertainty Propagation in HCCI/LTGC Engine Experiments'. *SAE International Journal of Engines* (2017). DOI: 10.4271/2017-01-0736.

[358] M. Cox, P. Harris and B. R.-L. Siebert. 'Evaluation of Measurement Uncertainty Based on the Propagation of Distributions Using Monte Carlo Simulation'. *Measurement Techniques* (2003). DOI: 10.1023/B:METE.0000008439.82231.ad.

[359] Jon P. Longtin. 'The uncertainty tree: Reducing the uncertainty of uncertainty analysis'. *Review of Scientific Instruments* (2002). DOI: 10.1063/1.1505654.

[360] Charles Ea Finney et al. 'A review of deterministic effects in cyclic variability of internal combustion engines'. *International Journal of Engine Research* (2015). DOI: 10.1177/1468087415572033.

[361] Brian Kaul et al. *High-dilution stoichiometric gasoline direct-injection (SGDI) combustion control development*. 2016.

[362] Brian Peterson, David L. Reuss and Volker Sick. 'High-speed imaging analysis of misfires in a spray-guided direct injection engine'. *Proceedings of the Combustion Institute* (2011). DOI: 10.1016/j.proci.2010.07.079.

[363] Bahram Bahri et al. 'Understanding and detecting misfire in an HCCI engine fuelled with ethanol'. *Applied Energy* (2013). DOI: 10.1016/j.apenergy.2013.03.004.

[364] Magnus Sjöberg and John E. Dec. 'Comparing late-cycle autoignition stability for single- and two-stage ignition fuels in HCCI engines'. *Proceedings of the Combustion Institute* (2007). DOI: 10.1016/j.proci.2006.08.010.

[365] Srijit Biswas et al. 'Assessing the potential of ethanol in the transition of biodiesel combustion to RCCI regimes under varying injection phasing strategies'. *Fuel* (2021). DOI: 10.1016/j.fuel.2021.121346.

[366] Ali Diané et al. 'Characterization, at Partial Loads, of the Combustion and Emissions of a Dual-Fuel Engine Burning Diesel and a Lean Gas Surrogate'. *Energies* (2023). DOI: 10.3390/en16155587.

[367] Rakesh Kumar Maurya. *Characteristics and Control of Low Temperature Combustion Engines*. Mechanical Engineering Series. 2018. ISBN: 978-3-319-68507-6. DOI: 10.1007/978-3-319-68508-3.

[368] J. A. Caton. *An introduction to thermodynamic cycle simulations for internal combustion engines*. 2015. ISBN: 978-1-119-03758-3.

[369] I. I. Vibe. 'Semi-empirical expression for combustion rate in engines'. *Proceedings of Conference on piston engines, USSR Academy of sciences*. Moscow, 1956.

[370] J I Ghojel. 'Review of the development and applications of the Wiebe function'. *International Journal of Engine Research* (2010). DOI: 10.1243/14680874JER06510.

[371] Y. Ding. 'Characterising Combustion in Diesel Engines'. Doctoral thesis. Delft University of Technology, 2011. URL: https://repository.tudelft.nl/islandora/object/uuid%3A10e25404-4b8e-443b-9f16-5e6e5c2a7444.

[372] Thomas F. Coleman and Yuying Li. 'An Interior Trust Region Approach for Nonlinear Minimization Subject to Bounds'. *SIAM Journal on Optimization* (1996). DOI: 10.1137/0806023.

PUBLICATIONS

Journal articles

• *As part of this thesis:*

(1). Konstantinos I. Kiouranakis et al. 'Methanol for heavy-duty internal combustion engines: Review of experimental studies and combustion strategies'. *Renewable and Sustainable Energy Reviews* (2025). DOI: 10.1016/j.rser.2025.115529

(2). Konstantinos I. Kiouranakis et al. 'Heat release behaviour in a natural gas lean-burn SI marine engine: Exploring the impact of bowl-in and squish combustion on performance and emissions'. *Applied Thermal Engineering* (2025). DOI: 10.1016/j.applthermaleng.2025.127509

(3). Konstantinos I. Kiouranakis et al. 'Combustion mode analysis of a large-bore methanol premixed dual-fuel engine with high methanol energy fractions'. *Energy Conversion and Management: X* (2025). DOI: 10.1016/j.ecmx.2025.101417

(4). Konstantinos I. Kiouranakis et al. 'Steering methanol premixed dual-fuel combustion with boundary conditions: Performance gains and mode shifts in a marine engine'. *Fuel* (2026). DOI: 10.1016/j.fuel.2026.139458

Conferences attended with papers

(1). Konstantinos I. Kiouranakis, Peter De Vos and Rinze Geertsma. 'Methanol as a Fuel in Shipping: Review and Outlook to ICE Research Within MENENS'. Series Title: Lecture Notes in Mobility. Springer, 2025. ISBN: 978-3-031-89443-5. DOI: 10.1007/978-3-031-89444-2_106

(2). Konstantinos I. Kiouranakis et al. 'Natural Gas for Marine Lean-Burn Spark Ignition Engines: A Combustion Stability Analysis'. *ASME 2024 ICE Forward Conference*. San Antonio, Texas, USA, 2024. DOI: 10.1115/ICEF2024-139218

(3). Konstantinos Ioannis Kiouranakis et al. 'Using multi-stage Wiebe to characterize the combustion of a marine natural gas lean-burn SI engine'. *31st CIMAC World Congress*. Zurich, 2025. DOI: 10.5281/ZENODO.15193328

ACKNOWLEDGMENTS

Surreal. This is the first word that comes to mind as I contemplate the end of this journey. I could never have imagined pursuing a Doctor of Philosophy degree; yet, having reached this point, I am certain of one thing: I will never stop pursuing learning and wisdom.

First and foremost, this PhD is owed to my supervisors and promoters, Peter de Vos and Rinze Geertsma, who gave me the chance to pursue it. I will always be grateful—not only for the opportunity to become a scientist, but for the space you created for me to grow as a human being. Looking back, I feel nothing but blessed that I can call you family in a way: you adopted me, trusted me, and let me keep doing what I was aspiring—to remain a student.

To Rinze: for reasons I still cannot explain, you were the first to believe in me and tell me I could chase a PhD. Beyond a supervisor, you have been a role model, and of course, a forever running buddy. To Peter: you opened your arms and became my academic father as my daily supervisor and promoter. Beyond our research, what will forever stay with me is your conviction that academia needs to remain rooted in teaching. By encouraging me to step into teaching—something I initially dreaded—you helped shape one of the most meaningful aspects of my academic journey.

However, this work would not have happened without also the people who guided me along the way. To Robbert Willems, who taught me so much about engine experiments: if my learning and research output during this PhD was a linear function of time, you turned it into an exponential one. Working with people like you is what I wish for my future self. To Harsh Sapra, who became not only an advisor but also a friend, offering both technical guidance and life advice. To Marcel Roberscheuten and the entire engine lab team at NLDA in Den Helder: you continually reminded me what "professor in practice" truly means. You helped me see that the place my soul wants to be is where theory and practice meet. To Menno Merts, who I wanted more actively involved as a supervisor, but always found time to share his interest and deep knowledge of combustion fundamentals.

To my colleagues. Thank you for bearing with me, and for still choosing to "disturb" the nerdy, often too distant office mate with conversations that made the days lighter. To my office mate Miguel Calvache: you sparked my interest in Spanish, made office life more beautiful, and became an hermano to me. To Vassili and Nicole: the siblings I gained during this journey, with whom I connected so effortlessly—after the initial push (thank you, Vassili) to realize it. To my colleague and forever friend, Kostas Z.: thank you for what you taught me about engines and combustion, but also about music and politics. To Abhishek: you were the first

person I called a friend in Delft and sparked my interest in philosophy—what a way to begin. Grateful to call you a forever friend. This list could go on for too long. If you are not mentioned by name, please do not mistake that for an appreciation lack. I carry you all with me, and I love you from the bottom of my heart.

To the MENENS project: without it as an entity, I would not have had the chance to immerse myself in my favorite subject of engines and serve a higher purpose of trying to make them more sustainable. In particular, I thank NLDA and TNO, and their lab teams, for our collaboration and their outstanding experimental work. Without your expertise, openness, and the effort to make the campaigns happen, I could not have completed this dissertation.

Now, to my family. And when I say family, I also mean my friends—my family by choice—most of whom are back in Greece, yet remained my motivation throughout these years. To Aggeliki: you stayed by my side through my move to the Netherlands and supported me. Wherever the life path led us to, I could not have made this journey without you. To Kitsios: you became my rock during the hardest personal period of this journey. You are my brother. To my other brother Bokias: thank you for sharing this journey with me in the Netherlands, and for bearing to live with my odd self. To my siblings, Niko, Kelly, and Nikita: you have been my role models, all in your own way. And I could not end with anyone else but my parents. I would be nobody without you. To my dad: despite all the hardships life placed in front of you, you kept standing—and you taught me what resilience is. To my one and only mum: you are beyond words. I love you exactly as you are.

I thank and love you all.

Konstantinos Ioannis Kiouranakis
Delft, April 2026

CURRICULUM VITAE

Konstantinos Ioannis Kiouranakis was born in Athens in May 1997. He holds a diploma degree in Naval Architecture and Marine Engineering from the National Technical University of Athens, from which he graduated in 2021. After completing his studies, he fulfilled his military service in Army Aviation and gained practical experience in maritime companies within the oil sector before beginning his PhD journey in July 2022. For the next four years, he pursued his doctoral research at Delft University of Technology and the Netherlands Defence Academy under the supervision of Peter de Vos and Rinze Geertsma, focusing on the exploration of methanol as a marine engine fuel through premixed combustion strategies.

Summary

Defossilizing maritime transport demands sustainable fuels that maintain marine engine efficiency and reliability. Methanol is a promising fuel due to its favorable properties and scalable renewable production, yet its low reactivity requires adapted combustion concepts. However, these premixed combustion concepts are hindered by knock and stability limits. This dissertation develops and applies in-cylinder pressure-based diagnostic frameworks to link combustion phenomena with overall performance for two premixed engine technologies: lean-burn spark ignition and premixed dual-fuel compression ignition. The methods and studies of this research provide insights into combustion mechanisms and operation constraints, establishing a foundation for optimizing premixed methanol strategies in support of maritime energy transition.

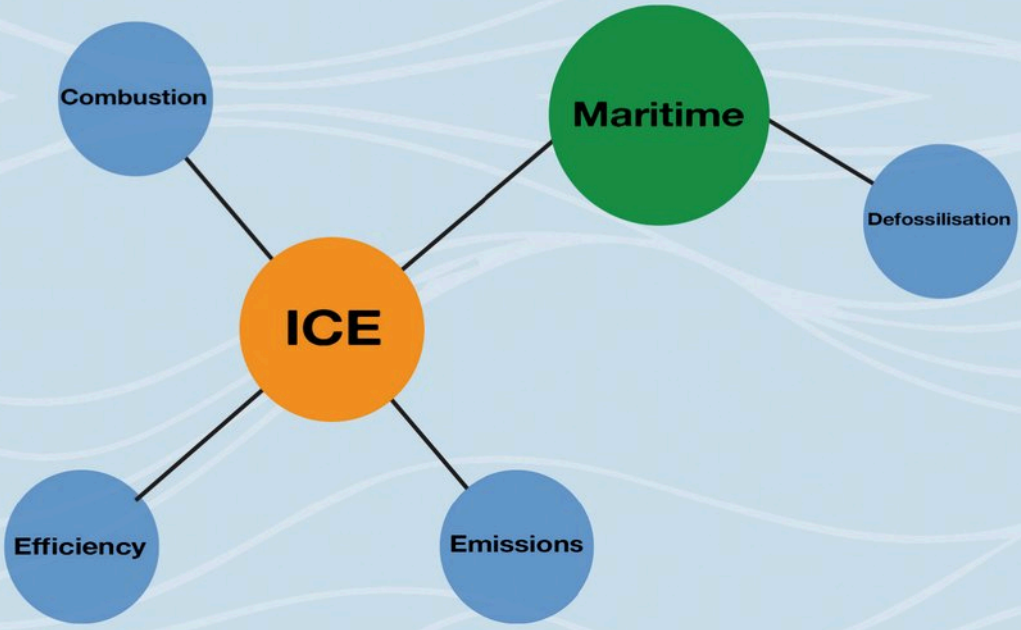

The human mind is such an extraordinary thing. It has invented the computer, split the atom, and sent ships into space - yet it has failed to solve the problem of human suffering.
- *Adapted from* Anthony de Mello